ISSN 1948-5204 (online)

World Journal of *Gastrointestinal Oncology*

World J Gastrointest Oncol 2022 May 15; 14(5): 947-1066

Published by Baishideng Publishing Group Inc

World Journal of Gastrointestinal Oncology

Contents

Monthly Volume 14 Number 5 May 15, 2022

CORRECTION

World Journal of Gastrointestinal Oncology

Monthly Volume 14 Number 5 May 15, 2022

Contents

ABOUT COVER

Editorial Board Member of *World Journal of Gastrointestinal Oncology*, Zilvinas Dambrauskas, MD, PhD, Professor, Department of Surgery and Institute for Digestive System Research, Lithuanian University of Health Sciences, Kaunas 50161, Lithuania. zilvinas.dambrauskas@lsmuni.lt

AIMS AND SCOPE

The primary aim of *World Journal of Gastrointestinal Oncology* (*WJGO*, *World J Gastrointest Oncol*) is to provide scholars and readers from various fields of gastrointestinal oncology with a platform to publish high-quality basic and clinical research articles and communicate their research findings online.

WJGO mainly publishes articles reporting research results and findings obtained in the field of gastrointestinal oncology and covering a wide range of topics including liver cell adenoma, gastric neoplasms, appendiceal neoplasms, biliary tract neoplasms, hepatocellular carcinoma, pancreatic carcinoma, cecal neoplasms, colonic neoplasms, colorectal neoplasms, duodenal neoplasms, esophageal neoplasms, gallbladder neoplasms, *etc*.

INDEXING/ABSTRACTING

The *WJGO* is now indexed in Science Citation Index Expanded (also known as SciSearch®), PubMed, PubMed Central, and Scopus. The 2021 edition of Journal Citation Reports® cites the 2020 impact factor (IF) for *WJGO* as 3.393; IF without journal self cites: 3.333; 5-year IF: 3.519; Journal Citation Indicator: 0.5; Ranking: 163 among 242 journals in oncology; Quartile category: Q3; Ranking: 60 among 92 journals in gastroenterology and hepatology; and Quartile category: Q3. The *WJGO*'s CiteScore for 2020 is 3.3 and Scopus CiteScore rank 2020: Gastroenterology is 70/136.

RESPONSIBLE EDITORS FOR THIS ISSUE

Production Editor: *Ying-Yi Yuan*; **Production Department Director:** *Xiang Li*; **Editorial Office Director:** *Ya-Juan Ma*.

NAME OF JOURNAL
World Journal of Gastrointestinal Oncology

ISSN
ISSN 1948-5204 (online)

LAUNCH DATE
February 15, 2009

FREQUENCY
Monthly

EDITORS-IN-CHIEF
Monjur Ahmed, Florin Burada

EDITORIAL BOARD MEMBERS
https://www.wjgnet.com/1948-5204/editorialboard.htm

PUBLICATION DATE
May 15, 2022

INSTRUCTIONS TO AUTHORS
https://www.wjgnet.com/bpg/gerinfo/204

GUIDELINES FOR ETHICS DOCUMENTS
https://www.wjgnet.com/bpg/GerInfo/287

GUIDELINES FOR NON-NATIVE SPEAKERS OF ENGLISH
https://www.wjgnet.com/bpg/gerinfo/240

PUBLICATION ETHICS
https://www.wjgnet.com/bpg/GerInfo/288

PUBLICATION MISCONDUCT
https://www.wjgnet.com/bpg/gerinfo/208

ARTICLE PROCESSING CHARGE
https://www.wjgnet.com/bpg/gerinfo/242

STEPS FOR SUBMITTING MANUSCRIPTS
https://www.wjgnet.com/bpg/GerInfo/239

ONLINE SUBMISSION
https://www.f6publishing.com

World Journal of Gastrointestinal Oncology

Submit a Manuscript: https://www.f6publishing.com

World J Gastrointest Oncol 2022 May 15; 14(5): 947-958

DOI: 10.4251/wjgo.v14.i5.947

ISSN 1948-5204 (online)

REVIEW

Gut microbiome in non-alcoholic fatty liver disease associated hepatocellular carcinoma: Current knowledge and potential for therapeutics

Imaad Said, Hassan Ahad, Adnan Said

Specialty type: Gastroenterology and hepatology

Provenance and peer review: Invited article; Externally peer reviewed.

Peer-review model: Single blind

Peer-review report's scientific quality classification

Grade A (Excellent): 0
Grade B (Very good): B
Grade C (Good): C
Grade D (Fair): 0
Grade E (Poor): 0

P-Reviewer: Gassler N, Germany; Shen J, China

Received: March 8, 2021
Peer-review started: March 8, 2021
First decision: March 29, 2021
Revised: April 14, 2021
Accepted: April 15, 2022
Article in press: April 15, 2022
Published online: May 15, 2022

Imaad Said, Brown University, Providence, RI 02912, United States

Hassan Ahad, Kansas University, Lawrence, KS 66045, United States

Adnan Said, Division of Gastroenterology and Hepatology, Department of Medicine, William S. Middleton VAMC, University of Wisconsin School of Medicine and Public Health, Madison, WI 53705, United States

Corresponding author: Adnan Said, FAASLD, MD, MS, Professor, Division of Gastroenterology and Hepatology, Department of Medicine, William S. Middleton VAMC, University of Wisconsin School of Medicine and Public Health, 4223 MFCB, 1685 Highland Avenue, Madison, WI 53705, United States. axs@medicine.wisc.edu

Abstract

Metabolic diseases such as nonalcoholic fatty liver disease (NAFLD) are rising in incidence and are an increasingly common cause of cirrhosis and hepatocellular carcinoma (HCC). The gut microbiome is closely connected to the liver *via* the portal vein, and has recently been identified as a predictor of liver disease state. Studies in NAFLD, cirrhosis and HCC have identified certain microbial signatures associated with these diseases, with the disease-associated microbiome changes collectively referred to as dysbiosis. The pathophysiologic underpinnings of these observations are an area of ongoing investigation, with current evidence demonstrating that the gut microbiome can influence liver disease and carcinogenesis *via* effects on intestinal permeability (leaky gut) and activation of the innate immune system. In the innate immune system, pathogen recognition receptors (Toll like receptors) on resident liver cells and macrophages cause liver inflammation, fibrosis, hepatocyte proliferation and reduced antitumor immunity, leading to chronic liver disease and carcinogenesis. Dysbiosis-associated changes include increase in secondary bile acids and reduced expression of FXR (nuclear receptor), which have also been associated with deleterious effects on lipid and carbohydrate metabolism associated with progressive liver disease. Longitudinal experimental and clinical studies are needed in different populations to examine these questions further. The role of therapeutics that modulate the microbiome is an emerging field with experimental studies showing the potential of diet, probiotics, fecal microbiota transplantation and prebiotics in improving liver disease in experimental models. Clinical studies are ongoing with preliminary

evidence showing improvement in liver enzymes and steatosis. The microbial profile is different in responders to cancer immunotherapy including liver cancer, but whether or not manipulation of the microbiome can be utilized to affect response is being investigated.

Key Words: Microbiome; Gut microbiome; Hepatocellular carcinoma; Nonalcoholic fatty liver disease; Pathophysiology; Treatment

Core Tip: The gut microbiome is intimately linked to nonalcoholic fatty liver disease, cirrhosis and hepatocellular carcinoma. The breakdown of the intestinal barrier in liver disease, innate immune system stimulation and bile acid profile changes are increasingly found in association with these diseases. Manipulation of the microbiome by diet, probiotics, prebiotics and other agents is a promising area of investigation.

Citation: Said I, Ahad H, Said A. Gut microbiome in non-alcoholic fatty liver disease associated hepatocellular carcinoma: Current knowledge and potential for therapeutics. *World J Gastrointest Oncol* 2022; 14(5): 947-958
URL: https://www.wjgnet.com/1948-5204/full/v14/i5/947.htm
DOI: https://dx.doi.org/10.4251/wjgo.v14.i5.947

INTRODUCTION

Liver cancer (hepatocellular carcinoma, HCC) is the seventh commonest cancer worldwide and the third commonest cause of cancer related mortality accounting for over 800000 deaths in 2020[1]. Over the past 4 decades in the US there has been a 4 fold increase in HCC incidence in the US[2].

Liver cancer is most commonly seen in association with cirrhosis of the liver as well as chronic hepatitis B (HBV) infection without cirrhosis[3]. Common causes of cirrhosis include non-alcoholic and alcoholic fatty liver disease, hepatitis C and hepatitis B infection as well as autoimmune and biliary diseases. Well known risk factors for liver cancer in cirrhosis and chronic HBV include male sex, smoking, alcohol excess, aflatoxin (rare), viral load in HBV, and metabolic factors such as diabetes and obesity[4].

Although the prevalence of hepatitis B and C are decreasing globally, liver cancer rates have increased due to the rise in cases of obesity, nonalcoholic fatty liver disease (NAFLD) and type 2 diabetes, largely fueled by a poor Western diet[5]. NAFLD related liver cancer is the fastest growing cause of liver cancer and related mortality in the US[6].

In NAFLD related HCC, factors such as age, genetic predisposition, diabetes and obesity have been found in association with the development of NAFLD-related HCC[6]. In NAFLD a significant minority of liver cancers (10%-15%) can occur even in the absence of cirrhosis and has been linked to the underlying liver inflammation, fibrosis with increased risk in diabetics[6]. The gut microbiome has been proposed as a leading risk factor associated with liver cancer. In obesity related metabolic diseases the microbial profile of the intestine has been linked to progressive liver disease and carcinogenesis both in experimental models and in human studies[7].

THE GUT MICROBIOME AND NAFLD-HCC

The gut microbiome

The gut microbiome refers to a multispecies community of resident microbes that includes a wide variety of bacteria, fungi, viruses as well as archaea, residing in the gut[8]. Nearly 100 trillion microbium occupy the intestinal tract particularly in the large intestine. Although small intestinal microbiota also exist this is a less well studied area compared to the large intestine. Most of the research in the human microbiome has been done on bacterial stool microorganisms which are a reasonable approximation of the intestinal microbiome. Studies of the microbiome in intestinal biopsies have been done to a lesser extent and there may be qualitative and quantitative differences in measuring the microbiome adherent to the mucosa *vs* present in stool.

The gut microbiome exhibits many benefits of commensalism for the host and plays an important role in regulating host immunity beginning in utero, maintaining a mucosal defense against pathogens, facilitating nutrient metabolism including assistance in digestion and as a prominent source of key vitamins and energy harvest[9]. The microbiome also plays a critical role in the pathogenesis of

metabolic diseases, inflammatory and autoimmune conditions both within the gastrointestinal tract and in remote sites[10].

The gut microbiome and liver disease

The liver receives the majority of its blood supply through the portal vein and is exposed to the microbiome either directly through microbial translocation or *via* microbial metabolites and products [11]. The homeostasis between gut microbes and host is mediated by an intact barrier function (tight junction) of colonic epithelial cells, thick mucus layer as well as IgA and antimicrobial surface peptides, achieved by interaction of the microbes and pathogen recognition receptors that promote a healthy tolerogenic immune response allowing symbiosis[12-14]. This exposure to the microbiome has a critical role in development of a normal immune response through priming and modulation of the immune response in the gut mucosa and the liver. This is exemplified in experiments in knockout mice lacking aspects of the innate immune system (*e.g.*, TLR5) in which dysbiosis has been reported[14].

Emerging evidence shows that in liver disease including metabolic fatty liver disease (NAFLD), cirrhosis and liver cancer, the microbiome varies significantly from the microbiome in healthy individuals both compositionally as well as functionally[11]. These diseases associated changes in the microbiome are referred to as dysbiosis and have been associated with metabolic liver disease and liver cancer in both animal experiments and in human studies. Dysbiosis, is strongly linked to fatty liver disease, type 2 diabetes and other metabolic disease[14]. The presence/absence of certain microorganisms can allow for identification of the severity of liver disease (serving as a diagnostic signature) and potentially guide emerging therapies. *Escherichia coli* (*E. coli*) is enriched in the gut of NAFLD patients with more advanced fibrosis and HCC[15] and Bacteroides bacteria were found in higher concentrations in cirrhotic patients with HCC patients as compared to cirrhotic patients without HCC [16].

In experimental models, antibiotics and gut sterilization can reduce the prevalence of HCCs in obese mice suggesting that microbiota dysbiosis plays a crucial role in the pathogenesis of HCC[17].

PATHOPHYSIOLOGY OF GUT DYSBIOSIS IN LIVER DISEASE AND LIVER CANCER

Leaky gut, endotoxemia, innate immune system and the inflammatory response

The intestinal microbiome in liver disease is potentially influenced by the liver disease itself, and in turn the intestinal microbiome can also influence the progression of liver disease.

In cirrhosis the underlying changes of portal hypertension influence intestine transit and permeability resulting in the so called "leaky gut" seen in cirrhosis[7]. This increased intestinal permeability allows increased passage of bacterial products, metabolites and bacteria *via* the portal vein to the liver resulting in endotoxinemia. Bacterial cell wall components such as lipopolysaccharide (LPS) from *Gram negative bacteria* and lipoteichoic acid (LTA) from *Gram positive bacteria* (also referred to as PAMPs or pathogen associated molecular pattern) are increased in the circulation in patients with increasing degree of advanced liver disease and in animal models of liver disease[7,18]. Measurements of LPS in portal vein, mean portal vein LPS levels increased in chronic liver injury from < 3 pg/mL in healthy volunteers to 4.9 pg/mL, 7.9 pg/mL and 10.2 pg/mL in patients with Child–Turcotte-Pugh cirrhosis stage A, B and C respectively[19].

In dysbiosis the host-microbiota balance is lost and the delivery of PAMPs like LPS and LTA *via* the portal vein, outside of the intestine where they exist in a symbiotic relationship with the host, is associated with activation of the innate immune systems *via* Pattern recognition receptors (such as Toll like receptors, TLR 4, 5 and TLR 9) found on the liver resident cells (hepatocytes, stellate cells) and liver resident macrophages (Kupffer cells)[11]. Activation of the immune response results in cytokine and chemokine expression and the recruitment of inflammatory cells in the liver, hepatocyte proliferation as well as hepatic stellate activation which result in progressive liver inflammation, fibrosis and liver cancer[7,19,20] (Figure 1).

Endotoxemia directly promotes chronic inflammation in the intestine as well as systemically in the liver, adipose tissue and vasculature though activation of cytokine and cell mediated pathways. This increases the risk of metabolic complications such as atherosclerosis, diabetes and nonalcoholic fatty liver disease which are common concurrent conditions[8,14]. The presence of NAFLD and liver diseases further impairs the ability of the liver to deal with gut derived endotoxins arriving *via* the portal vein. Chronic liver conditions such as NAFLD, particularly in the presence of diabetes are an increasing cause of liver cancer[6]. NAFLD patients with cirrhosis with HCC have an enhanced intestinal inflammatory status compared to those without HCC and healthy subjects, as demonstrated by the increased fecal calprotectin concentration[16]. Increased intestinal permeability, intestinal bacterial overgrowth and elevated serum endotoxin, all have been reported in NAFLD and NAFLD-HCC[7].

In experimental (mouse) models of liver cancer, TLR4 and the intestinal microbiota were not required for HCC initiation but are critical for HCC promotion. Activation of this innate immune system promotes liver cell proliferation *via* increased levels of the hepatomitogen epiregulin, and prevention of apoptosis (Figure 1). Gut sterilization restricted to late stages of hepatocarcinogenesis reduced HCC in

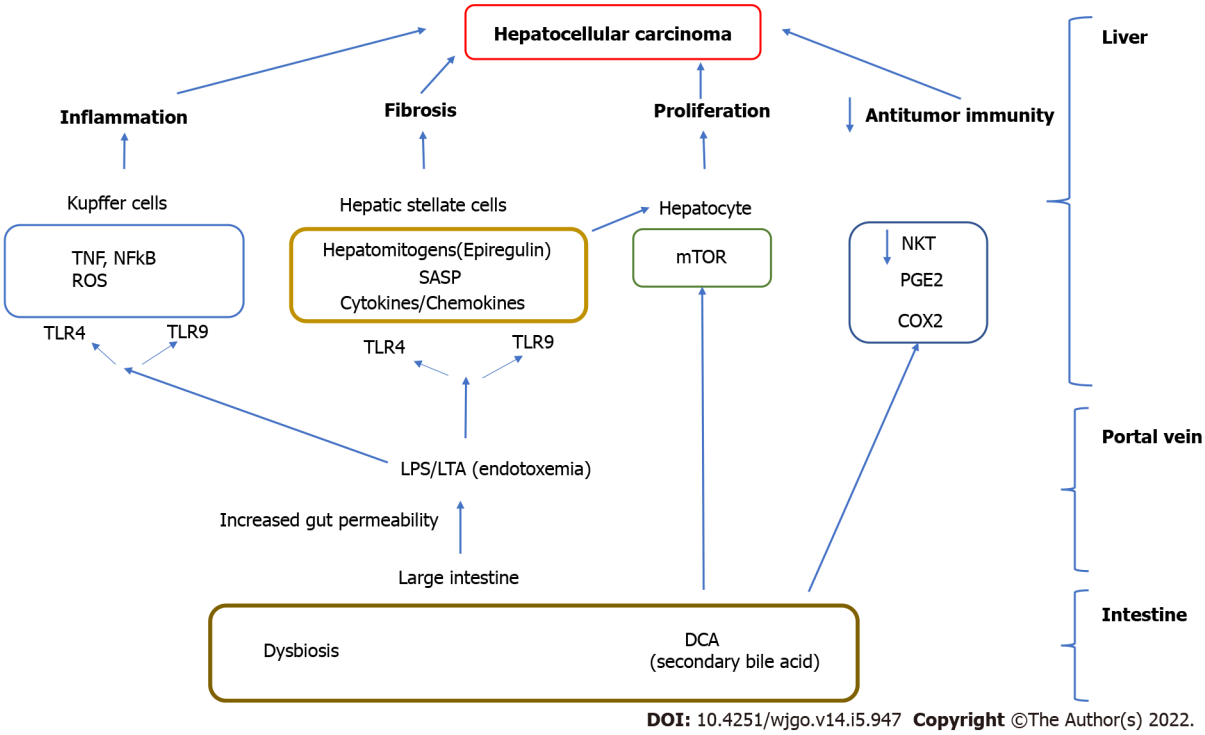

DOI: 10.4251/wjgo.v14.i5.947

Figure 1 Activation of the immune response results in cytokine and chemokine expression and the recruitment of inflammatory cells in the liver, hepatocyte proliferation as well as hepatic stellate activation which result in progressive liver inflammation, fibrosis and liver cancer.

this model. Germ-free status or TLR4 inactivation also reduce HCC by 80%-90% further attesting to the importance of the microbiome in carcinogenesis[17].

Intestinal permeability is increased in patients with compensated liver cirrhosis, regardless of the presence of HCC. A comparison of the patterns of cytokine and chemokine plasma levels between NAFLD related HCC in cirrhosis and NAFLD cirrhosis without HCC observed a specific inflammatory milieu in the HCC group_IL8, IL13, CCL3, CCL4, and CCL5 were significantly increased in the presence of HCC and, their plasma levels correlated with circulating activated monocytes and monocytic myeloid derived suppressor cells (mMDSCs). Activation of TLR4 by LPS is one of the most important inflammatory stimulations that can enhance the expression of CCL3, CCL4, and CCL5 by hepatic stellate cells (HSC) and monocytes[16].

LPS–TLR4 interaction also plays a role in hepatocarcinogenesis. IL8 has been associated with HCC development, tumor burden, and prognosis, similar to what has been reported for CCL2, CCL3, and CCL5. in mouse models the activation of HSC through TLR4 Leads to the secretion of CXCL1, the homologue of human IL8, causing neutrophil recruitment to the liver. Similar mechanisms have been postulated to promote mMDSC recruitment to the liver, favoring HCC progression[21].

LTA from Gram positive bacteria enhances the production of a Senescence associated secretory phenotype (SASP) of HSC in conjunction with an obesity induced gut microbial metabolite, deoxycholic acid (DCA) (secondary bile acid increased in the presence of dysbiosis in obesity). Cellular senescence a relatively recently described phenomenon is a complex process whereby senescent cells can induce cell cycle arrest as well as involve the secretion of factors that can result in tissue inflammation, repair and regeneration and affect the behavior of neighboring cells[22].

The phenotype of senescent cells involves secretion of a series of inflammatory cytokines, chemokines, matrix-remodeling factors, and growth factors. Whereas in early life and development the SASP may have anticancer effects (through cell cycle arrest) it has also been associated with the biology of aging, chronic inflammation and carcinogenesis in chronic conditions such as NAFLD. In one study of Steatohepatitis associated HCC increased production of senescence associated secretory factors like IL-6 were expressed by Fibroblasts in steatohepatitis associated cancers and non-tumoral stellate cells compared to convention HCCs)[23]. HCC development is promoted by this induction of cellular senescence and SASP in HSC in the tumor microenvironment. Corroborating these hypotheses, animal models of HCC demonstrate that vancomycin treatment significantly reduced obesity-associated liver cancer development. However, vancomycin treatment with DCA plus LTA significantly promoted liver cancer development, accompanied by increased levels of SASP factors[18].

Endotoxemia induced TLR 2 induction leads to COX2 mediated PGE production which suppresses antitumor immunity by inhibiting antitumor cytokine production from liver immune cells leading to HCC progression in a mouse model[7,18]. In human HCCs with noncirrhotic, NAFLD, COX2 overex-

pression and excess PGE production are detected[7,18]. Although these studies suggest that hepatocellular inflammation may be secondary to altered intestinal permeability and translocation of either intact bacteria or microbial cell components into circulation the causal link between them is not completely clarified[24].

The liver immune resident macrophages (Kupffer cells) and vascular system act to clear microbes that have penetrated the intestinal wall. Liver disease itself can cause dysfunction of this barrier and may promote increased intestinal permeability and translocation of bacteria or their components[25]. Liver disease in this model may directly contribute to the alteration of intestinal permeability and microbiome dysbiosis through portal hypertension.

Bile acids and interaction with gut microbiome, role in liver disease

Changes in bile acid metabolism are present in advanced liver disease: Bile acids have antimicrobial effects mediated directly or *via* induction of FXR nuclear receptors found in the intestine and liver that are closely linked with bile acid metabolism[26,27]. Bile antimicrobial properties are observed as a result of bile's capability of carrying out membrane-damaging effects. Electron microscopy and enzyme assay-based evidence has indicated in previous studies that, upon exposure to bile, cells shrink and lose intracellular material, thereby compromising membrane integrity[26]. Furthermore, bile has numerous other effects on bacterial stability such as changing the structure of RNA, inducing DNA damage, and alteration in protein structure, causing misfolding or denaturation, *via* detergent action[24]. The demonstration of the potential role of FXR against overgrowth is a possible area of potential research with utilization of synthetic FXR agonists in patients with reduced or obstructed bile flow who are at risk for bacterial overgrowth[27]. In cirrhosis there is decrease in total fecal bile acids and change in the bile acid profile which can result in intestinal bacterial overgrowth as bile acids have direct bacteriostatic effects[28-30]. Dysbiosis in liver disease has been associated with reduced Gram positives like *Ruminnococcacea* and increased *Enterobacteracieas* associated with decreased bile acid levels and with increased inflammation and LPS.

Bile acids are secreted by the liver and undergo extensive enterohepatic circulation in the small intestine and are influenced by the intestine microbiome. In obesity associated microbiomes there is increased conversion of primary bile acids like chenodeoxycholic acid to DCA which are toxic to the liver[31]. Unlike mice the human liver cannot convert DCA back to primary bile acids as it lacks the enzyme (7 hydroxylase) and secondary bile acids can accumulate to very high levels in the liver. After undergoing enterohepatic re-circulation increased DCA accumulation in the liver can cause oxidative injury to mitochondria and cell walls and increased reactive oxygen species development. Secondary BAs promote HCC development by activating SASP in hepatic stellate cells and hepatocyte proliferation *via* the hepatic mTOR pathway[32]. DCA has been associated with dysbiosis (Clostridium clusters) and development of HCC development in a obesity associated mouse model[33]. Since high fat diet can result in high DCA levels in healthy male volunteers, the DCA induced changes in stellate cells (SASP) may contribute to obesity associated HCC[33]. Increased DCA was associated with not only the increased relative abundance of specific bacterial groups, including *Bacteroidaceae* and *Lachnospiraceae spp.*, but also advanced fibrosis in NAFLD[34].

The production of bile acids in the liver and reabsorption in the ileum is regulated by a feedback mechanism with both bile acid induced activation of nuclear receptors like *FXR* in the intestine downregulating the apical bile salt pumps that transport bile back to the liver and activation of FXR nuclear receptors in the liver by bile acids downregulating their production. *TGR 5* is another universal bile acid sensing receptor that interacts with bile acids. Activation of these bile acid sensing receptors has been shown to have important anti-inflammatory and metabolic effects resulting in decreased liver lipogenesis, stellate cell activation, reduced gluconeogenesis resulting in improved liver metabolic profile[35].

Normal bile acids profiles are also involved in maintaining healthy intestinal epithelial barrier function *via* FXR and EGFR dependent pathways. The FXR dependent pathway is linked to the gut microbiota and liver disease *via* its regulation of bile acid concentration and composition. The presence of FXRs and their related target genes help maintain homeostasis of bile acid, glucose and fat levels in the liver and intestine. Inhibition of FXR disrupts this homeostasis and can lead to cholestasis, an excess buildup of bile acids in the liver. A lack of bile acids entering the intestine contributes to dysbiosis, which is commonly seen in conjunction with liver disease[31,36]. EGFR is important for the regeneration of liver cells post-injury, and the expression of this receptor is controlled by the bile acid profile in the gut-liver axis. An excess buildup of bile acids in the liver (caused by FXR inhibition, for example) results in overexpression of EGFR and its ligands, which is a trend commonly seen in patients with HCC[36].

Reduced levels of FXR expression have been found in mouse models that are associated with reduced expression of tumor suppressors (like SHP) and to liver cancer development.

In a mouse model of liver cancer, altering gut bacteria had an anti-tumor effect mediated *via* bile acid signaling that increased antitumor NKT cells in the liver. Primary bile acids were associated with antitumor effects *via* bile acid signaling through chemokines (CXCL16) whereas secondary bile acids were associated with reduced antitumor immunity. The use of vancomycin that reduced bacteria that convert primary to secondary bile acids were associated with increased NKT cell accumulation and reduced liver tumors[37].

Gut microbiome, metabolites and liver disease

The gut microbiome also impacts host metabolic processes such as energy extraction from food and is a major environmental factor contributing to NAFLD. The gut microbiota have the potential to increase intrahepatic fat through mechanisms such as altered appetite signaling, increased energy extraction from diet and altered expression of genes involved in de novo lipogenesis or oxidation[38,39]. There is evidence suggesting that microbiota may play a significant role in diurnal/circadian rhythm regulation a key process in mammalian metabolism that synchronizes metabolism to night and day light cycles [40]. In an animal model diurnal metabolic rhythms in metabolism were influenced by the intestinal microbiome *via* expression of intestinal epithelial histone deacetylase 3 (HDAC3) which takes inputs from the microbiota and circadian cycles and relays the signals from the inputs towards the host genes responsible for metabolism specifically in lipid transport promoting diet induced obesity[41]. Therefore, the possible disruption of the human microbiome can lead to worsening obesity and disruption of metabolic homeostasis leading to metabolic diseases like NAFLD and associate complications like cirrhosis and HCC.

Gut metabolites

Short chain fatty acids (SCFAs) are important for colonic epithelial integrity and serve as a valuable nutritional source in the colon. SCFA including formate, acetate, propionate and butyrate can enter the liver through portal vein and cause lipid accumulation and glucogenesis[38,42]. In NAFLD there are reduced levels of short chain anti-inflammatory fatty acids further affecting host energy absorption[43]. Other human NAFLD studies have shown increased SCFA levels (acetate and propionate) associated with reduced tREG cells and other markers of reduced immunologic progression of liver disease[44]. Circulating levels of butyrate are inversely related to portal hypertension, endotoxemia, and systemic inflammation in patients with cirrhosis**.** The effects of the microbiome on SCFA are still being investigated and discrepant results in studies may be due to variations in patient diet, age and other environmental factors. Based on the preponderance of preclinical data there is interest in investigation of the antisteatotic effects of SCFA supplementation in NAFLD.

Branched chain amino acids (BCAA) *vs* aromatic amino acids (AAA) balance can induce insulin resistance and steatosis and is associated with certain bacterial species (*Prevotella* and *Bacteroides*). BCAA have been positively associated with simple steatosis to NASH, NASH-cirrhosis and HCC, while Glutathione was inversely associated, although reverse effects are found in human and animal studies. Metabolites derived from aromatic amino acids can have anti-inflammatory effects in host cells[45].

Microbiota profiles in liver disease

Thus far there are no prospective longitudinal clinical studies showing correlation of microbial profile with HCC risk. Most studies are cross-sectional correlating microbial profiles with HCC risk while trying to control for other predictors. Functional studies that show a microbial risk profile development of HCC are animal based (mice based). In various models, germ free mice or sterilized mice have lower HCC risk. Administration of MAMPs can increase this risk (Table 1).

Identification of microbial signatures associated with HCC has the potential to be used for disease diagnostics in patients at risk of HCC. The microbiome also has the potential to be used for therapy (*e.g.*, in conjunction with cancer immunotherapy, see therapy section below).

The microbiome in obese individuals has reduced bacterial diversity and a higher potential for inflammation in a study of obesity, bimodal gene distribution was observed. Reduced bacterial diversity in obese individuals can lead to dysbiosis, which is associated with the development of liver diseases such as NAFLD and HCC - and so obesity is considered a risk factor for metabolic liver disease. A higher risk group was characterized by a higher prevalence of anti-inflammatory species such as *F. prausnitzii*, and an increased production potential of organic acids (including butyrate). In contrast, lower risk groups showed higher relative abundance of potentially proinflammatory *Bacteroides spp.* and genes involved in oxidative stress response. These groups were associated with insulin resistance but not BMI[46].

E. coli, E*nterobacteriaceae spp*., and *Klebsiella pneumonia* have been identified as ethanol-producing bacteria and were found to be relatively abundant in NAFLD patients[47,48]. In NAFLD advanced fibrosis was associated with an increased abundance of *Proteobacteria* and *E. coli* and a decrease in Firmicutes[49]. This gut microbiota profile promotes absorption of monosaccharides from the gut lumen, resulting in the induction of *de novo* hepatic lipogenesis[50].

Increased DCA was associated with not only the increased relative abundance of specific bacterial groups, including *Bacteroidaceae* and *Lachnospiraceae spp*., but also advanced fibrosis in NAFLD[48,51].

A study from China showed a microbial signature profile (distinct bacterial species) that were present in early stage HCC with cirrhosis compared to cirrhosis without HCC and healthy controls). While diversity of species was decreased in cirrhosis compared to controls it was increased in early-stage HCC compared to cirrhosis without HCC. Bacteria producing butyrate (potentially beneficial SCFA associated with improved gut barrier and liver immunity) were decreased in HCC while those producing LPS were increased[52].

Table 1 Microbiota profiles in liver disease

Study	Bacterial species increased	Bacterial species decreased	Putative impact of microbial change in group	Comparison group
Advanced fibrosis/cirrhosis				
Loomba *et al* [49], 2017, *Cell Metab*	Proteobacteria Include *E. coli*	Firmicutes	Higher incidence of enzymes for butyrate, and lower for lactate and acetate	NAFLD advanced fibrosis/cirrhosis compared to NAFLD mild/moderate fibrosis
Ponziani *et al* [18], 2019, *Hepatology*	**Phylum:** *Proteobacteria, Bacteroidetes, Cyanobacteria;* **Family:** *Lactobacillaceae, Enterobacteriaceae, Prevotellaceae, Bacteroidaceae, Streptococcaceae, Enterococcaceae, Veillonellaceae*	**Phylum:** *Verrucomicrobia;* **Family:** *Verrucomicrobiaceae; Methanobacteriaceae*	Intestinal inflammation, Increase in Intestinal permeability, increased systemic inflammation	NAFLD cirrhosis compared to healthy controls
HCC				
Ren *et al*[52], 2019, *Gut*	**Phylum:** *Acinetobacter*; **Genus:** *Gemmiger, Parabacteroides, Paraprevotella,* others	**Phylum:** *Verrucomicrobia*	Increased LPS producer with liver inflammation and oxidative damage; Decreased butyrate production resulting in intestinal mucosal disruption	Early HCC compared to cirrhosis
Ren *et al*[52], 2019, *Gut*	**Genus:** *Klebsiella, Haemophilus*	*Verrucomicrobia (Akkermansia);* **Genus:** *Alistipes, Phascolarctobacterium, Ruminococus*	Increased LPS producer with liver inflammation and oxidative damage; Decreased butyrate production resulting in intestinal mucosal disruption	Early HCC compared to healthy controls
Ponziani *et al* [16], 2019, *Hepatology*	**Phylum:** *Bacteroidetes*; **Family:** *Bacteroidaceae, Streptococcaceae, Enterococcaceae*	**Family:** *Verrucomicrobiaceae, Bifidobacteriaceae*	Intestinal inflammation, Increase in Intestinal permeability, increased systemic inflammation	HCC in NAFLD Compared to NAFLD cirrhosis without HCC
Grat M *et al* [15], 2016, *Transplant Proc*	*E. coli*		LPS and inflammation within liver	HCC cirrhosis Compared to non-HCC cirrhosis

Selected studies (human) showing different microbiota profiles in cirrhosis and hepatocellular carcinoma (HCC) with emphasis on non-alcoholic fatty liver disease associated HCC. HCC: Hepatocellular carcinoma; NAFLD: Non-alcoholic fatty liver disease; LPS: Lipopolysaccharide.

An Italian study showed *E. coli* overgrowth in the intestines of HCC and cirrhosis patients as well as increased levels of *Bacteroides* and *Ruminococcaceae spp*. and decreased levels of *Akkermensia* and *Bifidobacterium spp*. *Akkermansia* and *Bifidobacterium* were inversely correlated with calprotectin concentration, which in turn was associated with humoral and cellular inflammatory markers. A similar pattern was also observed for Bacteroides. This study suggests that gut microbiota profile and systemic inflammation are significantly correlated in NAFLD-HCC[18]. Another study also demonstrated *Bacteroides* and *Ruminococcaceae* increased but *Bifidobacterium* decreased in NAFLD-HCC[48].

The biggest differences in microbial profiles so far have been found between patients with cirrhosis and healthy patients and less so than those between cirrhosis with or without HCC. Thus the impact of the microbiome may be more in development of cirrhosis (the biggest risk factor for HCC) rather than HCC development itself. Differences in microbial profiles in studies from different countries suggest there are important regional differences, influenced by dietary, genetic or underlying cause of cirrhosis (*e.g.*, HBV HCC in Asia *vs* non HBV HCC in other part of the world) that should be accounted for in future studies.

Therapeutics, gut microbiome, role in liver cancer

Manipulation of the gut microbiome to alleviate disease including liver disease is a burgeoning area of research. Studies have looked at diet and impact on microbiome. The impact of using prebiotics, prebiotics and antibiotics to modulate the microbiome to impact liver disease is an area of active research as is the impact of the microbiome in influencing efficacy of liver cancer chemotherapeutics (Table 2).

There is epidemiologic evidence that dietary patterns and nutrients are associated with liver cancer (red meat, added sugar, particularly high fructose, processed food have been shown to pose a higher risk whereas fruit, vegetables, omega-3 oil (fish), coffee potentially lower risk). Animal (and some human) studies in liver disease also show high fat diet promoting worsened intestinal barrier function, decreased bacterial diversity and endotoxemia reaching the liver and adipose tissue promoting chronic inflammation and metabolic disease. Potential mechanisms whereby diet can influence cancer risk is through influencing inflammatory pathways, and potentially through modulation of the gut microbiome. A high fat diet results in a higher proportion of gram-negative bacteria - such as *Bacteroides*

Table 2 Therapeutics, gut microbiome, role in liver cancer

Study	Agents	Population	Outcomes
Animal models			
Borges Haubert *et al*[64], 2015, *Nutr Metab Insights*	*Prebiotics* fructoligosaccharides	NAFLD rat model	Decreased liver fat *via* decreased lipogenesis
Liu *et al*[65], 2020, *J Nutr Biochem*	*Probiotic* Lactobacillus rhamnosus	Mouse model of liver disease (HFD)	Reduced NASH frequency, reduced steatosis inflammation and apoptosis in liver
Zhou *et al*[56], 2017, *Sci Rep*	*FMT*	Mouse model of liver disease (HFD)	Decreased hepatic lipid and proinflammatory cytokines, increased lactobacillus, improved gut barrier function, reduced endotoxemia, increase butyrate
Yoshimoto *et al*[33], 2013, *Nature*	*Vancomycin*	Mouse model of liver disease (HFD)	Reduced liver cancer
Janssen *et al*[58], 2017, *Lipid Res*	Antibiotics (ampicillin, neomycin, vancomycin and metronidazole)	Mouse model of NAFLD	Decreased secondary bile acids, decreased liver inflammation and fibrosis
Friedman *et al*[63], 2018, *Gastroenterology*	FXR agonist obeticholic acid	Mouse model of NAFLD	Decreased endogenous bile acid; Increased bacterial profile with Gram + including Firmicutes
Humans studies			
Yang *et al*[5], 2020, *Br J Nutrition*	Diet and incident cancer risk-summary of studies	Worldwide epidemiologic studies of diet and liver cancer risk	*Higher risk for liver cancer:* Red Meat, Added Sugar, Processed food; *Lowered risk for liver cancer:* Vegetables, Fruits, Omega 3 oil, Coffee
Monem *et al*[55], 2017, *Euroasian J hepatogastro*	*Probiotics* Lactobacillus	NAFLD patients	Decreased AST and ALT
Bomhof *et al*[54], 2019, *Eur J Nutrition*	*Prebiotic* Oligofructose	NASH patients	Decreased hepatic inflammatory markers, deceased weight, improved glucose tolerance, decreased steatosis, decreased clostridium cluster XA and I and enhanced Bifidobacterium
Vrieze *et al*[57], 2012, *Gastroenterology*	FMT trial	FMT from lean donor to individuals with metabolic syndrome	Improved insulin sensitivity, Increase in butyrate producing bacteria

Selected studies (animal and human) of microbiome modulating therapies tested in non alcoholic steatohepatitis (NASH) and hepatocellular carcinoma (HCC) with emphasis on NASH HCC. NASH: Non alcoholic steatohepatitis; NAFLD: Non alcoholic fatty liver disease; HCC: Hepatocellular carcinoma; FMT: Fecal microbiota transplant; PD-1: Programmed death-1; FXR: Farnesoid X receptor.

- in the gut microbiome, resulting in a higher concentration of the LPS contained within the cell membrane of these bacteria. LPS activates toll-like receptors 4 and 9, which contributes to the fibrosis seen in NAFLD, NASH and HCC development[5,11,64].

Besides diet, other factors also regulate the microbiome and endotoxemia including genetics, and exogenous factors like exercise and alcohol.

Potential therapeutic strategies

Probiotics, prebiotics, fecal microbiota transplant (FMT), antibiotics for dysbiosis. No clinical studies have shown that intervening with the microbiome can influence the risk of HCC development in human trials thus far. In animal studies prebiotics (which are dietary fermentable substrates that can modulate microbiome growth) have been shown to reduce hepatic triglyceride accumulation *via* inhibition of lipogenesis and reduced expression of genes such as FAS[53].

In humans, supplementation with prebiotics such as oligofructose has been associated with decreased hepatic inflammatory markers. In a clinical trial with 14 participants, changes in body weight, glucose tolerance, and inflammatory markers among others were followed and observed over the course of 9 mo. The individuals treated with the prebiotics had markedly better markers than the individuals treated with the placebo and the overall rates of steatosis in patients treated with the prebiotic that were affected by non-alcoholic steatohepatitis did decrease[54].

Probiotics are live bacteria which are beneficial to the host. Probiotics in mice have been shown to enhance bile acid fecal excretion, reduce bile acid reabsorption in the intestine and reverse abnormal bile acid metabolism seen in dysbiosis. *Lactobacillus* and *Bifidobacterium spp*. have been reported to reduce gut inflammation and improve gut barrier function by remodeling the gut microbiota[53]. *Lactobacilli*, was administered orally to mice in a model of liver disease and reduced the frequency of NASH considerably while also reducing inflammation and fibrosis in the liver. In human studies, administration of *Lactobacillus acidophilus* reduced AST and ALT levels in NAFLD patients[55].

The modulation of gut microbiome *via* FMT has demonstrated decreased hepatic lipid accumulation and decreased pro-inflammatory cytokine levels after FMT in a mouse model of liver disease fed a high

fat diet[56]. Additionally, FMT increased the relative abundance of beneficial bacterial species of *Christensenellaceae* and *Lactobacillus*, improved gut barrier function, and increased butyrate production and reduced endotoxemia[58]. In a human trial, FMT from lean donors to individuals with metabolic syndrome temporarily increased insulin sensitivity whereas autologous FMT from the donors with metabolic syndrome did not show this change[57].

Antibiotics have been studied in experimental models of liver disease. In a mouse model of liver cancer, vancomycin treatment significantly reduced obesity-associated liver cancer development[18]. The use of antibiotics in a preclinical mouse model indicated that chronic oral administration of antibiotics decreased secondary bile acid levels, hepatic lipid accumulation, and attenuated hepatic inflammation and fibrosis *via* modulating the composition of gut microbiota[58,59].

In one study conducted on liver cancer model of mice, it was shown that various species of *Clostridium bacteria* can accumulate and potentially result in suppression of natural antitumor mechanisms against tumors found in the liver. Mice that were affected with the tumors were given antibiotic treatment that affected the state of the gut microbiome and resulted in a reduction in the growth of tumors in the liver as well as the metastasis of tumors originating in the liver. Antibiotics however may have divergent effects and Mahana *et al*[60] showed that mice treated with antibiotics exhibited severe insulin resistance and NAFLD associated with a change in composition of the gut microbiota from *Firmicutes* to *Bifidobacterium* and *Prevotella*.

The microbiome also has the potential to be used in conjunction with cancer immunotherapy. *Bacteroides* and *Bifidobacteria* species can assist T-cell-based immunotherapies in combating against cancer in the liver[61].

In a study of liver cancer undergoing immunotherapy (checkpoint inhibitor, anti-PD-1), gut microbiota profiles were different in patients responding to chemotherapy. These profiles varied during therapy and may enable early identification (within 6 wk changes in bacteria) of responders *vs* non responder to immunotherapy. Changes in the microbiome that correlated with response or non-response were seen as early as 6 wk. after start of immunotherapy[34]. Pathways by which the microbiome influenced cancer therapy efficacy may include the effect of certain bacterial species in improving host immunity, decreased intestinal permeability, decreased oxidative stress and decreased growth of pathogenic bacteria.

Probiotics and FMT are currently being investigated in cancer treatment as an adjuvant strategy to increase the efficacy of chemotherapy and immunotherapy[62].

FXR agonists that are in clinical use for patients with cholestatic liver diseases like PBC and being investigated for NAFLD have the potential to restore healthy gut microbiota and ameliorate metabolic diseases though effect on carbohydrate and lipid metabolism. In animal models, use of these agents have led to decreased endogenous bile acid levels and improved bacterial profile with increase in the proportion of Firmicutes[63].

CONCLUSION

Future directions

The role of the microbiome in chronic liver disease, particularly NAFLD and associated liver cancer is being elucidated through experimental and clinical studies. With the increasing epidemic of NAFLD and liver cancer this is an exciting and critical area of investigation.

Active areas of investigation include searching for effective HCC treatment and prevention in patients with chronic liver disease utilizing the knowledge gained from studies on the microbiome in liver disease. Utilizing the presence of distinct gut microbial profiles in earlier stage chronic liver disease, such as NAFLD and NASH, is emerging as an area for potential diagnostics as well as for therapeutics. Early identification of the signs of progressive liver disease, such as decreased microbiome diversity, increase in cytokine expression, and leaky gut may be important in preventing HCC development.

FOOTNOTES

Author contributions: Said A put forward the study concept and design; all authors did the manuscript writing and editing.

Conflict-of-interest statement: None of the authors have any relevant conflicts of interest.

Country/Territory of origin: United States

ORCID number: Imaad Said 0000-0002-7126-3794; Hassan Ahad 0000-0002-2527-6308; Adnan Said 0000-0001-9944-4071.

S-Editor: Wu YXJ
L-Editor: A
P-Editor: Wu YXJ

REFERENCES

1 **Sung H**, Ferlay J, Siegel RL, Laversanne M, Soerjomataram I, Jemal A, Bray F. Global Cancer Statistics 2020: GLOBOCAN Estimates of Incidence and Mortality Worldwide for 36 Cancers in 185 Countries. *CA Cancer J Clin* 2021; **71**: 209-249 [PMID: 33538338 DOI: 10.3322/caac.21660]
2 **Petrick JL**, Kelly SP, Altekruse SF, McGlynn KA, Rosenberg PS. Future of Hepatocellular Carcinoma Incidence in the United States Forecast Through 2030. *J Clin Oncol* 2016; **34**: 1787-1794 [PMID: 27044939 DOI: 10.1200/JCO.2015.64.7412]
3 **Massarweh NN**, El-Serag HB. Epidemiology of Hepatocellular Carcinoma and Intrahepatic Cholangiocarcinoma. *Cancer Control* 2017; **24**: 1073274817729245 [PMID: 28975830 DOI: 10.1177/1073274817729245]
4 **Fattovich G**, Stroffolini T, Zagni I, Donato F. Hepatocellular carcinoma in cirrhosis: incidence and risk factors. *Gastroenterology* 2004; **127**: S35-S50 [PMID: 15508101 DOI: 10.1053/j.gastro.2004.09.014]
5 **Yang WS**, Zeng XF, Liu ZN, Zhao QH, Tan YT, Gao J, Li HL, Xiang YB. Diet and liver cancer risk: a narrative review of epidemiological evidence. *Br J Nutr* 2020; **124**: 330-340 [PMID: 32234090 DOI: 10.1017/S0007114520001208]
6 **Said A**, Ghufran A. Epidemic of non-alcoholic fatty liver disease and hepatocellular carcinoma. *World J Clin Oncol* 2017; **8**: 429-436 [PMID: 29291167 DOI: 10.5306/wjco.v8.i6.429]
7 **Schwabe RF**, Greten TF. Gut microbiome in HCC - Mechanisms, diagnosis and therapy. *J Hepatol* 2020; **72**: 230-238 [PMID: 31954488 DOI: 10.1016/j.jhep.2019.08.016]
8 **Marchesi JR**, Adams DH, Fava F, Hermes GD, Hirschfield GM, Hold G, Quraishi MN, Kinross J, Smidt H, Tuohy KM, Thomas LV, Zoetendal EG, Hart A. The gut microbiota and host health: a new clinical frontier. *Gut* 2016; **65**: 330-339 [PMID: 26338727 DOI: 10.1136/gutjnl-2015-309990]
9 **Flint HJ**, Scott KP, Louis P, Duncan SH. The role of the gut microbiota in nutrition and health. *Nat Rev Gastroenterol Hepatol* 2012; **9**: 577-589 [PMID: 22945443 DOI: 10.1038/nrgastro.2012.156]
10 **Thaiss CA**, Zmora N, Levy M, Elinav E. The microbiome and innate immunity. *Nature* 2016; **535**: 65-74 [PMID: 27383981 DOI: 10.1038/nature18847]
11 **Yu LX**, Schwabe RF. The gut microbiome and liver cancer: mechanisms and clinical translation. *Nat Rev Gastroenterol Hepatol* 2017; **14**: 527-539 [PMID: 28676707 DOI: 10.1038/nrgastro.2017.72]
12 **Brown EM**, Sadarangani M, Finlay BB. The role of the immune system in governing host-microbe interactions in the intestine. *Nat Immunol* 2013; **14**: 660-667 [PMID: 23778793 DOI: 10.1038/ni.2611]
13 **McDole JR**, Wheeler LW, McDonald KG, Wang B, Konjufca V, Knoop KA, Newberry RD, Miller MJ. Goblet cells deliver luminal antigen to CD103+ dendritic cells in the small intestine. *Nature* 2012; **483**: 345-349 [PMID: 22422267 DOI: 10.1038/nature10863]
14 **Tilg H**, Zmora N, Adolph TE, Elinav E. The intestinal microbiota fuelling metabolic inflammation. *Nat Rev Immunol* 2020; **20**: 40-54 [PMID: 31388093 DOI: 10.1038/s41577-019-0198-4]
15 **Grąt M**, Wronka KM, Krasnodębski M, Masior Ł, Lewandowski Z, Kosińska I, Grąt K, Stypułkowski J, Rejowski S, Wasilewicz M, Gałęcka M, Szachta P, Krawczyk M. Profile of Gut Microbiota Associated With the Presence of Hepatocellular Cancer in Patients With Liver Cirrhosis. *Transplant Proc* 2016; **48**: 1687-1691 [PMID: 27496472 DOI: 10.1016/j.transproceed.2016.01.077]
16 **Ponziani FR**, Bhoori S, Castelli C, Putignani L, Rivoltini L, Del Chierico F, Sanguinetti M, Morelli D, Paroni Sterbini F, Petito V, Reddel S, Calvani R, Camisaschi C, Picca A, Tuccitto A, Gasbarrini A, Pompili M, Mazzaferro V. Hepatocellular Carcinoma Is Associated With Gut Microbiota Profile and Inflammation in Nonalcoholic Fatty Liver Disease. *Hepatology* 2019; **69**: 107-120 [PMID: 29665135 DOI: 10.1002/hep.30036]
17 **Dapito DH**, Mencin A, Gwak GY, Pradere JP, Jang MK, Mederacke I, Caviglia JM, Khiabanian H, Adeyemi A, Bataller R, Lefkowitch JH, Bower M, Friedman R, Sartor RB, Rabadan R, Schwabe RF. Promotion of hepatocellular carcinoma by the intestinal microbiota and TLR4. *Cancer Cell* 2012; **21**: 504-516 [PMID: 22516259 DOI: 10.1016/j.ccr.2012.02.007]
18 **Loo TM**, Kamachi F, Watanabe Y, Yoshimoto S, Kanda H, Arai Y, Nakajima-Takagi Y, Iwama A, Koga T, Sugimoto Y, Ozawa T, Nakamura M, Kumagai M, Watashi K, Taketo MM, Aoki T, Narumiya S, Oshima M, Arita M, Hara E, Ohtani N. Gut Microbiota Promotes Obesity-Associated Liver Cancer through PGE_2-Mediated Suppression of Antitumor Immunity. *Cancer Discov* 2017; **7**: 522-538 [PMID: 28202625 DOI: 10.1158/2159-8290.CD-16-0932]
19 **Lin RS**, Lee FY, Lee SD, Tsai YT, Lin HC, Lu RH, Hsu WC, Huang CC, Wang SS, Lo KJ. Endotoxemia in patients with chronic liver diseases: relationship to severity of liver diseases, presence of esophageal varices, and hyperdynamic circulation. *J Hepatol* 1995; **22**: 165-172 [PMID: 7790704 DOI: 10.1016/0168-8278(95)80424-2]
20 **Bellot P**, García-Pagán JC, Francés R, Abraldes JG, Navasa M, Pérez-Mateo M, Such J, Bosch J. Bacterial DNA translocation is associated with systemic circulatory abnormalities and intrahepatic endothelial dysfunction in patients with cirrhosis. *Hepatology* 2010; **52**: 2044-2052 [PMID: 20979050 DOI: 10.1002/hep.23918]
21 **Bigorgne AE**, John B, Ebrahimkhani MR, Shimizu-Albergine M, Campbell JS, Crispe IN. TLR4-Dependent Secretion by Hepatic Stellate Cells of the Neutrophil-Chemoattractant CXCL1 Mediates Liver Response to Gut Microbiota. *PLoS One* 2016; **11**: e0151063 [PMID: 27002851 DOI: 10.1371/journal.pone.0151063]

22 **Rodier F**, Campisi J. Four faces of cellular senescence. *J Cell Biol* 2011; **192**: 547-556 [PMID: 21321098 DOI: 10.1083/jcb.201009094]

23 **Lee JS**, Yoo JE, Kim H, Rhee H, Koh MJ, Nahm JH, Choi JS, Lee KH, Park YN. Tumor stroma with senescence-associated secretory phenotype in steatohepatitic hepatocellular carcinoma. *PLoS One* 2017; **12**: e0171922 [PMID: 28273155 DOI: 10.1371/journal.pone.0171922]

24 **Farhadi A**, Gundlapalli S, Shaikh M, Frantzides C, Harrell L, Kwasny MM, Keshavarzian A. Susceptibility to gut leakiness: a possible mechanism for endotoxaemia in non-alcoholic steatohepatitis. *Liver Int* 2008; **28**: 1026-1033 [PMID: 18397235 DOI: 10.1111/j.1478-3231.2008.01723.x]

25 **Balmer ML**, Slack E, de Gottardi A, Lawson MA, Hapfelmeier S, Miele L, Grieco A, Van Vlierberghe H, Fahrner R, Patuto N, Bernsmeier C, Ronchi F, Wyss M, Stroka D, Dickgreber N, Heim MH, McCoy KD, Macpherson AJ. The liver may act as a firewall mediating mutualism between the host and its gut commensal microbiota. *Sci Transl Med* 2014; **6**: 237ra66 [PMID: 24848256 DOI: 10.1126/scitranslmed.3008618]

26 **Begley M**, Gahan CG, Hill C. The interaction between bacteria and bile. *FEMS Microbiol Rev* 2005; **29**: 625-651 [PMID: 16102595 DOI: 10.1016/j.femsre.2004.09.003]

27 **Inagaki T**, Moschetta A, Lee YK, Peng L, Zhao G, Downes M, Yu RT, Shelton JM, Richardson JA, Repa JJ, Mangelsdorf DJ, Kliewer SA. Regulation of antibacterial defense in the small intestine by the nuclear bile acid receptor. *Proc Natl Acad Sci U S A* 2006; **103**: 3920-3925 [PMID: 16473946 DOI: 10.1073/pnas.0509592103]

28 **Schnabl B**, Brenner DA. Interactions between the intestinal microbiome and liver diseases. *Gastroenterology* 2014; **146**: 1513-1524 [PMID: 24440671 DOI: 10.1053/j.gastro.2014.01.020]

29 **Pijls KE**, Jonkers DM, Elamin EE, Masclee AA, Koek GH. Intestinal epithelial barrier function in liver cirrhosis: an extensive review of the literature. *Liver Int* 2013; **33**: 1457-1469 [PMID: 23879434 DOI: 10.1111/liv.12271]

30 **Kakiyama G**, Pandak WM, Gillevet PM, Hylemon PB, Heuman DM, Daita K, Takei H, Muto A, Nittono H, Ridlon JM, White MB, Noble NA, Monteith P, Fuchs M, Thacker LR, Sikaroodi M, Bajaj JS. Modulation of the fecal bile acid profile by gut microbiota in cirrhosis. *J Hepatol* 2013; **58**: 949-955 [PMID: 23333527 DOI: 10.1016/j.jhep.2013.01.003]

31 **Ridlon JM**, Kang DJ, Hylemon PB. Bile salt biotransformations by human intestinal bacteria. *J Lipid Res* 2006; **47**: 241-259 [PMID: 16299351 DOI: 10.1194/jlr.R500013-JLR200]

32 **Yamada S**, Takashina Y, Watanabe M, Nagamine R, Saito Y, Kamada N, Saito H. Bile acid metabolism regulated by the gut microbiota promotes non-alcoholic steatohepatitis-associated hepatocellular carcinoma in mice. *Oncotarget* 2018; **9**: 9925-9939 [PMID: 29515780 DOI: 10.18632/oncotarget.24066]

33 **Yoshimoto S**, Loo TM, Atarashi K, Kanda H, Sato S, Oyadomari S, Iwakura Y, Oshima K, Morita H, Hattori M, Honda K, Ishikawa Y, Hara E, Ohtani N. Obesity-induced gut microbial metabolite promotes liver cancer through senescence secretome. *Nature* 2013; **499**: 97-101 [PMID: 23803760 DOI: 10.1038/nature12347]

34 **Zheng Y**, Wang T, Tu X, Huang Y, Zhang H, Tan D, Jiang W, Cai S, Zhao P, Song R, Li P, Qin N, Fang W. Gut microbiome affects the response to anti-PD-1 immunotherapy in patients with hepatocellular carcinoma. *J Immunother Cancer* 2019; **7**: 193 [PMID: 31337439 DOI: 10.1186/s40425-019-0650-9]

35 **Chiang JYL**, Ferrell JM. Bile Acid Metabolism in Liver Pathobiology. *Gene Expr* 2018; **18**: 71-87 [PMID: 29325602 DOI: 10.3727/105221618X15156018385515]

36 **Komposch K**, Sibilia M. EGFR Signaling in Liver Diseases. *Int J Mol Sci* 2015; **17** [PMID: 26729094 DOI: 10.3390/ijms17010030]

37 **Ma C**, Han M, Heinrich B, Fu Q, Zhang Q, Sandhu M, Agdashian D, Terabe M, Berzofsky JA, Fako V, Ritz T, Longerich T, Theriot CM, McCulloch JA, Roy S, Yuan W, Thovarai V, Sen SK, Ruchirawat M, Korangy F, Wang XW, Trinchieri G, Greten TF. Gut microbiome-mediated bile acid metabolism regulates liver cancer *via* NKT cells. *Science* 2018; **360** [PMID: 29798856 DOI: 10.1126/science.aan5931]

38 **Ezzaidi N**, Zhang X, Coker OO, Yu J. New insights and therapeutic implication of gut microbiota in non-alcoholic fatty liver disease and its associated liver cancer. *Cancer Lett* 2019; **459**: 186-191 [PMID: 31185249 DOI: 10.1016/j.canlet.2019.114425]

39 **Jumpertz R**, Le DS, Turnbaugh PJ, Trinidad C, Bogardus C, Gordon JI, Krakoff J. Energy-balance studies reveal associations between gut microbes, caloric load, and nutrient absorption in humans. *Am J Clin Nutr* 2011; **94**: 58-65 [PMID: 21543530 DOI: 10.3945/ajcn.110.010132]

40 **Turnbaugh PJ**, Ley RE, Mahowald MA, Magrini V, Mardis ER, Gordon JI. An obesity-associated gut microbiome with increased capacity for energy harvest. *Nature* 2006; **444**: 1027-1031 [PMID: 17183312 DOI: 10.1038/nature05414]

41 **Field RE**, Romanus RJ. An improved gastrostomy technique. *IMJ Ill Med J* 1975; **148**: 610-611

42 **den Besten G**, Lange K, Havinga R, van Dijk TH, Gerding A, van Eunen K, Müller M, Groen AK, Hooiveld GJ, Bakker BM, Reijngoud DJ. Gut-derived short-chain fatty acids are vividly assimilated into host carbohydrates and lipids. *Am J Physiol Gastrointest Liver Physiol* 2013; **305**: G900-G910 [PMID: 24136789 DOI: 10.1152/ajpgi.00265.2013]

43 **Chu H**, Duan Y, Yang L, Schnabl B. Small metabolites, possible big changes: a microbiota-centered view of non-alcoholic fatty liver disease. *Gut* 2019; **68**: 359-370 [PMID: 30171065 DOI: 10.1136/gutjnl-2018-316307]

44 **Rau M**, Rehman A, Dittrich M, Groen AK, Hermanns HM, Seyfried F, Beyersdorf N, Dandekar T, Rosenstiel P, Geier A. Fecal SCFAs and SCFA-producing bacteria in gut microbiome of human NAFLD as a putative link to systemic T-cell activation and advanced disease. *United European Gastroenterol J* 2018; **6**: 1496-1507 [PMID: 30574320 DOI: 10.1177/2050640618804444]

45 **Han J**, Dzierlenga AL, Lu Z, Billheimer DD, Torabzadeh E, Lake AD, Li H, Novak P, Shipkova P, Aranibar N, Robertson D, Reily MD, Lehman-McKeeman LD, Cherrington NJ. Metabolomic profiling distinction of human nonalcoholic fatty liver disease progression from a common rat model. *Obesity (Silver Spring)* 2017; **25**: 1069-1076 [PMID: 28452429 DOI: 10.1002/oby.21855]

46 **Le Chatelier E**, Nielsen T, Qin J, Prifti E, Hildebrand F, Falony G, Almeida M, Arumugam M, Batto JM, Kennedy S, Leonard P, Li J, Burgdorf K, Grarup N, Jørgensen T, Brandslund I, Nielsen HB, Juncker AS, Bertalan M, Levenez F, Pons N, Rasmussen S, Sunagawa S, Tap J, Tims S, Zoetendal EG, Brunak S, Clément K, Doré J, Kleerebezem M, Kristiansen K, Renault P, Sicheritz-Ponten T, de Vos WM, Zucker JD, Raes J, Hansen T; MetaHIT consortium, Bork P, Wang J, Ehrlich

SD, Pedersen O. Richness of human gut microbiome correlates with metabolic markers. *Nature* 2013; **500**: 541-546 [PMID: 23985870 DOI: 10.1038/nature12506]

47 **Yuan J**, Chen C, Cui J, Lu J, Yan C, Wei X, Zhao X, Li N, Li S, Xue G, Cheng W, Li B, Li H, Lin W, Tian C, Zhao J, Han J, An D, Zhang Q, Wei H, Zheng M, Ma X, Li W, Chen X, Zhang Z, Zeng H, Ying S, Wu J, Yang R, Liu D. Fatty Liver Disease Caused by High-Alcohol-Producing Klebsiella pneumoniae. *Cell Metab* 2019; **30**: 675-688.e7 [PMID: 31543403 DOI: 10.1016/j.cmet.2019.08.018]

48 **Zhang C**, Yang M, Ericsson AC. The Potential Gut Microbiota-Mediated Treatment Options for Liver Cancer. *Front Oncol* 2020; **10**: 524205 [PMID: 33163393 DOI: 10.3389/fonc.2020.524205]

49 **Loomba R**, Seguritan V, Li W, Long T, Klitgord N, Bhatt A, Dulai PS, Caussy C, Bettencourt R, Highlander SK, Jones MB, Sirlin CB, Schnabl B, Brinkac L, Schork N, Chen CH, Brenner DA, Biggs W, Yooseph S, Venter JC, Nelson KE. Gut Microbiome-Based Metagenomic Signature for Non-invasive Detection of Advanced Fibrosis in Human Nonalcoholic Fatty Liver Disease. *Cell Metab* 2017; **25**: 1054-1062.e5 [PMID: 28467925 DOI: 10.1016/j.cmet.2017.04.001]

50 **Bäckhed F**, Ding H, Wang T, Hooper LV, Koh GY, Nagy A, Semenkovich CF, Gordon JI. The gut microbiota as an environmental factor that regulates fat storage. *Proc Natl Acad Sci U S A* 2004; **101**: 15718-15723 [PMID: 15505215 DOI: 10.1073/pnas.0407076101]

51 **Singh V**, Yeoh BS, Abokor AA, Golonka RM, Tian Y, Patterson AD, Joe B, Heikenwalder M, Vijay-Kumar M. Vancomycin prevents fermentable fiber-induced liver cancer in mice with dysbiotic gut microbiota. *Gut Microbes* 2020; **11**: 1077-1091 [PMID: 32223398 DOI: 10.1080/19490976.2020.1743492]

52 **Ren Z**, Li A, Jiang J, Zhou L, Yu Z, Lu H, Xie H, Chen X, Shao L, Zhang R, Xu S, Zhang H, Cui G, Sun R, Wen H, Lerut JP, Kan Q, Li L, Zheng S. Gut microbiome analysis as a tool towards targeted non-invasive biomarkers for early hepatocellular carcinoma. *Gut* 2019; **68**: 1014-1023 [PMID: 30045880 DOI: 10.1136/gutjnl-2017-315084]

53 **Chen YH**, Wu WK, Wu MS. Microbiota-Associated Therapy for Non-Alcoholic Steatohepatitis-Induced Liver Cancer: A Review. *Int J Mol Sci* 2020; **21** [PMID: 32825440 DOI: 10.3390/ijms21175999]

54 **Bomhof MR**, Parnell JA, Ramay HR, Crotty P, Rioux KP, Probert CS, Jayakumar S, Raman M, Reimer RA. Histological improvement of non-alcoholic steatohepatitis with a prebiotic: a pilot clinical trial. *Eur J Nutr* 2019; **58**: 1735-1745 [PMID: 29779170 DOI: 10.1007/s00394-018-1721-2]

55 **Abdel Monem SM**. Probiotic Therapy in Patients with Nonalcoholic Steatohepatitis in Zagazig University Hospitals. *Euroasian J Hepatogastroenterol* 2017; **7**: 101-106 [PMID: 29201787 DOI: 10.5005/jp-journals-10018-1226]

56 **Zhou D**, Pan Q, Shen F, Cao HX, Ding WJ, Chen YW, Fan JG. Total fecal microbiota transplantation alleviates high-fat diet-induced steatohepatitis in mice *via* beneficial regulation of gut microbiota. *Sci Rep* 2017; **7**: 1529 [PMID: 28484247 DOI: 10.1038/s41598-017-01751-y]

57 **Vrieze A**, Van Nood E, Holleman F, Salojärvi J, Kootte RS, Bartelsman JF, Dallinga-Thie GM, Ackermans MT, Serlie MJ, Oozeer R, Derrien M, Druesne A, Van Hylckama Vlieg JE, Bloks VW, Groen AK, Heilig HG, Zoetendal EG, Stroes ES, de Vos WM, Hoekstra JB, Nieuwdorp M. Transfer of intestinal microbiota from lean donors increases insulin sensitivity in individuals with metabolic syndrome. *Gastroenterology* 2012; **143**: 913-6.e7 [PMID: 22728514 DOI: 10.1053/j.gastro.2012.06.031]

58 **Janssen AWF**, Houben T, Katiraei S, Dijk W, Boutens L, van der Bolt N, Wang Z, Brown JM, Hazen SL, Mandard S, Shiri-Sverdlov R, Kuipers F, Willems van Dijk K, Vervoort J, Stienstra R, Hooiveld GJEJ, Kersten S. Modulation of the gut microbiota impacts nonalcoholic fatty liver disease: a potential role for bile acids. *J Lipid Res* 2017; **58**: 1399-1416 [PMID: 28533304 DOI: 10.1194/jlr.M075713]

59 **Safari Z**, Gérard P. The links between the gut microbiome and non-alcoholic fatty liver disease (NAFLD). *Cell Mol Life Sci* 2019; **76**: 1541-1558 [PMID: 30683985 DOI: 10.1007/s00018-019-03011-w]

60 **Mahana D**, Trent CM, Kurtz ZD, Bokulich NA, Battaglia T, Chung J, Müller CL, Li H, Bonneau RA, Blaser MJ. Antibiotic perturbation of the murine gut microbiome enhances the adiposity, insulin resistance, and liver disease associated with high-fat diet. *Genome Med* 2016; **8**: 48 [PMID: 27124954 DOI: 10.1186/s13073-016-0297-9]

61 **Longhi G**, van Sinderen D, Ventura M, Turroni F. Microbiota and Cancer: The Emerging Beneficial Role of Bifidobacteria in Cancer Immunotherapy. *Front Microbiol* 2020; **11**: 575072 [PMID: 33013813 DOI: 10.3389/fmicb.2020.575072]

62 **Vivarelli S**, Salemi R, Candido S, Falzone L, Santagati M, Stefani S, Torino F, Banna GL, Tonini G, Libra M. Gut Microbiota and Cancer: From Pathogenesis to Therapy. *Cancers (Basel)* 2019; **11** [PMID: 30609850 DOI: 10.3390/cancers11010038]

63 **Friedman ES**, Li Y, Shen TD, Jiang J, Chau L, Adorini L, Babakhani F, Edwards J, Shapiro D, Zhao C, Carr RM, Bittinger K, Li H, Wu GD. FXR-Dependent Modulation of the Human Small Intestinal Microbiome by the Bile Acid Derivative Obeticholic Acid. *Gastroenterology* 2018; **155**: 1741-1752.e5 [PMID: 30144429 DOI: 10.1053/j.gastro.2018.08.022]

64 **Borges Haubert NJ**, Marchini JS, Carvalho Cunha SF, Suen VM, Padovan GJ, Jordao AA Junior, Marchini Alves CM, Marchini JF, Vannucchi H. Choline and Fructooligosaccharide: Non-alcoholic Fatty Liver Disease, Cardiac Fat Deposition, and Oxidative Stress Markers. *Nutr Metab Insights* 2015; **8**: 1-6 [PMID: 25987847 DOI: 10.4137/NMI.S24385]

65 **Liu Q**, Liu Y, Li F, Gu Z, Liu M, Shao T, Zhang L, Zhou G, Pan C, He L, Cai J, Zhang X, Barve S, McClain CJ, Chen Y, Feng W. Probiotic culture supernatant improves metabolic function through FGF21-adiponectin pathway in mice. *J Nutr Biochem* 2020; **75**: 108256 [PMID: 31760308 DOI: 10.1016/j.jnutbio.2019.108256]

World Journal of Gastrointestinal Oncology

Submit a Manuscript: https://www.f6publishing.com

World J Gastrointest Oncol 2022 May 15; 14(5): 959-972

DOI: 10.4251/wjgo.v14.i5.959

ISSN 1948-5204 (online)

REVIEW

Helicobacter pylori, gastric microbiota and gastric cancer relationship: Unrolling the tangle

Christos Liatsos, Apostolis Papaefthymiou, Nikolaos Kyriakos, Michail Galanopoulos, Michael Doulberis, Marios Giakoumis, Evangelia Petridou, Christos Mavrogiannis, Theodore Rokkas, Jannis Kountouras

Specialty type: Gastroenterology and Hepatology

Provenance and peer review: Invited article; Externally peer reviewed.

Peer-review model: Single blind

Peer-review report's scientific quality classification

Grade A (Excellent): 0
Grade B (Very good): B
Grade C (Good): 0
Grade D (Fair): 0
Grade E (Poor): 0

P-Reviewer: Dong QJ, China

Received: March 19, 2021
Peer-review started: March 19, 2021
First decision: May 3, 2021
Revised: May 12, 2021
Accepted: April 9, 2022
Article in press: April 9, 2022
Published online: May 15, 2022

Christos Liatsos, Apostolis Papaefthymiou, Nikolaos Kyriakos, Michail Galanopoulos, Marios Giakoumis, Department of Gastroenterology, 401 General Military Hospital of Athens, Athens 11525, Greece

Apostolis Papaefthymiou, Gastroenterology, University Hospital of Larissa, Larissa 41336, Greece

Michael Doulberis, Division of Gastroenterology and Hepatology, Medical University Department, Kantonsspital Aarau, Aarau 1234, Switzerland

Evangelia Petridou, Department of Microbiology, "Agia Sofia" Paediatric Hospital, Goudi, Athens 11527, Greece

Christos Mavrogiannis, Gastrointestinal and Liver Unit, Faculty of Nursing, Kifissia General and Oncology Hospital, Kaliftaki, N.Kifisia 14564, Greece

Theodore Rokkas, Gastroenterological Clinic, Henry Dunant Hospital, Athens 11525, Greece

Jannis Kountouras, Department of Internal Medicine, Second Medical Clinic, Ippokration Hospital, Aristotle University of Thessaloniki, Thessaloniki 41336, Macedonia, Greece

Corresponding author: Christos Liatsos, FEBG, MD, PhD, Director, Department of Gastroenterology, 401 General Military Hospital of Athens, Panagioti Kanellopoulou Ave, Athens 11525, Greece. cliatsos@yahoo.com

Abstract

Helicobacter pylori infection (*Hp*-I) represents a typical microbial agent intervening in the complex mechanisms of gastric homeostasis by disturbing the balance between the host gastric microbiota and mucosa-related factors, leading to inflammatory changes, dysbiosis and eventually gastric cancer. The normal gastric microbiota shows diversity, with *Proteobacteria* [*Helicobacter pylori* (*H. pylori*) belongs to this family], *Firmicutes*, *Actinobacteria*, *Bacteroides* and *Fusobacteria* being the most abundant phyla. Most studies indicate that *H. pylori* has inhibitory effects on the colonization of other bacteria, harboring a lower diversity of them in the stomach. When comparing the healthy with the diseased stomach, there is a change in the composition of the gastric microbiome with increasing abundance of *H. pylori* (where present) in the gastritis stage, while as the gastric carcinogenesis cascade progresses to gastric cancer, the oral and intestinal-type

pathogenic microbial strains predominate. *Hp*-I creates a premalignant environment of atrophy and intestinal metaplasia and the subsequent alteration in gastric microbiota seems to play a crucial role in gastric tumorigenesis itself. Successful *H. pylori* eradication is suggested to restore gastric microbiota, at least in primary stages. It is more than clear that *Hp*-I, gastric microbiota and gastric cancer constitute a challenging tangle and the strong interaction between them makes it difficult to unroll. Future studies are considered of crucial importance to test the complex interaction on the modulation of the gastric microbiota by *H. pylori* as well as on the relationships between the gastric microbiota and gastric carcinogenesis.

Key Words: *Helicobacter pylori* infection; Gastric microbiota; Gastric cancer; Oncogenesis; Dysbiosis; *Helicobacter pylori* eradication

Core Tip: Gastric adenocarcinoma is a leading cause of cancer-related death in the world. Chronic gastric infection caused by *Helicobacter pylori* (*H. pylori*) is the strongest identified risk factor for gastric adenocarcinoma, prompting the World Health Organization to classify it as a class I carcinogen. It has been shown that in *H. pylori*-colonized patients, this pathogen accounts for more than 90% of all gastric microbiota modifying healthy microbiota and reducing its overall diversity. In this review, we tackle the complicated relationship between *H. pylori*, gastric microbiota and gastric cancer in an effort to unroll this tangle.

Citation: Liatsos C, Papaefthymiou A, Kyriakos N, Galanopoulos M, Doulberis M, Giakoumis M, Petridou E, Mavrogiannis C, Rokkas T, Kountouras J. *Helicobacter pylori*, gastric microbiota and gastric cancer relationship: Unrolling the tangle. *World J Gastrointest Oncol* 2022; 14(5): 959-972
URL: https://www.wjgnet.com/1948-5204/full/v14/i5/959.htm
DOI: https://dx.doi.org/10.4251/wjgo.v14.i5.959

INTRODUCTION

Gastric cancer (GC) has been recognized as a global health concern; it is still the fifth most frequent global malignancy and one of the main causes of cancer-related death[1]. Likewise, *Helicobacter pylori* infection (*Hp*-I), an important public health burden affecting more than half of the global population[2], is related with the majority of GC, with an estimate between 74.7% to more than 90% of the new non-cardia GC cases[1,3].

Regarding the interaction between *Hp*-I and GC, relevant mechanisms known for many years have been studied and are constantly being enriched with new data (Figure 1)[4-17]. In this regard, arising evidence indicates that *Helicobacter pylori* (*H. pylori*), as the most important member of abnormal gastric microbiota (GM), might induce gastric microbiome modifications[11] thereby possibly leading to gastric oncogenesis. The gastric flora may be involved in the *H. pylori*-related oncogenicity, and the variations in the GM composition of patients with GC, intestinal metaplasia (IM) and chronic gastritis are defined [18]. For instance, *Campylobacter* is among the most influential genera in *H. pylori*-associated atrophic gastritis and gastric atrophy-induced alterations of the GM, namely gastric dysbiosis, might contribute to gastric tumorigenic effect[1]. Moreover, *H. pylori*-related metabolic syndrome induces dysbiosis of gastrointestinal tract (GIT) microbiota, thereby contributing to lower and upper GIT carcinogenesis including GC[19-21]. However, the interaction between the host, microbiota and *H. pylori* in the pathogenesis of GC still has to be fully elucidated[22].

Based on recent data, this review attempts to unroll the tangle regarding the interaction between *Hp*-I, GM and GC.

GASTRIC MICROBIOTA COMPOSITION

The GIT (mainly intestine) is colonized by 1-4 × 10^{15} microorganisms, co-existing in a balanced relationship[22]; the GIT microbiota is estimated to be up to 2 kg and affects health and disease[23]. The majority of the bacteria found in the adults' gut consists of *Bacteroides and Parabacteroides*[23]. The anaerobic environment of intestinal lumen does not facilitate aerobic pathogens colonization and development under normal conditions, though anaerobic and facultative pathogenic species can invade it and promote diseases. Each site of the GIT has a unique distribution of microflora; when compared

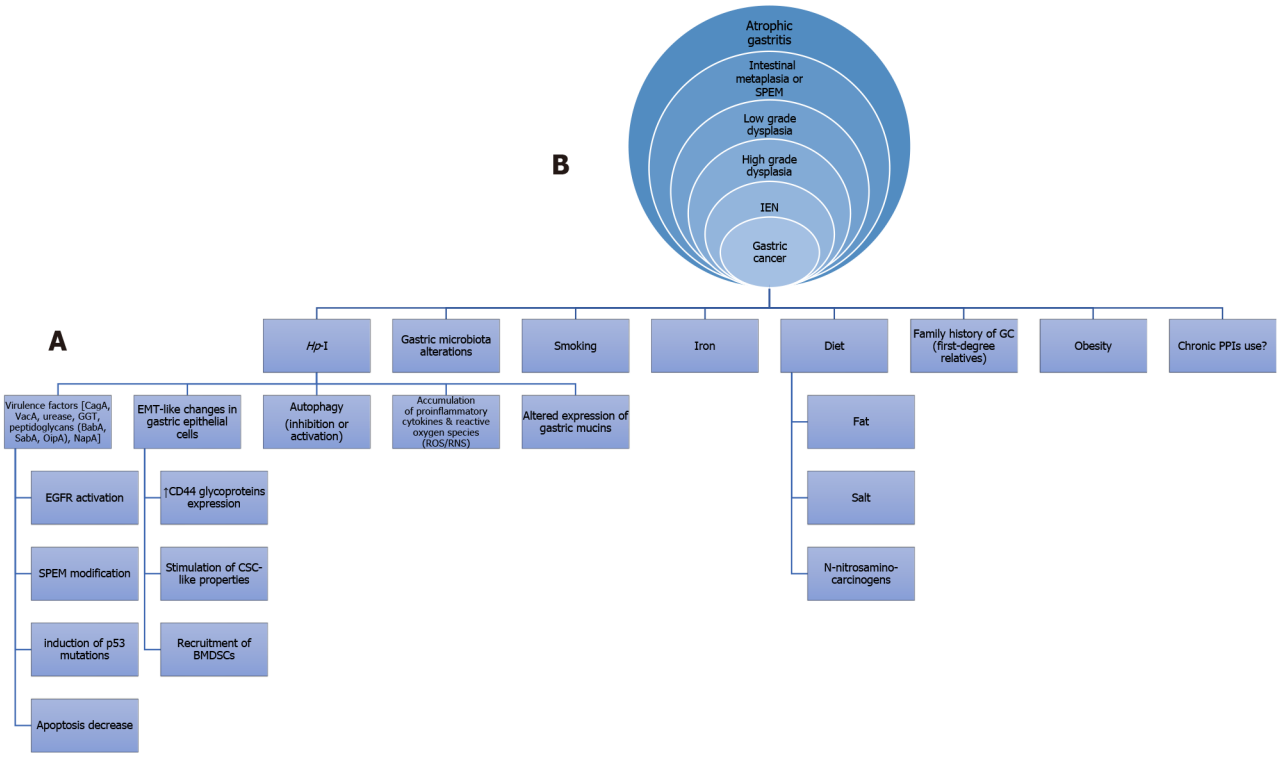

DOI: 10.4251/wjgo.v14.i5.959

Figure 1 Possible mechanisms involved (A) in the etiology of non-cardiac gastric cancer (intestinal type) resulting in the classical cascade of Correa histopathological precancerous lesions (B) as seen in an upper gastrointestinal endoscopy. *Hp*-I: *Helicobacter pylori* infection; GC: Gastric cancer; PPIs: Proton pump inhibitors; CagA: Cytotoxin-associated gene A; VacA: Vacuolating cytotoxin A; GGT: γ-glutamyl transpeptidase; BabA: Blood-group-antigen-binding adhesin; SabA: Sialic acid-binding adhesin; OipA: Outer inflammatory protein; NapA: Neutrophil activation protein A; EMT: Epithelial-mesenchymal transition; ROS/RNS: Reactive oxygen species/Reactive nitrogen species; EGFR: Epidermal growth factor receptor; SPEM: Spasmolytic polypeptide-expressing metaplasia; CSC: Cancer stem cell; BMDSCs: Bone marrow-derived stem cells; IEN: Intraepithelial neoplasia.

with the stomach and duodenum, bacteria density increases in the jejunum/ileum and colon. To yield the optimal conditions for their common interaction and survival, host and microbes have developed specific mechanisms; the disruption of those mechanisms triggers an imbalance in microbial species abundance, termed dysbiosis, which is incriminated for gut barrier dysfunction and induction of inflammatory response. In this regard, the failure to regulate the composition (microbial diversity), probably occurs during the beginning and course of several diseases including malignancies, such as GC[24].

Until recently, the gastric environment was considered as sterile, probably due to increased acidity, and the microbiota was believed to be isolated in the small intestine and colon. Subsequently, identifying *H. pylori* focused the attention on the gastric microbiota as "an ecological niche for bacteria" [23]. Emerging data have revealed that there is a broad range of microorganisms in the stomach with a density of 10^1 to 10^3 colony forming units/g[25,26]. Gastric microbiome is composed of bacteria ingested mainly through the ororespiratory tract and secondary from the intestine by transpyloric biliary reflux [27,28]. Most of those microorganisms cannot resist indigenous gastric defensive mechanisms and there are data indicating which microorganisms permanently colonize the gastric mucosa, other than *H. pylori*. Relative reports suggested that the predominant phyla in the gastric mucosa consist of *Streptococcus, Rothia, Lactobacillus, Veillonella, Prevotella, Neisseria* and *Hemophilus*, counting more than one hundred sorts[28,18]. Specifically, *H. pylori*, represents the most important member of the GM family with the highest relative abundance. Additional GM includes *Proteobacteria, Firmicutes, Actinobacteria, Bacteroidetes* and *Fusobacteria* being the 5 most abundant phyla[18], in children and adults[29]. In culture-based studies where cultures of gastric juice or mucosa biopsies were examined, numerous members of the *Firmicutes, Proteobacteria, Actinobacteria* and *Fusobacteria* phyla were identified, while yeasts were recognized in a relatively low abundance[30,31]. Laboratory molecular techniques with high sensitivity indicated that *Streptococcus, Prevotella, Neisseria, Veillonella* and *Rothia* represent the main bacterial populations in the gastric tissue, with Streptococcus being the most dominant genus[32-36]. Sung *et al* [37] revealed heterogeneity in the flora of gastric fluid and mucosa. Gastric mucosa has a greater flora richness while gastric juice has a greater flora diversity[37]. The presence of bacteria in gastric juice could be just transient as a result of their ingestion with food, drinks or saliva without colonizing the gastric mucosa so they create a fictional image of the real diversity[18].

More specifically, Bik *et al*[36] by introducing a small subunit 16S rDNA clone library approach, described a diverse population of 128 phylotypes (totally 1833 bacterial isolates obtained from gastric

biopsies of 23 healthy adults) within gastric mucosal samples with the majority of bacteria belonging to the five abovementioned major groups- *Proteobacteria, Firmicutes, Actinobacteria, Bacteroidetes* and *Fusobacteria* phyla[36]. A lot of similar studies confirmed the presence and proportion of these phyla[4, 38-41]. Table 1 shows the taxonomy of most prevalent GM at phylum and genus level.

IMPACT OF *HP*-I ON GASTRIC MICROBIOTA COMPOSITION

Regarding *Hp*-I, its impact on the GM remains to be clarified. While Bik *et al*[36] did not depict an impact of the occurrence of *H. pylori* in gastric biopsies on the composition of GM, several subsequent studies characterize *H. pylori* as the regulator of the GM community. Andersson *et al*[42] revealed that *H. pylori* was the dominant bacterium whenever isolated, though its absence was associated with a diverse microbiota. Analytically, in samples from *H. pylori*(+) individuals, *H. pylori* was the mainstay species (ninety percent) of the samples examined by 454 pyro-sequencing. Thirty-three phylotypes were recognized solely, 229 less when compared with *H. pylori*(-) individuals[42]. The abovementioned signifies that *H. pylori* has inhibitory effects on the colonization of other bacteria harboring a significantly lower diversity of them in the stomach. The GM in *H. pylori* negative patients was mainly dominated by the same phyla, though with diverse percent abundances: 52.6% *Proteobacteria,* 26.4% *Firmicutes,* 12% *Bacteroidetes* and 6.4% *Actinobacteria*[43]. The common genera observed in *H. pylori* negative individuals included *Gemella, Prevotella* and *Streptococcus*[42].

In another study which introduced DNA microarrays to characterize the GM in 12 corpus biopsy samples (eight *H. pylori* positive), Maldonado-Contreras *et al*[44] isolated 44 phyla with four dominant *Proteobacteria, Firmicutes, Actinobacteria,* and *Bacteroidetes. Hp*-I augmented the relative abundance of non-*H. pylori*—*Proteobacteria, Spirochaetes,* and *Acidobacteria* whereas lessening the relative abundance of *Actinobacteria, Bacteroidetes* and *Firmicutes,* compared to uninfected stomachs[44]. An additional study from Mongolia showed that patients infected with *H. pylori* exhibited a significantly lesser bacterial richness and Shannon and Simpson indices[45,46] compared with *H. pylori* negative arms. Moreover, enrichment of *Firmicutes, Fusobacteria, Bacteroidetes* and *Actinobacteria* at phylum level was shown in patients with *H. pylori* negative gastritis by the linear discriminant analysis effect size analysis[47].

Miao *et al*[48] studied the effect of *H. pylori* eradication in microbiota composition and found that GM profiles between *H. pylori* negative groups and previously *H. pylori* positive groups four months after successful eradication therapy were almost the same[48].

Table 2 shows the relative abundance of GM at phylum level among *H. pylori* positive and *H. pylori* negative patient groups. In particular, we present the minimum and the maximum values across the studies[36,42,43,47,48]. Also, we calculated the pooled percentages and the relative 95% confidence intervals. Among *H. pylori* positive patient groups, proteobacteria were more frequent, while among *H. pylori* negative patient groups, firmicutes and proteobacteria were more frequent.

IMPACT OF FACTORS ON GASTRIC MICROBIOTA COMPOSITION BEYOND *HP*-I

Beyond *H. pylori*, the composition of GM could be modified by some other factors such as dietary habits, age, ethnicity, medication use and severity of gastric mucosa inflammation[18,27,49-53].

Proton pump inhibitor (PPI) raises the pH in the stomach thereby altering the GM. Likewise, PPIs-driven gastric hypo-chlorhydria can cause substantial changes in gut microbiota composition[54,55]. Two possible mechanisms by which the mentioned PPIs can influence the GM composition have been proposed: (1) By targeting directly bacterial and fungal proton pumps; and (2) By disturbing the natural gastric microenvironment through the gastric pH alkalization[56]. More specifically, GM of patients on PPIs therapy has more abundant bacteria compared to patients on H2RAs and untreated control. The composition of microbiota was quite similar to that of oropharyngeal or fecal bacteria[26]. Paroni Sterbini *et al*[57] showed a significant increase in the relative abundance of *Streptococcus* in patients taking PPIs irrespective of *H. pylori* status; they revealed that *Streptococcus* can be an independent indicator of the gastric microbiome changes in dyspeptic patients secondary to the use of PPIs[57]. On the other hand, Parsons *et al*[40] by using 16S rRNA sequencing in gastric samples, showed that patients receiving PPIs had relatively few changes in the GM compared to healthy controls[39]. Besides, numerous reports indicated that the *H. pylori* moving from the antrum to body and fundus of the stomach is recorded particularly by long-term PPIs usage[58]. Thus, *Hp*-I eradication is proposed for patients who received long-term PPI usage in order to prevent the proinflammatory trigger and thereby decreasing GC potential. Antibiotic ingestion also effects gastrointestinal microflora. Mason *et al*[59] revealed that treatment with cefoperazone caused changes in GM with an overgrowth of *Enterococci* and a decrease of *Lactobacilli*[59].

Attempting to correlate gastric mucosal inflammation with GM, a rise in *Streptococcus* and a reduction in *Prevotella* was found in patients with atrophic gastritis *vs* healthy subjects[36]. Patients with autoimmune atrophic gastritis exhibited a larger concentration of *Firmicutes* than patients with chronic atrophic gastritis (CAG) and a greater variety of microbial species than *H. pylori*-induced atrophic

Table 1 Taxonomy of the most prevalent gastric microbiota at phylum and genus level

Phylum	Genus
Proteobacteria	*Helicobacter*, *Enterobacteriaceae* unknown, *Acinetobacter*, *Pseudomonas*, *Haemophilus*, *Agrobacterium*, *Halomonas*, *Shewanella*, *Sphingomonas*, *Methylobacterium*, *Aquabacterium*
Bacteroidetes	*Prevotella*, *Chryseobacterium*
Firmicutes	*Streptococcus*, *Clostridium*, *Lactobacillus*, *Staphylococcus*, *Faecalibacterium*, *Veillonella*, *Bacillus*, *Peptostreptococcus*, *Selenomonas*, *Phascolarctobacterium*, *Gemella*, *Roseburia*, *Megamonas*, *Gemmiger*, *Lactococcus*, *Granulicatera*, *Dialister*, *Alcaliphylus*, *Ruminococcus*, *Blautia*
Fusobacteria	*Fusobacterium*, *Leptotrichia*
Actinobacteria	*Propionobacterium*, *Corynebacterium*, *Arthrobacter*
Sprirochaetes	*Bacteroides*
Acidobacteria	*Streptophyta*, *Sphingobacterium*, *Pedobacter*

Table 2 Relative abundance of gastric microbiota at phylum level among *Helicobacter pylori* positive and *Helicobacter pylori* negative patient groups

Phylum	*H. pylori*-positive			*H. pylori*-negative		
	Minimum	Maximum	Pooled (95%CI)	Minimum	Maximum	Pooled (95%CI)
Proteobacteria	68.7	96.7	88.4 (75.4-95.9)	10.8	52.6	27.9 (12.7-43.9)
Bacteroeidetes	0.8	8.3	3.1 (1.1-6.0)	11.1	30.0	20.8 (12.7-28)
Firmicutes	1.3	14.7	6.2 (1.8-12.9)	16.3	29.9	31.1 (20.5-40.1)
Fusobacteria	0.1	1.6	1.1 (0.2-2.3)	1.1	6.1	3.5 (1.6-6.1)
Actinobacteria	0.2	3.1	1.2 (0.4-2.5)	2.8	46.8	16.7 (2.4-37.2)

Values are expressed as percentages. CI: Confidence interval; *H. pylori*: *Helicobacter pylori*.

gastritis. This might be due to the differences in gastric acidity between the two conditions or additional factors such as their different immune profiles[39]. Researchers from Mexico obtained gastric tissue from patients with non-atrophic gastritis (NAG), IM and intestinal type GC through extraction of DNA for microbiota analyses using microarray methods and showed that bacterial diversity steadily decreased from NAG to IM to GC[59].

THE INTERACTION BETWEEN GASTRIC MICROBIOTA AND GASTRIC CANCER

The existence of multiple homeostasis mechanisms that take place in the human stomach is a well-recognized phenomenon contributing to health maintenance by balancing the interaction between host gastric microbial diversity and mucosa-related factors[60,61]. When this balance is interrupted, a cascade of events occurs resulting in the emergence of inflammatory changes, dysbiosis and consequently, diseases including GC[36].

The mentioned hypochlorhydria appears to promote a decrease in microbial heterogeneity as well as the development of microorganisms which exhibit genotoxic changes, and raising the ratio of nitrate to nitrite reductase microbe capacities implicated in gastric oncogenesis. Furthermore, the bacterial balance differentiates by raising the stomach pH, giving growth mostly of oral bacteria, such as *Streptococcus anginosus, Peptostreptococcus stomatis, Slackia exigua and Parvimonas micra* as well as *Dialister pneumosintes*. Such bacteria might play a role in GC progression *via* the induction of various metabolic pathways[62]. Thus, to improve the understanding of the influence of promoting the survival and spread of potentially genotoxic bacteria in the stomach and other GIT locations, it will be critical to describe the properties of the mentioned PPIs in GM composition. Nevertheless, no consensus exists regarding the role of PPIs in GC development. Based on a number of metanalyses and studies, there is an increased GC risk in patients using PPIs for a long time period[63] (approximately 2.4 times more than non-users), despite *H. pylori* eradication[4,64,65].

Hp-I is a precise paradigm of the GM homeostasis disturbance sequelae[66]. The *H. pylori*-related inflammatory effects primarily act on the mucosal surface of the stomach variably affecting the production of mucin[67]. Differentiations of the latter seem to play a crucial role regarding the gastric carcinogenesis pathway[9]. Nevertheless, it should be stated that studies on the *H. pylori*-related mucin

production changes have not yet been able to sort out whether this GC sequelae results in dysbiosis in the stomach or, conversely, to microbial diversity. These effects could be the backbone of GC development, given the fact that at the last stage of gastric malignancy oral or intestinal-type bacteria are predominantly discovered, something not seen in premalignant conditions (chronic gastritis, atrophy and IM) where *H. pylori* abundancy is more than clear. Whether this phenomenon is due to tumor-related mucin type differentiation, possibly resulting in GC-related microbiota must be elucidated[68].

As already stated, earlier studies have shown that *H. pylori* negative individuals exhibit a significant variability in microbiota composition which mainly consists of P*roteobacteria, Firmicutes, Actinobacteria, Bacteroidetes* and *Fusobacteria*. On the contrary, the stomach of *H. pylori* positive patients is almost exclusively colonized by this infectious pathogen[42]. In line with this observation, it should be highlighted that from a specific point and beyond, the GC progress seems not to be related with *H. pylori* presence, since the gastric adenocarcinoma microbiota mainly consists of intestinal and oral bacterial genera, and in addition this progression can happen even after successful *H. pylori* treatment (Figure 2)[67]. Similar findings emerged from the study by Yu *et al*[27] who investigated 160 individuals with gastric malignancy residing in China and Mexico. They showed that in the non-cancerous gastric regions, the *H. pylori* presence was significantly high in contrast to the GC site with depletion even in the absence of *H. pylori*. The difference in microbiota diversity that patients with advanced malignant lesions exhibited was further verified in many studies which revealed a marked presence of *Lactobacillus, Streptococcaceae, Staphylococcus, Clostridium* and *Fusobacterium* among others, underlying the crucial role those intestinal microbes play[63,69]. Lastly, Robinson *et al*[70] showed, after utilizing an advanced computer-based search algorithm, that GC was the second most diversely abundant neoplasm in terms of bacterial DNA molecules with dominant species highly comprising *Pseudomonas* and not *H. pylori*.

The above studies and their subsequent findings have been verified to an accountable level by well-designed animal model experiments, especially in C57BL/6 mice, where their stomach microbiota consisted of similar bacteria categories to those found in humans, namely *Firmicutes, Bacteroidetes, Proteobacteria* and *Actinobacteria*[71]. For instance, according to Lofgren *et al*[72], the *H. pylori*-related gastritis not only resulted in decreased GM variety (as seen in human individuals), but also significantly extended the interval to gastric malignancy emergence, especially when the only pathogen was *H. pylori* . The above interesting outcome was confirmed by the study of Lertpiriyapong *et al*[73], who showed that by adding even a small number of intestinal commensal pathogens to monocolonized by *H. pylori* germ-free insulin-gastrin (INS-GAS) transgenic mouse models' stomach there was a progressive advancement to gastric neoplastic lesions.

Viewing the aforementioned data, while a role for *H. pylori* in gastric oncogenesis cannot be doubted, emerging data shows that additional bacteria in the GM also seem to be involved in the transformation of stomach epithelial cells[74]. Nevertheless, whether it is the *Hp*-I that stimulates growth of unwanted bacteria or *vice versa* warrants clarification.

In a survey, Jo *et al*[75] showed that in GC patients, the records of nitrosating/nitrate-reducing microbes other than *H. pylori* were no less than doubled in comparison with healthy controls exhibiting similar *H. pylori* status, albeit insignificantly. Thus, further basic research is necessary to illuminate whether GM alterations are crucial to GC development or are the result of alterations in the gastric setting.

Microbial infections have been incriminated for a variety of cancers by transforming host cells and triggering neoplastic characters and inflammatory reactions, disrupting cell configuration and altering their genoms. Therefore, it is rational to consider the possible role of the intestinal microbiota in gastric oncogenesis[76]. Furthermore, under the consideration that *H. pylori* plays a dominant role in Correa's cascade (*i.e.*, from NAG to atrophic gastritis and further to IM, dysplasia and GC), the inflammatory process of gastritis could be considered to be started and continued by *Hp*-I, which can colonize epithelium decades before neoplastic transformation. Ultimately, this transformation could develop owing to augmented pH of the stomach because of the loss of parietal cells and the multiplication of microbes other than *H. pylori*[18]. Certainly, the microbiota differs between patients with chronic gastritis, IM and GC. The later indicates the significant role of gut microbiota in *H. pylori*-related tumorigenic effect. In contrast, progressive alterations in gastric pH could also be anticipated through *H. pylori*-derived histological alterations, facilitating the gastric colonization from other bacteria[18]. Other investigators showed that the GC microbiota mainly included *Citrobacter*, *Achromobacter, Clostridium*, *Lactobacillus*, *Phyllobacterium* and *Rhodococcs*. Nevertheless, additional research is warranted to clarify the fingerprint of bacterial populations associated with gastric disorders in connection with the Correa's cascade sequence.

Currently, the comprehension of dysbiosis-related genotoxicity and inflammation needs to move from descriptive studies to functionally based studies which investigate the effects of specific taxa and bacteria-derived metabolites on the gastric mucosa. In this regard, the potential introduction of probiotics should be studied thoroughly in order to delineate its effectiveness in the rebalance of human microbiota synthesis[77].

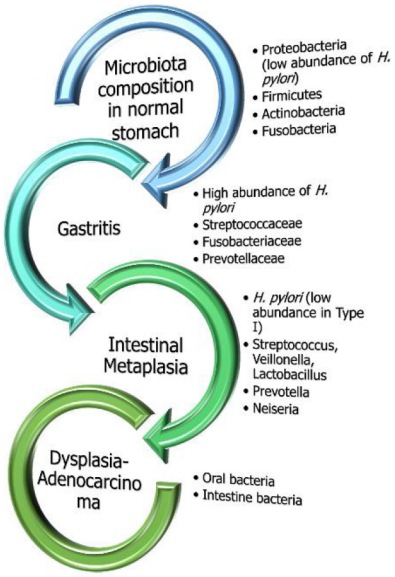

DOI: 10.4251/wjgo.v14.i5.959

Figure 2 Gastric microbial composition in the healthy and diseased stomach. Under normal healthy conditions without evidence of excessive inflammation, *Helicobacter pylori* (*H. pylori*) exists in very low abundance. On the contrary, in chronic gastritis, *H. pylori* is the predominant bacteria with the presence of other microorganisms as well but at lower rates. However, as the sequalae of carcinogenesis moves towards malignancy, oral or intestinal-type pathogens exclusively predominate.

INTERACTION BETWEEN *HP*-I, GASTRIC MICROBIOTA AND GASTRIC CANCER

The perpetuation of *Hp*-I reduces microbiota diversity and is connected with atrophy, IM and GC[78]. Although it represents the main genus in chronic gastritis with a mean relative abundance of 42% (varying from 0.01%-95%), *H. pylori* presents a dramatic decrease in GC tissues with a relative abundance of 6%. In this regard, recent data based on RNA sequencing analyses revealed that *H. pylori* entirely dominated the microbiota not only in infected patients but also in the majority of individuals categorized as *H. pylori*-uninfected using conventional approaches, thus implying an active role in all cases of GC development[78].

The vast majority of information regarding the role of GM in carcinogenesis derives from preclinical studies in INS-GAS transgenic mouse models. Complex microbiota has been associated with intensive gastric inflammation, epithelial damage, oxyntic gland atrophy, hyperplasia, metaplasia and dysplasia [71]. Moreover, co-infection with *H. pylori* in INS-GAS rodents predisposed to more severe gastric lesions and earlier development of early GC in comparison to *H. pylori*-infected germ-free INS-GAS mice[71]. Concerning the co-infective bacteria, complex microbiota and restricted microbiota consisting of only three species of commensal murine bacteria (*Clostridium sp*., *Lactobacillus murinus* and *Bacteroides sp*.) predisposed similarly to neoplasia generation in *H. pylori* positive models[73]. Further *in vivo* studies with *Hp*-I revealed that the co-infection with commensal microbiota accelerated the progression to gastric intraepithelial neoplasia and the progression to cancer, whereas the treatment with antibiotics delayed the gastric tumorigenesis in *H. pylori*-free and specific pathogen-free INS-GAS mice[73,79,80]. Moreover, the environment of gastric atrophy reduces the density of *H. pylori* aggregates to give rise to bacteria from other locations of the GIT, thus perpetuating the inflammatory process and genotoxicity, to induce malignant transformation. The overgrowth of such microbiome could partially contribute to the "point of no return" of carcinogenesis prevention after *H. pylori* eradication[81]. As already known, eradication of *H. pylori* is associated with a reduced risk of GC, although ambiguity exists over whether this is an isolated result from the eradication of the *H. pylori* or the modification of the whole GM, as bacterial diversity increases probably beneficially[80].

Interestingly, Eun *et al*[82] reported variations in the composition and diversity of GM among patients with chronic gastritis, IM and GC. More specifically, in the early stages of carcinogenesis, *H. pylori* may trigger the development of CAG, rather than direct induction of GC[82]. Subsequently, the resulting increased pH provokes changes in the constitution of GM thus facilitating the progression from CAG to IM and finally to GC[83]. On the other hand, subjects with GC showed a significant increase in the *Bacilli* class and *Streptococacceae* family whereas the *Epsilonproteobacteria* class and *Helicobacteriaceae* family were decreased[82]. As suggested by Correa *et al*[84], chronic *Hp*-I triggers a CAG with the mentioned defective acid secretion, thus facilitating the excessive colonization of gastric microflora with bacteria capable of reducing nitrate to nitrite, to form N-nitroso compounds that are carcinogenic[84,85]. In this regard, the GC microbiome is different from atrophic gastritis and possesses increased representation of nitrate reductases, with *Citrobacter, Achromobacter, Clostridium, Campylobacter,*

Deinococcus, Sulfurospirillum and *Phyllobacterium* representing ascendant species[79], thus accelerating the development of GC following *Hp*-I in INS-GAS mice when compared to germ-free mice that were monocolonized by *H. pylori*[71]. Relatively, chronic treatment with the mentioned PPIs increases the potential of atrophy among *H. pylori* positive subjects[86] in contrast to *H. pylori* negative individuals or patients receiving eradication treatment thus implying that the non-*H. pylori* microbiota could only promote gastric atrophy when co-existing with *H. pylori*[35,87].

The activity of gastritis is well known for its close relationship with *Hp*-I. A similar motif of diversity is suggested for further phyla, such as *Bacteroidetes* and increased abundances of *Firmicutes* or *Proteobacteria*, thus incriminating their dysbiosis for gastric carcinogenesis[87]. Nevertheless, despite the wide range of studies associating *Hp*-I with gastric dysbiosis, no data interpret the exact background of this interaction which seems to promote a sustained inflammation and genotoxicity[88]. A widely acceptable pattern suggests that chronic gastric inflammatory response to *H. pylori* may modify the gastric environment, paving the way to the growth of a dysbiotic gastric bacterial community; and *H. pylori* eradication reverses the gastric dysbiosis to a similar level to uninfected patients, and exerts beneficial effects on gut microbiota, achieving an increased probiotic and putative downregulation of drug-resistance[89]. More specifically, successful *H. pylori* eradication inhibited dysbiosis significantly ($P < 0.001$), although it remained higher than that of the *H. pylori* negative arm ($P = 0.025$). Nonetheless, treatment failure was associated with increased dysbiosis rate comparable to active *Hp*-I ($P = 0.351$)[89]. Intense dysbiosis was further found to be analogous to the progress from gastritis to atrophy, IM and GC (both $P < 0.001$)[89].

Pathophysiologically, the highly expressed VacA (vacuolating cytotoxin A), after *Hp*-I, binds to the receptor proteins tyrosine phosphatase α and β on gastric cells, thus generating pores to yield bacterial internalization[90]. Some data indicated that antibodies against VacA could be correlated with both peptic ulcer and gastric malignant disorders, thus it could be considered as a biomarker of both pathologies[91]. Additionally, *H. pylori* survival promoted by VacA is independent of CagA (cytotoxin-associated gene A) accumulation. VacA is connected with mucolopin 1 (transient receptor channel) which impedes the death of microbial cells through autophagic procedure and permits the formation of an intracellular niche in which *H. pylori* survives[91]. In this regard, infection of the AGS gastric adenocarcinoma cell line with *H. pylori* for 6 h, lead to autophagy that was dependent on VacA[92]. This implied that autophagy is activated by cells infected by *H. pylori* to evade the destructive effects of toxins thus promoting cell survival. In addition, others reported that 1 d exposure to VacA disturbs the antiphagocytic signaling and accumulates defective autophagosomes in cells[92]. Likewise, *H. pylori* controls the autophagocytic pathway as well as the expression of genes related to autophagy in both macrophages and gastric epithelial cells[93]. Therefore, it appears that during the initiation of carcinogenesis, the aforementioned pathway has a regulatory role and when suppressed, leads to premalignant disorders, induces oxidative stress, promotes cell growth, penetration and eventually metastases. Concerning GC, this could lead to precursor lesions extension[93]. Interestingly, there is a direct association between pathogens that induce dysbiosis and disturbed immune responses including apoptosis - autophagy and orodigestive cancers, including GC[93].

Besides, *H. pylori* releases a plethora of adhesins (BabA, BabB, SabA, AlpA and AlpB) which facilitate the opening of tight junctions (TJ) and adherent junctions (AJ)[94-96]. In this regard, *in vivo* CagA causes depolarization and disruption of the TJ barrier function in epithelial cells to the *H. pylori* attachment sites[7,94]. Additionally, after *in vitro* excessive administration, CagA binds to membrane e-cadherins, inhibits their interaction with β-catenin to disrupt the AJs' integrity and tightness[97]. *In vivo* cagA with *Lactobacillus* enhances the effect of *H. pylori* to human monocyte-derived dendritic cells (DC) leading to DC maturation and induction, beyond *H. pylori*, additional inflammatory mediators[93]. This implies that the bacteria that produce lactic acid could increase *H. pylori* related inflammation promoting gastric oncogenesis. The latter are in concordance with human GM studies displaying a plethora of *Lactobacillus* in *H. pylori*-connected IM and GC (intestinal type) *vs* NAG[62] and the increased *Lactobacillus* in INS-GAS mouse model studies infected with *H. pylori* and reduced commensals (*Clostridium, Lactobacillus,* and *Bacteroides*) which develop gastric intraepithelial neoplasia[73]. Nevertheless, other findings indicate a probiotic *Lactobacillus* strain that inhibits *H. pylori* colonization in a Mongolian gerbil model [98]. More relevant to biofilm-associated *H. pylori, Streptococcus mitis* interacts with *H. pylori* in co-culture studies, converting it to coccoid cells, as proteomic analysis reveals, signifying an apparent impact on gastric oncogenesis linked with *H. pylori*[99,100]. Moreover, experimental data on INS-GAS mice co-colonized with *H. pylori* and *Streptococcus Salivarius* showed more severe gastritis when compared with solely *Hp*-I only at 5 mo post-infection. The latter data signify strong interactions among several bacteria and *H. pylori* that in turn may affect *H. pylori*-related tumorigenesis[101]. Of note, *H. pylori*-induced biofilms are associated with resistance to *H. pylori* antibiotic eradication regimens[102]; *H. pylori* biofilms appear to be one of the main barriers to *H. pylori* eradication, by inhibiting antibiotics penetration and augmenting the expression of efflux pumps and mutations, several therapeutic failures and chronic infections[103].

Finally, the interplay between *H. pylori* and GM in the pathogenesis of GC can be dependent on Toll-like receptors through a perpetual stimulation by *H. pylori* and potentially by other microorganisms [104]. In this regard, *Hp*-I seems to create a premalignant environment of atrophy and IM and the subsequent alterations in GM in later stages play a more relevant role in carcinogenesis itself[105].

CONCLUSION

It is more than clear that *Hp*-I, GM and GC constitute a challenging tangle due to the strong interaction between them making it difficult to unroll it.

The stomach harbors a large and diverse bacterial community with *H. pylori*, a member of Proteobacteria phylum, being the most dominant and abundant genus. The main phyla colonizing the stomach are Proteobacteria, Bacteroidetes, Firmicutes, Fusobacteria and Actinobacteria. Most studies show that *H. pylori* has inhibitory effects on the colonization of other bacteria, harboring a lower diversity of them in the stomach. Other factors that influence GM are dietary habits, age, ethnicity, medication use (PPIs, antibiotics), gastric mucosa inflammation and GC. It is worthwhile to mention that GM differs in patients with chronic gastritis, IM, dysplasia or GC, but its role in GC has not yet been fully elucidated. Data shows that from a specific point and beyond, apart from *H. pylori*-related gastritis, the GC progress seems not to be related with *H. pylori* presence, since the gastric adenocarcinoma microbiota mainly consists of intestinal and oral bacterial genera, considering that this progression can happen even after successful *H. pylori* eradication. The above has been verified to an accountable level by well-designed animal model experiments. In accordance, beyond *H. pylori*'s role in gastric oncogenesis, other bacteria, *H. pylori*-stimulated or not, in GM also seem to be responsible for transformation of gastric epithelial cells.

To conclude, the aforementioned studies amongst others have begun to shed light into the maze of GC complex pathogenesis where abundant data show that beyond *H. pylori* related gastritis, additional pathogens might contribute to this type of cancer development. Nevertheless, large-scale experiments are needed to discern the exact role of different kinds of pathogens which reside in the stomach and their contribution to neoplasia emergence, aiding in the prediction of adverse prognosis of a specific microbiota diversity. Only then would the manipulation of GM be feasible, modifying the number and the types of the necessary commensals.

FOOTNOTES

Author contributions: Liatsos C conceived the idea, provided revisions to the scientific manuscript content and participated in the writing, corrections and completion of all stages of the manuscript; Papaefthymiou A, Kyriakos N, Galanopoulos M, Doulberis M and Giakoumis M participated in manuscript writing and literature data finding; Petridou E contributed to literature data finding and editing; Mavrogiannis C, Rokkas T and Papaefthymiou A provided revisions and editing of the manuscript; Kountouras J participated in the writing, reviewing and final editing of the manuscript.

Conflict-of-interest statement: The authors declare having no conflict of interests for this article.

Country/Territory of origin: Greece

ORCID number: Christos Liatsos 0000-0001-8025-0808; Apostolis Papaefthymiou 0000-0002-3563-4973; Nikolaos Kyriakos 0000-0002-7395-6594; Michail Galanopoulos 0000-0002-7544-2810; Michael Doulberis 0000-0002-0396-5081; Marios Giakoumis 0000-0002-9909-5454; Evangelia Petridou 0000-0002-4926-4408; Christos Mavrogiannis 0000-0001-6163-5884; Theodore Rokkas 0000-0001-6475-3026; Jannis Kountouras 0000-0001-6459-5136.

S-Editor: Chang KL
L-Editor: Filipodia
P-Editor: Chang KL

REFERENCES

1 **Bray F**, Ferlay J, Soerjomataram I, Siegel RL, Torre LA, Jemal A. Global cancer statistics 2018: GLOBOCAN estimates of incidence and mortality worldwide for 36 cancers in 185 countries. *CA Cancer J Clin* 2018; **68**: 394-424 [PMID: 30207593 DOI: 10.3322/caac.21492]

2 **Hooi JKY**, Lai WY, Ng WK, Suen MMY, Underwood FE, Tanyingoh D, Malfertheiner P, Graham DY, Wong VWS, Wu JCY, Chan FKL, Sung JJY, Kaplan GG, Ng SC. Global Prevalence of Helicobacter pylori Infection: Systematic Review and Meta-Analysis. *Gastroenterology* 2017; **153**: 420-429 [PMID: 28456631 DOI: 10.1053/j.gastro.2017.04.022]

3 **de Martel C**, Ferlay J, Franceschi S, Vignat J, Bray F, Forman D, Plummer M. Global burden of cancers attributable to infections in 2008: a review and synthetic analysis. *Lancet Oncol* 2012; **13**: 607-615 [PMID: 22575588 DOI:

10.1016/S1470-2045(12)70137-7]
4 **Cheung KS**, Leung WK. Long-term use of proton-pump inhibitors and risk of gastric cancer: a review of the current evidence. *Therap Adv Gastroenterol* 2019; **12**: 1756284819834511 [PMID: 30886648 DOI: 10.1177/1756284819834511]
5 **Liatsos C**, Rokkas T. The Effect of Chronic Use of Proton Pump Inhibitors on Gastric Cancer: Should We Be Aware of It? *Dig Dis* 2018; **36**: 395-396 [PMID: 29874647 DOI: 10.1159/000489629]
6 **Moss SF**. The Clinical Evidence Linking *Helicobacter pylori* to Gastric Cancer. *Cell Mol Gastroenterol Hepatol* 2017; **3**: 183-191 [PMID: 28275685 DOI: 10.1016/j.jcmgh.2016.12.001]
7 **Amieva MR**, Vogelmann R, Covacci A, Tompkins LS, Nelson WJ, Falkow S. Disruption of the epithelial apical-junctional complex by Helicobacter pylori CagA. *Science* 2003; **300**: 1430-1434 [PMID: 12775840 DOI: 10.1053/j.gastro.2015.09.004]
8 **Kountouras J**, Kapetanakis N, Zavos C, Polyzos SA, Romiopoulos I, Tsiaousi E, Anastasiadou K, Giorgakis N, Vardaka E, Nikolaidou C, Venizelos I, Katsinelos P. Helicobacter pylori might contribute to cancer and/or bone marrow-derived stem cell-related gastrointestinal oncogenesis. *Oncogene* 2015; **34**: 670 [PMID: 24469039 DOI: 10.1038/onc.2013.602]
9 **Babu SD**, Jayanthi V, Devaraj N, Reis CA, Devaraj H. Expression profile of mucins (MUC2, MUC5AC and MUC6) in Helicobacter pylori infected pre-neoplastic and neoplastic human gastric epithelium. *Mol Cancer* 2006; **5**: 10 [PMID: 16545139 DOI: 10.1186/1476-4598-5-10]
10 **Kountouras J**, Doulberis M, Papaefthymiou A, Polyzos SA, Vardaka E, Tzivras D, Dardiotis E, Deretzi G, Giartza-Taxidou E, Grigoriadis S, Katsinelos P. A perspective on risk factors for esophageal adenocarcinoma: emphasis on Helicobacter pylori infection. *Ann N Y Acad Sci* 2019; **1452**: 12-17 [PMID: 31310338 DOI: 10.1111/nyas.14168]
11 **Zhang S**, Shi D, Li M, Li Y, Wang X, Li W. The relationship between gastric microbiota and gastric disease. *Scand J Gastroenterol* 2019; **54**: 391-396 [PMID: 30945954 DOI: 10.1080/00365521.2019.1591499]
12 **Burkitt MD**, Duckworth CA, Williams JM, Pritchard DM. Helicobacter pylori-induced gastric pathology: insights from *in vivo* and *ex vivo* models. *Dis Model Mech* 2017; **10**: 89-104 [PMID: 28151409 DOI: 10.1242/dmm.027649]
13 **Yuan G**, Chen Y, He S. Family History of Gastric Cancer and Helicobacter pylori Treatment. *N Engl J Med* 2020; **382**: 2171 [PMID: 32459942 DOI: 10.1056/NEJMc2003542]
14 **Chooi YC**, Ding C, Magkos F. The epidemiology of obesity. *Metabolism* 2019; **92**: 6-10 [PMID: 30253139 DOI: 10.1016/j.metabol.2018.09.005]
15 **Choi IJ**, Kim CG, Lee JY, Kim YI, Kook MC, Park B, Joo J. Family History of Gastric Cancer and *Helicobacter pylori* Treatment. *N Engl J Med* 2020; **382**: 427-436 [PMID: 31995688 DOI: 10.1056/NEJMoa1909666]
16 **Choi IJ**, Kook MC, Kim YI, Cho SJ, Lee JY, Kim CG, Park B, Nam BH. Helicobacter pylori Therapy for the Prevention of Metachronous Gastric Cancer. *N Engl J Med* 2018; **378**: 1085-1095 [PMID: 29562147 DOI: 10.1056/NEJMoa1708423]
17 **Díaz P**, Valenzuela Valderrama M, Bravo J, Quest AFG. *Helicobacter pylori* and Gastric Cancer: Adaptive Cellular Mechanisms Involved in Disease Progression. *Front Microbiol* 2018; **9**: 5 [PMID: 29403459 DOI: 10.3389/fmicb.2018.00005]
18 **Alarcón T**, Llorca L, Perez-Perez G. Impact of the Microbiota and Gastric Disease Development by Helicobacter pylori. *Curr Top Microbiol Immunol* 2017; **400**: 253-275 [PMID: 28124157 DOI: 10.1007/978-3-319-50520-6_11]
19 **Kountouras J**, Boziki M, Polyzos SA, Katsinelos P, Gavalas E, Zeglinas C, Tzivras D, Romiopoulos I, Giorgakis N, Anastasiadou K, Vardaka E, Kountouras C, Kazakos E, Giartza-Taxidou E, Deretzi G, Dardiotis E, Kotronis G, Doulberis M. The Emerging Role of Helicobacter Pylori-Induced Metabolic Gastrointestinal Dysmotility and Neurodegeneration. *Curr Mol Med* 2017; **17**: 389-404 [PMID: 29256351 DOI: 10.2174/1566524018666171219094837]
20 **Kountouras J**, Polyzos SA, Doulberis M, Zeglinas C, Artemaki F, Vardaka E, Deretzi G, Giartza-Taxidou E, Tzivras D, Vlachaki E, Kazakos E, Katsinelos P, Mantzoros CS. Potential impact of Helicobacter pylori-related metabolic syndrome on upper and lower gastrointestinal tract oncogenesis. *Metabolism* 2018; **87**: 18-24 [PMID: 29936174 DOI: 10.1016/j.metabol.2018.06.008]
21 **Saetang J**, Sangkhathat S. Diets link metabolic syndrome and colorectal cancer development (Review). *Oncol Rep* 2017; **37**: 1312-1320 [PMID: 28098913 DOI: 10.3892/or.2017.5385]
22 **Schulz C**, Koch N, Schütte K, Pieper DH, Malfertheiner P. H. pylori and its modulation of gastrointestinal microbiota. *J Dig Dis* 2015; **16**: 109-117 [PMID: 25624012 DOI: 10.1111/1751-2980.12233]
23 **Sgambato D**, Miranda A, Romano L, Romano M. Gut microbiota and gastric disease. *Minerva Gastroenterol Dietol* 2017; **63**: 345-354 [PMID: 28206729 DOI: 10.23736/S1121-421X.17.02380-7]
24 **Wang L**, Peng F, Peng C, Du JR. Gut Microbiota in Tumor Microenvironment: A Critical Regulator in Cancer Initiation and Development as Potential Targets for Chinese Medicine. *Am J Chin Med* 2021; **49**: 609-626 [PMID: 33683187 DOI: 10.1142/S0192415X21500270]
25 **Sheh A**, Fox JG. The role of the gastrointestinal microbiome in Helicobacter pylori pathogenesis. *Gut Microbes* 2013; **4**: 505-531 [PMID: 23962822 DOI: 10.4161/gmic.26205]
26 **Wroblewski LE**, Peek RM Jr, Wilson KT. Helicobacter pylori and gastric cancer: factors that modulate disease risk. *Clin Microbiol Rev* 2010; **23**: 713-739 [PMID: 20930071 DOI: 10.1128/CMR.00011-10]
27 **Sanduleanu S**, Jonkers D, De Bruine A, Hameeteman W, Stockbrügger RW. Non-Helicobacter pylori bacterial flora during acid-suppressive therapy: differential findings in gastric juice and gastric mucosa. *Aliment Pharmacol Ther* 2001; **15**: 379-388 [PMID: 11207513 DOI: 10.1046/j.1365-2036.2001.00888.x]
28 **Yu G**, Torres J, Hu N, Medrano-Guzman R, Herrera-Goepfert R, Humphrys MS, Wang L, Wang C, Ding T, Ravel J, Taylor PR, Abnet CC, Goldstein AM. Molecular Characterization of the Human Stomach Microbiota in Gastric Cancer Patients. *Front Cell Infect Microbiol* 2017; **7**: 302 [PMID: 28730144 DOI: 10.3389/fcimb.2017.00302]
29 **Harris PR**, Smythies LE, Smith PD, Perez-Perez GI. Role of childhood infection in the sequelae of H. pylori disease. *Gut Microbes* 2013; **4**: 426-438 [PMID: 24275060 DOI: 10.4161/gmic.26943]
30 **Savage DC**. Microbial ecology of the gastrointestinal tract. *Annu Rev Microbiol* 1977; **31**: 107-133 [PMID: 334036 DOI: 10.1146/annurev.mi.31.100177.000543]
31 **Adamsson I**, Nord CE, Lundquist P, Sjöstedt S, Edlund C. Comparative effects of omeprazole, amoxycillin plus

metronidazole *vs* omeprazole, clarithromycin plus metronidazole on the oral, gastric and intestinal microflora in Helicobacter pylori-infected patients. *J Antimicrob Chemother* 1999; **44**: 629-640 [PMID: 10552979 DOI: 10.1093/jac/44.5.629]

32 **Schulz C**, Schütte K, Malfertheiner P. Helicobacter pylori and Other Gastric Microbiota in Gastroduodenal Pathologies. *Dig Dis* 2016; **34**: 210-216 [PMID: 27028228 DOI: 10.1159/000443353]

33 **Yang I**, Woltemate S, Piazuelo MB, Bravo LE, Yepez MC, Romero-Gallo J, Delgado AG, Wilson KT, Peek RM, Correa P, Josenhans C, Fox JG, Suerbaum S. Different gastric microbiota compositions in two human populations with high and low gastric cancer risk in Colombia. *Sci Rep* 2016; **6**: 18594 [PMID: 26729566 DOI: 10.1038/srep18594]

34 **Hu Y**, He LH, Xiao D, Liu GD, Gu YX, Tao XX, Zhang JZ. Bacterial flora concurrent with Helicobacter pylori in the stomach of patients with upper gastrointestinal diseases. *World J Gastroenterol* 2012; **18**: 1257-1261 [PMID: 22468090 DOI: 10.3748/wjg.v18.i11.1257]

35 **Engstrand L**, Lindberg M. Helicobacter pylori and the gastric microbiota. *Best Pract Res Clin Gastroenterol* 2013; **27**: 39-45 [PMID: 23768551 DOI: 10.1016/j.bpg.2013.03.016]

36 **Bik EM**, Eckburg PB, Gill SR, Nelson KE, Purdom EA, Francois F, Perez-Perez G, Blaser MJ, Relman DA. Molecular analysis of the bacterial microbiota in the human stomach. *Proc Natl Acad Sci U S A* 2006; **103**: 732-737 [PMID: 16407106 DOI: 10.1073/pnas.0506655103]

37 **Sung J**, Kim N, Kim J, Jo HJ, Park JH, Nam RH, Seok YJ, Kim YR, Lee DH, Jung HC. Comparison of Gastric Microbiota Between Gastric Juice and Mucosa by Next Generation Sequencing Method. *J Cancer Prev* 2016; **21**: 60-65 [PMID: 27051651 DOI: 10.15430/JCP.2016.21.1.60]

38 **Zilberstein B**, Quintanilha AG, Santos MA, Pajecki D, Moura EG, Alves PR, Maluf Filho F, de Souza JA, Gama-Rodrigues J. Digestive tract microbiota in healthy volunteers. *Clinics (Sao Paulo)* 2007; **62**: 47-54 [PMID: 17334549 DOI: 10.1590/S1807-59322007000100008]

39 **Katsinelos T**, Doulberis M, Polyzos SA, Papaefthymiou A, Katsinelos P, Kountouras J. Molecular Links Between Alzheimer's Disease and Gastrointestinal Microbiota: Emphasis on Helicobacter pylori Infection Involvement. *Curr Mol Med* 2019; **20**: 3-12 [PMID: 31530263 DOI: 10.2174/1566524019666190917125917]

40 **Parsons BN**, Ijaz UZ, D'Amore R, Burkitt MD, Eccles R, Lenzi L, Duckworth CA, Moore AR, Tiszlavicz L, Varro A, Hall N, Pritchard DM. Comparison of the human gastric microbiota in hypochlorhydric states arising as a result of Helicobacter pylori-induced atrophic gastritis, autoimmune atrophic gastritis and proton pump inhibitor use. *PLoS Pathog* 2017; **13**: e1006653 [PMID: 29095917 DOI: 10.1371/journal.ppat.1006653]

41 **Espinoza JL**, Matsumoto A, Tanaka H, Matsumura I. Gastric microbiota: An emerging player in Helicobacter pylori-induced gastric malignancies. *Cancer Lett* 2018; **414**: 147-152 [PMID: 29138097 DOI: 10.1016/j.canlet.2017.11.009]

42 **Andersson AF**, Lindberg M, Jakobsson H, Bäckhed F, Nyrén P, Engstrand L. Comparative analysis of human gut microbiota by barcoded pyrosequencing. *PLoS One* 2008; **3**: e2836 [PMID: 18665274 DOI: 10.1371/journal.pone.0002836]

43 **Llorca L**, Pérez-Pérez G, Urruzuno P, Martinez MJ, Iizumi T, Gao Z, Sohn J, Chung J, Cox L, Simón-Soro A, Mira A, Alarcón T. Characterization of the Gastric Microbiota in a Pediatric Population According to Helicobacter pylori Status. *Pediatr Infect Dis J* 2017; **36**: 173-178 [PMID: 27820723 DOI: 10.1097/INF.0000000000001383]

44 **Maldonado-Contreras A**, Goldfarb KC, Godoy-Vitorino F, Karaoz U, Contreras M, Blaser MJ, Brodie EL, Dominguez-Bello MG. Structure of the human gastric bacterial community in relation to Helicobacter pylori status. *ISME J* 2011; **5**: 574-579 [PMID: 20927139 DOI: 10.1038/ismej.2010.149]

45 **Shannon CE**. A Mathematical Theory of Communication. *Bell Syst Tech J* 1948; **27**: 379-423 [DOI: 10.1002/j.1538-7305.1948.tb01338.x]

46 **Simpson EH**. Measurement of Diversity. *Nature* 1949; **163**: 688-688 [DOI: 10.1038/163688a0]

47 **Gantuya B**, El-Serag HB, Matsumoto T, Ajami NJ, Oyuntsetseg K, Azzaya D, Uchida T, Yamaoka Y. Gastric Microbiota in Helicobacter pylori-Negative and -Positive Gastritis Among High Incidence of Gastric Cancer Area. *Cancers (Basel)* 2019; 11 [PMID: 30974798 DOI: 10.3390/cancers11040504]

48 **Miao R**, Wan C, Wang Z. The relationship of gastric microbiota and Helicobacter pylori infection in pediatrics population. *Helicobacter* 2020; **25**: e12676 [PMID: 31762120 DOI: 10.1111/hel.12676]

49 **Wroblewski LE**, Peek RM Jr. Helicobacter pylori, Cancer, and the Gastric Microbiota. *Adv Exp Med Biol* 2016; **908**: 393-408 [PMID: 27573782 DOI: 10.1007/978-3-319-41388-4_19]

50 **Chan YK**, Estaki M, Gibson DL. Clinical consequences of diet-induced dysbiosis. *Ann Nutr Metab* 2013; **63** Suppl 2: 28-40 [PMID: 24217034 DOI: 10.1159/000354902]

51 **Fan W**, Huo G, Li X, Yang L, Duan C. Impact of diet in shaping gut microbiota revealed by a comparative study in infants during the six months of life. *J Microbiol Biotechnol* 2014; **24**: 133-143 [PMID: 24169452 DOI: 10.4014/jmb.1309.09029]

52 **Goldsmith JR**, Sartor RB. The role of diet on intestinal microbiota metabolism: downstream impacts on host immune function and health, and therapeutic implications. *J Gastroenterol* 2014; **49**: 785-798 [PMID: 24652102 DOI: 10.1007/s00535-014-0953-z]

53 **David LA**, Maurice CF, Carmody RN, Gootenberg DB, Button JE, Wolfe BE, Ling AV, Devlin AS, Varma Y, Fischbach MA, Biddinger SB, Dutton RJ, Turnbaugh PJ. Diet rapidly and reproducibly alters the human gut microbiome. *Nature* 2014; **505**: 559-563 [PMID: 24336217 DOI: 10.1038/nature12820]

54 **Takagi T**, Naito Y, Inoue R, Kashiwagi S, Uchiyama K, Mizushima K, Tsuchiya S, Okayama T, Dohi O, Yoshida N, Kamada K, Ishikawa T, Handa O, Konishi H, Okuda K, Tsujimoto Y, Ohnogi H, Itoh Y. The influence of long-term use of proton pump inhibitors on the gut microbiota: an age-sex-matched case-control study. *J Clin Biochem Nutr* 2018; **62**: 100-105 [PMID: 29371761 DOI: 10.3164/jcbn.17-78]

55 **Lo WK**, Chan WW. Proton pump inhibitor use and the risk of small intestinal bacterial overgrowth: a meta-analysis. *Clin Gastroenterol Hepatol* 2013; **11**: 483-490 [PMID: 23270866 DOI: 10.1016/j.cgh.2012.12.011]

56 **Vesper BJ**, Jawdi A, Altman KW, Haines GK 3rd, Tao L, Radosevich JA. The effect of proton pump inhibitors on the human microbiota. *Curr Drug Metab* 2009; **10**: 84-89 [PMID: 19149516 DOI: 10.2174/138920009787048392]

57 **Paroni Sterbini F**, Palladini A, Masucci L, Cannistraci CV, Pastorino R, Ianiro G, Bugli F, Martini C, Ricciardi W, Gasbarrini A, Sanguinetti M, Cammarota G, Posteraro B. Effects of Proton Pump Inhibitors on the Gastric Mucosa-Associated Microbiota in Dyspeptic Patients. *Appl Environ Microbiol* 2016; **82**: 6633-6644 [PMID: 27590821 DOI: 10.1128/AEM.01437-16]

58 **Malfertheiner P**, Kandulski A, Venerito M. Proton-pump inhibitors: understanding the complications and risks. *Nat Rev Gastroenterol Hepatol* 2017; **14**: 697-710 [PMID: 28930292 DOI: 10.1038/nrgastro.2017.117]

59 **Mason KL**, Erb Downward JR, Falkowski NR, Young VB, Kao JY, Huffnagle GB. Interplay between the gastric bacterial microbiota and Candida albicans during postantibiotic recolonization and gastritis. *Infect Immun* 2012; **80**: 150-158 [PMID: 21986629 DOI: 10.1128/IAI.05162-11]

60 **Aviles-Jimenez F**, Vazquez-Jimenez F, Medrano-Guzman R, Mantilla A, Torres J. Stomach microbiota composition varies between patients with non-atrophic gastritis and patients with intestinal type of gastric cancer. *Sci Rep* 2014; **4**: 4202 [PMID: 24569566 DOI: 10.1038/srep04202]

61 **Noto JM**, Peek RM Jr. The gastric microbiome, its interaction with Helicobacter pylori, and its potential role in the progression to stomach cancer. *PLoS Pathog* 2017; **13**: e1006573 [PMID: 28982167 DOI: 10.1371/journal.ppat.1006573]

62 **Coker OO**, Dai Z, Nie Y, Zhao G, Cao L, Nakatsu G, Wu WK, Wong SH, Chen Z, Sung JJY, Yu J. Mucosal microbiome dysbiosis in gastric carcinogenesis. *Gut* 2018; **67**: 1024-1032 [PMID: 28765474 DOI: 10.1136/gutjnl-2017-314281]

63 **Brusselaers N**, Wahlin K, Engstrand L, Lagergren J. Maintenance therapy with proton pump inhibitors and risk of gastric cancer: a nationwide population-based cohort study in Sweden. *BMJ Open* 2017; **7**: e017739 [PMID: 29084798 DOI: 10.1136/bmjopen-2017-017739]

64 **Song H**, Zhu J, Lu D. Long-term proton pump inhibitor (PPI) use and the development of gastric pre-malignant lesions. *Cochrane Database Syst Rev* 2014; CD010623 [PMID: 25464111 DOI: 10.1002/14651858.CD010623.pub2]

65 **Eslami L**, Nasseri-Moghaddam S. Meta-analyses: does long-term PPI use increase the risk of gastric premalignant lesions? *Arch Iran Med* 2013; **16**: 449-458 [PMID: 23906249]

66 **Vogiatzi P**, Cassone M, Luzzi I, Lucchetti C, Otvos L Jr, Giordano A. Helicobacter pylori as a class I carcinogen: physiopathology and management strategies. *J Cell Biochem* 2007; **102**: 264-273 [PMID: 17486575 DOI: 10.1002/jcb.21375]

67 **Rajilic-Stojanovic M**, Figueiredo C, Smet A, Hansen R, Kupcinskas J, Rokkas T, Andersen L, Machado JC, Ianiro G, Gasbarrini A, Leja M, Gisbert JP, Hold GL. Systematic review: gastric microbiota in health and disease. *Aliment Pharmacol Ther* 2020; **51**: 582-602 [PMID: 32056247 DOI: 10.1111/apt.15650]

68 **Vogtmann E**, Goedert JJ. Epidemiologic studies of the human microbiome and cancer. *Br J Cancer* 2016; **114**: 237-242 [PMID: 26730578 DOI: 10.1038/bjc.2015.465]

69 **Dicksved J**, Lindberg M, Rosenquist M, Enroth H, Jansson JK, Engstrand L. Molecular characterization of the stomach microbiota in patients with gastric cancer and in controls. *J Med Microbiol* 2009; **58**: 509-516 [PMID: 19273648 DOI: 10.1099/jmm.0.007302-0]

70 **Robinson KM**, Crabtree J, Mattick JS, Anderson KE, Dunning Hotopp JC. Distinguishing potential bacteria-tumor associations from contamination in a secondary data analysis of public cancer genome sequence data. *Microbiome* 2017; **5**: 9 [PMID: 28118849 DOI: 10.1186/s40168-016-0224-8]

71 **Lofgren JL**, Whary MT, Ge Z, Muthupalani S, Taylor NS, Mobley M, Potter A, Varro A, Eibach D, Suerbaum S, Wang TC, Fox JG. Lack of commensal flora in Helicobacter pylori-infected INS-GAS mice reduces gastritis and delays intraepithelial neoplasia. *Gastroenterology* 2011; **140**: 210-220 [PMID: 20950613 DOI: 10.1053/j.gastro.2010.09.048]

72 **Rolig AS**, Cech C, Ahler E, Carter JE, Ottemann KM. The degree of Helicobacter pylori-triggered inflammation is manipulated by preinfection host microbiota. *Infect Immun* 2013; **81**: 1382-1389 [PMID: 23429529 DOI: 10.1128/IAI.00044-13]

73 **Lertpiriyapong K**, Whary MT, Muthupalani S, Lofgren JL, Gamazon ER, Feng Y, Ge Z, Wang TC, Fox JG. Gastric colonisation with a restricted commensal microbiota replicates the promotion of neoplastic lesions by diverse intestinal microbiota in the Helicobacter pylori INS-GAS mouse model of gastric carcinogenesis. *Gut* 2014; **63**: 54-63 [PMID: 23812323 DOI: 10.1136/gutjnl-2013-305178]

74 **Liu X**, Shao L, Liu X, Ji F, Mei Y, Cheng Y, Liu F, Yan C, Li L, Ling Z. Alterations of gastric mucosal microbiota across different stomach microhabitats in a cohort of 276 patients with gastric cancer. *EBioMedicine* 2019; **40**: 336-348 [PMID: 30584008 DOI: 10.1016/j.ebiom.2018.12.034]

75 **Jo HJ**, Kim J, Kim N, Park JH, Nam RH, Seok YJ, Kim YR, Kim JS, Kim JM, Lee DH, Jung HC. Analysis of Gastric Microbiota by Pyrosequencing: Minor Role of Bacteria Other Than Helicobacter pylori in the Gastric Carcinogenesis. *Helicobacter* 2016; **21**: 364-374 [PMID: 26915731 DOI: 10.1111/hel.12293]

76 **Eyvazi S**, Vostakolaei MA, Dilmaghani A, Borumandi O, Hejazi MS, Kahroba H, Tarhriz V. The oncogenic roles of bacterial infections in development of cancer. *Microb Pathog* 2020; **141**: 104019 [PMID: 32006638 DOI: 10.1016/j.micpath.2020.104019]

77 **Homan M**, Orel R. Are probiotics useful in Helicobacter pylori eradication? *World J Gastroenterol* 2015; **21**: 10644-10653 [PMID: 26457024 DOI: 10.3748/wjg.v21.i37.10644]

78 **Li TH**, Qin Y, Sham PC, Lau KS, Chu KM, Leung WK. Alterations in Gastric Microbiota After H. Pylori Eradication and in Different Histological Stages of Gastric Carcinogenesis. *Sci Rep* 2017; **7**: 44935 [PMID: 28322295 DOI: 10.1038/srep44935]

79 **Thorell K**, Bengtsson-Palme J, Liu OH, Palacios Gonzales RV, Nookaew I, Rabeneck L, Paszat L, Graham DY, Nielsen J, Lundin SB, Sjöling Å. *In Vivo* Analysis of the Viable Microbiota and Helicobacter pylori Transcriptome in Gastric Infection and Early Stages of Carcinogenesis. *Infect Immun* 2017; **85** [PMID: 28694295 DOI: 10.1128/IAI.00031-17]

80 **Lee CW**, Rickman B, Rogers AB, Muthupalani S, Takaishi S, Yang P, Wang TC, Fox JG. Combination of sulindac and antimicrobial eradication of Helicobacter pylori prevents progression of gastric cancer in hypergastrinemic INS-GAS mice. *Cancer Res* 2009; **69**: 8166-8174 [PMID: 19826057 DOI: 10.1158/0008-5472.CAN-08-3856]

81 **Mera RM**, Bravo LE, Camargo MC, Bravo JC, Delgado AG, Romero-Gallo J, Yepez MC, Realpe JL, Schneider BG, Morgan DR, Peek RM Jr, Correa P, Wilson KT, Piazuelo MB. Dynamics of *Helicobacter pylori* infection as a determinant

of progression of gastric precancerous lesions: 16-year follow-up of an eradication trial. *Gut* 2018; **67**: 1239-1246 [PMID: 28647684 DOI: 10.1136/gutjnl-2016-311685]

82 **Eun CS**, Kim BK, Han DS, Kim SY, Kim KM, Choi BY, Song KS, Kim YS, Kim JF. Differences in gastric mucosal microbiota profiling in patients with chronic gastritis, intestinal metaplasia, and gastric cancer using pyrosequencing methods. *Helicobacter* 2014; **19**: 407-416 [PMID: 25052961 DOI: 10.1111/hel.12145]

83 **Dias-Jácome E**, Libânio D, Borges-Canha M, Galaghar A, Pimentel-Nunes P. Gastric microbiota and carcinogenesis: the role of non-Helicobacter pylori bacteria - A systematic review. *Rev Esp Enferm Dig* 2016; **108**: 530-540 [PMID: 27604361 DOI: 10.17235/reed.2016.4261/2016]

84 **Correa P**, Haenszel W, Cuello C, Tannenbaum S, Archer M. A model for gastric cancer epidemiology. *Lancet* 1975; **2**: 58-60 [PMID: 49653 DOI: 10.1016/s0140-6736(75)90498-5]

85 **Plottel CS**, Blaser MJ. Microbiome and malignancy. *Cell Host Microbe* 2011; **10**: 324-335 [PMID: 22018233 DOI: 10.1016/j.chom.2011.10.003]

86 **Naylor G**, Axon A. Role of bacterial overgrowth in the stomach as an additional risk factor for gastritis. *Can J Gastroenterol* 2003; **17** Suppl B: 13B-17B [PMID: 12845343 DOI: 10.1155/2003/350347]

87 **Gao JJ**, Zhang Y, Gerhard M, Mejias-Luque R, Zhang L, Vieth M, Ma JL, Bajbouj M, Suchanek S, Liu WD, Ulm K, Quante M, Li ZX, Zhou T, Schmid R, Classen M, Li WQ, You WC, Pan KF. Association Between Gut Microbiota and *Helicobacter pylori*-Related Gastric Lesions in a High-Risk Population of Gastric Cancer. *Front Cell Infect Microbiol* 2018; **8**: 202 [PMID: 29971220 DOI: 10.3389/fcimb.2018.00202]

88 **Pereira-Marques J**, Ferreira RM, Pinto-Ribeiro I, Figueiredo C. Helicobacter pylori Infection, the Gastric Microbiome and Gastric Cancer. *Adv Exp Med Biol* 2019; **1149**: 195-210 [PMID: 31016631 DOI: 10.1007/5584_2019_366]

89 **Guo Y**, Zhang Y, Gerhard M, Gao JJ, Mejias-Luque R, Zhang L, Vieth M, Ma JL, Bajbouj M, Suchanek S, Liu WD, Ulm K, Quante M, Li ZX, Zhou T, Schmid R, Classen M, Li WQ, You WC, Pan KF. Effect of *Helicobacter pylori* on gastrointestinal microbiota: a population-based study in Linqu, a high-risk area of gastric cancer. *Gut* 2020; **69**: 1598-1607 [PMID: 31857433 DOI: 10.1136/gutjnl-2019-319696]

90 **Rieder G**, Fischer W, Haas R. Interaction of Helicobacter pylori with host cells: function of secreted and translocated molecules. *Curr Opin Microbiol* 2005; **8**: 67-73 [PMID: 15694859 DOI: 10.1016/j.mib.2004.12.004]

91 **Li Q**, Liu J, Gong Y, Yuan Y. Serum VacA antibody is associated with risks of peptic ulcer and gastric cancer: A meta-analysis. *Microb Pathog* 2016; **99**: 220-228 [PMID: 27568203 DOI: 10.1016/j.micpath.2016.08.030]

92 **Terebiznik MR**, Raju D, Vázquez CL, Torbricki K, Kulkarni R, Blanke SR, Yoshimori T, Colombo MI, Jones NL. Effect of Helicobacter pylori's vacuolating cytotoxin on the autophagy pathway in gastric epithelial cells. *Autophagy* 2009; **5**: 370-379 [PMID: 19164948 DOI: 10.4161/auto.5.3.7663]

93 **Castaño-Rodríguez N**, Kaakoush NO, Lee WS, Mitchell HM. Dual role of Helicobacter and Campylobacter species in IBD: a systematic review and meta-analysis. *Gut* 2017; **66**: 235-249 [PMID: 26508508 DOI: 10.1136/gutjnl-2015-310545]

94 **Dubois A**, Borén T. Helicobacter pylori is invasive and it may be a facultative intracellular organism. *Cell Microbiol* 2007; **9**: 1108-1116 [PMID: 17388791 DOI: 10.1111/j.1462-5822.2007.00921.x]

95 **Weydig C**, Starzinski-Powitz A, Carra G, Löwer J, Wessler S. CagA-independent disruption of adherence junction complexes involves E-cadherin shedding and implies multiple steps in Helicobacter pylori pathogenicity. *Exp Cell Res* 2007; **313**: 3459-3471 [PMID: 17692843 DOI: 10.1016/j.yexcr.2007.07.015]

96 **Saadat I**, Higashi H, Obuse C, Umeda M, Murata-Kamiya N, Saito Y, Lu H, Ohnishi N, Azuma T, Suzuki A, Ohno S, Hatakeyama M. Helicobacter pylori CagA targets PAR1/MARK kinase to disrupt epithelial cell polarity. *Nature* 2007; **447**: 330-333 [PMID: 17507984 DOI: 10.1038/nature05765]

97 **Murata-Kamiya N**, Kurashima Y, Teishikata Y, Yamahashi Y, Saito Y, Higashi H, Aburatani H, Akiyama T, Peek RM Jr, Azuma T, Hatakeyama M. Helicobacter pylori CagA interacts with E-cadherin and deregulates the beta-catenin signal that promotes intestinal transdifferentiation in gastric epithelial cells. *Oncogene* 2007; **26**: 4617-4626 [PMID: 17237808 DOI: 10.1038/sj.onc.1210251]

98 **Merino JS**, García A, Pastene E, Salas A, Saez K, González CL. Lactobacillus fermentum UCO-979C strongly inhibited Helicobacter pylori SS1 in Meriones unguiculatus. *Benef Microbes* 2018; **9**: 625-627 [PMID: 29633633 DOI: 10.3920/BM2017.0160]

99 **Krzyżek P**. Commentary: Proteomics Analysis Revealed that Crosstalk between *Helicobacter pylori* and *Streptococcus mitis* May Enhance Bacterial Survival and Reduces Carcinogenesis. *Front Microbiol* 2017; **8**: 2381 [PMID: 29238340 DOI: 10.3389/fmicb.2017.02381]

100 **Khosravi Y**, Dieye Y, Loke MF, Goh KL, Vadivelu J. Streptococcus mitis induces conversion of Helicobacter pylori to coccoid cells during co-culture in vitro. *PLoS One* 2014; **9**: e112214 [PMID: 25386948 DOI: 10.1371/journal.pone.0112214]

101 **Shen Z**, Dzink-Fox J, Wilson KT, Whary MT, Muthupalani S, Piazuelo MB, Bravo LE, Suerbaum S, Fox JG, Josenhans C. Tu1288 - Co-Colonization of Helicobacter Pylori with Staphylococcus Epidermidis or Streptococcus Salivarius Differ in the Progression of Gastritis in Ins-Gas Mice. *Gastroenterology* 2018; **154**: s924-s925 [DOI: 10.1016/S0016-5085(18)33114-7]

102 **Kazakos EI**, Dorrell N, Polyzos SA, Deretzi G, Kountouras J. Comment on "Effect of biofilm formation by clinical isolates of Helicobacter pylori on the efflux-mediated resistance to commonly used antibiotics". *World J Gastroenterol* 2017; **23**: 6194-6196 [PMID: 28970736 DOI: 10.3748/wjg.v23.i33.6194]

103 **Moghadam MT**, Chegini Z, Khoshbayan A, Farahani I, Shariati A. Helicobacter pylori Biofilm and New Strategies to Combat it. *Curr Mol Med* 2021; **21**: 549-561 [PMID: 33272177 DOI: 10.2174/1566524020666201203165649]

104 **Pimentel-Nunes P**, Gonçalves N, Boal-Carvalho I, Afonso L, Lopes P, Roncon-Albuquerque R Jr, Henrique R, Moreira-Dias L, Leite-Moreira AF, Dinis-Ribeiro M. Helicobacter pylori induces increased expression of Toll-like receptors and decreased Toll-interacting protein in gastric mucosa that persists throughout gastric carcinogenesis. *Helicobacter* 2013; **18**: 22-32 [PMID: 23061653 DOI: 10.1111/hel.12008]

105 **González Torre JA**, Cruz-Gómez ÁJ, Belenguer A, Sanchis-Segura C, Ávila C, Forn C. Hippocampal dysfunction is

associated with memory impairment in multiple sclerosis: A volumetric and functional connectivity study. *Mult Scler* 2017; **23**: 1854-1863 [PMID: 28086035 DOI: 10.1177/1352458516688349]

World Journal of Gastrointestinal Oncology

Submit a Manuscript: https://www.f6publishing.com

World J Gastrointest Oncol 2022 May 15; 14(5): 973-988

DOI: 10.4251/wjgo.v14.i5.973

ISSN 1948-5204 (online)

REVIEW

EFNA1 in gastrointestinal cancer: Expression, regulation and clinical significance

Ling-Yu Chu, Bin-Liang Huang, Xu-Chun Huang, Yu-Hui Peng, Jian-Jun Xie, Yi-Wei Xu

Specialty type: Oncology

Provenance and peer review: Invited article; Externally peer reviewed.

Peer-review model: Single blind

Peer-review report's scientific quality classification

Grade A (Excellent): 0
Grade B (Very good): B
Grade C (Good): C
Grade D (Fair): 0
Grade E (Poor): 0

P-Reviewer: Farouk S, Egypt; Kałuzińska Ż, Poland

Received: April 20, 2021
Peer-review started: April 20, 2021
First decision: August 19, 2021
Revised: September 17, 2021
Accepted: April 1, 2022
Article in press: April 1, 2022
Published online: May 15, 2022

Ling-Yu Chu, Jian-Jun Xie, Department of Biochemistry and Molecular Biology, Shantou University Medical College, Shantou 515041, Guangdong Province, China

Bin-Liang Huang, Xu-Chun Huang, Yu-Hui Peng, Yi-Wei Xu, Department of Clinical Laboratory Medicine, The Cancer Hospital of Shantou University Medical College, Shantou 515041, Guangdong Province, China

Yu-Hui Peng, Yi-Wei Xu, Guangdong Esophageal Cancer Research Institute, The Cancer Hospital of Shantou University Medical College, Shantou 515041, Guangdong Province, China

Corresponding author: Yi-Wei Xu, PhD, Senior Technologist, Department of Clinical Laboratory Medicine, The Cancer Hospital of Shantou University Medical College, No. 7 Raoping road, Shantou 515041, Guangdong Province, China. 14yyxu@stu.edu.cn

Abstract

Ephrin-A1 is a protein that in humans is encoded by the *EFNA1* gene. The ephrins and EPH-related receptors comprise the largest subfamily of receptor protein-tyrosine kinases which play an indispensable role in normal growth and development or in the pathophysiology of various tumors. The role of *EFNA1* in tumorigenesis and development is complex and depends on the cell type and microenvironment which in turn affect the expression of *EFNA1*. This article reviews the expression, prognostic value, regulation and clinical significance of *EFNA1* in gastrointestinal tumors.

Key Words: *EFNA1*; Expression; Tumorigenesis; Clinical implication; gastrointestinal cancer

Core Tip: Ephrin-A1, a protein that in humans is encoded by the *EFNA1* gene, is the ligand of EphA2. Studies have shown that the EphA2 receptor and its ligand ephrin-A1 are expressed in a variety of malignant tumors and the interaction between the two promotes the migration of tumor vascular endothelial cells. In addition, studies have shown that *EFNA1* widely affects tumor growth through enhancing tumor angiogenesis, malignant cell events and invasiveness. EFNA1 is also up-regulated in gastrointestinal tumors and is closely related to the prognosis of gastrointestinal tumors. Therefore, this article reviews the expression, prognostic value, regulation and clinical significance of *EFNA1* in gastrointestinal tumors.

Citation: Chu LY, Huang BL, Huang XC, Peng YH, Xie JJ, Xu YW. *EFNA1* in gastrointestinal cancer: Expression, regulation and clinical significance. *World J Gastrointest Oncol* 2022; 14(5): 973-988
URL: https://www.wjgnet.com/1948-5204/full/v14/i5/973.htm
DOI: https://dx.doi.org/10.4251/wjgo.v14.i5.973

INTRODUCTION

Current theory suggests that a tumor is an "organ" that contains a diverse collection of cells. Different cells sense changes in the external environment through signaling molecules on the surface of cell membrane or plasma membrane. It regulates a series of biological behaviors, such as tumor occurrence, development, invasion and metastasis[1]. Receptor tyrosine kinases (RTKs) can directly transmit external information to the nucleus and are key molecules in the signal transduction pathways through which cells convert external stimuli into biological behavior. The Eph (erythropoietin-producing hepatoma-amplified sequence) receptor family is the largest known family of RTKs[2]. By interacting with its ephrin ligands, Eph receptors regulate physiological and pathological processes, including the formation of tissues and organs, signal transmission of the nervous system, angiogenesis and cell-to-cell adhesion[3]. Studies have shown that the EphA2 receptor and its ligand ephrin-A1 are expressed in a variety of malignant tumors and the interaction between the two promotes the migration of tumor vascular endothelial cells[4]. Therefore, in recent years, the role of ephrins in the occurrence and development of tumors has become a hot topic in cancer research.

Studies have shown that *EFNA1* widely affects tumor growth through enhancing tumor angiogenesis [5,6], malignant cell events[7,8] and invasiveness[9-11]. It is up-regulated in gastrointestinal tumors (such as esophageal cancer (EC)[12], colorectal cancer (CRC)[13], and hepatocellular carcinoma (HCC) [14]) and is closely related to the prognosis of gastrointestinal tumors[12-16]. This article summarizes the research progress on *EFNA1* in terms of gene composition, protein structure, expression, regulation and biological effects. On this basis, the role of *EFNA1* in tumors and its regulatory mechanisms are described in detail as well as its potential clinical significance in gastric cancer (GC), HCC, CRC, EC and some common gastrointestinal cancers.

THE EPHRIN FAMILY AND STRUCTURAL CHARACTERISTICS

The Eph family contains 14 tyrosine kinase receptors[17] and is the largest known RTK family. The Eph receptor is located on the cell membrane and can directly receive stimulation from the external environment. Eph receptors can also be divided into two categories: A and B, where EphA is comprised of 8 members and EphB is comprised of six members. Eph receptors contain a typical transmembrane structure and belong to transmembrane proteins[18,19]. The typical Eph family receptor structure involves an extracellular domain consisting of a globular domain, a unique cysteine-rich motif and two fibronectin type III motifs. The extracellular domain and the intracellular domain are connected by a short transmembrane domain. The intracellular membrane region is relatively conserved and includes the domain with tyrosine kinase activity, a sterile alpha motif domain and a C-terminal postsynaptic density protein, discs large, zonula occludens (PDZ) domain[20]. Ephrin ligands are divided into two subclasses according to the way they attach to the membrane. Type A ephrins are firmly anchored to the cell membrane with the aid of glycosylphosphatidylinositol (GPI) and include five members (ephrins A1-A5). Type B ephrins are transmembrane proteins[18,19] and include three members (ephrins B1-B3). Ephrin-B contains a PDZ-binding region and there is also a conserved tyrosine residue that can be phosphorylated. Ephrin-A is rather special in that it only contains a receptor-binding region which is coupled to the cell membrane through a GPI anchor. This structure also leads to the specificity of ephrin-A signal transduction (Figure 1).

Ephrin-A1 was first discovered in 1990 as a soluble protein produced by human umbilical vein endothelial cells (HUVECs) in response to treatment with tumor necrosis factor (TNF). However, it was not confirmed until 1994 to be a ligand for EphA2 which had been considered an independent RTK

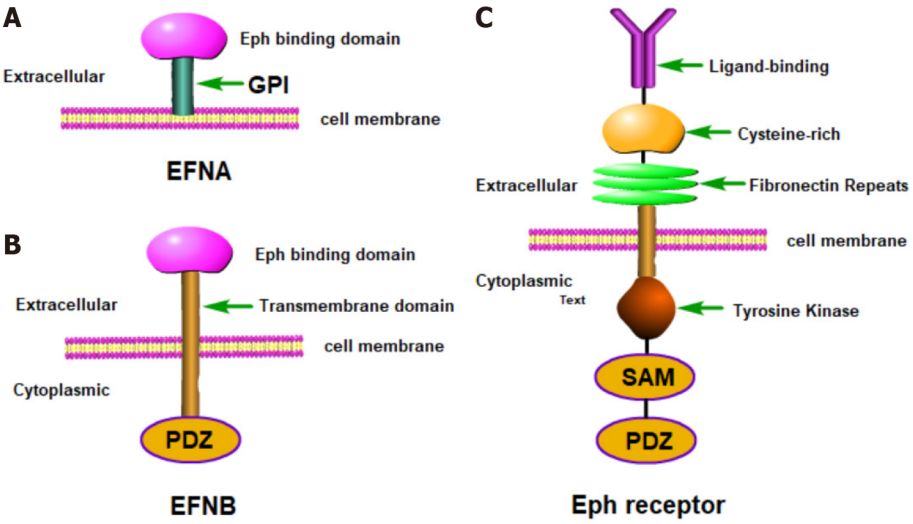

DOI: 10.4251/wjgo.v14.i5.973

Figure 1 Ephrin-A signal transduction. A: Structure of ephrinA ligands; B: Structure of ephrinB ligands; C: Eph/Ephrin interaction map. GPI: Glycosylphosphatidylinositol; PDZ: Postsynaptic density 95-Discs large Zonula occludentes-1-protein; SAM: Sterile alpha motif.

kinase before then[21,22]. Ephrin-A1 is a single-chain protein molecule containing 205 amino acid residues, has a molecular weight of 22-KD and is a membrane-coupled ligand protein. The *EFNA1* gene, encoding ephrine-A1, is located on chromosome Iq22[20,23]. *EFNA1* is 7024 bp in length and contains 5 exons (Table 1 and Figure 2). The length of exon 1 is 194 bp and includes the entire 5' untranslated region (5'UTR). Exons 2 and 3 are 295 bp and 65 bp, respectively, and encode most of the amino acid sequence of the central junction domain. The C-terminus of ephrin-A1 is encoded by exon 4 and the first half of exon 5 (the latter half is the 3' untranslated region (3' UTR)). As early as 1996, a study by Daniel *et al*[24] found that soluble ephrin-A1 can induce HUVECs cultured *in vitro* to form capillary-like structures, suggesting that ephrin-A1 has the potential to promote angiogenesis.

The binding of Eph receptor to ephrin ligand is very complicated. The same Eph receptor can bind different ephrins and the same ligand can also interact with multiple Eph receptors. EphA2 is the most common receptor for ephrin-A1. The signal transduction by the EphA2 receptor and ephrin-A1 is unique in that they can mediate two-way signal transmission. They can act as receptors or ligands for each other and transmit signals to the cells in which they are located. At present, the signal transmitted by the EphA2 receptor is usually referred to as forward signaling, and the intracellular signal transduction mediated by ephrin-A1 is called the reverse signaling[25,26]. For EphA2 to be activated by ephrin-A1, it must form oligomers in a ligand-dependent manner, indicating that the activation of the EphA2 receptor depends on the interaction between it and the ephrin-A1 Ligand[27]. When EphA2 is activated through ephrin-A1 binding, the tyrosines in their intracellular regions are phosphorylated to form a binding site for another protein, ultimately resulting in the signal transduction complex.

EFNA1 AND GASTROINTESTINAL CANCERS

Expression and prognostic value of ephrin-A1 in gastrointestinal cancers

Ephrin is up-regulated in various subtypes of tumor tissues and the up-regulation is closely related to tumor growth[28]. Among the ephrins, ephrin-A1 is highly expressed in human gastrointestinal cancers such as GC, CRC, and EC, as well as HCC. The degree of up-regulation of its expression is closely related to the malignancy of the tumor, metastatic potential and prognosis of the patient[13,29]. We summarize the expression of ephrin-A1 in gastrointestinal cancers and its prognostic value in Table 2.

Gastric cancer

As a tumor-related secreted protein, ephrin-A1 is highly expressed in most GC tissues and cells. Further studies have found that there is a positive correlation between the expression level of *EFNA1* and the degree of malignancy of GC[30-41]. *EFNA1* is highly expressed in GC tissues but is low or not expressed in benign GC lesions, and its expression surges with increases in malignancy[30]. Overexpression of ephrin-A1 in GC tumors was reported for 57% of patients in one study and 72.7% of patients in another study, and the overexpression of ephrin-A1 was significantly related to TNM staging and lymph node metastasis[31]. Studies by Miyazaki *et al*[32] found that *EFNA1* is highly expressed in GC, and its high expression may be related to the occurrence, development, invasion and metastasis of GC. *EFNA1* expression increases with both clinical stage and lymph node metastasis and decreases in the degree of

Table 1 *EFNA1* gene information

Gene name (known as)	Position and length	Exon number	Encoding mRNA and protein	5'UTR	CDS	3'UTR
EFNA1 (ephrin-A1; B61; EFL1; GMAN; ECKLG)	1q22; 7024bp	5 (1..194, 3464..3759, 5682..5693, 5855..5905,6082..7024)	NM_004428.3, 1552bp, NM_182685.2, 1486 bp; NP_004419.2 , 205aa, NP_872626.1, 183 aa	1..103	103..194, 3464..3759, 5682..5693, 5855..5905,6082..7024	6192..7024

CDS: Coding DNA Sequence.

tissue differentiation, which indicates the malignant degree of GC. Yuan *et al*[33] studied 176 cases of human GC and found that *EFNA1* mRNA and protein are highly expressed in GC, suggesting a pre-transcriptional regulatory mechanism in GC. In addition, the study also found that *EFNA1* is greatly expressed in the highly invasive cancer cell line AGS compared with moderately invasive cancer cell lines, suggesting that high expression of ephrin-A1 is related to a more aggressive behavior. These results suggest that *EFNA1* plays an important role in progression and metastasis after human GC resection.

Genetic variation of miRNA binding sites may change the susceptibility of individuals to many cancers. Li *et al*[34] selected 525 GC patients and 501 controls, and selected 3 miRNA binding-site single nucleotide polymorphisms (SNPs) from 30 untranslated regions (UTRs) of GC-related genes to study their relationship with GC susceptibility. It was found that rs12904 in the *EFNA1* gene was significantly related to the risk of GC. In addition, luciferase detection showed that *EFNA1* mRNA is the target of hsamiR-200c, and expression of the rs12904G>A isoform resulted in a change of luciferase expression. In summary, these findings indicate that the miR-200c binding site containing the SNP (rs12904G>A) can regulate the expression of *EFNA1* and is related to GC susceptibility[34-36]. Zhuo *et al*[37] found that a lncRNA, GMAN, was increased in GC tissues and was associated with GC metastasis and decreased survival rates. GMAN regulates the translation of *EFNA1* mRNA by competitively binding antisense GMAN RNA, thereby affecting the invasion and metastasis of GC cells; and up-regulation of GMAN is associated with a poor prognosis of GC.

Colorectal cancer

EFNA1 is highly expressed in most CRC tissues and cells. In recent years, studies based on the relationship between *EFNA1* and CRC have shown that it plays an important role in CRC cell growth, invasion, metastasis and angiogenesis[42-52]. Potla *et al*[42] found that overexpression of *EFNA1* can promote the growth of HT29 CRC cells. Ephrin-A1 activates EphA2 to weaken the connections between tumor cells, resulting in increased adhesion of tumor cells to the extracellular matrix (ECM) and enhanced invasion into the matrix. All of these are important characteristics of tumor cells for acquiring the ability to invade and metastasize. Shi *et al*[43] selected 14 genes through a literature analysis and compared their expression in rectal cancer tissues and para-cancerous tissues, as well as rectal adenomas and cancer tissues. Among them, the gene copy number and mRNA expression of *EFNA1* increased in the progression from adenoma to cancer, indicating that *EFNA1* may be a driving gene to promote rectal cancer. Studies have also evaluated the genetic association between *EFNA1* polymorphisms and susceptibility to CRC. The results showed that, compared with the normal control group, expression of *EFNA1* in CRC is increased, suggesting that *EFNA1* is involved in the occurrence of CRC and may be used as a diagnostic biomarker for CRC. In addition, it was also found that the rs12904G/A variant is significantly associated with a lower risk of CRC compared with the AA genotype[44,45]. A study by Rosenberg *et al*[46] showed that the CRC epithelial cell line Caco-2 simultaneously expresses ephrin-A1 (B61) and its receptor EphA2 (Eck). The ephrin-A1 and EphA2 are co-localized in the same cell and play a role in the development, migration and barrier function of CRC epithelial cells helping to maintain the homeostasis and continuity of the epithelial barrier.

Kataoka *et al*[47] detected the expression of *EFNA1* in CRC specimens and found that 62.5% (25/37) expressed ephrin-A1 to a greater extent which correlated with low survival rate and poor prognosis. Overexpression of *EFNA1* in CRC stages I and II is more significant than in stages III and IV, and overexpression in tumors < 5 cm is greater than that in tumors > 5 cm. This data suggests an importance of *EFNA1* in the early stages of CRC progression. However, the prognostic role of *EFNA1* in CRC patients is still controversial. Robertis *et al*[48] reported that low expression of *EFNA1* in CRC cells is indicative of poor patient prognosis, including poor disease-free survival, cancer-specific survival and progression-free survival. However, two other gene chip analyses showed that the prognosis of patients with high *EFNA1* expression is worse than that of patients with low expression[49,50]. In addition, multivariate analysis showed that *EFNA1* expression is an independent prognostic factor of CRC[49,50]. Therefore, a large sample, multi-center clinical study is needed to verify the prognostic value of *EFNA1* in CRC.

Table 2 *EFNA1* prognostic value in gastrointestinal cancers

Tumor type	Sample type	Expression	Methods	Prognosis value	Notes	Ref.
Gastric cancer	Tissues	Increased	RT-PCR	(-)	*EFNA1* expression is related to GC stage, depth of invasion, lymph node metastasis and recurrence	Nakamura *et al* [30], 2005
	Tissues	Increased	IHC	Poor DSS	(-)	Miyazaki *et al* [32], 2013
	Tissues	Increased	IHC, RT-PCR	Poor DSS	*EFNA1* expression is related to TNM and lymph node metastasis	Yuan *et al*[33], 2009
	Tissues	Increased	RT-PCR	(-)	SNP (rs12904G>A) can regulate the expression of *EFNA1* and is related to GC susceptibility	Li *et al*[34], 2014
	Tissues	Increased	(-)	(-)	*EFNA1* expression increase the susceptibility of GC	Zhu *et al*[35], 2015
	Tissues	Increased	(-)	(-)	*EFNA1* expression may be related to GC susceptibility	Lee *et al*[36], 2015
	Tissues	Increased	IHC, RT-PCR	Poor DSS	GMAN up-regulates the expression of *EFNA1* and promotes the transfer of GC	Zhou *et al*[37], 2019
Colorectal cancer	Cells	(-)	(-)	(-)	*EFNA1* overexpression can inhibit the growth of HT29 cells	Potla *et al*[42], 2002
	Tissues	Increased	IHC, RT-PCR	(-)	The expression of *EFNA1* promotes the development of rectal adenocarcinoma to rectal cancer	Shi *et al*[43], 2012
	Tissues	Increased	(-)	(-)	*EFNA1* may be used as a diagnostic biomarker for the characteristics of CRC. In addition, the rs12904G/A variant is related to the susceptibility to CRC	Mao *et al*[44], 2013
	Cells	(-)	(-)	(-)	Eck and B61 are co-expressed in the same cell, suggesting the existence of an autocrine loop	Rosenberg *et al* [46], 1997
	Tissues	Increased	RT-PCR	Poor DSS	Decreased survival	Kataoka *et al* [47], 2004
	Cells	Reduced	(-)	Poor DSS	*EFNA1* can be used as a prognostic marker for CRC	Robertis *et al* [48], 2017
	Tissues	Increased	RT-PCR	Poor DSS	*EFNA1* is an independent prognostic factor for CRC	Yamamoto *et al* [49], 2013
	Serum	Increased	IHC, QRT-PCR	Poor DSS	*EFNA1* may be used for the identification of CRC	Lip *et al*[50], 2008
Hepatocellular carcinoma	Tissues	Increased	RT-PCR	Poor DSS	The high expression of *EFNA1* protein is related to histological differentiation, portal vein tumor thrombus and lymph node metastasis	Zhang *et al*[54], 2007
	Tissues	Increased	RT-PCR	Poor DSS	*EFNA1* is an independent prognostic factor of HCC	Wada *et al*[55], 2014
	Tissues	Increased	IHC	Poor DSS	*EFNA1* is involved in the mechanism of AFP induction in HCC	Lida *et al*[57], 2005
	Tissues, Serum	Increased	IHC, RT-PCR	Poor DSS	The expression of *EFNA1* is positively correlated with AFP	Cui *et al*[58], 2010
Esophageal cancer	Tissues	Increased	IHC, RT-PCR	Poor DSS	Decreased survival	Xu *et al*[59], 2005
	Tissues	Increased	(-)	Poor DSS	Decreased survival	Chen *et al*[60], 2019
	Cells	Increased	RT-PCR	(-)	High expression of *EFNA1* decreased the viability of ESCC cells	Yang *et al*[61], 2015

AFP: Alpha-fetoprotein; CRC: Colorectal cancer; DSS: Disease free survival; ESCC: Esophageal squamous cell carcinoma; GC: Gastric cancer; HCC: Hepatocellular carcinoma; IHC: Immunocytochemistry; RT-PCR: Reverse transcription-polymerase chain reaction; SNP: Single nucleotide polymorphism.

Hepatocellular carcinoma

EFNA1 is widely expressed in HCC tissues[53-58]. Its expression is lowest in normal liver tissues, increases in liver cirrhosis tissues and is further increased in HCC tissues[54,57,58]. Existing studies have shown that the expression of *EFNA1* is related to HCC tissue differentiation and lymph node

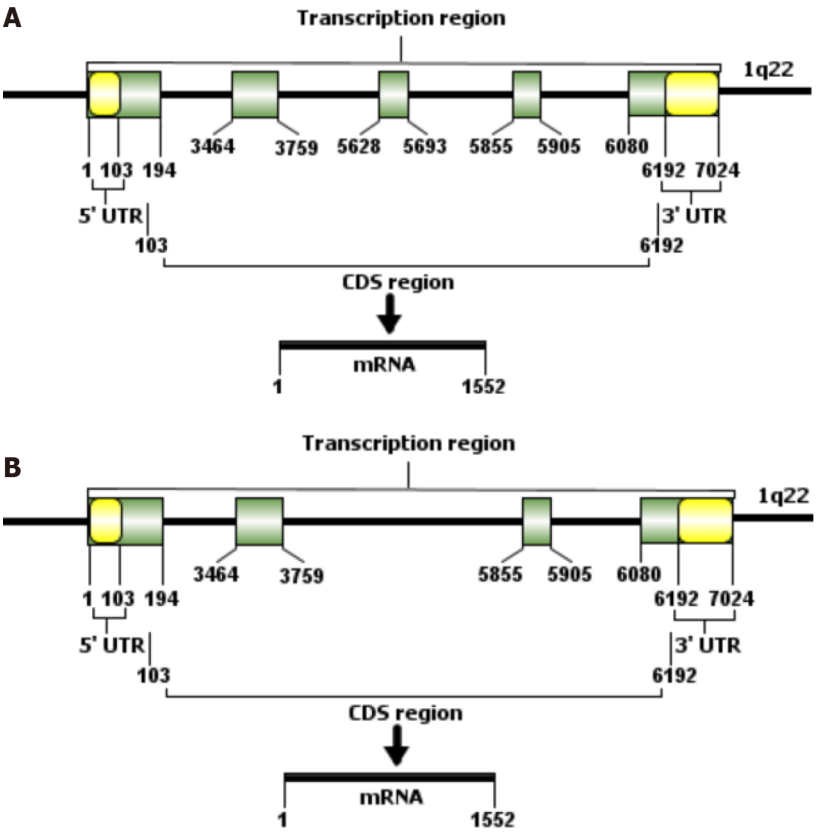

DOI: 10.4251/wjgo.v14.i5.973

Figure 2 Schematic representation of the *EFNA1* chromosomal gene. A: mRNA (NM_004428.3) schematic; B: mRNA (NM_182685.2) schematic.

metastasis. In addition, overexpression of *EFNA1* indicates poor prognosis[14,54]. Cox multivariate analysis showed that *EFNA1* is an independent prognostic factor of HCC, suggesting that the expression of *EFNA1* may be a useful indicator for predicting the high risk of recurrence after radical resection of HCC[55].

In HCC, ephrin-A1 is closely related to expression of alpha-fetoprotein (AFP) and can indicate poor prognosis in patients with AFP[57,58]. A study by Lida *et al*[57] showed that ephrin-A1 induces the expression of genes related to the cell cycle (p21), angiogenesis, and cell-cell interaction (Rho, integrins, and matrix metalloproteinases) in HCC cells, and these ephrin-A1-induced genes are also activated in HCC tissues overexpressing AFP. Part of the reason for the poor prognosis of HCC patients with AFP is the expression of ephrin-A1 which induces the expression of tumor cell growth, angiogenesis, invasion and metastasis-related genes. In addition, Cui *et al*[58] found that the frequency of *EFNA1* expression in HCC tissues is higher than that of AFP (91% and 45%, respectively). In HCC cell lines and tissues, ephrin-A1 is positively correlated with AFP expression. In terms of secreted proteins, ephrin-A1 is detected in the supernatant of most primary HCC cell lines and it was clearly found that serum ephrin-A1 Levels in HCC patients are elevated. This suggests that *EFNA1* can be used as a useful serum marker to measure the development and progress of HCC.

Esophageal cancer

At present, there are few studies on *EFNA1* in EC. Existing studies have confirmed that *EFNA1* is highly expressed in esophageal squamous cell carcinoma (ESCC) tissues and cells, and is indicative of a relatively poor prognosis[59-61]. Xu *et al*[59] used immunohistochemistry and reverse transcription-polymerase chain reaction (RT-PCR) to analyze the expression of *EFNA1* protein and mRNA in ESCC tissue. The results showed that 84.4% (146/173) sample positively expressed and 15.6% (27/173) sample negatively expressed *EFNA1*. In addition to overall survival, *EFNA1* protein expressions were significantly associated with histological grade, number of lymph node metastasis and clinical stage for patients with ESCC in the univariate analysis. In addition, studies have also shown that ephrin-A1 and EphA2 often co-localize in the tumor area and vascular endothelial cells in ESCC, and their expression is related to co-localization[59]. A study by Chen *et al*[60] showed that the expression level of *EFNA1* in ESCC tissues is higher than that in normal tissues. Survival analysis showed that *EFNA1* expression is associated with shorter overall survival. Regarding the expression of *EFNA1* in ESCC and its prognostic role, more studies are needed to further confirm these results.

Role of EFNA1 in gastrointestinal cancers

EFNA1 is differentially-expressed in many gastrointestinal cancers and high expression of *EFNA1* may have an important function in the formation of the malignant phenotype of gastrointestinal cancers[28-61]. The effects of differential *EFNA1* expression on gastrointestinal cancers are mainly manifested in the following aspects.

Regulation of gastrointestinal cancer cell growth

Ephrin-A1 exerts an inhibitory effect on the growth of GC, CRC, HCC and ESCC cells. Both anchorage-dependent and anchorage-independent growth of tumor cells overexpressing EphA2 was observed to be reduced by treatment with ephrin-A1-Fc, an ephrin-A1 fused to the Fc domain of IgG[30,62]. The EphA2 receptor is activated by its ligand ephrin-A1, triggering the down-regulation of the total expression of EphA2 in GC cells resulting in a net inhibition of the proliferation of GC cells[33]. Potla *et al*[42] found that in three-dimensional spheroid cultures of HT29 colon cancer cells, an increase of *EFNA1* expression reduces the growth of tumor cells. Shi *et al*[43] reported that the expression of *EFNA1* mRNA increases in the progression from rectal adenoma to rectal cancer. In addition, a recent study conducted by Yamamoto *et al*[49] showed that *EFNA1* is an independent prognostic factor for CRC and its loss of function is related to decreased proliferation, invasion and migration of CRC cell lines.

Eph/Ephrin can also regulate the effects of other growth factors on cell growth. Miao *et al*[63] reported that when EphA2 is activated by ephrin-A1, the Ras/Erk pathway can be inhibited to reduce cell growth induced by platelet-derived growth factor, vascular endothelial growth factor (VEGF) and epidermal growth factor. In addition, the overexpression of *EFNA1* is related to the growth and proliferation of gastrointestinal cancer cells and may play the role of a cell growth factor or growth promoting factor[64]. Therefore, in a sense, *EFNA1* can be considered as a potential growth factor[65] and its abnormal expression in cancers can affect tumor growth and formation.

Regulation of gastrointestinal cancer cells adhesion

Malignant tumor cells often exhibit low cell adhesion which can be due to a lack of cadherin function. Ephrin-A1 has been shown to recruit the Src family kinase Fyn into lipid rafts which is followed by redistribution of vinculin, activation of the mitogen-activated protein kinase pathway, protein tyrosine phosphorylation and increased cell-substrate adhesion[66,67]. In addition, studies have shown that the amount of ephrin-A1 determines the extent of EphA2-dependent, integrin-mediated cell adhesion[68]. In cancer cells lacking cadherin, cell-to-cell contact is reduced. Therefore, EphA2 cannot bind to ephrin-A1 attached to the adjacent cell membrane and cannot undergo tyrosine phosphorylation which facilitates cancer cell detachment from surrounding cells leading to cancer cell spread and increased invasion.

Studies have shown that cadherin can significantly affect the expression and subcellular localization of ephrin-A1/EphA2, and ephrin-A1/EphA2 in turn can also regulate the function of cadherin[69]. EphA2 promotes tumor growth by enhancing the adhesion of tumor cells to the extracellular matrix increasing anchorage-independent growth and angiogenesis[70]. The specific mechanism may be related to the dysfunction of the cadherin glycoprotein in the phosphorylation or distribution of EphA2 at the sites of cell contact[71].

Regulation of gastrointestinal cancer cells migration

EFNA1 not only plays a role in normal physiological processes but also plays an important role in pathological processes such as tumor formation[72,73]. It has been reported that ephrin-A1 and EphA2 are up-regulated in most gastrointestinal tumors and this up-regulation is related to tumor formation and tumor migration[73-75]. Microarray analysis of 220 CRC samples and RT-PCR analysis of 146 CRC samples showed that loss of ephrin-A1 after siRNA knockdown decreases cell proliferation, invasion and migration. Expression of *EFNA1* is a high-risk indicator for predicting recurrence and cancer-related death after radical resection of CRC[49]. Leguchi *et al*[76] showed that when tumor cells treated with PBS or ephrin-A1-Fc are injected into mice, tumor cells in the lungs can be detected, but that ephrin-A1-Fc treatment increased lung permeability and enhanced tumor metastasis, whereas neutralization by anti- ephrin-A1 antibody reduced the effect.

The regulation of Eph/Ephrin on cancer cell migration is mainly through its influence on the function of integrins. Miao *et al*[77] showed that when EphA2 is activated, it can inactivate integrin function, inhibit cell spreading, migration and integrin-dependent cell adhesion. They also found that when EphA2 is activated with ephrin-A1, EphA2 can quickly recruit the tyrosine phospholipase SHP2, which can dephosphorylate focal adhesion kinase (FAK) and paxillin, leading to the dissociation of the EphA2 and FAK complex[77,78]. Other data also indicate that the activation of ephrin-A1 can generally increase the adhesion of cells to the extracellular matrix and promote cell migration[79-81].

EFNA1 AND TUMOR ANGIOGENESIS

Tumor angiogenesis is a common pathological phenomenon in carcinogenesis and directly regulates the pathological process of tumor growth, invasion and metastasis. Tumor angiogenesis can bring nutrients and oxygen necessary for tumor cell growth and discharge metabolic waste. At the same time, new blood vessels can be used as a metastasis channel to mediate distant metastasis of tumors[82]. Angiogenesis is regulated by a variety of pro-angiogenic factors and anti-angiogenic factors. Currently, five major protein families are considered to be key regulators of tumor angiogenesis, namely VEGF and its receptor family, angiopoietin and the TIE receptor family, Notch receptor family, Eph/ephrin family and Slit ligand/Robo receptor family[1,83]. Among them, ephrin-A1 and its main receptor EphA2, as the main members of the Eph/ephrin family, are not only significantly expressed in a variety of malignant tumors but are also closely related to normal and tumor angiogenesis.

Role of EFNA1 in tumor angiogenesis

In 2000, Ogawa *et al*[84] first reported that ephrin-A1/EphA2 plays an important role in tumor angiogenesis, showing that overexpression of ephrin-A1 in tumor cells promotes tumor angiogenesis, whereas down-regulation of ephrin-A1 expression inhibits tumor cell-induced endothelial cell migration and reduces microvascular density. Functional changes such as migration of vascular endothelial cells, play a key role in tumor angiogenesis. Ephrin-A1 is mainly expressed in tumor cells while EphA2 is mainly expressed in tumor blood vessels. Therefore, it is speculated that tumor cells expressing ephrin-A1 have the effect of attracting endothelial cells expressing EphA2 leading to formation of new blood vessels and angiogenesis. EphA2 expressed on the surface of endothelial cells is a key component in the regulation of angiogenesis. Blocking EphA2 can limit the migration of endothelial cells, vascular reorganization and VEGF-induced angiogenesis.

EphA2 can promote the migration of tumor vascular endothelium and ephrin-A1 has been confirmed to act as a chemical inducer in the process of vascular remodeling[85], suggesting that the interaction between the two in tumor cells and vascular endothelial cells is jointly involved in tumor angiogenesis [85,86]. Combination of the two can promote the migration of tumor vascular endothelial cells and promote the formation of capillary-like structures in tissues and endothelial cells by affecting the cytoskeleton, matrix adhesion and/or cell adhesion. Inhibition of EphA2 activation also reduces tumor angiogenesis, further supporting an important role for EphA2 in tumor neovascularization, invasion and metastasis[85-87]. Pandy *et al*[85] confirmed that ephrin-A1, not fibroblast growth factors, specifically regulates TNF-α-induced angiogenesis in mice *in vivo*. This suggests that the induction of ephrin-A1 and subsequent activation of its receptor EphA2 may regulate angiogenesis mediated by TNF-α.

Ogawa *et al*[84] found that ephrin-A1 and EphA2 are stably expressed in some endothelial cells within gastrointestinal tumors including EC and CRC. In CRC, the expression of ephrin-A1/EphA2 is up-regulated in tumor areas with higher blood vessel density. In small volume CRC tumors (< 5 cm), the expression of ephrin-A1 and EphA2 is higher[47,88]. Liu *et al*[89] used the microvessel density (MVD) method to label tumor blood vessels with CD34 and directly observe and quantify tumor angiogenesis as well as observe tumor invasion and metastasis. The results of the study showed that MVD in GC tissue is higher than that in adjacent tissues and normal gastric mucosa. MVD increases with the decrease of GC differentiation and increases in infiltration depth, lymph node metastasis and tumor diameter and it is closely related to increased tumor malignancy and metastasis. It is also positively correlated with the expression of EphA2 and ephrin-A1. This suggests that ephrin-A1 may play a role in promoting vascularization and play an important role in the formation of blood vessels in GC.

Possible mechanisms of EFNA1-promoted tumor angiogenesis

There is sufficient experimental evidence to show that EphA2 activation on endothelial cells is necessary for ephrin-A1 to exert its angiogenic effect *in vitro* and *in vivo*[90]. The mechanism by which *EFNA1* induces angiogenesis is not fully understood. So far, only a few studies have shed light on the molecular mechanism of ephrin-A1-induced angiogenesis. Based on this, we summarize the possible mechanism by which ephrin-A1 promotes tumor angiogenesis (Figure 3).

Erk-associated signaling pathways

EFNA1 can be activated *via* the ERK1/2 pathway through EphA2 and promote the proliferation, migration and angiogenesis of HUVECs[91,92]. Activation of EphA2 by ephrin-A1 can promote the migration of endothelial cells and the formation of capillary structures by regulating the morphology, migration, adhesion and proliferation of vascular endothelial cells. Interaction between the two has also been confirmed to induce angiogenesis *in vivo*[93]. For example, ephrin-A1-Fc can increase the adhesion of HUVECs by activating integrins and promoting vascular function[94].

Pratt *et al*[95] have shown that ephrin-A1-mediated stimulation of EphA2 receptor tyrosine kinase can transmit signals from the cell membrane through MAP kinase. These signals are transmitted to the nucleus by inducing the transcription of Elk-1 and are transmitted back to the cell membrane through

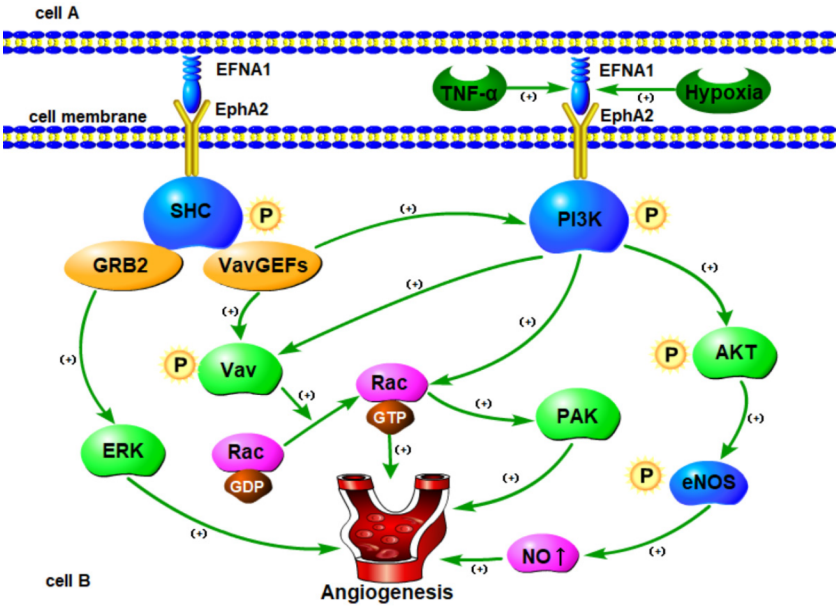

DOI: 10.4251/wjgo.v14.i5.973

Figure 3 Possible molecular mechanisms by which *EFNA1* induces angiogenesis. PI3K: Phosphatidylinositol 3-hydroxy kinase; eNOS: Endothelialnitric oxide synthase; TNF-α: Tumor necrosis factor α; PAK: p21-activated kinase.

the destabilization of the cell's attachment to the ECM. In addition, studies have shown that the biochemical mechanism of EphA2 signaling involves the activation-dependent interaction between tyrosine phosphorylation of EphA2 and SHC adaptor protein. SHC in turn bridges EphA2 to GRB2 which contributes to ERK kinase activation and nuclear translocation.

Growth factors and cytokines mediated signaling pathways

In different types of cells, growth factors and cytokines can induce the expression of *EFNA* ligands. Ephrin-A1 was the first *EFNA* ligand identified and shown to be an immediate early gene product induced by TNF-α in cultured HUVECs[21]. Unlike other angiogenic factors induced by TNF-α[96,97], Cheng *et al*[98] showed that *EFNA1* induction does not require NF-kB or p42/44 MAPK signaling, but rather activation of the JNK and p38MAPK signaling pathways[99]. Both of these pathways have been shown to regulate actin reorganization and cell migration in endothelial cells[100,101]. Therefore, regulating the expression of *EFNA1* by p38 MAPK and JNK is consistent with the role of *EFNA1* in endothelial cell migration and blood vessel assembly. In addition, Hess *et al*[102] showed that TNF-α can up-regulate the expression of *EFNA1* by acting on HUVECs leading to increased phosphorylation of EphA2 resulting in increased angiogenesis and enhanced cell chemotaxis. Phosphorylation of EphA2 caused by ephrin-A1 can activate phosphatidylinositol 3-hydroxy kinase (PI3K) and up-regulate Rac1 activity thereby causing endothelial cell migration to increase and promote angiogenesis[102].

In addition to TNF-α, ephrin-A1 is also induced by lipopolysaccharide[103], interleukin-1β[21,103], and VEGF in HUVECs and microvascular endothelial cells[98]. The study of Cheng *et al*[98] showed that similar to TNF-α, VEGF induces ephrin-A1 as an immediate early gene product. Blocking EphA receptor signaling inhibits VEGF-induced endothelial cell survival, migration, *in vitro* sprouting and *in vivo* angiogenesis indicating that EphA receptor activation is necessary for VEGF-induced angiogenesis[98]. Ojima[104] and Chen *et al*[105] showed that soluble ephrin-A1-Fc can promote the tube formation and migration of HUVECs, while EphA2-Fc can antagonize the interaction between EphA2 and ephrin-A1 thereby reducing VEGF-induced endothelial cell migration and proliferation.

Vav-mediated signaling pathways

Studies have shown that *EFNA1* stimulates endothelial cell migration and assembly in culture[84,106], while EphA2 receptor-dependent endothelial cell migration and assembly require activation of Rac1 GTPase[107]. In addition, Vav2 and/or Vav3 are required for ephrin-A1-induced endothelial cell migration/assembly and Rac1 activation[107,108]. Therefore, Hunter *et al*[108] studied ephrin-A1 and Vav and found that when ephrin-A1 binds to EphA2, EphA2 is phosphorylated by tyrosine. Activated EphA2 can directly recruit Vav-GEFs through the SH2 region so that the Vav protein can be phosphorylated and activated directly or indirectly. In addition, by recruiting p85, EphA2 receptors can also up-regulate phosphatidylinositol-3,4,5-trisphosphate levels through the PH domain and enhance Vav-GEF activity. The activated Vav-GEFs subsequently increase Rac1-GTP levels and promote endothelial cell migration and angiogenesis.

eNOS-mediated signaling pathways

The promotion and inhibition of ephrin-A1 on the same signal pathway has also been observed in different cell or tumor types. It is well known that endothelial nitric oxide synthase (eNOS) and NO play a key role in endothelial cell migration and angiogenesis[109]. There is ample evidence that eNOS is mainly expressed in tumor vascular endothelial cells, and the NO produced by it plays a direct role in tumor angiogenesis induced by various angiogenic factors[110,111]. Hypoxia is one of the most common and important features in the tumor microenvironment which helps induce a variety of angiogenic factors[112].

Therefore, Song *et al*[113] explored the mechanism of *EFNA1* regulating angiogenesis by observing the effect of hypoxia on the expression and secretion of ephrin-A1 in tumor cells and the possible relationship between *EFNA1* and eNOS/NO in tumor angiogenesis. Studies have shown that the upregulation of membrane-bound ephrin-A1 induced by hypoxia may interact with EphA2 receptors on endothelial cells in the tumor microenvironment and induce eNOS phosphorylation and increase NO production through PI3K/AKT-dependent pathways thereby promoting tumor angiogenesis. These results show that the PI3K/AKT/eNOS signaling cascade may be a common pathway for hypoxia-induced ephrin-A1-dependent angiogenesis.

Rac-PAK signaling pathways

Studies have shown that in the vasculature, stimulating vascular smooth muscle cells with ephrin-A1 can inhibit cell proliferation through the inactivation of Rac1 and p21-activated kinase (PAK)[107]. Therefore, ephrin-A1 stimulation leads to inactivation of Rac1 and inhibition of cell proliferation in smooth muscle cells of the blood vessel wall leading to a loss of blood vessels. On the contrary, ephrin-A1 activates Rac1 and induces cell migration and blood vessel assembly of endothelial cells and promotes the sprouting and branching of new capillaries from existing blood vessels[107,114].

However, another study using rat vascular smooth muscle cells showed that ephrin-A1-mediated morphological changes are related to the inhibition of Rac1 and PAK1 activity and are antagonized by the expression of a constitutively-active Rac mutant[115]. The use of siRNA to inhibit the synthesis of Rac1 enhanced the ephrin-A1-induced inhibition of proliferation. Sphingosine-1-phosphate (S1P), a lipid mediator known to inhibit Rac activation in vascular smooth muscle cells, amplifies the effect of ephrin-A1. In conclusion, the authors emphasized the role of the Rac/PAK pathway in ephrin-A1-mediated cell proliferation inhibition. In this way, ephrin-A1 alone or in synergy with S1P can participate in vascular instability which is a prerequisite for angiogenesis[107,115].

TARGETED THERAPY OF *EFNA1* IN GASTROINTESTINAL CANCERS

EFNA1 is widely expressed in gastrointestinal cancer tissues, especially in highly aggressive cancer cells, suggesting that ephrin-A1 can be used as an important surface marker of gastrointestinal cancer cells and has potential diagnostic and prognostic value. The close relationship between *EFNA1* and the occurrence and development of gastrointestinal cancers has been confirmed which could represent a breakthrough in the search for new cancer treatment drugs.

Yang *et al*[61] found that *EFNA1* is involved in the resistance of ESCC cells to Photofrin-mediated photodynamic therapy (PDT). *EFNA1* is up-regulated in PDT-resistant ESCC cells and simultaneous incubation with oligomeric ephrin-A1 and soluble ephrin-A1 leads to significant resistance of ESCC cells to Photofrin-PDT[61]. These findings suggest that in ESCC, ephrin-A1 may be an attractive research direction and target for PDT resistance.

Studies have shown that in CRC, the combination of ephrin-A1-Fc and EphA2 can make EphA2 phosphorylated, and the complex formed moves into the cell and gradually degrades, thereby achieving the effect of inhibiting tumor progression[30]. In addition, the overexpression of EphA2 in CRC leads to resistance to chemotherapy[48] and the activation of EphA2 after ephrin-A1 treatment restores the efficacy of cetuximab against CRC cells[116]. These studies show that the combination of ephrin-A1 and cetuximab in tumor treatment provides a method for reversing CRC chemotherapy resistance but more preclinical and clinical studies are needed for confirmation.

Aiming at the specific binding between the G-H loop of ephrin-A1 and the ligand binding domain of EphA2[117], investigators have screened for small molecule antagonists that can selectively block Eph receptors thereby preventing the activation of EphA2[118]. For example, lithocholic acid (LCA), as a small molecule compound, can compete to hinder the binding of ephrin-A1 and EphA2. Its role is to interact with the G-H loop of ephrin-A1 and hinder the binding of ephrin-A1 to its receptor[119]. In addition, anti-EphA2 antibody and EphA2-Fc fusion protein have also been used to block the activation of EphA2,and significant anti-tumor angiogenesis effects have been observed *in vitro* and *in vivo*[120-122]. The activation of EphA2 receptors in tumor cells can block the activation of some important oncogenes[123,124] and ephrin-A1-Fc is currently the most widely used EphA2 receptor agonist. Duggineni *et al*[125] have designed and synthesized peptide molecules that can functionally bind to ephrin-A1 based on the characteristics of the ephrin-A1-binding domain. Such peptides can be expected to become new drugs for tumor suppression, targeted therapy and tumor imaging.

CONCLUSION

In summary, *EFNA1* plays an important role in the occurrence, development and angiogenesis of gastrointestinal tumors and its mechanism of promoting angiogenesis has also been studied in depth. However, the research on *EFNA1* and pancreatic cancer is still in the initial exploration stage. In future work, the clinical application of *EFNA1* in pancreatic cancer still needs more experiments and clinical studies to conduct a comprehensive verification of the system. In addition, the specific molecular mechanism of *EFNA1* in tumor progression is still poorly understood, and many aspects remain to be explored.

Rac/PAK, PI3K/AKT, ERK and other pathways are involved in tumor angiogenesis mediated by *EFNA1*/EphA2. *EFNA1* is expressed in tumor cells and tumor-related blood vessels. Current research mainly focuses on the function and mechanism of *EFNA1* in tumor cells and vascular endothelial cells. Tumors are dependent on angiogenesis but there are few reports on whether ephrin-A1 on the surface of tumor cells is related to EphA2 receptors on the surface of vascular endothelial cells or how they interact.

Ephrin-A1 has always been considered a GPI-coupled membrane-coupled ligand and its activation requires cell-to-cell contact. However, in 2008, Wykosky *et al*[126] found that ephrin-A1 can be secreted from malignant glioma cells and breast cancer cells into the cell supernatant and still retain its ability to activate EphA2. This suggests that ephrin-A1 derived from tumor cells not only acts on adjacent vascular endothelial cells to induce angiogenesis through a paracrine mechanism, but may also act on distant blood vessels to promote angiogenesis.

Hypoxia and inflammation are two major characteristics of the tumor microenvironment. Accompanied by many pathological processes, such as tumor occurrence, development, invasion, metastasis and angiogenesis, they also regulate the expression and function of tumor-related proteins. Studies have found that in solid tumors with hypoxia due to ischemia, the expression of *EFNA1* can be significantly upregulated[127]. Vihanto *et al*[128] also found, using a rat skin hypoxia model, that the expression of ephrin and Eph receptors in skin epithelial cells increases under hypoxic conditions. If it is possible to clarify the effect of hypoxia on the expression of *EFNA1* in gastrointestinal tumor cells, especially the effect on the secretion of soluble *EFNA1*, it may further reveal the function of *EFNA1* in gastrointestinal tumors.

Research on *EFNA1* in gastrointestinal tumor formation, tumor cell apoptosis and angiogenesis are still in its infancy. Further analysis and study of its signal transduction mechanisms in gastrointestinal tumors will help clarify the mechanism of tumor progression, invasion and metastasis, and provide a more reliable theoretical basis for tumor therapy.

FOOTNOTES

Author contributions: Chu LY collected data and wrote the manuscript; Huang BL and Huang XC collected data; Xu YW, Peng YH and Xie JJ supervised the work, revised the manuscript and contributed equally to this work.

Supported by the Natural Science Foundation of China, No. 81972801; the Guangdong Basic and Applied Basic Research Foundation, No. 2019A1515011873; the Medical Project of Science and Technology Planning of Shantou, No. 200605115266724; and the 2020 Li Ka Shing Foundation Cross-Disciplinary Research Grant, No. 2020LKSFG01B.

Conflict-of-interest statement: The authors have no conflicts of interest to declare.

Country/Territory of origin: China

ORCID number: Ling-Yu Chu 0000-0002-4682-0931; Bin-Liang Huang 0000-0001-6932-858X; Xu-Chun Huang 0000-0002-5999-3532; Yu-Hui Peng 0000-0002-1866-4679; Jian-Jun Xie 0000-0002-5141-5076; Yi-Wei Xu 0000-0002-8670-592X.

S-Editor: Wang LL
L-Editor: Filipodia
P-Editor: Wang LL

REFERENCES

1 **Ziyad S**, Iruela-Arispe ML. Molecular mechanisms of tumor angiogenesis. *Genes Cancer* 2011; **2**: 1085-1096 [PMID: 22866200 DOI: 10.1177/1947601911432334]
2 **Himanen JP**, Rajashankar KR, Lackmann M, Cowan CA, Henkemeyer M, Nikolov DB. Crystal structure of an Eph receptor-ephrin complex. *Nature* 2001; **414**: 933-938 [PMID: 11780069 DOI: 10.1038/414933a]
3 **Arvanitis D**, Davy A. Eph/ephrin signaling: networks. *Genes Dev* 2008; **22**: 416-429 [PMID: 18281458 DOI: 10.1101/gad.1630408]
4 **Cheng N**, Brantley DM, Liu H, Lin Q, Enriquez M, Gale N, Yancopoulos G, Cerretti DP, Daniel TO, Chen J. Blockade of EphA receptor tyrosine kinase activation inhibits vascular endothelial cell growth factor-induced angiogenesis. *Mol Cancer Res* 2002; **1**: 2-11 [PMID: 12496364]
5 **Ma TT**, Wang L, Wang JL, Liu YJ, Chen YC, He HJ, Song Y. Hypoxia-Induced Cleavage Of Soluble ephrinA1 From Cancer Cells Is Mediated By MMP-2 And Associates With Angiogenesis In Oral Squamous Cell Carcinoma. *Onco Targets Ther* 2019; **12**: 8491-8499 [PMID: 31686863 DOI: 10.2147/OTT.S213252]
6 **Brantley-Sieders DM**, Fang WB, Hwang Y, Hicks D, Chen J. Ephrin-A1 facilitates mammary tumor metastasis through an angiogenesis-dependent mechanism mediated by EphA receptor and vascular endothelial growth factor in mice. *Cancer Res* 2006; **66**: 10315-10324 [PMID: 17079451 DOI: 10.1158/0008-5472.CAN-06-1560]
7 **Genander M**, Frisén J. Ephrins and Eph receptors in stem cells and cancer. *Curr Opin Cell Biol* 2010; **22**: 611-616 [PMID: 20810264 DOI: 10.1016/j.ceb.2010.08.005]
8 **Khodayari N**, Mohammed KA, Lee H, Kaye F, Nasreen N. MicroRNA-302b targets Mcl-1 and inhibits cell proliferation and induces apoptosis in malignant pleural mesothelioma cells. *Am J Cancer Res* 2016; **6**: 1996-2009 [PMID: 27725905]
9 **Salem AF**, Gambini L, Udompholkul P, Baggio C, Pellecchia M. Therapeutic Targeting of Pancreatic Cancer *via* EphA2 Dimeric Agonistic Agents. *Pharmaceuticals (Basel)* 2020; **13** [PMID: 32397624 DOI: 10.3390/ph13050090]
10 **Hamaoka Y**, Negishi M, Katoh H. EphA2 is a key effector of the MEK/ERK/RSK pathway regulating glioblastoma cell proliferation. *Cell Signal* 2016; **28**: 937-945 [PMID: 27132626 DOI: 10.1016/j.cellsig.2016.04.009]
11 **Miao H**, Gale NW, Guo H, Qian J, Petty A, Kaspar J, Murphy AJ, Valenzuela DM, Yancopoulos G, Hambardzumyan D, Lathia JD, Rich JN, Lee J, Wang B. EphA2 promotes infiltrative invasion of glioma stem cells *in vivo* through cross-talk with Akt and regulates stem cell properties. *Oncogene* 2015; **34**: 558-567 [PMID: 24488013 DOI: 10.1038/onc.2013.590]
12 **Miyazaki T**, Kato H, Fukuchi M, Nakajima M, Kuwano H. EphA2 overexpression correlates with poor prognosis in esophageal squamous cell carcinoma. *Int J Cancer* 2003; **103**: 657-663 [PMID: 12494475 DOI: 10.1002/ijc.10860]
13 **Hao Y**, Li G. Role of *EFNA1* in tumorigenesis and prospects for cancer therapy. *Biomed Pharmacother* 2020; **130**: 110567 [PMID: 32745910 DOI: 10.1016/j.biopha.2020.110567]
14 **Ieguchi K**. Eph as a target in inflammation. *Endocr Metab Immune Disord Drug Targets* 2015; **15**: 119-128 [PMID: 25772170 DOI: 10.2174/1871530315666150316121302]
15 **Shi L**, Itoh F, Itoh S, Takahashi S, Yamamoto M, Kato M. Ephrin-A1 promotes the malignant progression of intestinal tumors in Apc(min/+) mice. *Oncogene* 2008; **27**: 3265-3273 [PMID: 18246128 DOI: 10.1038/sj.onc.1210992]
16 **Hong HN**, Won YJ, Shim JH, Kim HJ, Han SH, Kim BS, Kim HS. Cancer-associated fibroblasts promote gastric tumorigenesis through EphA2 activation in a ligand-independent manner. *J Cancer Res Clin Oncol* 2018; **144**: 1649-1663 [DOI: 10.1007/s00432-018-2683-8]
17 **Luo H**, Wan X, Wu Y, Wu J. Cross-linking of EphB6 resulting in signal transduction and apoptosis in Jurkat cells. *J Immunol* 2001; **167**: 1362-1370 [PMID: 11466354 DOI: 10.4049/jimmunol.167.3.1362]
18 **Ferluga S**, Hantgan R, Goldgur Y, Himanen JP, Nikolov DB, Debinski W. Biological and structural characterization of glycosylation on ephrin-A1, a preferred ligand for EphA2 receptor tyrosine kinase. *J Biol Chem* 2013; **288**: 18448-18457 [PMID: 23661698 DOI: 10.1074/jbc.M113.464008]
19 **Kullander K**, Klein R. Mechanisms and functions of Eph and ephrin signalling. *Nat Rev Mol Cell Biol* 2002; **3**: 475-486 [PMID: 12094214 DOI: 10.1038/nrm856]
20 **Wykosky J**, Debinski W. The EphA2 receptor and ephrinA1 Ligand in solid tumors: function and therapeutic targeting. *Mol Cancer Res* 2008; **6**: 1795-1806 [PMID: 19074825 DOI: 10.1158/1541-7786.MCR-08-0244]
21 **Holzman LB**, Marks RM, Dixit VM. A novel immediate-early response gene of endothelium is induced by cytokines and encodes a secreted protein. *Mol Cell Biol* 1990; **10**: 5830-5838 [PMID: 2233719 DOI: 10.1128/mcb.10.11.5830-5838.1990]
22 **Lindberg RA**, Hunter T. cDNA cloning and characterization of eck, an epithelial cell receptor protein-tyrosine kinase in the eph/elk family of protein kinases. *Mol Cell Biol* 1990; **10**: 6316-6324 [PMID: 2174105 DOI: 10.1128/mcb.10.12.6316-6324.1990]
23 **Xiao T**, Xiao Y, Wang W, Tang YY, Xiao Z, Su M. Targeting EphA2 in cancer. *J Hematol Oncol* 2020; **13**: 114 [DOI: 10.1186/s13045-020-00944-9]
24 **Daniel TO**, Stein E, Cerretti DP, St John PL, Robert B, Abrahamson DR. ELK and LERK-2 in developing kidney and microvascular endothelial assembly. *Kidney Int Suppl* 1996; **57**: S73-S81 [PMID: 8941926]
25 **Luxey M**, Jungas T, Laussu J, Audouard C, Garces A, Davy A. Eph:ephrin-B1 forward signaling controls fasciculation of sensory and motor axons. *Dev Biol* 2013; **383**: 264-274 [PMID: 24056079 DOI: 10.1016/j.ydbio.2013.09.010]
26 **Allen-Sharpley MR**, Cramer KS. Coordinated Eph-ephrin signaling guides migration and axon targeting in the avian auditory system. *Neural Dev* 2012; **7**: 29 [PMID: 22908944 DOI: 10.1186/1749-8104-7-29]
27 **Bocharov EV**, Mayzel ML, Volynsky PE, Goncharuk MV, Ermolyuk YS, Schulga AA, Artemenko EO, Efremov RG, Arseniev AS. Spatial structure and pH-dependent conformational diversity of dimeric transmembrane domain of the receptor tyrosine kinase EphA1. *J Biol Chem* 2008; **283**: 29385-29395 [PMID: 18728013 DOI: 10.1074/jbc.M803089200]
28 **Hafner C**, Schmitz G, Meyer S, Bataille F, Hau P, Langmann T, Dietmaier W, Landthaler M, Vogt T. Differential gene expression of Eph receptors and ephrins in benign human tissues and cancers. *Clin Chem* 2004; **50**: 490-499 [PMID:

14726470 DOI: 10.1373/clinchem.2003.026849]
29 **Ieguchi K**, Maru Y. Roles of EphA1/A2 and ephrin-A1 in cancer. *Cancer Sci* 2019; **110**: 841-848 [PMID: 30657619 DOI: 10.1111/cas.13942]
30 **Nakamura R**, Kataoka H, Sato N, Kanamori M, Ihara M, Igarashi H, Ravshanov S, Wang YJ, Li ZY, Shimamura T, Kobayashi T, Konno H, Shinmura K, Tanaka M, Sugimura H. EPHA2/*EFNA1* expression in human gastric cancer. *Cancer Sci* 2005; **96**: 42-47 [PMID: 15649254 DOI: 10.1111/j.1349-7006.2005.00007.x]
31 **Katoh Y**, Katoh M. Comparative integromics on Ephrin family. *Oncol Rep* 2006; **15**: 1391-1395 [PMID: 16596216]
32 **Miyazaki K**, Inokuchi M, Takagi Y, Kato K, Kojima K, Sugihara K. EphA4 is a prognostic factor in gastric cancer. *BMC Clin Pathol* 2013; **13**: 19 [PMID: 23738943 DOI: 10.1186/1472-6890-13-19]
33 **Yuan WJ**, Ge J, Chen ZK, Wu SB, Shen H, Yang P, Hu B, Zhang GW, Chen ZH. Over-expression of EphA2 and EphrinA-1 in human gastric adenocarcinoma and its prognostic value for postoperative patients. *Dig Dis Sci* 2009; **54**: 2410-2417 [PMID: 19101799 DOI: 10.1007/s10620-008-0649-4]
34 **Li Y**, Nie Y, Cao J, Tu S, Lin Y, Du Y, Li Y. G-A variant in miR-200c binding site of *EFNA1* alters susceptibility to gastric cancer. *Mol Carcinog* 2014; **53**: 219-229 [PMID: 23065816 DOI: 10.1002/mc.21966]
35 **Zhu H**, Yang M, Zhang H, Chen X, Yang X, Zhang C, Qin Q, Cheng H, Sun X. Genome-wide association pathway analysis to identify candidate single nucleotide polymorphisms and molecular pathways for gastric adenocarcinoma. *Tumour Biol* 2015; **36**: 5635-5639 [PMID: 25687184 DOI: 10.1007/s13277-015-3236-2]
36 **Lee JH**, Kim Y, Choi JW, Kim YS. Genetic variants and risk of gastric cancer: a pathway analysis of a genome-wide association study. *Springerplus* 2015; **4**: 215 [PMID: 25992311 DOI: 10.1186/s40064-015-1005-8]
37 **Zhuo W**, Liu Y, Li S, Guo D, Sun Q, Jin J, Rao X, Li M, Sun M, Jiang M, Xu Y, Teng L, Jin Y, Si J, Liu W, Kang Y, Zhou T. Long Noncoding RNA GMAN, Up-regulated in Gastric Cancer Tissues, Is Associated With Metastasis in Patients and Promotes Translation of Ephrin A1 by Competitively Binding GMAN-AS. *Gastroenterology* 2019; **156**: 676-691.e11 [PMID: 30445010 DOI: 10.1053/j.gastro.2018.10.054]
38 **Bennett BD**, Wang Z, Kuang WJ, Wang A, Groopman JE, Goeddel DV, Scadden DT. Cloning and characterization of HTK, a novel transmembrane tyrosine kinase of the EPH subfamily. *J Biol Chem* 1994; **269**: 14211-14218 [PMID: 8188704]
39 **Yan SX**, Wang DG, Chen YJ, Liu HC, Xu YC. Expression of EphA2 and Ephrin a1 in gastric cancer tissues with helicobacter pylori infection and its relationship with distant metastasis. *Medicine and Philosophy* 2016; **37**: 63-66 [DOI: 10.1046/j.1443-9573.2002.00078_3_2.x]
40 **Kiyokawa E**, Takai S, Tanaka M, Iwase T, Suzuki M, Xiang YY, Naito Y, Yamada K, Sugimura H, Kino I. Overexpression of ERK, an EPH family receptor protein tyrosine kinase, in various human tumors. *Cancer Res* 1994; **54**: 3645-3650 [PMID: 8033077]
41 **Coffman KT**, Hu M, Carles-Kinch K, Tice D, Donacki N, Munyon K, Kifle G, Woods R, Langermann S, Kiener PA, Kinch MS. Differential EphA2 epitope display on normal *vs* malignant cells. *Cancer Res* 2003; **63**: 7907-7912 [PMID: 14633720]
42 **Potla L**, Boghaert ER, Armellino D, Frost P, Damle NK. Reduced expression of EphrinA1 (*EFNA1*) inhibits three-dimensional growth of HT29 colon carcinoma cells. *Cancer Lett* 2002; **175**: 187-195 [PMID: 11741747 DOI: 10.1016/s0304-3835(01)00613-9]
43 **Shi ZZ**, Zhang YM, Shang L, Hao JJ, Zhang TT, Wang BS, Liang JW, Chen X, Zhang Y, Wang GQ, Wang MR. Genomic profiling of rectal adenoma and carcinoma by array-based comparative genomic hybridization. *BMC Med Genomics* 2012; **5**: 52 [PMID: 23158542 DOI: 10.1186/1755-8794-5-52]
44 **Mao YY**, Jing FY, Jin MJ, Li YJ, Ding Y, Guo J, Wang FJ, Jiang LF, Chen K. rs12904 polymorphism in the 3'UTR of *EFNA1* is associated with colorectal cancer susceptibility in a Chinese population. *Asian Pac J Cancer Prev* 2013; 14: 5037-5041 [DOI: 10.7314/apjcp.2013.14.9.5037]
45 **Simonian M**, Mosallaei M, Khosravi S, Salehi R. rs12904 polymorphism in the 3'-untranslated region of ephrin A1 Ligand and the risk of sporadic colorectal cancer in the Iranian population. *J Cancer Res Ther* 2019; **15**: 15-19 [PMID: 30880748 DOI: 10.4103/jcrt.JCRT_766_17]
46 **Rosenberg IM**, Göke M, Kanai M, Reinecker HC, Podolsky DK. Epithelial cell kinase-B61: an autocrine loop modulating intestinal epithelial migration and barrier function. *Am J Physiol* 1997; **273**: G824-G832 [PMID: 9357823 DOI: 10.1152/ajpgi.1997.273.4.G824]
47 **Kataoka H**, Igarashi H, Kanamori M, Ihara M, Wang JD, Wang YJ, Li ZY, Shimamura T, Kobayashi T, Maruyama K, Nakamura T, Arai H, Kajimura M, Hanai H, Tanaka M, Sugimura H. Correlation of EPHA2 overexpression with high microvessel count in human primary colorectal cancer. *Cancer Sci* 2004; **95**: 136-141 [PMID: 14965363 DOI: 10.1111/j.1349-7006.2004.tb03194.x]
48 **De Robertis M**, Loiacono L, Fusilli C, Poeta ML, Mazza T, Sanchez M, Marchionni L, Signori E, Lamorte G, Vescovi AL, Garcia-Foncillas J, Fazio VM. Dysregulation of EGFR Pathway in EphA2 Cell Subpopulation Significantly Associates with Poor Prognosis in Colorectal Cancer. *Clin Cancer Res* 2017; **23**: 159-170 [PMID: 27401248 DOI: 10.1158/1078-0432.CCR-16-0709]
49 **Yamamoto H**, Tei M, Uemura M, Takemasa I, Uemura Y, Murata K, Fukunaga M, Ohue M, Ohnishi T, Ikeda K, Kato T, Okamura S, Ikenaga M, Haraguchi N, Nishimura J, Mizushima T, Mimori K, Doki Y, Mori M. Ephrin-A1 mRNA is associated with poor prognosis of colorectal cancer. *Int J Oncol* 2013; **42**: 549-555 [PMID: 23258614 DOI: 10.3892/ijo.2012.1750]
50 **Lips EH**, van Eijk R, de Graaf EJ, Oosting J, de Miranda NF, Karsten T, van de Velde CJ, Eilers PH, Tollenaar RA, van Wezel T, Morreau H. Integrating chromosomal aberrations and gene expression profiles to dissect rectal tumorigenesis. *BMC Cancer* 2008; **8**: 314 [PMID: 18959792 DOI: 10.1186/1471-2407-8-314]
51 **Xiong Y**, Li KX, Wei H, Jiao L, Yu SY, Zeng L. Eph/ephrin signalling serves a bidirectional role in lipopolysaccharide-induced intestinal injury. *Mol Med Rep* 2018; **18**: 2171-2181 [DOI: 10.3892/mmr.2018.9169]
52 **Brantley-Sieders DM**, Chen J. Eph receptor tyrosine kinases in angiogenesis: from development to disease. *Angiogenesis* 2004; **7**: 17-28 [PMID: 15302992 DOI: 10.1023/B:AGEN.0000037340.33788.87]

53 **Sepehri Z**, Kiani Z, Kohan F, Alavian SM, Ghavami S. Toll like receptor 4 and hepatocellular carcinoma; A systematic review. *Life Sci* 2017; **179**: 80-87 [PMID: 28472619 DOI: 10.1016/j.lfs.2017.04.025]

54 **Zhang G**, Zhang SJ, Zhao YF, Wu Y, Li Z, Wang JX. Expression and clinical significance of Ephrin-A1 in primary hepatocellular carcinoma. *Zhonghua Waikexue Zazhi* 2007; **45**: 499-502 [PMID: 17686315]

55 **Wada H**, Yamamoto H, Kim C, Uemura M, Akita H, Tomimaru Y, Hama N, Kawamoto K, Kobayashi S, Eguchi H, Umeshita K, Doki Y, Mori M, Nagano H. Association between ephrin-A1 mRNA expression and poor prognosis after hepatectomy to treat hepatocellular carcinoma. *Int J Oncol* 2014; **45**: 1051-1058 [PMID: 24969670 DOI: 10.3892/ijo.2014.2519]

56 **Yu HT**, Guo PY, Xie XZ, Chen G. The effect of regulated EphA1/EphrinA1 signaling axis on endothelial progenitor cells to promote their angiogenesis potency in hepatocellular carcinoma. *Wenzhou Yixueyuan Xuebao* 2019; **49**: 791-796 [DOI: 10.1158/1538-7445.am2018-101]

57 **Iida H**, Honda M, Kawai HF, Yamashita T, Shirota Y, Wang BC, Miao H, Kaneko S. Ephrin-A1 expression contributes to the malignant characteristics of {alpha}-fetoprotein producing hepatocellular carcinoma. *Gut* 2005; **54**: 843-851 [PMID: 15888795 DOI: 10.1136/gut.2004.049486]

58 **Cui XD**, Lee MJ, Yu GR, Kim IH, Yu HC, Song EY, Kim DG. *EFNA1* Ligand and its receptor EphA2: potential biomarkers for hepatocellular carcinoma. *Int J Cancer* 2010; **126**: 940-949 [PMID: 19642143 DOI: 10.1002/ijc.24798]

59 **Xu F**, Zhong W, Li J, Shanshen Z, Cui J, Nesland JM, Suo Z. Predictive value of EphA2 and EphrinA-1 expression in oesophageal squamous cell carcinoma. *Anticancer Res* 2005; **25**: 2943-2950 [PMID: 16080548]

60 **Chen FF**, Zhang SR, Peng H, Chen YZ, Cui XB. Integrative genomics analysis of hub genes and their relationship with prognosis and signaling pathways in esophageal squamous cell carcinoma. *Mol Med Rep* 2019; **20**: 3649-3660 [PMID: 31485619 DOI: 10.3892/mmr.2019.10608]

61 **Yang PW**, Chiang TH, Hsieh CY, Huang YC, Wong LF, Hung MC, Tsai JC, Lee JM. The effect of ephrin-A1 on resistance to Photofrin-mediated photodynamic therapy in esophageal squamous cell carcinoma cells. *Lasers Med Sci* 2015; **30**: 2353-2361 [PMID: 26450615 DOI: 10.1007/s10103-015-1812-8]

62 **Wykosky J**, Gibo DM, Stanton C, Debinski W. EphA2 as a novel molecular marker and target in glioblastoma multiforme. *Mol Cancer Res* 2005; **3**: 541-551 [PMID: 16254188 DOI: 10.1158/1541-7786.MCR-05-0056]

63 **Miao H**, Wei BR, Peehl DM, Li Q, Alexandrou T, Schelling JR, Rhim JS, Sedor JR, Burnett E, Wang B. Activation of EphA receptor tyrosine kinase inhibits the Ras/MAPK pathway. *Nat Cell Biol* 2001; **3**: 527-530 [PMID: 11331884 DOI: 10.1038/35074604]

64 **Easty DJ**, Hill SP, Hsu MY, Fallowfield ME, Florenes VA, Herlyn M, Bennett DC. Up-regulation of ephrin-A1 during melanoma progression. *Int J Cancer* 1999; **84**: 494-501 [PMID: 10502726 DOI: 10.1002/(sici)1097-0215(19991022)84:5<]

65 **Tuzi NL**, Gullick WJ. eph, the largest known family of putative growth factor receptors. *Br J Cancer* 1994; **69**: 417-421 [PMID: 8123468 DOI: 10.1038/bjc.1994.77]

66 **Davy A**, Gale NW, Murray EW, Klinghoffer RA, Soriano P, Feuerstein C, Robbins SM. Compartmentalized signaling by GPI-anchored ephrin-A5 requires the Fyn tyrosine kinase to regulate cellular adhesion. *Genes Dev* 1999; **13**: 3125-3135 [PMID: 10601038 DOI: 10.1101/gad.13.23.3125]

67 **Huai J**, Drescher U. An ephrin-A-dependent signaling pathway controls integrin function and is linked to the tyrosine phosphorylation of a 120-kDa protein. *J Biol Chem* 2001; **276**: 6689-6694 [DOI: 10.1074/jbc.m008127200]

68 **Pasquale EB**. Eph receptor signalling casts a wide net on cell behaviour. *Nat Rev Mol Cell Biol* 2005; **6**: 462-475 [PMID: 15928710 DOI: 10.1038/nrm1662]

69 **Orsulic S**, Kemler R. Expression of Eph receptors and ephrins is differentially regulated by E-cadherin. *J Cell Sci* 2000; **113**: 1793-1802 [PMID: 10769210]

70 **Lu C**, Shahzad MM, Wang H, Landen CN, Kim SW, Allen J, Nick AM, Jennings N, Kinch MS, Bar-Eli M, Sood AK. EphA2 overexpression promotes ovarian cancer growth. *Cancer Biol Ther* 2008; **7**: 1098-1103 [PMID: 18443431 DOI: 10.4161/cbt.7.7.6168]

71 **Zantek ND**, Azimi M, Fedor-Chaiken M, Wang B, Brackenbury R, Kinch MS. E-cadherin regulates the function of the EphA2 receptor tyrosine kinase. *Cell Growth Differ* 1999; **10**: 629-638 [PMID: 10511313]

72 **Surawska H**, Ma PC, Salgia R. The role of ephrins and Eph receptors in cancer. *Cytokine Growth Factor Rev* 2004; **15**: 419-433 [PMID: 15561600 DOI: 10.1016/j.cytogfr.2004.09.002]

73 **Dodelet VC**, Pasquale EB. Eph receptors and ephrin ligands: embryogenesis to tumorigenesis. *Oncogene* 2000; **19**: 5614-5619 [PMID: 11114742 DOI: 10.1038/sj.onc.1203856]

74 **Chen J**, Zhuang G, Frieden L, Debinski W. Eph receptors and Ephrins in cancer: common themes and controversies. *Cancer Res* 2008; **68**: 10031-10033 [PMID: 19074866 DOI: 10.1158/0008-5472.CAN-08-3010]

75 **Wimmer-Kleikamp SH**, Lackmann M. Eph-modulated cell morphology, adhesion and motility in carcinogenesis. *IUBMB Life* 2005; **57**: 421-431 [PMID: 16012051 DOI: 10.1080/15216540500138337]

76 **Ieguchi K**, Tomita T, Omori T, Komatsu A, Deguchi A, Masuda J, Duffy SL, Coulthard MG, Boyd A, Maru Y. ADAM12-cleaved ephrin-A1 contributes to lung metastasis. *Oncogene* 2014; **33**: 2179-2190 [PMID: 23686306 DOI: 10.1038/onc.2013.180]

77 **Miao H**, Burnett E, Kinch M, Simon E, Wang B. Activation of EphA2 kinase suppresses integrin function and causes focal-adhesion-kinase dephosphorylation. *Nat Cell Biol* 2000; **2**: 62-69 [PMID: 10655584 DOI: 10.1038/35000008]

78 **Hynes RO**. Integrins: versatility, modulation, and signaling in cell adhesion. *Cell* 1992; **69**: 11-25 [PMID: 1555235 DOI: 10.1016/0092-8674(92)90115-s]

79 **Davy A**, Robbins SM. Ephrin-A5 modulates cell adhesion and morphology in an integrin-dependent manner. *EMBO J* 2000; **19**: 5396-5405 [DOI: 10.1093/emboj/19.20.5396]

80 **Meyer S**, Hafner C, Guba M, Flegel S, Geissler EK, Becker B, Koehl GE, Ors öE, Landthaler M, Vogt T. Ephrin-B2 overexpression enhances integrin-mediated ECM-attachment and migration of B16 melanoma cells. *Int J Oncol* 2005; **27**: 1197-1206 [DOI: 10.3892/ijo.27.5.1197]

81 **Huynh-Do U**, Vindis C, Liu H, Cerretti DP, McGrew JT, Enriquez M, Chen J, Daniel TO. Ephrin-B1 transduces signals

to activate integrin-mediated migration, attachment and angiogenesis. *J Cell Sci* 2002; **115**: 3073-3081 [PMID: 12118063]

82 **Folkman J**. Role of angiogenesis in tumor growth and metastasis. *Semin Oncol* 2002; **29**: 15-18 [PMID: 12516034 DOI: 10.1053/sonc.2002.37263]

83 **Carmeliet P**, Jain RK. Molecular mechanisms and clinical applications of angiogenesis. *Nature* 2011; **473**: 298-307 [PMID: 21593862 DOI: 10.1038/nature10144]

84 **Ogawa K**, Pasqualini R, Lindberg RA, Kain R, Freeman AL, Pasquale EB. The ephrin-A1 Ligand and its receptor, EphA2, are expressed during tumor neovascularization. *Oncogene* 2000; **19**: 6043-6052 [PMID: 11146556 DOI: 10.1038/sj.onc.1204004]

85 **Pandey A**, Shao H, Marks RM, Polverini PJ, Dixit VM. Role of B61, the ligand for the Eck receptor tyrosine kinase, in TNF-alpha-induced angiogenesis. *Science* 1995; **268**: 567-569 [PMID: 7536959 DOI: 10.1126/science.7536959]

86 **Pasquale EB**. Eph-ephrin bidirectional signaling in physiology and disease. *Cell* 2008; **133**: 38-52 [PMID: 18394988 DOI: 10.1016/j.cell.2008.03.011]

87 **Brantley-Sieders DM**, Fang WB, Hicks DJ, Zhuang G, Shyr Y, Chen J. Impaired tumor microenvironment in EphA2-deficient mice inhibits tumor angiogenesis and metastatic progression. *FASEB J* 2005; **19**: 1884-1886 [PMID: 16166198 DOI: 10.1096/fj.05-4038fje]

88 **Ieguchi K**, Tomita T, Takao T, Omori T, Mishima T, Shimizu I, Tognolini M, Lodola A, Tsunoda T, Kobayashi S, Wada S, Maru Y. Analysis of ADAM12-Mediated Ephrin-A1 Cleavage and Its Biological Functions. *Int J Mol Sci* 2021; **22** [PMID: 33804570 DOI: 10.3390/ijms22052480]

89 **Liu H**, Guo JW, Liu JH, Zuo LF. EphA2/EphrinA1 expressions in human gastric carcinoma and their relationship with angiogenesis. *ACTA academiae medicinae militaris tertiae* 2008; **30**: 2183-2186 [DOI: 10.1007/bf02911180]

90 **Chu M**, Zhang C. Inhibition of angiogenesis by leflunomide *via* targeting the soluble ephrin-A1/EphA2 system in bladder cancer. *Sci Rep* 2018; **8**: 1539 [PMID: 29367676 DOI: 10.1038/s41598-018-19788-y]

91 **Tang FY**, Chiang EP, Shih CJ. Green tea catechin inhibits ephrin-A1-mediated cell migration and angiogenesis of human umbilical vein endothelial cells. *J Nutr Biochem* 2007; **18**: 391-399 [PMID: 17049832 DOI: 10.1016/j.jnutbio.2006.07.004]

92 **Vaught D**, Brantley-Sieders DM, Chen J. Eph receptors in breast cancer: roles in tumor promotion and tumor suppression. *Breast Cancer Res* 2008; **10**: 217 [PMID: 19144211 DOI: 10.1186/bcr2207]

93 **Saik JE**, Gould DJ, Keswani AH, Dickinson ME, West JL. Biomimetic hydrogels with immobilized ephrinA1 for therapeutic angiogenesis. *Biomacromolecules* 2011; **12**: 2715-2722 [PMID: 21639150 DOI: 10.1021/bm200492h]

94 **Moon JJ**, Lee SH, West JL. Synthetic biomimetic hydrogels incorporated with ephrin-A1 for therapeutic angiogenesis. *Biomacromolecules* 2007; **8**: 42-49 [PMID: 17206786 DOI: 10.1021/bm060452p]

95 **Pratt RL**, Kinch MS. Activation of the EphA2 tyrosine kinase stimulates the MAP/ERK kinase signaling cascade. *Oncogene* 2002; **21**: 7690-7699 [PMID: 12400011 DOI: 10.1038/sj.onc.1205758]

96 **Boyle EM**, Jr. , Kovacich JC, Canty TG, Jr., Morgan EN, Chi E, Verrier ED, Pohlman TH. Inhibition of nuclear factor-kappa B nuclear localization reduces human E-selectin expression and the systemic inflammatory response. *Circulation* 1998; **98**: II282-288 [DOI: 10.1046/j.1440-1797.2000.005003a105.x]

97 **Yoshida S**, Ono M, Shono T, Izumi H, Ishibashi T, Suzuki H, Kuwano M. Involvement of interleukin-8, vascular endothelial growth factor, and basic fibroblast growth factor in tumor necrosis factor alpha-dependent angiogenesis. *Mol Cell Biol* 1997; **17**: 4015-4023 [PMID: 9199336 DOI: 10.1128/MCB.17.7.4015]

98 **Cheng N**, Brantley DM, Chen J. The ephrins and Eph receptors in angiogenesis. *Cytokine Growth Factor Rev* 2002; **13**: 75-85 [PMID: 11750881 DOI: 10.1016/s1359-6101(01)00031-4]

99 **Cheng N**, Chen J. Tumor necrosis factor-alpha induction of endothelial ephrin A1 expression is mediated by a p38 MAPK- and SAPK/JNK-dependent but nuclear factor-kappa B-independent mechanism. *J Biol Chem* 2001; **276**: 13771-13777 [PMID: 11278471 DOI: 10.1074/jbc.M009147200]

100 **Shi CS**, Leonardi A, Kyriakis J, Siebenlist U, Kehrl JH. TNF-mediated activation of the stress-activated protein kinase pathway: TNF receptor-associated factor 2 recruits and activates germinal center kinase related. *J Immunol* 1999; **163**: 3279-3285 [PMID: 10477597]

101 **Rousseau S**, Houle F, Landry J, Huot J. p38 MAP kinase activation by vascular endothelial growth factor mediates actin reorganization and cell migration in human endothelial cells. *Oncogene* 1997; **15**: 2169-2177 [PMID: 9393975 DOI: 10.1038/sj.onc.1201380]

102 **Hess AR**, Margaryan NV, Seftor EA, Hendrix MJ. Deciphering the signaling events that promote melanoma tumor cell vasculogenic mimicry and their link to embryonic vasculogenesis: role of the Eph receptors. *Dev Dyn* 2007; **236**: 3283-3296 [PMID: 17557303 DOI: 10.1002/dvdy.21190]

103 **Ivanov AI**, Steiner AA, Scheck AC, Romanovsky AA. Expression of Eph receptors and their ligands, ephrins, during lipopolysaccharide fever in rats. *Physiol Genomics* 2005; **21**: 152-160 [PMID: 15671251 DOI: 10.1152/physiolgenomics.00043.2004]

104 **Ojima T**, Takagi H, Suzuma K, Oh H, Suzuma I, Ohashi H, Watanabe D, Suganami E, Murakami T, Kurimoto M, Honda Y, Yoshimura N. EphrinA1 inhibits vascular endothelial growth factor-induced intracellular signaling and suppresses retinal neovascularization and blood-retinal barrier breakdown. *Am J Pathol* 2006; **168**: 331-339 [PMID: 16400034 DOI: 10.2353/ajpath.2006.050435]

105 **Chen J**, Hicks D, Brantley-Sieders D, Cheng N, McCollum GW, Qi-Werdich X, Penn J. Inhibition of retinal neovascularization by soluble EphA2 receptor. *Exp Eye Res* 2006; **82**: 664-673 [PMID: 16359662 DOI: 10.1016/j.exer.2005.09.004]

106 **Bergers G**, Benjamin LE. Tumorigenesis and the angiogenic switch. *Nat Rev Cancer* 2003; **3**: 401-410 [PMID: 12778130 DOI: 10.1038/nrc1093]

107 **Brantley-Sieders DM**, Caughron J, Hicks D, Pozzi A, Ruiz JC, Chen J. EphA2 receptor tyrosine kinase regulates endothelial cell migration and vascular assembly through phosphoinositide 3-kinase-mediated Rac1 GTPase activation. *J Cell Sci* 2004; **117**: 2037-2049 [PMID: 15054110 DOI: 10.1242/jcs.01061]

108 **Hunter SG**, Zhuang G, Brantley-Sieders D, Swat W, Cowan CW, Chen J. Essential role of Vav family guanine nucleotide exchange factors in EphA receptor-mediated angiogenesis. *Mol Cell Biol* 2006; **26**: 4830-4842 [PMID: 16782872 DOI: 10.1128/MCB.02215-05]

109 **Fukumura D**, Gohongi T, Kadambi A, Izumi Y, Ang J, Yun CO, Buerk DG, Huang PL, Jain RK. Predominant role of endothelial nitric oxide synthase in vascular endothelial growth factor-induced angiogenesis and vascular permeability. *Proc Natl Acad Sci U S A* 2001; **98**: 2604-2609 [PMID: 11226286 DOI: 10.1073/pnas.041359198]

110 **Gallo O**, Masini E, Morbidelli L, Franchi A, Fini-Storchi I, Vergari WA, Ziche M. Role of nitric oxide in angiogenesis and tumor progression in head and neck cancer. *J Natl Cancer Inst* 1998; **90**: 587-596 [PMID: 9554441 DOI: 10.1093/jnci/90.8.587]

111 **Fukumura D**, Kashiwagi SS, Jain RK. The role of nitric oxide in tumour progression. *Nat Rev Cancer* 2006; **6**: 521-34 [DOI: 10.1038/nrc1910]

112 **Acker T**, Plate KH. Role of hypoxia in tumor angiogenesis-molecular and cellular angiogenic crosstalk. *Cell Tissue Res* 2003; **314**: 145-155 [PMID: 12898211 DOI: 10.1007/s00441-003-0763-8]

113 **Song Y**, Zhao XP, Song K, Shang ZJ. Ephrin-A1 is up-regulated by hypoxia in cancer cells and promotes angiogenesis of HUVECs through a coordinated cross-talk with eNOS. *PLoS One* 2013; **8**: e74464 [PMID: 24040255 DOI: 10.1371/journal.pone.0074464]

114 **Zhuang G**, Hunter S, Hwang Y, Chen J. Regulation of EphA2 receptor endocytosis by SHIP2 Lipid phosphatase *via* phosphatidylinositol 3-Kinase-dependent Rac1 activation. *J Biol Chem* 2007; **282**: 2683-2694 [PMID: 17135240 DOI: 10.1074/jbc.M608509200]

115 **Deroanne C**, Vouret-Craviari V, Wang B, Pouysségur J. EphrinA1 inactivates integrin-mediated vascular smooth muscle cell spreading *via* the Rac/PAK pathway. *J Cell Sci* 2003; **116**: 1367-1376 [PMID: 12615978 DOI: 10.1242/jcs.00308]

116 **Cuyàs E**, Queralt B, Martin-Castillo B, Bosch-Barrera J, Menendez JA. EphA2 receptor activation with ephrin-A1 Ligand restores cetuximab efficacy in NRAS-mutant colorectal cancer cells. *Oncol Rep* 2017; **38**: 263-270 [PMID: 28560458 DOI: 10.3892/or.2017.5682]

117 **Himanen JP**, Goldgur Y, Miao H, Myshkin E, Guo H, Buck M, Nguyen M, Rajashankar KR, Wang B, Nikolov DB. Ligand recognition by A-class Eph receptors: crystal structures of the EphA2 Ligand-binding domain and the EphA2/ephrin-A1 complex. *EMBO Rep* 2009; **10**: 722-728 [PMID: 19525919 DOI: 10.1038/embor.2009.91]

118 **Noberini R**, Koolpe M, Peddibhotla S, Dahl R, Su Y, Cosford ND, Roth GP, Pasquale EB. Small molecules can selectively inhibit ephrin binding to the EphA4 and EphA2 receptors. *J Biol Chem* 2008; **283**: 29461-29472 [PMID: 18728010 DOI: 10.1074/jbc.M804103200]

119 **Giorgio C**, Hassan Mohamed I, Flammini L, Barocelli E, Incerti M, Lodola A, Tognolini M. Lithocholic acid is an Eph-ephrin ligand interfering with Eph-kinase activation. *PLoS One* 2011; **6**: e18128 [PMID: 21479221 DOI: 10.1371/journal.pone.0018128]

120 **Kiewlich D**, Zhang J, Gross C, Xia W, Larsen B, Cobb RR, Biroc S, Gu JM, Sato T, Light DR, Heitner T, Willuda J, Vogel D, Monteclaro F, Citkowicz A, Roffler SR, Zajchowski DA. Anti-EphA2 antibodies decrease EphA2 protein levels in murine CT26 colorectal and human MDA-231 breast tumors but do not inhibit tumor growth. *Neoplasia* 2006; **8**: 18-30 [DOI: 10.1593/neo.05544]

121 **Brantley DM**, Cheng N, Thompson EJ, Lin Q, Brekken RA, Thorpe PE, Muraoka RS, Cerretti DP, Pozzi A, Jackson D, Lin C, Chen J. Soluble Eph A receptors inhibit tumor angiogenesis and progression in vivo. *Oncogene* 2002; **21**: 7011-7026 [PMID: 12370823 DOI: 10.1038/sj.onc.1205679]

122 **Jackson D**, Gooya J, Mao S, Kinneer K, Xu L, Camara M, Fazenbaker C, Fleming R, Swamynathan S, Meyer D, Senter PD, Gao C, Wu H, Kinch M, Coats S, Kiener PA, Tice DA. A human antibody-drug conjugate targeting EphA2 inhibits tumor growth in vivo. *Cancer Res* 2008; **68**: 9367-9374 [PMID: 19010911 DOI: 10.1158/0008-5472.CAN-08-1933]

123 **Tandon M**, Vemula SV, Sharma A, Ahi YS, Mittal S, Bangari DS, Mittal SK. EphrinA1-EphA2 interaction-mediated apoptosis and FMS-like tyrosine kinase 3 receptor ligand-induced immunotherapy inhibit tumor growth in a breast cancer mouse model. *J Gene Med* 2012; **14**: 77-89 [DOI: 10.1002/jgm.1649]

124 **Fang WB**, Brantley-Sieders DM, Hwang Y, Ham AJ, Chen J. Identification and functional analysis of phosphorylated tyrosine residues within EphA2 receptor tyrosine kinase. *J Biol Chem* 2008; **283**: 16017-16026 [PMID: 18387945 DOI: 10.1074/jbc.M709934200]

125 **Duggineni S**, Mitra S, Lamberto I, Han X, Xu Y, An J, Pasquale EB, Huang Z. Design and Synthesis of Potent Bivalent Peptide Agonists Targeting the EphA2 Receptor. *ACS Med Chem Lett* 2013; **4** [PMID: 24167659 DOI: 10.1021/mL3004523]

126 **Wykosky J**, Palma E, Gibo DM, Ringler S, Turner CP, Debinski W. Soluble monomeric EphrinA1 is released from tumor cells and is a functional ligand for the EphA2 receptor. *Oncogene* 2008; **27**: 7260-7273 [PMID: 18794797 DOI: 10.1038/onc.2008.328]

127 **Bishop-Bailey D**. Tumour vascularisation: a druggable target. *Curr Opin Pharmacol* 2009; **9**: 96-101 [PMID: 19056315 DOI: 10.1016/j.coph.2008.10.004]

128 **Vihanto MM**, Plock J, Erni D, Frey BM, Frey FJ, Huynh-Do U. Hypoxia up-regulates expression of Eph receptors and ephrins in mouse skin. *FASEB J* 2005; **19**: 1689-1691 [PMID: 16081502 DOI: 10.1096/fj.04-3647fje]

World Journal of Gastrointestinal Oncology

Submit a Manuscript: https://www.f6publishing.com

World J Gastrointest Oncol 2022 May 15; 14(5): 989-1001

DOI: 10.4251/wjgo.v14.i5.989

ISSN 1948-5204 (online)

MINIREVIEWS

Scoping out the future: The application of artificial intelligence to gastrointestinal endoscopy

Scott B Minchenberg, Trent Walradt, Jeremy R Glissen Brown

Specialty type: Gastroenterology and hepatology

Provenance and peer review: Invited article; Externally peer reviewed.

Peer-review model: Single blind

Peer-review report's scientific quality classification

Grade A (Excellent): A
Grade B (Very good): 0
Grade C (Good): C, C
Grade D (Fair): 0
Grade E (Poor): 0

P-Reviewer: Costache RS, Romania; Hanada E, Japan; Ma J, China

Received: February 26, 2021
Peer-review started: February 26, 2021
First decision: May 3, 2021
Revised: June 21, 2021
Accepted: April 20, 2022
Article in press: April 20, 2022
Published online: May 15, 2022

Scott B Minchenberg, Trent Walradt, Department of Internal Medicine, Beth Israel Deaconess Medical Center, Boston, MA 02130, United States

Jeremy R Glissen Brown, Division of Gastroenterology, Beth Israel Deaconess Medical Center, Boston, MA 02130, United States

Corresponding author: Jeremy R Glissen Brown, MD, Academic Fellow, Division of Gastroenterology, Beth Israel Deaconess Medical Center, 330 Brookline Avenue, Boston, MA 02130, United States. jglissen@bidmc.harvard.edu

Abstract

Artificial intelligence (AI) is a quickly expanding field in gastrointestinal endoscopy. Although there are a myriad of applications of AI ranging from identification of bleeding to predicting outcomes in patients with inflammatory bowel disease, a great deal of research has focused on the identification and classification of gastrointestinal malignancies. Several of the initial randomized, prospective trials utilizing AI in clinical medicine have centered on polyp detection during screening colonoscopy. In addition to work focused on colorectal cancer, AI systems have also been applied to gastric, esophageal, pancreatic, and liver cancers. Despite promising results in initial studies, the generalizability of most of these AI systems have not yet been evaluated. In this article we review recent developments in the field of AI applied to gastrointestinal oncology.

Key Words: Artificial intelligence; Oncology; Gastroenterology; Endoscopy; Machine learning; Computer-assisted decision making; Computer-aided detection; Computer-aided diagnosis

Core Tip: Artificial intelligence (AI) technologies have become a topic of intense investigation in clinical medicine. In gastrointestinal oncology AI has been employed in multiple areas, with notable progress seen in computer-aided detection and computer-aided diagnosis. Most efforts have focused on colorectal cancer, but AI systems have also been developed for malignancies involving the esophagus, stomach, pancreas and liver. Although studies in this field have demonstrated excellent diagnostic characteristics, many have limited external validity. This article will review the current evidence for AI technologies applied to the detection and diagnosis of gastrointestinal malignancies.

Citation: Minchenberg SB, Walradt T, Glissen Brown JR. Scoping out the future: The application of artificial intelligence to gastrointestinal endoscopy. *World J Gastrointest Oncol* 2022; 14(5): 989-1001
URL: https://www.wjgnet.com/1948-5204/full/v14/i5/989.htm
DOI: https://dx.doi.org/10.4251/wjgo.v14.i5.989

INTRODUCTION

The first documented gastrointestinal (GI) endoscopic procedure was performed by Dr. Adolph Kussmaul in the 19th century using a modified Desormeaux device illuminated by a gasoline lamp with reflective mirrors[1]. Since the 1800s, there have been remarkable technological advancements in the field of endoscopy allowing for diagnostic and therapeutic interventions ranging from early detection of cancerous lesions to the treatment of life-threatening gastrointestinal bleeding. Mastering endoscopic techniques takes years of training followed by decades of experience. Even among experts, however, there is still considerable interprovider variability and room for improvement in the detection rate of gastrointestinal malignancies.

Artificial intelligence (AI) represents an attractive solution to these issues. Over the past two decades, numerous systems have been developed for computer-aided detection (CADe) and computer-aided diagnosis (CADx) of gastrointestinal lesions. Furthermore, some of the first prospective, randomized trials applying AI in clinical medicine have evaluated CADe for colorectal polyps[2]. Additional randomized trials are underway evaluating a broad spectrum of AI technologies in GI oncology. As products become commercially available, it will be important for gastroenterologists to familiarize themselves with technologies and the data supporting them.

DEFINITIONS

AI refers to technology designed to mimic human intelligence. A subset of AI is machine learning, a technique in which computers use data to improve their performance without explicit instruction. The majority of AI systems studied in GI oncology are based off two major approaches: traditional machine learning and deep neural networks.

Traditional machine learning is based on a set of algorithms that require a significant amount of input in order to make a particular decision. Much of the learning for traditional machine learning is based on pattern recognition relating to features such as color, texture, intensity, and shape. Many studies utilizing traditional machine learning implemented support vector machines (SVM) or a modified form of SVM. The crux of SVM is based on identifying hyperplanes allowing for the separation of data points. Initially this method was selected because of its high ratio of accuracy to computational power, allowing for application in real time. As technology pushed forth in the 21st century, various groups began exploring the use of deep neural networks, in many cases convolutional neural networks (CNN), for the detection and diagnosis of concerning lesions. Deep neural networks function by extracting data *via* a series of filters that is then processed by a neural network while preserving spatial and temporal features. This allows for dynamic learning while the algorithm extracts clinically relevant data.

Most machine learning models have several settings defined by the developer known as hyperparameters. These parameters are used to optimize the performance of the model. They are generally classified as model hyperparameters (*e.g.*, number of layers in a neural network) and training hyperparameters (*e.g.*, learning rate).

When developing a machine learning model, data is divided into training, validation and test datasets. The training dataset is used to create the model. The validation dataset is used to optimize hyperparameters and evaluate for overfitting. The test dataset is used to evaluate the performance of the model.

Preprocessing refers to the methods applied to images prior to analysis by the machine learning model. Techniques include histogram equalization to adjust contrast and gaussian filtering to remove noise. Transformation of the images can be achieved *via* resizing and processing through multiple layers, where deeper layers typically contain an increasing number of dimensions.

Data augmentation is a process to artificially enlarge a dataset when developing an AI algorithm. It is typically performed *via* rotation, flipping, shear, and zoom of the original data, thus expanding the amount of data in the training dataset.

Trials applying AI in GI oncology typically report the following metrics: sensitivity, specificity, positive predictive value (PPV), negative predictive value (NPV), accuracy, precision and area under the receiver operating characteristic curve (AuROC). In order to measure the performance of a detection method or segmentation task, the intersection over union (IoU) can be calculated by dividing the area of overlap (overlap of prediction label and ground-truth labels) by the area of union (area of both the predicted and ground-truth labels). The IoU varies from study to study, and a predetermined threshold is typically set to determine true positive (TP) and false positive (FP**).** Often an IoU ≥ 0.25-0.5 defines a true positive (TP) and an IoU < 0.25-0.5 is considered a false positive (FP). Many prospective studies use a clinical definition of true positive as the number of correctly identified lesions by either AI or endoscopists. Using the discussed parameters, various AI-based approaches for the detection of GI cancers can be compared.

COLONOSCOPY

Globally, colorectal cancer (CRC) is the third most commonly diagnosed cancer and the fourth leading cause of death[3]. Colonoscopy has been associated with a decrease in the incidence and mortality of CRC through the detection and removal of precancerous polyps[4,5]. Adenoma detection rate (ADR) is often used as a gold standard metric for colonoscopy quality, and studies have shown that ADR may be inversely proportional to the rate of interval CRC after colonoscopy[6]. Studies have also shown, however, that roughly one fifth of adenomas are missed, even by expert endoscopists[7]. Evidence suggests that unrecognized polyps that appear within the endoscopic field of view are an important contributor to this problem. For instance, Aslanian *et al*[8] demonstrated that nurse observation during colonoscopy resulted in a trend towards improvement in the ADR. In addition, Marcondes *et al*[9] demonstrated that the ADR declines at the end of the day, suggesting endoscopist factors such as fatigue may play a role in polyp detection. Several CADe systems based on traditional machine learning techniques or deep learning have been designed as an attempt to combat these problems, serve as a safety net or "second set of eyes" during colonoscopy, and thus augment ADR.

Once polyps are identified, polyp characterization is the next crucial step. Optical biopsy refers to the use of endoscopy to predict histology *in vivo*. The successful application of optical biopsy to polyps would reduce costs associated with pathologic assessment and prevent unnecessary polypectomies. Computer-based optical biopsy also has the potential to level the playing field for advanced endoscopic techniques such as endocytoscopy (a specialized endoscopic imaging modality that allows for ultra-high level of magnification during live endoscopy) and allow providers to use these techniques with less interprovider variability. The American Society of Gastrointestinal Endoscopy Preservation and Incorporation of Valuable Endoscopic Innovations (PIVI) proposed standards for "resect and discard" (≥ 90% agreement with histopathology for post-polypectomy surveillance intervals) and "diagnose-and-leave" (≥ 90% NPV for adenomatous histology) strategies for diminutive polyps[10]. A systematic review and meta-analysis revealed that optical biopsy using narrow-band imaging (NBI) met the PIVI-2 threshold for the "diagnose-and-leave" strategy, but only in the sub-group of expert endoscopists[11]. Not surprisingly, multiple CADx systems for the characterization of colorectal polyps have been developed to capitalize on the promises of optical biopsy and overcome the limitations of current technologies.

CADe

Perhaps the most well-studied application of AI in gastroenterology is polyp detection (Figure 1). Researchers in this field initially developed methods that recognized manually extracted polyp features such as shape, color and texture[12]. These early efforts were based on the analysis of static endoscopic images or video frames[12,13]. The most recent technologies employ deep-learning algorithms that are capable of detecting polyps in real-time[14,15]. There are now commercially available AI-based polyp detection technologies available in the United States, Europe and Asia[16-18].

Several prospective, randomized trials have been performed that have examined the efficacy of applying CADe to colonoscopy using deep learning methods (Table 1)[2,19-24]. Mohan *et al*[25] performed a meta-analysis, including 6 of these trials with a pooled patient population of 4962 patients. They found that ADR was significantly higher when using CADe assisted colonoscopy compared with standard colonoscopy [relative risk = 1.5, 95% confidence interval (CI): 1.3-1.72; $P < 0.0001$]. Colonoscopy withdrawal time was slighter greater in the CADe assisted group (mean difference = 0.38 minutes, 95%CI: 0.05-0.72; $P = 0.02$).

Although these findings are promising, these trials have several limitations. First, the augmented ADR seen in these trials was largely driven by improved detection of diminutive adenomas (size < 5 mm), the clinical benefit of which remains an area of active debate[26]. Secondly, only one trial was double-blinded[23]. In the single-blind trials, being observed may have facilitated a "competitive spirit"

Table 1 Characteristics of randomized trials applying computer-aided detection to colonoscopy

Ref.	Training/validation datasets	Testing datasets	AI system	ADR with AI (%)	ADR without AI (%)	Withdrawal time with AI (min)	Withdrawal time without AI (min)
Wang *et al* [2], 2019	5545 images from 1290 colonoscopy videos performed in China. Images were labeled by endoscopists. Training: 4495 images. Validation: 1050 images.	CVC-ClinicDb: 612 image frames of polyps from 29 colonoscopy videos performed in Spain. Polyp location manually annotated by endoscopists. 27113 images from 1138 colonoscopy videos performed in China. 20% contained histologically confirmed polyps. Videos of 138 histologically confirmed polyps from 110 patients in China. 54 full-length colonoscopy videos from 54 patients in China.	CNN based on SegNet architecture.	29	20	6.9	6.4
Wang *et al* [23], 2020				34	28	7.5	7.0
Liu *et al*[24], 2020				29	21	6.6	6.7
Repici *et al* [19], 2020	Based on data from previous clinical trial[74]. Videos of 2684 histologically confirmed polyps from 840 patients in Europe and the US. Training and validation: 2346 polyps from 735 patients. Testing: 338 polyps from 105 patients.		GI-Genius, Medtronic; CNN, details not available.	55	40	7.0	7.3
Gong *et al* [20], 2020	All images were obtained from colonoscopies of > 5000 patients in China. Trained 3 DCNNs on still images: DCNN 1: 3264 *in-vitro*, 10180 *in-vivo*, and 4230 unqualified images used to train the system to determine whether a scope was inside or outside the body. 1000 images per category used for testing. DCNN 2: 5189 images of the cecum and 5630 non-cecum images used to train the system to identify the cecum. 500 images per category used for testing. DCNN 3: 2602 clear images, 1877 images in cleansing process, and 1899 blurry images used to train the system to recognize slipping. 200 images per category used for testing. k-fold cross-validation procedure was implemented with k = 10.		DCNN 1-3 trained and tested in four independent convolutional neural networks: VGG16 [75], DenseNet-169 [76], ResNet-50[77], Inception-v3[78].	16	8	6.4	4.8
Liu *et al*[21], 2020	151 videos containing endoscopist-confirmed polyps and 384 polyp-negative videos from colonoscopies in China. Training and validation: 101 polyp-positive cases and 300 polyp-negative cases. Testing: 46 polyp-positive cases and 88 polyp-negative cases.		CADe system, Henan Xuanweitang Medical Information Technology; 3-dimensional CNN.	39	24	6.8	6.7
Su *et al* [22], 2020	23612 images from colonoscopies of > 4000 patients in China. Images were labeled by 2 endoscopists. Training: 15951. Validation: 3681. Testing: 3980. 5 DCNN models were created to time the withdrawal phase, supervise withdrawal stability, evaluate bowel preparation, and detect colorectal polyps in real time.		Model B, based on AlexNet architecture [79]. BP based on ZFNet[80] and Model PD YOLO V2[81]. Model E developed using a DCNN with one fully connected layer.	29	17	7.0	5.7

AI: Artificial intelligence; ADR: Adenoma detection rate; CADe: Computer-aided detection; CNN: Convolutional neural networks; DCNN: Deep convolutional neural network; GI: Gastrointestinal.

or Hawthorne effect in provider participants, leading to improved inspection techniques[8]. Third, all but one of these trials were performed at a single center[19]. Thus, the results of these studies may not be broadly generalizable. Given these promises and limitations, the European Society of Gastrointestinal Endoscopy published guidelines in 2019 suggesting "the possible incorporation of computer aided diagnosis… into colonoscopy, if acceptable and reproducible accuracy for colorectal neoplasia is demonstrated in high quality multicenter *in vivo* clinical studies[27]." Guidance and guidelines have been produced to aid gastroenterologists in conducting, reviewing and interpreting CADe studies with the goal of accelerating the entrance of this technology into routine clinical practice[28].

CADx

CADx systems for the characterization of colorectal polyps have been developed using a variety of imaging modalities including white light endoscopy, magnifying NBI (M-NBI), autofluorescence endoscopy, endocytoscopy, and magnifying chromoendoscopy (Figure 2). The majority of studies examining these technologies are retrospective in nature. Only six prospective trials have been performed, and none of them were randomized controlled trials[10,29-33]. Aihara *et al*[32] published the first prospective CADx trial for colorectal lesions in 2013. Investigators used autofluorescence endoscopy to distinguish between neoplastic and non-neoplastic lesions. They evaluated 32 patients with 102 colorectal lesions. The CADx system had a sensitivity, specificity, PPV, and NPV of 94.2%,

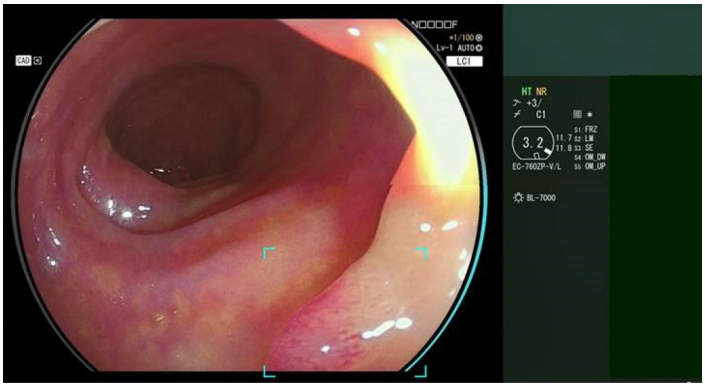

DOI: 10.4251/wjgo.v14.i5.989

Figure 1 Example output from a computer-aided detection system using white light endoscopy (Fujifilm Corp., Tokyo). When a lesion is detected the endoscopist is notified by a hollow, bounded box. Used with the permission of Fujifilm.

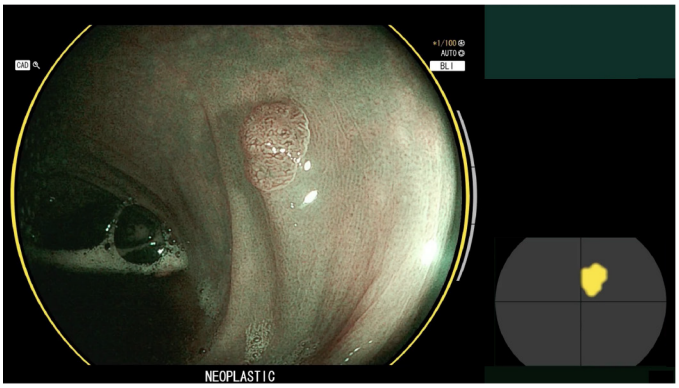

DOI: 10.4251/wjgo.v14.i5.989

Figure 2 Example output from a computer-aided diagnosis system using narrow-band imaging (Fujifilm Corp., Tokyo). The system predicts whether or not the lesion of interest is neoplastic. Used with the permission of Fujifilm.

88.9%, 95.6%, and 85.2% respectively[32]. Kuiper *et al*[30] performed another trial using autofluorescence endoscopy and CADx that included 87 patients with 207 colorectal lesions. This study achieved a NPV 73.5%. In a subsequent study using the next generation model of the same device on 27 patients with 137 diminutive colorectal polyps, Rath *et al*[31] reported an improved NPV of 96.1% meeting the PIVI-2 criteria for the "diagnose-and-leave" strategy. A more recent study utilizing autofluorescence endoscopy was published by Horiuchi *et al*[33] in 2019. The authors evaluated 95 patients with 429 diminutive colorectal polyps and found a NPV for rectosigmoid polyps of 93.4%. When evaluating rectosigmoid and non-rectosigmoid polyps together, however, the NPV decreased to 80.8%. Kominami *et al*[29] utilized M-NBI in a study of 41 patients with 118 colorectal lesions. That trial achieved a NPV of 93.3% and the recommendations for follow-up colonoscopy based on the CADx system and pathology were identical for 92.7% of patients. Thus, their system surpassed the PIVI criteria for both the "diagnose-and-leave" and the "resect-and-discard" strategies. Mori *et al*[10] performed the largest prospective CADx trial to date, which included 325 patients with 466 diminutive polyps. The CADx algorithm in this trial analyzed endocytoscopy images after application of NBI or methylene blue dye. The authors found that for the 250 rectosigmoid polyps in their study, using the most conservative estimate, the NPV was 93.7%, meeting the PIVI-2 threshold to support a "diagnose-and-leave" strategy.

ESOPHAGOGASTRODUODENOSCOPY

Many upper GI malignant processes, including esophageal and gastric pre-cancerous and cancerous lesions are easy to miss and can be confused with benign processes such as esophagitis or gastritis. In addition, if a patient has numerous lesions, it becomes difficult to determine which lesions require biopsy. Even with a significant amount of training, 20%-25% of early gastric cancer is missed when utilizing high-definition white light endoscopy[34]. Consequently, much work has focused on using AI to improve the detection and diagnosis of these increasingly prevalent lesions.

Detection of early gastric cancer

In 2015, Miyaki *et al*[35] utilized SVM to delineate early gastric cancer using esophagogastroduodenoscopy (EGD) with M-NBI on 95 patients from a single hospital in Japan. This was the first study to delineate gastric cancerous lesions relative to noncancerous reddened lesions or surrounding tissue using an SVM based traditional machine learning algorithm[35]. This idea was expanded on by Kanesaka *et al*[36] who utilized SVM in real time with M-NBI to detect lesions concerning for early gastric cancers. In this retrospective study the CADe system achieved an accuracy, sensitivity, and specificity of 96.3%, 96.7%, and 95%, respectively[36]. Kanesaka *et al*[36] demonstrated the power of SVM relating to detection of gastric cancer but their study was limited by its sample size (81 test images), lesion type (focused only on depressed-type lesions), and selection bias. In 2018, Hirasawa *et al*[37] developed a CNN-based system for detecting early and advanced gastric cancer. This system was trained on 13584 images and tested on 2296 from 69 patients demonstrating a sensitivity of 92.2% and a PPV of 30.6%[37]. Most false positives were related to gastritis[37]. Overall, this study provided sufficient evidence that a deep neural network-based approach was feasible for the detection of early gastric cancer, but several limitations were also noted. Li *et al*[38] applied a CNN based system to M-NBI for the detection of early gastric cancer. This system was trained on 2088 images and tested on 341 images achieving an accuracy, sensitivity, and specificity of 90.91%, 91.18%, and 90.64%, respectively, with a significant improvement in sensitivity relative to "expert" endoscopists[38]. The accuracy, sensitivity, and specificity of the Li *et al*[38] study were lower than results published by Kanesaka *et al*[36] with SVM. These differences, however, are difficult to compare directly given varied nomenclature and histologic interpretation by groups from different countries.

Zhu *et al*[39] developed another CNN-based system in 2019 with the ability to determine the invasion depth of gastric cancer. 790 images were used for training and 203 images were used to test the system[39]. They were able to achieve a sensitivity and specificity of 76.47% and 95.56%, respectively, with a PPV and NPV of 89.66% and 88.97%, respectively on the test dataset[40]. They also demonstrated that the CNN-based system had a significantly higher accuracy for the determination of invasion depth compared to a small group of 17 endoscopists[39]. This study was the first to use CNN to evaluate the depth of gastric cancer and has significant potential clinical utility. Major limitations include a small sample size, lack of validation and testing on video or live endoscopy, and the fact that the data was collected from a single center using a single type of endoscope.

Wu *et al*[39] described the use of CNN to help eliminate blind spots and detect early gastric cancer. In regards to classifying gastric locations, their CNN-based approach had an accuracy of 90% and 65.9% when dividing the stomach into 10 and 26 parts respectively[39]. For the detection of early gastric cancer, this study achieved promising results with an accuracy of 92.5%, sensitivity of 94.0%, specificity of 91.0%, PPV of 91.3%, and NPV of 93.8%[39]. In 2021, Wu *et al*[39,40] published the first multi-center randomized control trial investigating the detection of blind spots and early gastric cancer using an updated version of their CNN based AI discussed above. In this study, 1050 patients from 5 hospitals were randomized to receive AI-assisted endoscopy or standard-of-care endoscopy. The AI-assisted group had significantly fewer blind spots. The accuracy, sensitivity, and specificity of the system were 84.69%, 100%, and 84.29% respectively for the detection of gastric cancer[40]. The trial yielded a lower accuracy and specificity relative to previous publications and the single center study by Li *et al*[38] However, this was the first study of its kind to evaluate a CNN-based system prospectively in a randomized clinical trial.

Barrett's esophagus

In the United States, esophageal adenocarcinoma accounts for approximately two thirds of newly diagnosed esophageal cancers and is associated with a poor prognosis if identified in the late stages[41]. When identified, esophageal premalignant lesions can be treated *via* ablation or endoscopic resection, drastically improving outcomes[42,43]. Traditionally, "random" biopsies were obtained with a relatively low diagnostic yield as lesions concerning for neoplasia in patients with Barrett's esophagus (BE) are often challenging to identify. Recently, several groups have studied the implementation of AI during EGD for screening and surveillance of BE. In 2016, van der Sommen *et al*[44] published the first study using machine learning for the detection of early neoplastic lesions in BE. The algorithm achieved a sensitivity of 86% and specificity of 87%[44] but the initial algorithm did not outperform an expert endoscopist during the length of their study. Swager *et al*[45] expanded on this concept and developed a machine learning algorithm for volumetric laser endomicroscopy (VLE). The resultant system achieved a sensitivity and specificity of 90% and 93%, respectively[45]. It also outperformed a clinical VLE prediction score[45]. In 2019, the ARGOS consortium developed a CADe system to detect Berrett's lesions using white light endoscopy (WLE), which achieved an accuracy, sensitivity, and specificity of 92%, 95%, and 85%, respectively[46]. Although their approach yielded highly accurate results, it was tested on high quality images and limited by human perceptual bias as the algorithm was trained to detect abnormalities based on variations in color and texture. The ARGOS consortium sought to improve on their initial approach by developing a deep learning-based CADe system built on a hybrid ResNet-UNet CNN[47]. This method achieved 89% accuracy, 90% sensitivity, and 88% specificity for the detection of neoplasms and nondysplastic BE[47]. Their deep-learning based CADe system also out

performed 53 international endoscopic assessors ranging in experience from research fellows with no endoscopic expertise to board-certified endoscopists with greater than 5 years of experience[47]. The authors also implemented their algorithm during live endoscopic procedures on 10 patients with BE [48]. The system achieved an accuracy, sensitivity, and specificity of 90%, 91%, and 89%, respectively during clinical use[48]. Hashimoto *et al*[49] also demonstrated the power of a CNN-based algorithm for the detection and classification of early esophageal neoplasia. On 458 test images they achieved a sensitivity of 96.4%, specificity of 94.2%, and accuracy of 95.4% at a speed allowing for implementation during live endoscopy[49]. Though we are starting to see the implementation of CNN-based systems prospectively in the clinical trial setting, in the near future we will likely see the first publication of multi-center, randomized clinical trials utilizing AI for the detection of neoplasia in patient with BE.

Detection of esophageal squamous cell carcinoma

In 2019, Horie *et al*[50] published the first study applying CNN-based systems to EGD for the detection of esophageal cancer. This was a single center trial that used 8428 images from 384 patients for training and 1118 images from 97 patients for testing[50]. The system achieved a sensitivity of 98% and specificity of 79% with a PPV of 40% and NPV of 95% for the diagnosis of esophageal cancer[50]. Shadows were the most common cause of false positives and background mucosal inflammation was the most common cause of a false negative[50]. Cai *et al*[51] utilized CNN for the detection of esophageal squamous cell carcinoma (SCC) by initially training it with 2428 images from 746 patients and testing it on 187 images form 52 patients. They achieved an accuracy, sensitivity, specificity, PPV, and NPV of 91.4%, 97.8%, 85.4%, 86.4%, and 97.6% respectively[51]. They also demonstrated that the use of CNN significantly increased both accuracy and sensitivity of esophageal SCC detection by junior, mid-level, and senior endoscopists while reviewing still images[51]. Guo *et al*[52] trained a CNN-based system on 6473 narrow-band images that was validated using 6671 images and which achieved a sensitivity of 98.04% and a specificity of 95.03% for the detection of precancerous lesions or early esophageal SCC. Authors also tested the system on 27 non-magnifying videos and achieved a per-frame sensitivity of 60.8% and per-lesion sensitivity of 100%[52]. When applied to 20 magnifying videos, the per-frame sensitivity increased to 96.1%, and the per-lesion sensitivity remained at 100%[52]. Another group using CNN with endoscopy to detect SCC demonstrated no significant difference in accuracy, sensitivity, and specificity between AI diagnosis or endoscopist diagnosis using narrow-band imaging or white light imaging[53]. Liu *et al*[54] constructed a 2 stream CNN system achieving an accuracy of 85.83%, sensitivity of 94.23%, and specificity of 94.67% outperforming SVM based methods with the same data set. Fukuda *et al*[55], developed a CNN based algorithm to detect SCC with NBI/BLI to detect and characterize suspicious lesions. For lesion detection, the system achieved a sensitivity, specificity, and accuracy of 91%, 51%, and 63% respectively[55]. The algorithm outperformed experts with regards to sensitivity but underperformed when it came to specificity and accuracy[55]. However, when it came to characterization of lesions, the CNN based algorithm outperformed expert endoscopists by achieving a specificity, sensitivity, and accuracy of 86%, 89%, and 88% respectively[55]. As can be seen for many other CADe and CADx systems, over a relatively short time period, we have seen significant advances in the early detection of pre-malignant lesions and a shift from traditional machine learning to deep neural networks.

CAPSULE ENDOSCOPY

Traditional endoscopic techniques allow for the visualization of the esophagus, stomach, duodenum, terminal ileum, and colon. With the advent of push enteroscopy, we have the ability to reach the proximal jejunum, but are still unable to explore most of the small intestine. Capsule endoscopy (CE) uses a 26 mm × 11 mm pill sized video camera that is swallowed and allows for the wireless transmission of video from the whole GI tract. CE allows for visualization of portions of the jejunum and ileum previously unreachable or difficult to reach. Unlike traditional endoscopy, CE is unable to be controlled by an operator so important pathology can be missed, and there is no way to intervene immediately if an abnormality is identified. CE is also limited by an eight- to twelve-hour battery life and the risk of obstruction in patients with strictures. Even with its limitations, CE has become an important tool for the diagnosis of GI pathology.

Decades after its initial conception, the first CE was approved for use in 2001 by the Food and Drug Administration (FDA), ushering in a new era of discovery[56]. As the practice of CE became more mainstream, physicians were tasked with interpreting many hours of video averaging between 30-120 min with a staggering 50000-60000 frames per study[57,58]. It is an incredibly arduous task for an endoscopist to maintain their attention and consistently identify evidence of pathology in as little as 1 frame while combing through hours upon hours of video. The miss rate in this setting has been reported to be at least 50% in a small blinded study from 2012[59]. Recently we have seen the parallel development of AI algorithms to help interpret the swaths of data generated by CE studies. Initially the development approach was based on traditional machine learning with many studies utilizing SVM, but the field has made a substantial shift towards deep learning primary through CNN, which, in general

have afforded favorable performance characteristics.

A major application of CE is the ability to noninvasively identify polyps and lesions concerning for malignancy throughout the GI tract. Early efforts consisted of traditional machine learning algorithms such as SVC that were designed to identify the presence or absence of a polyp instance. One early paper using a binary classifier based on geometrical analysis demonstrated 47% sensitivity per frame and over 81% sensitivity per polyp with a specificity of 90%[60]. Using a boosting-based approach, Silva *et al*[61] achieved a sensitivity of 91.0% and a specificity of 95.2% for polyp detection with CE. This was expanded on by Iakovidis *et al*[62], whose color feature-based pattern recognition was utilized to subclassify lesions. Liu *et al*[63] implemented multiscale textural features and an SVM based feature selection method to enhance the process of polyp classification that was 97.3% accurate, 97.8% sensitive, and 96.7% specific. Various groups sought to improve traditional machine learning approaches by using a genetic fuzzy based improved kernel SVM[64] and by using ensemble learning[65].

A study from 2020 investigated the application of a CNN based system to CE for the detection of protruding lesions including polyps, nodules, epithelial tumors, submucosal tumors and venous structures[66]. In this particular study the sensitivity and specificity for detecting any protruding lesion [on test images] were 90.7% and 79.8% respectively[66]. Subgroup analysis of the data yielded a sensitivity of 86.5% for polyp detection[66]. When applied to patients the sensitivity for protruding lesions increased to 98.6%[66]. Currently, the well-established SVM-based detection methods for polyps appear to be superior for the detection/classification of polyps but perhaps further training and studies are required for CNN to outperform SVMs, and all of these studies are pre-clinical.

ENDOSCOPIC ULTRASOUND

AI applications for endoscopic ultrasound (EUS) are still in nascent stages. The majority of work utilizing AI for EUS has focused on diagnosing pancreatic cancer. A variety of conventional machine learning techniques including PCA, SVM and artificial neural networks have been utilized[67-69]. Recently, Kuwahara *et al*[70] performed the first deep learning based study using a CNN to predict malignancy in intraductal papillary mucinous neoplasms. They trained their algorithm on 3970 still images and achieved a sensitivity, specificity, PPV, NPV, and accuracy of 95.7%, 92.6%, 91.7%, 96.2%, and 94.0%, respectively. Of note, the human accuracy for predicting IPMN malignancy in this study was only 56.0%. In 2020, Marya *et al*[71] performed a retrospective study using a CNN-system to differentiate autoimmune pancreatitis from pancreatic ductal adenocarcinoma (PDAC). The system was 90% sensitive and 93% specific for differentiating autoimmune pancreatitis from PDAC.

Outside of the field of pancreatic cancer, Minoda *et al*[72] published a retrospective study evaluating the ability of a CNN-system to diagnose gastrointestinal stromal tumors among subepithelial lesions (SEL) using EUS images. Among 30 SELs ≥ 20 mm the system achieved an accuracy, sensitivity, and specificity or 90.0%, 91.7%, and 83.3% respectively. Finally, Marya *et al*[73] utilized a CNN to identify focal liver lesions (FLL) and classify them as malignant or benign. The authors included a total of 210685 EUS images in their study. Their algorithm correctly identified 92% of FLLs. When evaluating video data, they achieved a sensitivity of 100% and specificity of 80% for the classification of malignant FLLs.

CONCLUSION

AI technology applied to gastrointestinal oncology has an exciting and potent future and the potential to decrease morbidity, mortality and costs. Research groups have demonstrated how AI can augment the detection and diagnosis of numerous GI malignancies. This field is growing rapidly, but it is still in its infancy. Although we have recently seen the first prospective, randomized trials emerging in several spaces, most studies in this field are still retrospective. Furthermore, the majority of datasets used to train the algorithms used in these studies were collected from single-center databases in heterogenous patient populations. Consequently, these studies are at high risk of selection bias and with models at risk for overfitting. In order to create robust tools ready for general clinical practice, multicenter, randomized controlled clinical trials conducted by endoscopists of various skill levels on diverse patient populations and utilizing robustly trained and validated models are needed. Additionally, it will be important to monitor the efficacy of these tools in the real-world setting. Finally, clinicians will need to collaborate with lawmakers and other stakeholders to determine how best to regulate these technologies and establish clear policies on accountability. In clinical practice today, AI serves as a "safety net" for physicians. It is there to serve as a second set of eyes to support a diagnosis only. We believe it will be many years before AI is used to make definitive diagnosis or drive management decisions. Gastroenterologists should work to familiarize themselves with the strength and limitations of these technologies so they can take an active role in a future AI-assisted healthcare system.

FOOTNOTES

Author contributions: Minchenberg SB and Walradt T contributed equally to the work and should be listed as co-first authors; Minchenberg SB, Walradt T, and Glissen Brown JR contributed to manuscript concept and layout; Minchenberg SB and Walradt T contributed to drafting of the manuscript; All authors read and approved the final manuscript.

Conflict-of-interest statement: All authors disclose no financial relationships relevant to this publication.

Country/Territory of origin: United States

ORCID number: Scott B Minchenberg 0000-0002-0445-5956; Trent Walradt 0000-0003-1081-0923; Jeremy R Glissen Brown 0000-0002-7204-7241.

Corresponding Author's Membership in Professional Societies: American College of Gastroenterology; American Gastroenterological Association; and American Society for Gastrointestinal Endoscopy.

S-Editor: Gong ZM
L-Editor: A
P-Editor: Gong ZM

REFERENCES

1 **Rehnberg V**, Walters E. The life and work of Adolph Kussmaul 1822-1902: 'Sword swallowers in modern medicine'. *J Intensive Care Soc* 2017; **18**: 71-72 [PMID: 28979542 DOI: 10.1177/1751143716676822]
2 **Wang P**, Berzin TM, Glissen Brown JR, Bharadwaj S, Becq A, Xiao X, Liu P, Li L, Song Y, Zhang D, Li Y, Xu G, Tu M, Liu X. Real-time automatic detection system increases colonoscopic polyp and adenoma detection rates: a prospective randomised controlled study. *Gut* 2019; **68**: 1813-1819 [PMID: 30814121 DOI: 10.1136/gutjnl-2018-317500]
3 **Bray F**, Ferlay J, Soerjomataram I, Siegel RL, Torre LA, Jemal A. Global cancer statistics 2018: GLOBOCAN estimates of incidence and mortality worldwide for 36 cancers in 185 countries. *CA Cancer J Clin* 2018; **68**: 394-424 [PMID: 30207593 DOI: 10.3322/caac.21492]
4 **Nishihara R**, Wu K, Lochhead P, Morikawa T, Liao X, Qian ZR, Inamura K, Kim SA, Kuchiba A, Yamauchi M, Imamura Y, Willett WC, Rosner BA, Fuchs CS, Giovannucci E, Ogino S, Chan AT. Long-term colorectal-cancer incidence and mortality after lower endoscopy. *N Engl J Med* 2013; **369**: 1095-1105 [PMID: 24047059 DOI: 10.1056/NEJMoa1301969]
5 **Kahi CJ**, Imperiale TF, Juliar BE, Rex DK. Effect of screening colonoscopy on colorectal cancer incidence and mortality. *Clin Gastroenterol Hepatol* 2009; **7**: 770-5; quiz 711 [PMID: 19268269 DOI: 10.1016/j.cgh.2008.12.030]
6 **Kaminski MF**, Regula J, Kraszewska E, Polkowski M, Wojciechowska U, Didkowska J, Zwierko M, Rupinski M, Nowacki MP, Butruk E. Quality indicators for colonoscopy and the risk of interval cancer. *N Engl J Med* 2010; **362**: 1795-1803 [PMID: 20463339 DOI: 10.1056/NEJMoa0907667]
7 **Ahn SB**, Han DS, Bae JH, Byun TJ, Kim JP, Eun CS. The Miss Rate for Colorectal Adenoma Determined by Quality-Adjusted, Back-to-Back Colonoscopies. *Gut Liver* 2012; **6**: 64-70 [PMID: 22375173 DOI: 10.5009/gnl.2012.6.1.64]
8 **Aslanian HR**, Shieh FK, Chan FW, Ciarleglio MM, Deng Y, Rogart JN, Jamidar PA, Siddiqui UD. Nurse observation during colonoscopy increases polyp detection: a randomized prospective study. *Am J Gastroenterol* 2013; **108**: 166-172 [PMID: 23381064 DOI: 10.1038/ajg.2012.237]
9 **Marcondes FO**, Gourevitch RA, Schoen RE, Crockett SD, Morris M, Mehrotra A. Adenoma Detection Rate Falls at the End of the Day in a Large Multi-site Sample. *Dig Dis Sci* 2018; **63**: 856-859 [PMID: 29397494 DOI: 10.1007/s10620-018-4947-1]
10 **Mori Y**, Kudo SE, Misawa M, Saito Y, Ikematsu H, Hotta K, Ohtsuka K, Urushibara F, Kataoka S, Ogawa Y, Maeda Y, Takeda K, Nakamura H, Ichimasa K, Kudo T, Hayashi T, Wakamura K, Ishida F, Inoue H, Itoh H, Oda M, Mori K. Real-Time Use of Artificial Intelligence in Identification of Diminutive Polyps During Colonoscopy: A Prospective Study. *Ann Intern Med* 2018; **169**: 357-366 [PMID: 30105375 DOI: 10.7326/M18-0249]
11 **ASGE Technology Committee**, Abu Dayyeh BK, Thosani N, Konda V, Wallace MB, Rex DK, Chauhan SS, Hwang JH, Komanduri S, Manfredi M, Maple JT, Murad FM, Siddiqui UD, Banerjee S. ASGE Technology Committee systematic review and meta-analysis assessing the ASGE PIVI thresholds for adopting real-time endoscopic assessment of the histology of diminutive colorectal polyps. *Gastrointest Endosc* 2015; **81**: 502.e1-502.e16 [PMID: 25597420 DOI: 10.1016/j.gie.2014.12.022]
12 **Iakovidis DK**, Maroulis DE, Karkanis SA. An intelligent system for automatic detection of gastrointestinal adenomas in video endoscopy. *Comput Biol Med* 2006; **36**: 1084-1103 [PMID: 16293240 DOI: 10.1016/j.compbiomed.2005.09.008]
13 **Maroulis DE**, Iakovidis DK, Karkanis SA, Karras DA. CoLD: a versatile detection system for colorectal lesions in endoscopy video-frames. *Comput Methods Programs Biome***70**: 151-166 [PMID: 12507791 DOI: 10.1016/s0169-2607(02)00007-x]

14 **Cogan T**, Cogan M, Tamil L. MAPGI: Accurate identification of anatomical landmarks and diseased tissue in gastrointestinal tract using deep learning. *Comput Biol Med* 2019; **111**: 103351 [PMID: 31325742 DOI: 10.1016/j.compbiomed.2019.103351]

15 **Bilal M**, Glissen Brown JR, Berzin TM. Using Computer-Aided Polyp Detection During Colonoscopy. *Am J Gastroenterol* 2020; **115**: 963-966 [PMID: 32618638 DOI: 10.14309/ajg.0000000000000646]

16 **Cybernet Systems Co., Ltd**. EndoBRAIN - Artificial intelligence system that supports optical diagnosis of colorectal polyps - was approved by PMDA (Pharmaceuticals and Medical Devices Agency), a regulatory body in Japan. 2018. Available from: https://www.cybernet.jp/english/documents/pdf/news/press/2018/20181210.pdf

17 **Medtronic**. Medtronic Launches the First Artificial Intelligence System for Colonoscopy at United European Gastroenterology Week 2019 | Medtronic. 2019. Available from: https://newsroom.medtronic.com/news-releases/news-release-details/medtronic-launches-first-artificial-intelligence-system/

18 **FDA**. FDA Authorizes Marketing of First Device that Uses Artificial Intelligence to Help Detect Potential Signs of Colon Cancer. 2021. Available from: https://www.fda.gov/news-events/press-announcements/fda-authorizes-marketing-first-device-uses-artificial-intelligence-help-detect-potential-signs-colon

19 **Repici A**, Badalamenti M, Maselli R, Correale L, Radaelli F, Rondonotti E, Ferrara E, Spadaccini M, Alkandari A, Fugazza A, Anderloni A, Galtieri PA, Pellegatta G, Carrara S, Di Leo M, Craviotto V, Lamonaca L, Lorenzetti R, Andrealli A, Antonelli G, Wallace M, Sharma P, Rosch T, Hassan C. Efficacy of Real-Time Computer-Aided Detection of Colorectal Neoplasia in a Randomized Trial. *Gastroenterology* 2020; **159**: 512-520.e7 [PMID: 32371116 DOI: 10.1053/j.gastro.2020.04.062]

20 **Gong D**, Wu L, Zhang J, Mu G, Shen L, Liu J, Wang Z, Zhou W, An P, Huang X, Jiang X, Li Y, Wan X, Hu S, Chen Y, Hu X, Xu Y, Zhu X, Li S, Yao L, He X, Chen D, Huang L, Wei X, Wang X, Yu H. Detection of colorectal adenomas with a real-time computer-aided system (ENDOANGEL): a randomised controlled study. *Lancet Gastroenterol Hepatol* 2020; **5**: 352-361 [PMID: 31981518 DOI: 10.1016/S2468-1253(19)30413-3]

21 **Liu WN**, Zhang YY, Bian XQ, Wang LJ, Yang Q, Zhang XD, Huang J. Study on detection rate of polyps and adenomas in artificial-intelligence-aided colonoscopy. *Saudi J Gastroenterol* 2020; **26**: 13-19 [PMID: 31898644 DOI: 10.4103/sjg.SJG_377_19]

22 **Su JR**, Li Z, Shao XJ, Ji CR, Ji R, Zhou RC, Li GC, Liu GQ, He YS, Zuo XL, Li YQ. Impact of a real-time automatic quality control system on colorectal polyp and adenoma detection: a prospective randomized controlled study (with videos). *Gastrointest Endosc* 2020; **91**: 415-424.e4 [PMID: 31454493 DOI: 10.1016/j.gie.2019.08.026]

23 **Wang P**, Liu X, Berzin TM, Glissen Brown JR, Liu P, Zhou C, Lei L, Li L, Guo Z, Lei S, Xiong F, Wang H, Song Y, Pan Y, Zhou G. Effect of a deep-learning computer-aided detection system on adenoma detection during colonoscopy (CADe-DB trial): a double-blind randomised study. *Lancet Gastroenterol Hepatol* 2020; **5**: 343-351 [PMID: 31981517 DOI: 10.1016/S2468-1253(19)30411-X]

24 **Liu P**, Wang P, Glissen Brown JR, Berzin TM, Zhou G, Liu W, Xiao X, Chen Z, Zhang Z, Zhou C, Lei L, Xiong F, Li L, Liu X. The single-monitor trial: an embedded CADe system increased adenoma detection during colonoscopy: a prospective randomized study. *Therap Adv Gastroenterol* 2020; **13**: 1756284820979165 [PMID: 33403003 DOI: 10.1177/1756284820979165]

25 **Mohan BP**, Facciorusso A, Khan SR, Chandan S, Kassab LL, Gkolfakis P, Tziatzios G, Triantafyllou K, Adler DG. Real-time computer aided colonoscopy versus standard colonoscopy for improving adenoma detection rate: A meta-analysis of randomized-controlled trials. *EClinicalMedicine* 2020; **29-30**: 100622 [PMID: 33294821 DOI: 10.1016/j.eclinm.2020.100622]

26 **Lieberman D**, Sullivan BA, Hauser ER, Qin X, Musselwhite LW, O'Leary MC, Redding TS 4th, Madison AN, Bullard AJ, Thomas R, Sims KJ, Williams CD, Hyslop T, Weiss D, Gupta S, Gellad ZF, Robertson DJ, Provenzale D. Baseline Colonoscopy Findings Associated With 10-Year Outcomes in a Screening Cohort Undergoing Colonoscopy Surveillance. *Gastroenterology* 2020; **158**: 862-874.e8 [PMID: 31376388 DOI: 10.1053/j.gastro.2019.07.052]

27 **Bisschops R**, East JE, Hassan C, Hazewinkel Y, Kamiński MF, Neumann H, Pellisé M, Antonelli G, Bustamante Balen M, Coron E, Cortas G, Iacucci M, Yuichi M, Longcroft-Wheaton G, Mouzyka S, Pilonis N, Puig I, van Hooft JE, Dekker E. Advanced imaging for detection and differentiation of colorectal neoplasia: European Society of Gastrointestinal Endoscopy (ESGE) Guideline - Update 2019. *Endoscopy* 2019; **51**: 1155-1179 [PMID: 31711241 DOI: 10.1055/a-1031-7657]

28 **Liu X**, Cruz Rivera S, Moher D, Calvert MJ, Denniston AK; SPIRIT-AI and CONSORT-AI Working Group. Reporting guidelines for clinical trial reports for interventions involving artificial intelligence: the CONSORT-AI extension. *Lancet Digit Health* 2020; **2**: e537-e548 [PMID: 33328048 DOI: 10.1016/S2589-7500(20)30218-1]

29 **Kominami Y**, Yoshida S, Tanaka S, Sanomura Y, Hirakawa T, Raytchev B, Tamaki T, Koide T, Kaneda K, Chayama K. Computer-aided diagnosis of colorectal polyp histology by using a real-time image recognition system and narrow-band imaging magnifying colonoscopy. *Gastrointest Endosc* 2016; **83**: 643-649 [PMID: 26264431 DOI: 10.1016/j.gie.2015.08.004]

30 **Kuiper T**, Alderlieste YA, Tytgat KM, Vlug MS, Nabuurs JA, Bastiaansen BA, Löwenberg M, Fockens P, Dekker E. Automatic optical diagnosis of small colorectal lesions by laser-induced autofluorescence. *Endoscopy* 2015; **47**: 56-62 [PMID: 25264763 DOI: 10.1055/s-0034-1378112]

31 **Rath T**, Tontini GE, Vieth M, Nägel A, Neurath MF, Neumann H. In vivo real-time assessment of colorectal polyp histology using an optical biopsy forceps system based on laser-induced fluorescence spectroscopy. *Endoscopy* 2016; **48**: 557-562 [PMID: 27009081 DOI: 10.1055/s-0042-102251]

32 **Aihara H**, Saito S, Inomata H, Ide D, Tamai N, Ohya TR, Kato T, Amitani S, Tajiri H. Computer-aided diagnosis of neoplastic colorectal lesions using 'real-time' numerical color analysis during autofluorescence endoscopy. *Eur J Gastroenterol Hepatol* 2013; **25**: 488-494 [PMID: 23249604 DOI: 10.1097/MEG.0b013e32835c6d9a]

33 **Horiuchi H**, Tamai N, Kamba S, Inomata H, Ohya TR, Sumiyama K. Real-time computer-aided diagnosis of diminutive rectosigmoid polyps using an auto-fluorescence imaging system and novel color intensity analysis software. *Scand J Gastroenterol* 2019; **54**: 800-805 [PMID: 31195905 DOI: 10.1080/00365521.2019.1627407]

34 **Kaise M**. Advanced endoscopic imaging for early gastric cancer. *Best Pract Res Clin Gastroenterol* 2015; **29**: 575-587 [PMID: 26381303 DOI: 10.1016/j.bpg.2015.05.010]

35 **Miyaki R**, Yoshida S, Tanaka S, Kominami Y, Sanomura Y, Matsuo T, Oka S, Raytchev B, Tamaki T, Koide T, Kaneda K, Yoshihara M, Chayama K. A computer system to be used with laser-based endoscopy for quantitative diagnosis of early gastric cancer. *J Clin Gastroenterol* 2015; **49**: 108-115 [PMID: 24583752 DOI: 10.1097/MCG.0000000000000104]

36 **Kanesaka T**, Lee TC, Uedo N, Lin KP, Chen HZ, Lee JY, Wang HP, Chang HT. Computer-aided diagnosis for identifying and delineating early gastric cancers in magnifying narrow-band imaging. *Gastrointest Endosc* 2018; **87**: 1339-1344 [PMID: 29225083 DOI: 10.1016/j.gie.2017.11.029]

37 **Hirasawa T**, Aoyama K, Tanimoto T, Ishihara S, Shichijo S, Ozawa T, Ohnishi T, Fujishiro M, Matsuo K, Fujisaki J, Tada T. Application of artificial intelligence using a convolutional neural network for detecting gastric cancer in endoscopic images. *Gastric Cancer* 2018; **21**: 653-660 [PMID: 29335825 DOI: 10.1007/s10120-018-0793-2]

38 **Li L**, Chen Y, Shen Z, Zhang X, Sang J, Ding Y, Yang X, Li J, Chen M, Jin C, Chen C, Yu C. Convolutional neural network for the diagnosis of early gastric cancer based on magnifying narrow band imaging. *Gastric Cancer* 2020; **23**: 126-132 [PMID: 31332619 DOI: 10.1007/s10120-019-00992-2]

39 **Niu PH**, Zhao LL, Wu HL, Zhao DB, Chen YT. Artificial intelligence in gastric cancer: Application and future perspectives. *World J Gastroenterol* 2020; **26**: 5408-5419 [PMID: 33024393 DOI: 10.3748/wjg.v26.i36.5408]

40 **Zhu Y**, Wang QC, Xu MD, Zhang Z, Cheng J, Zhong YS, Zhang YQ, Chen WF, Yao LQ, Zhou PH, Li QL. Application of convolutional neural network in the diagnosis of the invasion depth of gastric cancer based on conventional endoscopy. *Gastrointest Endosc* 2019; **89**: 806-815.e1 [PMID: 30452913 DOI: 10.1016/j.gie.2018.11.011]

41 **Patel N**, Benipal B. Incidence of Esophageal Cancer in the United States from 2001-2015: A United States Cancer Statistics Analysis of 50 States. *Cureus* 2018; **10**: e3709 [PMID: 30788198 DOI: 10.7759/cureus.3709]

42 **Behrens A**, Pech O, Graupe F, May A, Lorenz D, Ell C. Barrett's adenocarcinoma of the esophagus: better outcomes through new methods of diagnosis and treatment. *Dtsch Arztebl Int* 2011; **108**: 313-319 [PMID: 21629515 DOI: 10.3238/arztebl.2011.0313]

43 **Phoa KN**, Pouw RE, Bisschops R, Pech O, Ragunath K, Weusten BL, Schumacher B, Rembacken B, Meining A, Messmann H, Schoon EJ, Gossner L, Mannath J, Seldenrijk CA, Visser M, Lerut T, Seewald S, ten Kate FJ, Ell C, Neuhaus H, Bergman JJ. Multimodality endoscopic eradication for neoplastic Barrett oesophagus: results of an European multicentre study (EURO-II). *Gut* 2016; **65**: 555-562 [PMID: 25731874 DOI: 10.1136/gutjnl-2015-309298]

44 **van der Sommen F**, Zinger S, Curvers WL, Bisschops R, Pech O, Weusten BL, Bergman JJ, de With PH, Schoon EJ. Computer-aided detection of early neoplastic lesions in Barrett's esophagus. *Endoscopy* 2016; **48**: 617-624 [PMID: 27100718 DOI: 10.1055/s-0042-105284]

45 **Swager AF**, van der Sommen F, Klomp SR, Zinger S, Meijer SL, Schoon EJ, Bergman JJGHM, de With PH, Curvers WL. Computer-aided detection of early Barrett's neoplasia using volumetric laser endomicroscopy. *Gastrointest Endosc* 2017; **86**: 839-846 [PMID: 28322771 DOI: 10.1016/j.gie.2017.03.011]

46 **de Groof J**, van der Sommen F, van der Putten J, Struyvenberg MR, Zinger S, Curvers WL, Pech O, Meining A, Neuhaus H, Bisschops R, Schoon EJ, de With PH, Bergman JJ. The Argos project: The development of a computer-aided detection system to improve detection of Barrett's neoplasia on white light endoscopy. *United European Gastroenterol J* 2019; **7**: 538-547 [PMID: 31065371 DOI: 10.1177/2050640619837443]

47 **de Groof AJ**, Struyvenberg MR, van der Putten J, van der Sommen F, Fockens KN, Curvers WL, Zinger S, Pouw RE, Coron E, Baldaque-Silva F, Pech O, Weusten B, Meining A, Neuhaus H, Bisschops R, Dent J, Schoon EJ, de With PH, Bergman JJ. Deep-Learning System Detects Neoplasia in Patients With Barrett's Esophagus With Higher Accuracy Than Endoscopists in a Multistep Training and Validation Study With Benchmarking. *Gastroenterology* 2020; **158**: 915-929.e4 [PMID: 31759929 DOI: 10.1053/j.gastro.2019.11.030]

48 **de Groof AJ**, Struyvenberg MR, Fockens KN, van der Putten J, van der Sommen F, Boers TG, Zinger S, Bisschops R, de With PH, Pouw RE, Curvers WL, Schoon EJ, Bergman JJGHM. Deep learning algorithm detection of Barrett's neoplasia with high accuracy during live endoscopic procedures: a pilot study (with video). *Gastrointest Endosc* 2020; **91**: 1242-1250 [PMID: 31926965 DOI: 10.1016/j.gie.2019.12.048]

49 **Hashimoto R**, Requa J, Dao T, Ninh A, Tran E, Mai D, Lugo M, El-Hage Chehade N, Chang KJ, Karnes WE, Samarasena JB. Artificial intelligence using convolutional neural networks for real-time detection of early esophageal neoplasia in Barrett's esophagus (with video). *Gastrointest Endosc* 2020; **91**: 1264-1271.e1 [PMID: 31930967 DOI: 10.1016/j.gie.2019.12.049]

50 **Horie Y**, Yoshio T, Aoyama K, Yoshimizu S, Horiuchi Y, Ishiyama A, Hirasawa T, Tsuchida T, Ozawa T, Ishihara S, Kumagai Y, Fujishiro M, Maetani I, Fujisaki J, Tada T. Diagnostic outcomes of esophageal cancer by artificial intelligence using convolutional neural networks. *Gastrointest Endosc* 2019; **89**: 25-32 [PMID: 30120958 DOI: 10.1016/j.gie.2018.07.037]

51 **Cai SL**, Li B, Tan WM, Niu XJ, Yu HH, Yao LQ, Zhou PH, Yan B, Zhong YS. Using a deep learning system in endoscopy for screening of early esophageal squamous cell carcinoma (with video). *Gastrointest Endosc* 2019; **90**: 745-753.e2 [PMID: 31302091 DOI: 10.1016/j.gie.2019.06.044]

52 **Guo L**, Xiao X, Wu C, Zeng X, Zhang Y, Du J, Bai S, Xie J, Zhang Z, Li Y, Wang X, Cheung O, Sharma M, Liu J, Hu B. Real-time automated diagnosis of precancerous lesions and early esophageal squamous cell carcinoma using a deep learning model (with videos). *Gastrointest Endosc* 2020; **91**: 41-51 [PMID: 31445040 DOI: 10.1016/j.gie.2019.08.018]

53 **Ohmori M**, Ishihara R, Aoyama K, Nakagawa K, Iwagami H, Matsuura N, Shichijo S, Yamamoto K, Nagaike K, Nakahara M, Inoue T, Aoi K, Okada H, Tada T. Endoscopic detection and differentiation of esophageal lesions using a deep neural network. *Gastrointest Endosc* 2020; **91**: 301-309.e1 [PMID: 31585124 DOI: 10.1016/j.gie.2019.09.034]

54 **Liu G**, Hua J, Wu Z, Meng T, Sun M, Huang P, He X, Sun W, Li X, Chen Y. Automatic classification of esophageal lesions in endoscopic images using a convolutional neural network. *Ann Transl Med* 2020; **8**: 486 [PMID: 32395530 DOI: 10.21037/atm.2020.03.24]

55 **Fukuda H**, Ishihara R, Kato Y, Matsunaga T, Nishida T, Yamada T, Ogiyama H, Horie M, Kinoshita K, Tada T. Comparison of performances of artificial intelligence versus expert endoscopists for real-time assisted diagnosis of

esophageal squamous cell carcinoma (with video). *Gastrointest Endosc* 2020; **92**: 848-855 [PMID: 32505685 DOI: 10.1016/j.gie.2020.05.043]

56 **Adler SN**. The history of time for capsule endoscopy. *Ann Transl Med* 2017; **5**: 194 [PMID: 28567374 DOI: 10.21037/atm.2017.03.90]

57 **ASGE Technology Committee**, Wang A, Banerjee S, Barth BA, Bhat YM, Chauhan S, Gottlieb KT, Konda V, Maple JT, Murad F, Pfau PR, Pleskow DK, Siddiqui UD, Tokar JL, Rodriguez SA. Wireless capsule endoscopy. *Gastrointest Endosc* 2013; **78**: 805-815 [PMID: 24119509 DOI: 10.1016/j.gie.2013.06.026]

58 **McAlindon ME**, Ching HL, Yung D, Sidhu R, Koulaouzidis A. Capsule endoscopy of the small bowel. *Ann Transl Med* 2016; **4**: 369 [PMID: 27826572 DOI: 10.21037/atm.2016.09.18]

59 **Zheng Y**, Hawkins L, Wolff J, Goloubeva O, Goldberg E. Detection of lesions during capsule endoscopy: physician performance is disappointing. *Am J Gastroenterol* 2012; **107**: 554-560 [PMID: 22233695 DOI: 10.1038/ajg.2011.461]

60 **Mamonov AV**, Figueiredo IN, Figueiredo PN, Tsai YH. Automated polyp detection in colon capsule endoscopy. *IEEE Trans Med Imaging* 2014; **33**: 1488-1502 [PMID: 24710829 DOI: 10.1109/TMI.2014.2314959]

61 **Silva J**, Histace A, Romain O, Dray X, Granado B. Toward embedded detection of polyps in WCE images for early diagnosis of colorectal cancer. *Int J Comput Assist Radiol Surg* 2014; **9**: 283-293 [PMID: 24037504 DOI: 10.1007/s11548-013-0926-3]

62 **Iakovidis DK**, Koulaouzidis A. Automatic lesion detection in capsule endoscopy based on color saliency: closer to an essential adjunct for reviewing software. *Gastrointest Endosc* 2014; **80**: 877-883 [PMID: 25088924 DOI: 10.1016/j.gie.2014.06.026]

63 **Liu G**, Yan G, Kuang S, Wang Y. Detection of small bowel tumor based on multi-scale curvelet analysis and fractal technology in capsule endoscopy. *Comput Biol Med* 2016; **70**: 131-138 [PMID: 26829705 DOI: 10.1016/j.compbiomed.2016.01.021]

64 **K G**, C R. Heuristic Classifier for Observe Accuracy of Cancer Polyp Using Video Capsule Endoscopy. *Asian Pac J Cancer Prev* 2017; **18**: 1681-1688 [PMID: 28670889 DOI: 10.22034/APJCP.2017.18.6.1681]

65 **Vieira PM**, Freitas NR, Valente J, Vaz IF, Rolanda C, Lima CS. Automatic detection of small bowel tumors in wireless capsule endoscopy images using ensemble learning. *Med Phys* 2020; **47**: 52-63 [PMID: 31299096 DOI: 10.1002/mp.13709]

66 **Saito H**, Aoki T, Aoyama K, Kato Y, Tsuboi A, Yamada A, Fujishiro M, Oka S, Ishihara S, Matsuda T, Nakahori M, Tanaka S, Koike K, Tada T. Automatic detection and classification of protruding lesions in wireless capsule endoscopy images based on a deep convolutional neural network. *Gastrointest Endosc* 2020; **92**: 144-151.e1 [PMID: 32084410 DOI: 10.1016/j.gie.2020.01.054]

67 **Das A**, Nguyen CC, Li F, Li B. Digital image analysis of EUS images accurately differentiates pancreatic cancer from chronic pancreatitis and normal tissue. *Gastrointest Endosc* 2008; **67**: 861-867 [PMID: 18179797 DOI: 10.1016/j.gie.2007.08.036]

68 **Săftoiu A**, Vilmann P, Dietrich CF, Iglesias-Garcia J, Hocke M, Seicean A, Ignee A, Hassan H, Streba CT, Ioncică AM, Gheonea DI, Ciurea T. Quantitative contrast-enhanced harmonic EUS in differential diagnosis of focal pancreatic masses (with videos). *Gastrointest Endosc* 2015; **82**: 59-69 [PMID: 25792386 DOI: 10.1016/j.gie.2014.11.040]

69 **Zhu M**, Xu C, Yu J, Wu Y, Li C, Zhang M, Jin Z, Li Z. Differentiation of pancreatic cancer and chronic pancreatitis using computer-aided diagnosis of endoscopic ultrasound (EUS) images: a diagnostic test. *PLoS One* 2013; **8**: e63820 [PMID: 23704940 DOI: 10.1371/journal.pone.0063820]

70 **Kuwahara T**, Hara K, Mizuno N, Okuno N, Matsumoto S, Obata M, Kurita Y, Koda H, Toriyama K, Onishi S, Ishihara M, Tanaka T, Tajika M, Niwa Y. Usefulness of Deep Learning Analysis for the Diagnosis of Malignancy in Intraductal Papillary Mucinous Neoplasms of the Pancreas. *Clin Transl Gastroenterol* 2019; **10**: 1-8 [PMID: 31117111 DOI: 10.14309/ctg.0000000000000045]

71 **Marya NB**, Powers PD, Chari ST, Gleeson FC, Leggett CL, Abu Dayyeh BK, Chandrasekhara V, Iyer PG, Majumder S, Pearson RK, Petersen BT, Rajan E, Sawas T, Storm AC, Vege SS, Chen S, Long Z, Hough DM, Mara K, Levy MJ. Utilisation of artificial intelligence for the development of an EUS-convolutional neural network model trained to enhance the diagnosis of autoimmune pancreatitis. *Gut* 2021; **70**: 1335-1344 [PMID: 33028668 DOI: 10.1136/gutjnl-2020-322821]

72 **Minoda Y**, Ihara E, Komori K, Ogino H, Otsuka Y, Chinen T, Tsuda Y, Ando K, Yamamoto H, Ogawa Y. Efficacy of endoscopic ultrasound with artificial intelligence for the diagnosis of gastrointestinal stromal tumors. *J Gastroenterol* 2020; **55**: 1119-1126 [PMID: 32918102 DOI: 10.1007/s00535-020-01725-4]

73 **Marya NB**, Powers PD, Fujii-Lau L, Abu Dayyeh BK, Gleeson FC, Chen S, Long Z, Hough DM, Chandrasekhara V, Iyer PG, Rajan E, Sanchez W, Sawas T, Storm AC, Wang KK, Levy MJ. Application of artificial intelligence using a novel EUS-based convolutional neural network model to identify and distinguish benign and malignant hepatic masses. *Gastrointest Endosc* 2021; **93**: 1121-1130.e1 [PMID: 32861752 DOI: 10.1016/j.gie.2020.08.024]

74 **Repici A**, Wallace MB, East JE, Sharma P, Ramirez FC, Bruining DH, Young M, Gatof D, Irene Mimi Canto M, Marcon N, Cannizzaro R, Kiesslich R, Rutter M, Dekker E, Siersema PD, Spaander M, Kupcinskas L, Jonaitis L, Bisschops R, Radaelli F, Bhandari P, Wilson A, Early D, Gupta N, Vieth M, Lauwers GY, Rossini M, Hassan C. Efficacy of Per-oral Methylene Blue Formulation for Screening Colonoscopy. *Gastroenterology* 2019; **156**: 2198-2207.e1 [PMID: 30742834 DOI: 10.1053/j.gastro.2019.02.001]

75 **Simonyan K**, Zisserman A. Very Deep Convolutional Networks for Large-Scale Image Recognition. arXiv preprint arXiv:1409.1556. 2014

76 **Huang G**, Liu Z, van der Maaten L, Weinberger KQ. Densely Connected Convolutional Networks. In: 2017 IEEE Conference on Computer Vision and Pattern Recognition (CVPR), 2017: 2261-2269 [DOI: 10.1109/CVPR.2017.243]

77 **He K**, Zhang X, Ren S, Sun J. Deep Residual Learning for Image Recognition. In: 2016 IEEE Conference on Computer Vision and Pattern Recognition (CVPR), 2016: 770-778 [DOI: 10.1109/CVPR.2016.90]

78 **Szegedy C**, Vanhoucke V, Ioffe S, Shlens J, Wojna Z. Rethinking the Inception Architecture for Computer Vision. In: 2016 IEEE Conference on Computer Vision and Pattern Recognition (CVPR), 2016: 2818-2826 [DOI: 10.1109/CVPR.2016.308]

79 **Zhang X**, Pan W, Xiao P. In-Vivo Skin Capacitive Image Classification Using AlexNet Convolution Neural Network. In: 2018 IEEE 3rd International Conference on Image, Vision and Computing (ICIVC), 2018: 439–443 [DOI: 10.1109/ICIVC.2018.8492860]

80 **Antioquia AMC**, Stanley Tan D, Azcarraga A, Cheng WH, Hua KL. ZipNet: ZFNet-level Accuracy with 48× Fewer Parameters. In: 2018 IEEE Visual Communications and Image Processing (VCIP), 2018: 1-4 [DOI: 10.1109/VCIP.2018.8698672]

81 **Algorry AM**, García AG, Wofmann AG. Real-Time Object Detection and Classification of Small and Similar Figures in Image Processing. In: 2017 International Conference on Computational Science and Computational Intelligence (CSCI), 2017: 516-519 [DOI: 10.1109/CSCI.2017.87]

World Journal of Gastrointestinal Oncology

Submit a Manuscript: https://www.f6publishing.com

World J Gastrointest Oncol 2022 May 15; 14(5): 1002-1013

DOI: 10.4251/wjgo.v14.i5.1002

ISSN 1948-5204 (online)

ORIGINAL ARTICLE

Retrospective Study

Pretreatment serum albumin-to-alkaline phosphatase ratio is an independent prognosticator of survival in patients with metastatic gastric cancer

Yu-Ting Li, Xiao-Shu Zhou, Xiao-Ming Han, Jing Tian, You Qin, Tao Zhang, Jun-Li Liu

Specialty type: Oncology

Provenance and peer review: Unsolicited article; Externally peer reviewed.

Peer-review model: Single blind

Peer-review report's scientific quality classification
Grade A (Excellent): 0
Grade B (Very good): B
Grade C (Good): C, C
Grade D (Fair): 0
Grade E (Poor): 0

P-Reviewer: de Melo FF, Brazil; Mishra TS, India; Silano F, Brazil

Received: November 9, 2021
Peer-review started: November 9, 2021
First decision: December 12, 2021
Revised: December 26, 2021
Accepted: April 21, 2022
Article in press: April 21, 2022
Published online: May 15, 2022

Yu-Ting Li, Xiao-Shu Zhou, You Qin, Tao Zhang, Jun-Li Liu, Cancer Center, Union Hospital, Tongji Medical College, Huazhong University of Science and Technology, Wuhan 430022, Hubei Province, China

Xiao-Ming Han, Department of Ultrasound Medicine, Jingmen Second People's Hospital, Jingchu University of Technology Affiliated Central Hospital, Jingmen 448000, Hubei Province, China

Jing Tian, Department of Oncology, Hubei Cancer Hospital, The Seventh Clinical School Affiliated of Tongji Medical College, Huazhong University of Science and Technology, Wuhan 430000, Hubei Province, China

Corresponding author: Jun-Li Liu, MD, PhD, Associate Chief Physician, Associate Professor, Cancer Center, Union Hospital, Tongji Medical College, Huazhong University of Science and Technology, Jianghan Road, Wuhan 430022, Hubei Province, China. junli78@foxmail.com

Abstract

BACKGROUND

Previous studies have suggested that a low albumin-to-alkaline phosphatase ratio (AAPR) is associated with a lower survival rate in patients with various malignancies. However, the relationship between pretreatment AAPR and the prognosis of patients with gastric cancer (GC) remains unclear.

AIM

To investigate the prognostic value of AAPR in distant metastatic GC.

METHODS

A total of 191 patients with distant metastatic cancer from a single institute were enrolled in this study. Pretreatment clinical data, including serum albumin and alkaline phosphatase levels, were collected. A chi-square test or Fisher's exact test was applied to evaluate the correlations between AAPR and various clinical parameters in GC patients. The Kaplan–Meier method and Cox proportional hazards regression model were used to evaluate the prognostic efficacy of AAPR in metastatic GC patients. A two-sided *P* value lower than 0.05 was considered statistically significant.

RESULTS

A receiver operating characteristic curve indicated that 0.48 was the optimal threshold value for AAPR. AAPR ≤ 0.48 was significantly associated with bone ($P < 0.05$) and liver metastasis ($P < 0.05$). Patients with high levels of AAPR had better survival in terms of overall survival (OS) and progression-free survival (PFS), regardless of the presence of liver/bone metastasis. Pretreatment AAPR was found to be a favorable predictor of OS and PFS based on a multivariate cox regression model. AAPR-M system, constructed based on AAPR and number of metastatic sites, showed superior predictive ability relative to the number of metastatic sites for predicting survival.

CONCLUSION

Pretreatment AAPR may serve as an independent prognostic factor for predicting PFS and OS in patients with metastatic GC. Furthermore, AAPR may assist clinicians with individualizing treatment.

Key Words: Albumin-to-alkaline phosphatase ratio; Gastric cancer; overall survival; Progression-free survival

Core Tip: Previous studies have suggested that a low albumin-to-alkaline phosphatase ratio (AAPR) is associated with inferior survival in patients with various malignancies. However, the relationship between pretreatment AAPR and the prognosis of patients with gastric cancer (GC) remains unclear. In this study, we showed that pretreatment AAPR was a favorable predictor of overall survival (OS) and progression-free survival (PFS) by the multivariate cox regression model with hazard ratios of 0.476 and 0.527, respectively. Pretreatment AAPR may serve as an independent prognostic factor for predicting PFS and OS in patients with metastatic cancer. Furthermore, AAPR may assist clinicians with individualizing treatment.

Citation: Li YT, Zhou XS, Han XM, Tian J, Qin Y, Zhang T, Liu JL. Pretreatment serum albumin-to-alkaline phosphatase ratio is an independent prognosticator of survival in patients with metastatic gastric cancer. *World J Gastrointest Oncol* 2022; 14(5): 1002-1013

URL: https://www.wjgnet.com/1948-5204/full/v14/i5/1002.htm

DOI: https://dx.doi.org/10.4251/wjgo.v14.i5.1002

INTRODUCTION

Despite the decline in incidence and mortality over the last decade[1], gastric cancer (GC) is still a severe threat to human health, especially in Eastern Asia, including China, Japan, and Korea[2]. Although more effective treatment regimens have been developed for patients with GC, the prognosis of this disease remains poor, especially for those with distant metastasis, and the 5-year overall survival (OS) rate is only 5.3%[3]. Currently, the recognized tumor-node-metastasis staging system does not provide accurate prognostic information and does not aid clinical decision-making for patients with metastatic cancers[4,5]. Therefore, low cost, easy to obtain, and reliable biomarkers are needed to accurately predict survival for patients with metastatic cancers.

Various biomarkers such as serum levels of programmed cell death ligand 1[6], the platelet-to-lymphocyte ratio[7], the neutrophil-to-lymphocyte ratio[8], and serum levels of high-density lipoprotein cholesterol[9], carcinoembryonic antigen, and carbohydrate antigen 19-9[10], are all currently used prognostic indicators for GC in patients. Nevertheless, the predictive powers of these respective markers are not conclusive and need further validation before being integrated into standard clinical practice. Hence, there is still an urgent need to identify precise predictors of survival for GC patients.

The albumin-to-alkaline phosphatase ratio (AAPR), which is calculated as albumin divided by alkaline phosphatase (ALP), has been shown to be closely associated with clinical outcomes in numerous types of cancer, including hepatocellular carcinoma (HCC)[11], cholangiocarcinoma[12], non-small cell lung cancer (NSCLC)[13,14], small cell lung cancer[15], nasopharyngeal carcinoma[16], and pancreatic ductal adenocarcinoma[17]. Recently, AAPR was found to be significantly decreased in patients with resectable GC, and low level AAPR predicted poor prognosis in GC[18]. However, as far as we know, the use of AAPR as a prognostic indicator of survival in metastatic GC patients has not yet been verified. Therefore, in this study, we focused on the association between AAPR and metastatic GC and evaluated its prognostic capability in patients with metastatic GC.

MATERIALS AND METHODS

Patients and eligibility

From May 2011 to September 2018, we retrospectively enrolled 191 patients diagnosed with distant metastatic GC at the Cancer Center of the Union Hospital of Huazhong University of Science and Technology (Wuhan, China). The inclusion criteria were as follows: the presence of pathologically proven GC; clinically diagnosed distant metastasis; absence of concurrent malignancies; and availability of pretreatment laboratory tests.

This study was retrospectively designed and in line with the Helsinki Declaration's principles and followed existing national legislation. A waiver of informed consent was obtained for the study because this was a retrospective study, and anonymous analyses were employed in place to protect patient confidentiality, meaning there was minimal risk to the patients. The study was approved by the Institutional Ethical Board of Wuhan Union Hospital of Tongji Medical College, Huazhong University of Science and Technology.

Clinical data collection

Clinical data, such as age, sex, smoking status, sites of metastasis, and histopathology, were collected from the hospital medical system. Furthermore, laboratory data, including pretreatment serum levels of albumin and ALP, were collected from the hospital's laboratory service. The AAPR was calculated by dividing the serum albumin by the serum ALP.

Follow-up assessment

Follow-up was performed by a review of medical records and telephone conversation. The last follow-up date was January 31, 2019. The primary endpoints were OS and progression-free survival (PFS). OS refers to the interval between the dates of diagnosis to the date of death due to any cause or last follow-up. PFS was calculated from the date of diagnosis to the date of disease progression or the date of the last follow-up without evidence of progression.

Statistical analyses

All statistical analyses were performed using SPSS software version 23.0 (IBM, Chicago, IL, United States). Receiver operating characteristic (ROC) curve analysis was utilized to estimate the optimal cut-off value of AAPR. A chi-square test or Fisher's exact test was applied to evaluate the correlations between AAPR and various clinical parameters. Propensity score matching was utilized to balance out selection biases. We employed a logistic regression model to estimate propensity scores for all patients. One-to-one nearest-neighbor matching was used between low and high-level AAPR using a 0.1 caliper width. The score-matched pairs were used in the subsequent analyses. Kaplan-Meier (K-M) method was applied to create survival curves using a log-rank test. We employed a Cox proportional hazards model to identify variables that affected the survival of patients with metastatic GC, using univariate and multivariate analyses. A two-sided P value lower than 0.05 was considered statistically significant.

RESULTS

Patient characteristics

From May 2011 to September 2018, a total of 191 patients with GC were recruited for our study. The demographics and clinical characteristics of the participants are presented in Table 1. The median age was 56 (range: 20-78) years, and 60 (31.4%) patients were older than 60 years. Among the patients, 105 (55.0%) were male and 45 (23.6%) had a history of smoking. The majority (57.1%) of these patients developed metastasis at only one site. There were 57 (29.8%) patients with liver metastasis and 24 (12.6%) patients with bone metastasis. Approximately half of the patients had poorly differentiated carcinoma (40.3%). A total of 146 (76.4%) patients received Taxane- or fluorouracil-based combination chemotherapy as a first-line treatment.

A ROC curve identified 0.48 as the optimal threshold value of AAPR (Supplementary Figure 1). The distribution of clinical characteristics between the two groups is listed in Table 1. AAPR ≤ 0.48 was significantly associated with bone (P = 0.023) and liver metastasis (P = 0.000). Higher AAPR values were more often observed in female patients, and patients who had metastasis in one site upon diagnosis. The median follow-up period was 8.9 (range, 1–62.13) months, and 41 patients were still alive at the last follow-up session. Fifty-eight pairs of patients were generated using propensity score matching who showed no significant differences (Table 1).

K-M survival analysis of AAPR

K-M survival analysis of AAPR for OS and PFS was also conducted as a preliminary evaluation of the prognostic capabilities of AAPR. This K-M analysis suggested that high AAPR values were correlated with longer OS [hazard ratio (HR) = 0.536, 95% confidence interval (CI) = 0.385–0.745, P < 0.05] and PFS

Table 1 Baseline patient information and characteristics

Characteristics	Before propensity matching			After propensity matching		
	AAPR ≤ 0.48 (*n* = 86)	AAPR > 0.48 (*n* = 105)	*P* value	AAPR ≤ 0.48 (*n* = 58)	AAPR > 0.48 (*n* = 58)	*P* value
Gender						0.265
Male	56	49	0.011	32	26	
Female	30	56		26	32	
Age						
≤ 60	59	72	0.996	39	40	0.842
> 60	27	33		19	18	
Smoking status						
No	61	85	0.018	44	48	0.359
Yes	25	20		14	10	
Number of involved sites						
One	41	68	0.018	30	24	0.264
Multiple	45	37		28	34	
Liver metastasis						
No	48	86	0.000	44	44	1.000
Yes	38	19		14	14	
Bone metastasis						
No	70	97	0.023	50	50	1.00
Yes	16	8		8	8	
Pathology						
High differentiated	3	1	0.201	1	0	0.334
Moderately differentiated	3	4		3	2	
Poorly differentiated	31	46		17	25	
Signet ring cell	13	25		9	13	
Others	2	3		1	1	
Unknown	34	26		27	17	
Treatment regimens						
Combination chemotherapy	63	83	0.520	45	44	0.378
Fluorouracil or taxane alone	11	7		7	3	
Radiotherapy	1	2		1	2	
Best supportive care	11	13		5	9	

AAPR: Albumin-to-alkaline phosphatase ratio.

(HR = 0.611, 95%CI = 0.446–0.837, $P < 0.05$) (Figure 1A and B). The median OS (mOS) and PFS values of patients with AAPR ≤ 0.48 were 7.73 and 4.37 months, respectively, which were significantly shorter compared with patients in the high AAPR group (> 0.48), which had a median OS and PFS of 11.57 and 8.63 months, respectively. Among propensity-matched pairs of patients, similar results were obtained for OS (HR = 0.634, 95%CI = 0.426–0.944, $P < 0.05$) and PFS (HR = 0.584, 95%CI = 0.385–0.884, $P < 0.05$) (Figure 1C and D).

Subgroup analyses

We conducted subgroup analyses to investigate the relationship between AAPR and survival according to the number of sites with metastasis, with or without bone/Liver metastasis. Patients with low AAPR values showed markedly worse OS (HR = 0.512, 95%CI = 0.344–0.763, $P < 0.05$) and PFS (HR = 0.553, 95%CI = 0.376–0.811, $P < 0.05$) compared with those with high AAPR values in the subgroup without

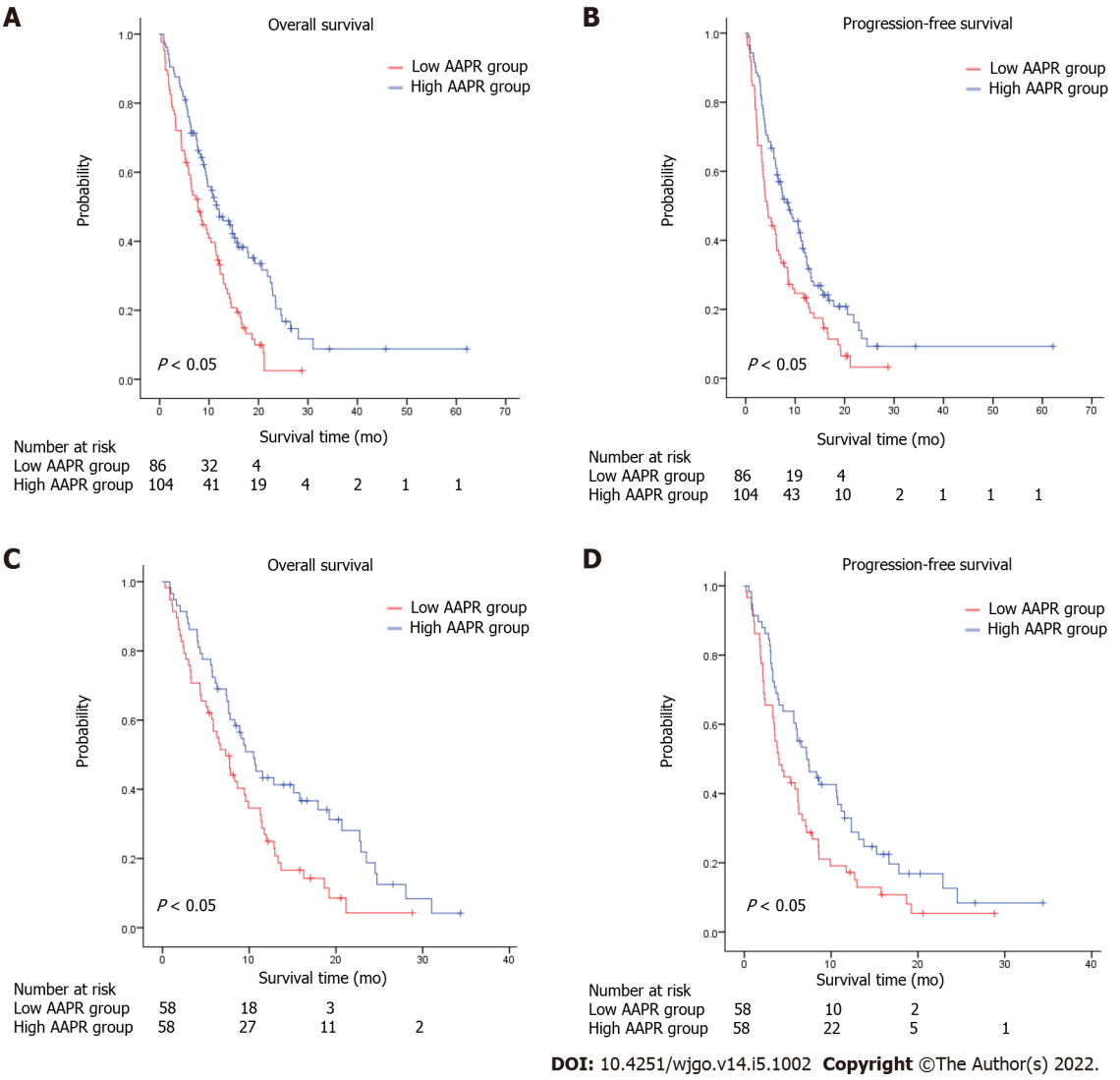

DOI: 10.4251/wjgo.v14.i5.1002

Figure 1 Kaplan-Meier survival estimates between subgroups according to albumin-to-alkaline phosphatase ratio. A: Overall survival (OS) according to albumin-to-alkaline phosphatase ratio (AAPR) before propensity matching; B: Progression-free survival (PFS) according to AAPR before propensity matching; C: OS according to AAPR after propensity matching; D: PFS according to AAPR after propensity matching. AAPR: Albumin-to-alkaline phosphatase ratio.

liver metastasis (Figure 2A and B). Similarly, in the subgroup without bone metastasis, an AAPR ≤ 0.48 was significantly correlated with worse OS (HR = 0.522, 95%CI = 0.366–0.744, $P < 0.05$) and PFS (HR = 0.607, 95%CI = 0.433–0.850, $P < 0.05$) (Figure 2C and D). Not surprisingly, patients with high AAPR values had better OS and PFS in the subgroup without liver/bone metastasis (OS: HR = 0.541, 95%CI = 0.347–0.842, $P < 0.05$; PFS: HR = 0.589, 95%CI = 0.384–0.902, $P < 0.05$) (Figure 2E and F). In patients with one site of metastasis, AAPR > 0.48 was associated with better survival in terms of OS (HR = 0.540, 95%CI = 0.343–0.849, $P < 0.05$) and PFS (HR = 0.567, 95%CI = 0.370–0.869, $P < 0.05$) (Figure 3A and B). Patients receiving fluorouracil or taxane alone as a first-line treatment had a relative short mOS (mOS: 2.40 mo, 95%CI = 1.88–2.92) in the low AAPR group, which was much shorter than in the high AAPR group (mOS: 6.27 mo, 95%CI = 3.27–9.26) (Supplementary Table 1). In contrast, patients who received combination chemotherapy in the low AAPR group had better survival outcomes (mOS: 10.37 mo, 95%CI = 7.40–13.33) (Supplementary Table 1).

Univariate and multivariate analyses

Univariate and multivariate analyses were conducted to estimate the predictive value of AAPR. As shown in Tables 2 and 3, univariate analysis demonstrated that high AAPR levels (HR = 0.611, 95%CI = 0.446–0.837, $P < 0.05$), combined chemotherapy as first-line treatment regimen (HR = 0.448, 95%CI = 0.313–0.639, $P < 0.05$), and only one metastasis site (HR = 1.484, 95%CI = 1.083–2.034, $P < 0.05$) were significantly associated with better PFS in patients with metastatic GC. Meanwhile, high AAPR levels (HR = 0.536, 95%CI = 0.385–0.745, $P < 0.05$), male (HR = 0.705, 95%CI = 0.510–0.975, $P < 0.05$), only one metastasis site (HR = 1.748, 95%CI = 1.264–2.417, $P < 0.05$), and combination chemotherapy as first-line treatment regimen (HR = 0.334, 95%CI = 0.232–0.480, $P < 0.05$) were determined to be favorable

Table 2 Univariate and multivariate analyses of prognostic factors for overall survival for all patients

Variables	Univariate analyses		Multivariate analyses	
	HR (95%CI)	*P* value	HR (95%CI)	*P* value
Gender (male *vs* female)	0.705 (0.510-0.975)	0.035	0.746 (0.508-1.094)	0.133
Age (> 60 *vs* ≤ 60)	1.125 (0.794-1.594)	0.509	0.808 (0.541-1.207)	0.298
Smoking status (Yes *vs* No)	1.451 (0.970-2.173)	0.070	1.364 (0.851-2.188)	0.197
Number of involved sites (multiple *vs* one)	1.748 (1.264-2.417)	0.001	1.425 (1.018-1.997)	0.038
Liver metastasis (Yes *vs* No)	0.950 (0.674-1.339)	0.731	0.758 (0.511-1.124)	0.167
Bone metastasis (Yes *vs* No)	1.319 (0.822-2.115)	0.251	1.395 (0.843-2.307)	0.195
Treatment regimens (combination chemotherapy *vs* others)	0.334 (0.232-0.480)	0.000	0.269 (0.175-0.411)	0.000
AAPR (> 0.48 *vs* ≤ 0.48)	0.536 (0.385-0.745)	0.000	0.476 (0.328-0.691)	0.000

HR: Hazard ratio; CI: Confidence interval; AAPR: Albumin-to-alkaline phosphatase ratio.

Table 3 Univariate and multivariate analyses of prognostic factors for progression-free survival for all patients

Variables	Univariate analyses		Multivariate analyses	
	HR (95%CI)	*P* value	HR (95%CI)	*P* value
Gender (male *vs* female)	0.759 (0.554-1.041)	0.087	0.772 (0.529-1.126)	0.179
Age (> 60 *vs* ≤ 60)	1.162 (0.830-1.626)	0.382	0.955 (0.654-1.395)	0.813
Smoking status (Yes *vs* No)	0.805 (0.550-1.177)	0.262	1.227 (0.781-1.927)	0.375
Number of involved sites (multiple *vs* one)	1.484 (1.083-2.034)	0.014	1.223 (0.880-1.701)	0.231
Liver metastasis (Yes *vs* No)	0.950 (0.674-1.339)	0.770	0.737 (0.506-1.073)	0.112
Bone metastasis (Yes *vs* No)	1.219 (0.762-1.951)	0.409	1.232 (0.754-2.011)	0.405
Treatment regimens (combination chemotherapy *vs* others)	0.448 (0.313-0.639)	0.000	0.398 (0.263-0.594)	0.000
AAPR (> 0.48 *vs* ≤ 0.48)	0.611 (0.446-0.837)	0.002	0.527 (0.370-0.751)	0.000

HR: Hazard ratio; CI: Confidence interval; AAPR: Albumin-to-alkaline phosphatase ratio.

prognostic indicators of OS. Subsequent multivariate analyses revealed that AAPR was a significant predictor of both OS (HR = 0.476, 95%CI = 0.328–0.691, $P < 0.05$) and PFS (HR = 0.527, 95%CI = 0.370–0.751, $P < 0.05$) in patients with metastatic GC. AAPR > 0.48 was found to be associated with a favorable prognosis in patients with metastatic GC. Combination chemotherapy predicted better OS (HR = 0.269, 95%CI = 0.175–0.411, $P < 0.05$) and PFS (HR = 0.398, 95%CI = 0.263–0.594, $P < 0.05$) in patients with metastatic GC. We also determined that the number of metastatic sites involved was also an independent prognostic factor of OS (HR = 1.425, 95%CI = 1.018–1.997, $P < 0.05$).

Predictive value of AAPR-M system

According to a previous study conducted in 2016, several factors were associated with worse prognosis, including age, carcinomatosis, and a larger burden of metastatic disease[19]. In our study, the number of metastatic sites was an independent prognostic factor. A combined model named AAPR-M was constructed based on AAPR and number of metastatic sites aimed at finding more prognostic factors for metastatic GC. We classified the patients into three groups according to this innovative AAPR-M system. Patients with high AAPR levels and only one metastatic site were assigned to a low-risk group, patients with more than one metastatic site and a low AAPR level were assigned to a high-risk group, while the others were grouped into a medium-risk group. Strong association with increased death and progression were documented for patients with high risk according to AAPR-M system. The median OS was 14.03 (95%CI: 10.32–17.75) *vs* 9.60 (95%CI: 7.59–11.61) *vs* 5.83 (95%CI: 3.18–8.48) months in the high, medium and low-risk groups, respectively (Figure 4A). Similar results were found in PFS (Figure 4B), suggesting that this AAPR-M system had a very strong predictive ability for survival in patients with metastatic GC.

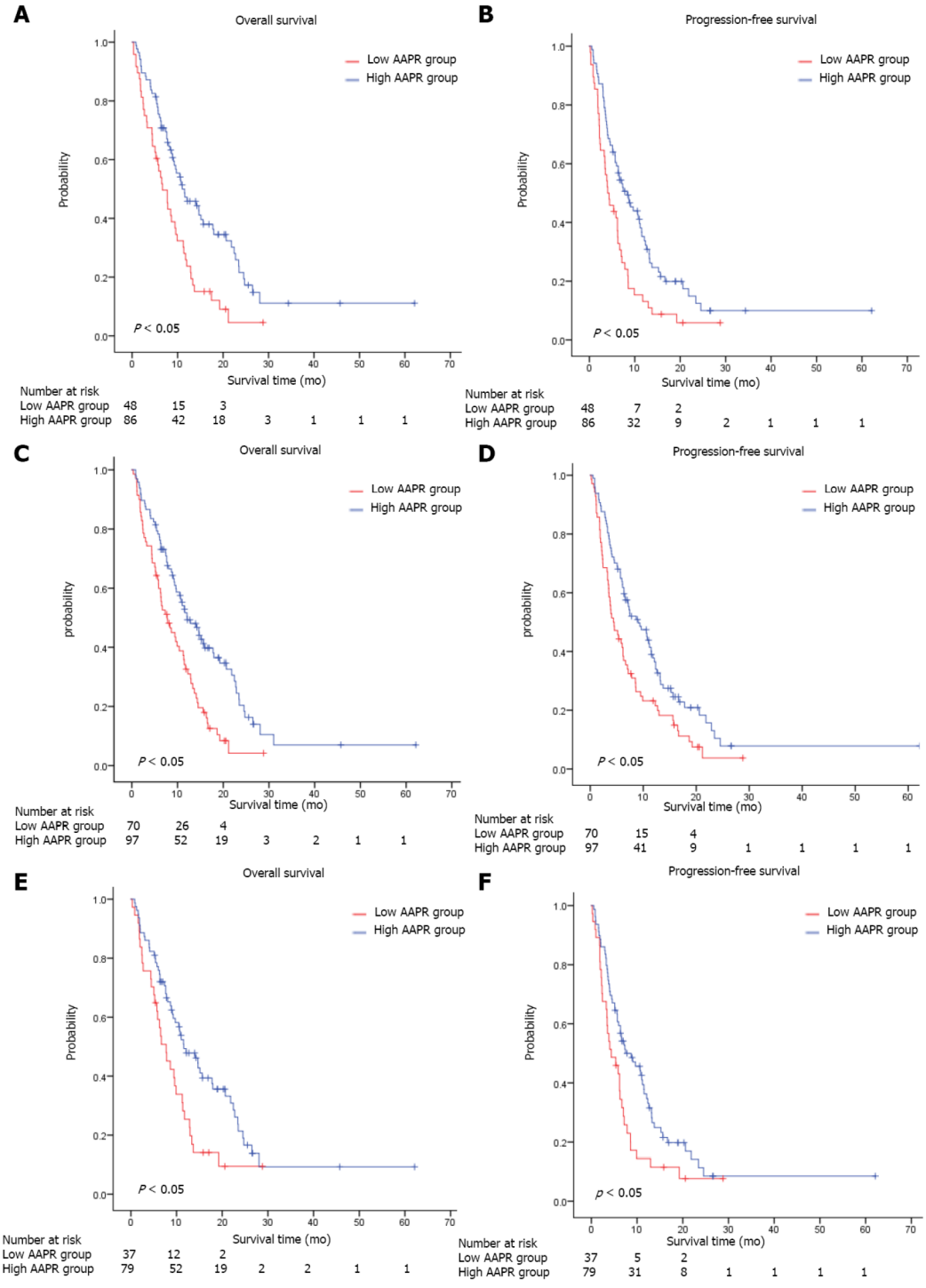

DOI: 10.4251/wjgo.v14.i5.1002

Figure 2 Kaplan–Meier survival estimates of overall survival and progression-free survival according to albumin-to-alkaline phosphatase ratio levels in patients (A and B) without liver metastasis, (C and D) without bone metastasis, (E and F) without liver or bone metastasis.
AAPR: Albumin-to-alkaline phosphatase ratio.

We applied area under the curve (AUC) values to compare the predictive ability between AAPR, the number of metastatic sites, and AAPR-M. AAPR-M showed greater AUC compared with the number of metastatic sites in terms of 1-year OS, 2-year OS, and 1-year PFS (Figure 5). The AAPR-M system had a larger χ^2 value relative to the number of metastatic sites for 1-year OS (7.451 *vs* 6.071), 2-year OS (8.831 *vs* 1.779), and 1-year PFS (4.239 *vs* 2.454) prediction in likelihood ratio test analysis. This suggested that AAPR-M was superior to the number of metastatic sites for predicting survival.

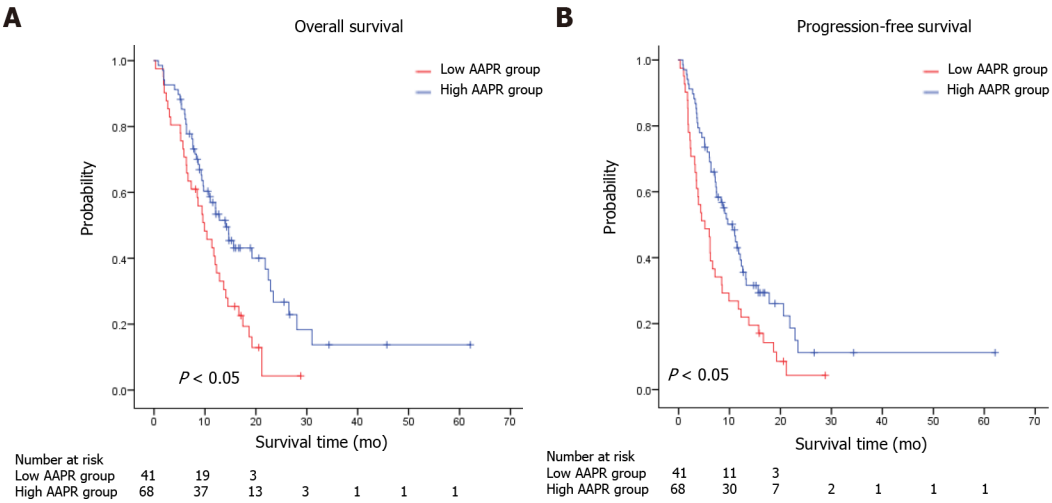

DOI: 10.4251/wjgo.v14.i5.1002

Figure 3 Kaplan–Meier survival estimates of overall survival and progression-free survival according to albumin-to-alkaline phosphatase ratio levels in patients with one site of metastasis. A: Overall survival according to abumin-to-alkaline phosphatase ratio (AAPR); B: Progression-free survival according to AAPR. AAPR: Albumin-to-alkaline phosphatase ratio.

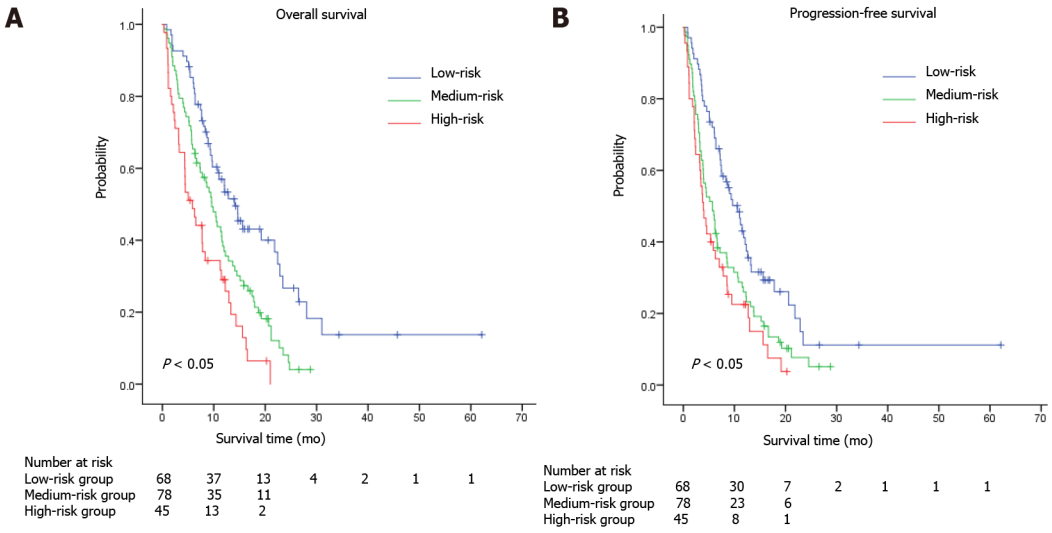

DOI: 10.4251/wjgo.v14.i5.1002

Figure 4 Kaplan–Meier survival estimates of overall survival (A) and progression-free survival (B) according to the AAPR-M risk system (combination of albumin-to-alkaline phosphatase ratio and number of metastatic sites) in metastatic gastric patients.

DISCUSSION

This study evaluated the prognostic relevance of AAPR in patients with metastatic GC and, to the best of our knowledge, was the first study to focus on the relationship between the AAPR and prognosis in metastatic GC. This study demonstrated that smaller AAPR values were correlated with inferior clinical outcomes in terms of OS and PFS in patients with metastatic GC. Furthermore, multivariate analysis demonstrated that AAPR was an independent prognostic indicator of metastatic GC.

Albumin is one of the major plasma proteins that indicate an individual's nutritional status. This protein is involved in maintaining intravascular oncotic pressure, scavenging free radicals, and maintaining steroid hormone hemostasis[20]. Previous studies have demonstrated that hypoalbuminemia is a prognostic indicator in colorectal cancer[21] and glioblastoma multiforme[22]. Notably, low levels of preoperative serum albumin are correlated with poor OS in GC patients after surgery[23], indicating that albumin is a prognostic biomarker for GC.

ALP is a ubiquitous membrane-bound glycoprotein that exist in several mammalian tissues such as liver, bone, and kidney[24]. Serum ALP is closely associated with the presence of liver and bone metastasis in malignant diseases[25-27]. Serum ALP is also an independent predictor of various cancers

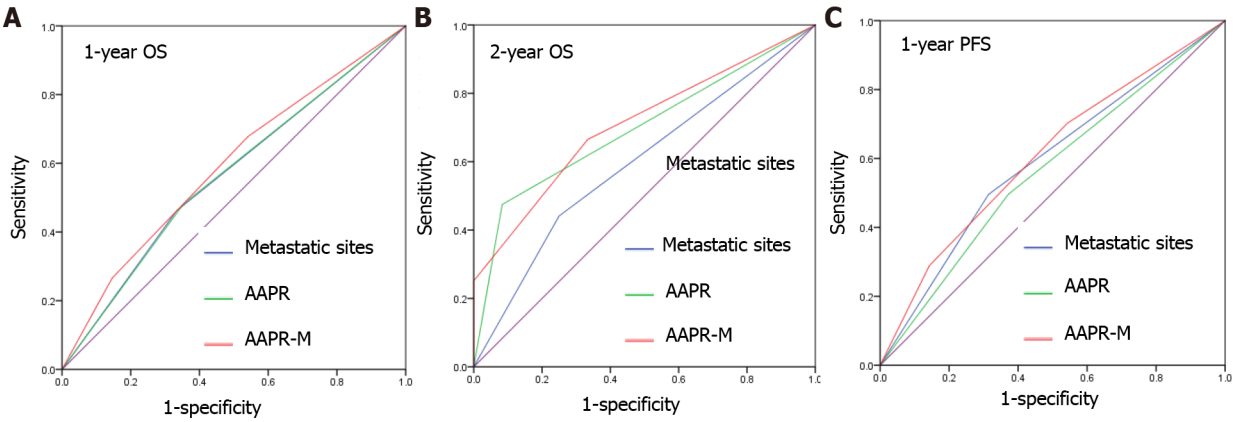

DOI: 10.4251/wjgo.v14.i5.1002

Figure 5 Receiver operating characteristic analysis of the albumin-to-alkaline phosphatase ratio, number of metastatic sites, and AAPR-M system in 1-year overall survival (A), 2-year overall survival (B), and 1-year progression-free survival (C) prediction. PFS: Progression-free survival; OS: Overall survival; AAPR: Albumin-to-alkaline phosphatase ratio.

including breast cancer[28], nasopharyngeal carcinoma[29], prostate cancer[30], and GC[31].

As both albumin and ALP are prognostic indicators of survival in several types of cancer, Chan *et al* [32] derived the albumin-to-alkaline phosphatase ratio to put these two parameters together, and found that AAPR was a superior prognostic indicator compared with albumin and ALP alone in patients with HCC. Thereafter, the prognostic capability of AAPR has been verified in several types of cancer, and the majority of data indicates that low AAPR values are correlated with poorer survival[11,13,16]. Three meta-analyses were recently conducted and a consistent conclusion was drawn, namely, that cancer patients with higher AAPR levels have better survival than patients with lower levels[33-35]. However, the prognostic significance of pretreatment AAPR in GC remains unclear. We suspected, however, that AAPR would be a promising prognostic indicator in patients with metastatic GC.

Therefore, we used pretreatment AAPR as a predictor of survival in patients with metastatic GC. In our cohort, an AAPR lower than 0.48 was associated with more metastatic sites, as well as the presence of liver and bone metastasis. In accordance with our findings, Li *et al*[13] demonstrated that elevated AAPR values were more likely to be found in patients with one site of metastasis and advanced NSCLC. A significant correlation was also discovered between patients with liver/bone metastasis and lower AAPR values[13]. Hence, we speculated that high AAPR values at diagnosis may reflect a relatively less aggressive stage of metastatic GC.

Patients with high AAPR values had significantly longer OS and PFS compared to patients with low AAPR values in our study, suggesting that high AAPR values were correlated with favorable survival in metastatic GC. Furthermore, univariate and multivariate cox regression analyses revealed that AAPR was an independent predictor of survival in terms of OS and PFS in patients with metastatic GC. All of these results collectively suggest that AAPR is an excellent predictor of survival in patients with metastatic GC. We demonstrated that patients with low-level AAPR level received fluorouracil or taxane alone as first-line treatment had an mOS of less than 3 months, while patients received combination chemotherapy had an mOS more than 10 months. For patients with rapidly progressing cancers may aggravate in a short time, and loss the chance of treatment. It is particularly important to precisely confirm the gastric patients with advanced malignant disease who are expected to have a poor prognosis. These results gave us a hint that for patients with low AAPR was associated with poor prognosis, and stronger treatment regimens were needed to prolong survival time. Further analysis showed that AAPR-M system may serve as a supplementary strategy to further improve prognostic efficiency for metastatic GC.

However, this study had several limitations. First, this study was retrospective in design, and all of the data was collected from a single institution, which may have introduced bias in the results. Multicenter prospective studies are needed to verify and extend these findings. Second, the cut-off value of AAPR was obtained from a ROC curve in this study. To date, a consensus regarding the optimal threshold has not been reached, and external validation is required. Third, only pretreatment AAPR was adopted to evaluate its prognostic capability in metastatic GC; thus, whether dynamic AAPR is related to the prognosis of GC is unclear. Fourth, our conclusions were restricted by the small sample size, and high quality, large scale, prospective cohort studies are needed to validate these conclusions.

CONCLUSION

In conclusion, as far as we know, our study demonstrated that pretreatment AAPR is an independent prognostic indicator of both OS and PFS in patients with metastatic GC for the first time. Patients with high levels of pretreatment AAPR showed better survival compared with those with low levels. To verify the prognostic efficacy of AAPR, prospective studies are needed.

ARTICLE HIGHLIGHTS

Research background

Previous studies have suggested that a low albumin-to-alkaline phosphatase ratio (AAPR) is associated with a lower survival rate in patients with various malignancies.

Research motivation

The predictive ability had been established in several malignancies, however, the relationship between pretreatment AAPR and the prognosis of patients with gastric cancer (GC) remains unclear.

Research objectives

To investigate the prognostic value of AAPR in distant metastatic GC.

Research methods

From May 2011 to September 2018, we retrospectively enrolled 191 patients who were diagnosed with distant metastatic GC.

Research results

Patients with high levels of AAPR had better survival in terms of overall survival (OS) and progression-free survival (PFS), regardless of the presence of liver/bone metastasis. Pretreatment AAPR was found to be a favorable predictor of OS and PFS based on a multivariate cox regression model. AAPR-M system, constructed based on AAPR and number of metastatic sites, showed superior predictive ability relative to the number of metastatic sites for predicting survival.

Research conclusions

Patients with high levels of pretreatment AAPR showed better survival compared with those with low levels.

Research perspectives

Prospective studies are needed to verify the prognostic efficacy of AAPR.

FOOTNOTES

Author contributions: Liu JL, Tian J, Zhang T, and Li YT contributed to the study conception and design and data analysis; Zhou XS and Han XM collected the data; Li YT drafted the first version of the manuscript; Qin Y and Liu JL verified the data and edited the manuscript; The revision of the manuscript was performed by Zhang T and Tian J; The final version submitted for publication was critically reviewed and approved by all the authors.

Institutional review board statement: The study was approved by the Institutional Ethical Board of Wuhan Union Hospital of Tongji Medical College, Huazhong University of Science and Technology.

Informed consent statement: A waiver of informed consent was obtained for the study because this was a retrospective study, and anonymous analyses were employed in place to protect patient confidentiality, meaning there was minimal risk to the patients.

Conflict-of-interest statement: The authors declare that they have no conflict of interest.

Data sharing statement: The datasets generated during and/or analyzed during the current study are available from the corresponding author on reasonable request.

Country/Territory of origin: China

ORCID number: Jun-Li Liu 0000-0001-9082-692X.

S-Editor: Wu YXJ
L-Editor: A
P-Editor: Wu YXJ

REFERENCES

1 **Stock M**, Otto F. Gene deregulation in gastric cancer. *Gene* 2005; **360**: 1-19 [PMID: 16154715 DOI: 10.1016/j.gene.2005.06.026]
2 **Bray F**, Ferlay J, Soerjomataram I, Siegel RL, Torre LA, Jemal A. Global cancer statistics 2018: GLOBOCAN estimates of incidence and mortality worldwide for 36 cancers in 185 countries. *CA Cancer J Clin* 2018; **68**: 394-424 [PMID: 30207593 DOI: 10.3322/caac.21492]
3 **Jim MA**, Pinheiro PS, Carreira H, Espey DK, Wiggins CL, Weir HK. Stomach cancer survival in the United States by race and stage (2001-2009): Findings from the CONCORD-2 study. *Cancer* 2017; **123** Suppl 24: 4994-5013 [PMID: 29205310 DOI: 10.1002/cncr.30881]
4 **Koizumi W**, Narahara H, Hara T, Takagane A, Akiya T, Takagi M, Miyashita K, Nishizaki T, Kobayashi O, Takiyama W, Toh Y, Nagaie T, Takagi S, Yamamura Y, Yanaoka K, Orita H, Takeuchi M. S-1 plus cisplatin *vs* S-1 alone for first-line treatment of advanced gastric cancer (SPIRITS trial): a phase III trial. *Lancet Oncol* 2008; **9**: 215-221 [PMID: 18282805 DOI: 10.1016/S1470-2045(08)70035-4]
5 **Lordick F**, Luber B, Lorenzen S, Hegewisch-Becker S, Folprecht G, Wöll E, Decker T, Endlicher E, Röthling N, Schuster T, Keller G, Fend F, Peschel C. Cetuximab plus oxaliplatin/Leucovorin/5-fluorouracil in first-line metastatic gastric cancer: a phase II study of the Arbeitsgemeinschaft Internistische Onkologie (AIO). *Br J Cancer* 2010; **102**: 500-505 [PMID: 20068568 DOI: 10.1038/sj.bjc.6605521]
6 **Takahashi N**, Iwasa S, Sasaki Y, Shoji H, Honma Y, Takashima A, Okita NT, Kato K, Hamaguchi T, Yamada Y. Serum levels of soluble programmed cell death ligand 1 as a prognostic factor on the first-line treatment of metastatic or recurrent gastric cancer. *J Cancer Res Clin Oncol* 2016; **142**: 1727-1738 [PMID: 27256004 DOI: 10.1007/s00432-016-2184-6]
7 **Wang J**, Qu J, Li Z, Che X, Liu J, Teng Y, Jin B, Zhao M, Liu Y, Qu X. Pretreatment platelet-to-lymphocyte ratio is associated with the response to first-line chemotherapy and survival in patients with metastatic gastric cancer. *J Clin Lab Anal* 2018; **32** [PMID: 28238215 DOI: 10.1002/jcla.22185]
8 **Zhang Y**, Lu JJ, Du YP, Feng CX, Wang LQ, Chen MB. Prognostic value of neutrophil-to-lymphocyte ratio and platelet-to-lymphocyte ratio in gastric cancer. *Medicine (Baltimore)* 2018; **97**: e0144 [PMID: 29561419 DOI: 10.1097/MD.0000000000010144]
9 **Tamura T**, Inagawa S, Hisakura K, Enomoto T, Ohkohchi N. Evaluation of serum high-density lipoprotein cholesterol levels as a prognostic factor in gastric cancer patients. *J Gastroenterol Hepatol* 2012; **27**: 1635-1640 [PMID: 22647147 DOI: 10.1111/j.1440-1746.2012.07189.x]
10 **Sisik A**, Kaya M, Bas G, Basak F, Alimoglu O. CEA and CA 19-9 are still valuable markers for the prognosis of colorectal and gastric cancer patients. *Asian Pac J Cancer Prev* 2013; **14**: 4289-4294 [PMID: 23991991 DOI: 10.7314/apjcp.2013.14.7.4289]
11 **Li Q**, Lyu Z, Wang L, Li F, Yang Z, Ren W. Albumin-to-Alkaline Phosphatase Ratio Associates with Good Prognosis of Hepatitis B Virus-Positive HCC Patients. *Onco Targets Ther* 2020; **13**: 2377-2384 [PMID: 32256088 DOI: 10.2147/OTT.S242034]
12 **Zhang F**, Lu S, Tian M, Hu K, Chen R, Zhang B, Ren Z, Shi Y, Yin X. Albumin-to-Alkaline Phosphatase Ratio is an Independent Prognostic Indicator in Combined Hepatocellular and Cholangiocarcinoma. *J Cancer* 2020; **11**: 5177-5186 [PMID: 32742464 DOI: 10.7150/jca.45633]
13 **Li D**, Yu H, Li W. Albumin-to-alkaline phosphatase ratio at diagnosis predicts survival in patients with metastatic non-small-cell lung cancer. *Onco Targets Ther* 2019; **12**: 5241-5249 [PMID: 31303770 DOI: 10.2147/OTT.S203321]
14 **Zhou S**, Jiang W, Wang H, Wei N, Yu Q. Predictive value of pretreatment albumin-to-alkaline phosphatase ratio for overall survival for patients with advanced non-small cell lung cancer. *Cancer Med* 2020; **9**: 6268-6280 [PMID: 32691996 DOI: 10.1002/cam4.3244]
15 **Li X**, Li B, Zeng H, Wang S, Sun X, Yu Y, Wang L, Yu J. Prognostic value of dynamic albumin-to-alkaline phosphatase ratio in limited stage small-cell lung cancer. *Future Oncol* 2019; **15**: 995-1006 [PMID: 30644319 DOI: 10.2217/fon-2018-0818]
16 **Kim JS**, Keam B, Heo DS, Han DH, Rhee CS, Kim JH, Jung KC, Wu HG. The Prognostic Value of Albumin-to-Alkaline Phosphatase Ratio before Radical Radiotherapy in Patients with Non-metastatic Nasopharyngeal Carcinoma: A Propensity Score Matching Analysis. *Cancer Res Treat* 2019; **51**: 1313-1323 [PMID: 30699498 DOI: 10.4143/crt.2018.503]
17 **Zhang K**, Dong S, Jing YH, Gao HF, Chen LY, Hua YQ, Chen H, Chen Z. Albumin-to-alkaline phosphatase ratio serves as a prognostic indicator in unresectable pancreatic ductal adenocarcinoma: a propensity score matching analysis. *BMC Cancer* 2020; **20**: 541 [PMID: 32517802 DOI: 10.1186/s12885-020-07023-9]
18 **Wang Y**, Xiong F, Yang J, Xia T, Jia Z, Shen J, Xu C, Feng J, Lu Y. Decreased albumin-to-alkaline phosphatase ratio predicted poor survival of resectable gastric cancer patients. *J Gastrointest Oncol* 2021; **12**: 1338-1350 [PMID: 34532092 DOI: 10.21037/jgo-21-430]

19 **Dixon M**, Mahar AL, Helyer LK, Vasilevska-Ristovska J, Law C, Coburn NG. Prognostic factors in metastatic gastric cancer: results of a population-based, retrospective cohort study in Ontario. *Gastric Cancer* 2016; **19**: 150-159 [PMID: 25421300 DOI: 10.1007/s10120-014-0442-3]

20 **Esper DH**, Harb WA. The cancer cachexia syndrome: a review of metabolic and clinical manifestations. *Nutr Clin Pract* 2005; **20**: 369-376 [PMID: 16207677 DOI: 10.1177/0115426505020004369]

21 **Heys SD**, Walker LG, Deehan DJ, Eremin OE. Serum albumin: a prognostic indicator in patients with colorectal cancer. *J R Coll Surg Edinb* 1998; **43**: 163-168 [PMID: 9654876]

22 **Schwartzbaum JA**, Lal P, Evanoff W, Mamrak S, Yates A, Barnett GH, Goodman J, Fisher JL. Presurgical serum albumin levels predict survival time from glioblastoma multiforme. *J Neurooncol* 1999; **43**: 35-41 [PMID: 10448869 DOI: 10.1023/a:1006269413998]

23 **Liu BZ**, Tao L, Chen YZ, Li XZ, Dong YL, Ma YJ, Li SG, Li F, Zhang WJ. Preoperative Body Mass Index, Blood Albumin and Triglycerides Predict Survival for Patients with Gastric Cancer. *PLoS One* 2016; **11**: e0157401 [PMID: 27309531 DOI: 10.1371/journal.pone.0157401]

24 **Schoppet M**, Shanahan CM. Role for alkaline phosphatase as an inducer of vascular calcification in renal failure? *Kidney Int* 2008; **73**: 989-991 [PMID: 18414436 DOI: 10.1038/ki.2008.104]

25 **Han KS**, Hong SJ. Serum alkaline phosphatase differentiates prostate-specific antigen flare from early disease progression after docetaxel chemotherapy in castration-resistant prostate cancer with bone metastasis. *J Cancer Res Clin Oncol* 2014; **140**: 1769-1776 [PMID: 24858569 DOI: 10.1007/s00432-014-1710-7]

26 **Kim JM**, Kwon CH, Joh JW, Park JB, Ko JS, Lee JH, Kim SJ, Park CK. The effect of alkaline phosphatase and intrahepatic metastases in large hepatocellular carcinoma. *World J Surg Oncol* 2013; **11**: 40 [PMID: 23432910 DOI: 10.1186/1477-7819-11-40]

27 **Zhang L**, Gong Z. Clinical Characteristics and Prognostic Factors in Bone Metastases from Lung Cancer. *Med Sci Monit* 2017; **23**: 4087-4094 [PMID: 28835603 DOI: 10.12659/msm.902971]

28 **Chen B**, Dai D, Tang H, Chen X, Ai X, Huang X, Wei W, Xie X. Pre-treatment serum alkaline phosphatase and lactate dehydrogenase as prognostic factors in triple negative breast cancer. *J Cancer* 2016; **7**: 2309-2316 [PMID: 27994669 DOI: 10.7150/jca.16622]

29 **Li G**, Gao J, Tao YL, Xu BQ, Tu ZW, Liu ZG, Zeng MS, Xia YF. Increased pretreatment levels of serum LDH and ALP as poor prognostic factors for nasopharyngeal carcinoma. *Chin J Cancer* 2012; **31**: 197-206 [PMID: 22237040 DOI: 10.5732/cjc.011.10283]

30 **Li D**, Lv H, Hao X, Hu B, Song Y. Prognostic value of serum alkaline phosphatase in the survival of prostate cancer: evidence from a meta-analysis. *Cancer Manag Res* 2018; **10**: 3125-3139 [PMID: 30214305 DOI: 10.2147/CMAR.S174237]

31 **Namikawa T**, Ishida N, Tsuda S, Fujisawa K, Munekage E, Iwabu J, Munekage M, Uemura S, Tsujii S, Tamura T, Yatabe T, Maeda H, Kitagawa H, Kobayashi M, Hanazaki K. Prognostic significance of serum alkaline phosphatase and lactate dehydrogenase levels in patients with unresectable advanced gastric cancer. *Gastric Cancer* 2019; **22**: 684-691 [PMID: 30417313 DOI: 10.1007/s10120-018-0897-8]

32 **Chan AW**, Chan SL, Mo FK, Wong GL, Wong VW, Cheung YS, Chan HL, Yeo W, Lai PB, To KF. Albumin-to-alkaline phosphatase ratio: a novel prognostic index for hepatocellular carcinoma. *Dis Markers* 2015; **2015**: 564057 [PMID: 25737613 DOI: 10.1155/2015/564057]

33 **Guo X**, Zou Q, Yan J, Zhen X, Gu H. Prognostic effect of pretreatment albumin-to-alkaline phosphatase ratio in human cancers: A meta-analysis. *PLoS One* 2020; **15**: e0237793 [PMID: 32822383 DOI: 10.1371/journal.pone.0237793]

34 **Tian G**, Li G, Guan L, Yang Y, Li N. Pretreatment albumin-to-alkaline phosphatase ratio as a prognostic indicator in solid cancers: A meta-analysis with trial sequential analysis. *Int J Surg* 2020; **81**: 66-73 [PMID: 32745716 DOI: 10.1016/j.ijsu.2020.07.024]

35 **Xie H**, Wei L, Tang S, Gan J. Prognostic Value of Pretreatment Albumin-to-Alkaline Phosphatase Ratio in Cancer: A Meta-Analysis. *Biomed Res Int* 2020; **2020**: 6661097 [PMID: 33376729 DOI: 10.1155/2020/6661097]

World Journal of Gastrointestinal Oncology

Submit a Manuscript: https://www.f6publishing.com

World J Gastrointest Oncol 2022 May 15; 14(5): 1014-1026

DOI: 10.4251/wjgo.v14.i5.1014

ISSN 1948-5204 (online)

ORIGINAL ARTICLE

Retrospective Study

Preoperative prediction of malignant potential of 2-5 cm gastric gastrointestinal stromal tumors by computerized tomography-based radiomics

Xue-Feng Sun, Hai-Tao Zhu, Wan-Ying Ji, Xiao-Yan Zhang, Xiao-Ting Li, Lei Tang, Ying-Shi Sun

Specialty type: Radiology, nuclear medicine and medical imaging

Provenance and peer review: Unsolicited article; Externally peer reviewed.

Peer-review model: Single blind

Peer-review report's scientific quality classification

Grade A (Excellent): A
Grade B (Very good): B, B
Grade C (Good): 0
Grade D (Fair): 0
Grade E (Poor): 0

P-Reviewer: Katayama Y, Japan; Tanaka T, Japan; Toyota S, Japan

Received: December 1, 2021
Peer-review started: December 1, 2021
First decision: December 27, 2021
Revised: December 29, 2021
Accepted: April 21, 2022
Article in press: April 21, 2022
Published online: May 15, 2022

Xue-Feng Sun, Hai-Tao Zhu, Wan-Ying Ji, Xiao-Yan Zhang, Xiao-Ting Li, Lei Tang, Ying-Shi Sun, Key laboratory of Carcinogenesis and Translational Research (Ministry of Education/Beijing), Department of Radiology, Peking University Cancer Hospital & Institute, Beijing 100142, China

Corresponding author: Ying-Shi Sun, MD, Chief Doctor, Key laboratory of Carcinogenesis and Translational Research (Ministry of Education/Beijing), Department of Radiology, Peking University Cancer Hospital & Institute, No. 52 Fucheng Road, Haidian District, Beijing 100142, China. sys27@163.com

Abstract

BACKGROUND

The use of endoscopic surgery for treating gastrointestinal stromal tumors (GISTs) between 2 and 5 cm remains controversial considering the potential risk of metastasis and recurrence. Also, surgeons are facing great difficulties and challenges in assessing the malignant potential of 2-5 cm gastric GISTs.

AIM

To develop and evaluate computerized tomography (CT)-based radiomics for predicting the malignant potential of primary 2-5 cm gastric GISTs.

METHODS

A total of 103 patients with pathologically confirmed gastric GISTs between 2 and 5 cm were enrolled. The malignant potential was categorized into low grade and high grade according to postoperative pathology results. Preoperative CT images were reviewed by two radiologists. A radiological model was constructed by CT findings and clinical characteristics using logistic regression. Radiomic features were extracted from preoperative contrast-enhanced CT images in the arterial phase. The XGboost method was used to construct a radiomics model for the prediction of malignant potential. Nomogram was established by combing the radiomics score with CT findings. All of the models were developed in a training group (n = 69) and evaluated in a test group (n = 34).

RESULTS

The area under the curve (AUC) value of the radiological, radiomics, and nomogram models was 0.753 (95% confidence interval [CI]: 0.597-0.909), 0.919

(95%CI: 0.828-1.000), and 0.916 (95%CI: 0.801-1.000) in the training group *vs* 0.642 (95%CI: 0.379-0.870), 0.881 (95%CI: 0.772-0.990), and 0.894 (95%CI: 0.773-1.000) in the test group, respectively. The AUC of the nomogram model was significantly larger than that of the radiological model in both the training group (Z = 2.795, P = 0.0052) and test group (Z = 2.785, P = 0.0054). The decision curve of analysis showed that the nomogram model produced increased benefit across the entire risk threshold range.

CONCLUSION

Radiomics may be an effective tool to predict the malignant potential of 2-5 cm gastric GISTs and assist preoperative clinical decision making.

Key Words: Gastrointestinal stromal tumors; Gastric gastrointestinal stromal tumors; Computed tomography; Malignant potential; Radiomics; Nomogram

Core Tip: The use of endoscopic surgery in gastrointestinal stromal tumors (GISTs) between 2 and 5 cm remains controversial considering the potential risk of metastasis and recurrence. Also, surgeons are facing great difficulties and challenges in assessing the malignant potential of 2-5 cm gastric GISTs. This study aimed to develop and evaluate computerized tomography-based radiomics for predicting the malignant potential of primary 2-5 cm gastric GISTs.

Citation: Sun XF, Zhu HT, Ji WY, Zhang XY, Li XT, Tang L, Sun YS. Preoperative prediction of malignant potential of 2-5 cm gastric gastrointestinal stromal tumors by computerized tomography-based radiomics. *World J Gastrointest Oncol* 2022; 14(5): 1014-1026

URL: https://www.wjgnet.com/1948-5204/full/v14/i5/1014.htm

DOI: https://dx.doi.org/10.4251/wjgo.v14.i5.1014

INTRODUCTION

Gastrointestinal stromal tumors (GISTs) are the most common mesenchymal tumors in the gastrointestinal tract and account for the majority of submucosal tumors[1,2]. They most frequently appear in the stomach (50%-60%) and small intestine (30%-35%) and rarely in the colorectum (5%) and esophagus (< 1%)[3,4]. GISTs are clinically heterogeneous with varying degrees of malignant potential. Therefore, preoperative evaluation of the biological behavior of GISTs is important for surgical decision making[3,5].

Endoscopic resection is an effective and safe method for treating gastric GISTs smaller than 2 cm[6-8]. Nevertheless, whether endoscopic surgery can be used for resecting gastric GISTs between 2 and 5 cm remains controversial considering the potential risk of metastasis and recurrence[6,9]. Also, surgeons are facing great difficulties and challenges in assessing the malignant potential of 2-5 cm gastric GISTs.

The frequencies of 2 to 5 cm gastric GISTs metastases with mitotic counts larger than 5/50 high-power fields (HPFs) and smaller than 5/50 HPFs are 16% and 1.9%, respectively[10]. Based on mitotic counts, several risk stratification systems have been proposed to assess the recurrence risk after complete resection of primary GISTs[10-12]. Gastric GISTs are generally associated with a better prognosis than non-gastric GISTs[10]. The modified National Institutes of Health (NIH) criteria classify GISTs into four categories (very low, low, intermediate, and high risk) according to tumor location, mitotic count, tumor size, and tumor rupture. The modified NIH criteria have become a commonly accepted risk stratification tool for GISTs due to their important value in assessing prognosis after operation[13-15]. However, these criteria are only postoperatively applied as the mitosis count of the specimen available after excision is a significant criterion factor.

Preoperative prediction of the malignant potential and prognosis of these GISTs is crucial for clinical decision-making. Preoperative biopsy is a common method for determining the characteristics of suspected lesions. Yet, this method has several disadvantages, such as the lack of adequate tissue for fine-needle biopsy, the possible failure to obtain mitosis counts with improper sampling, or the underestimation of mitotic grades, which increase the difficulty of response evaluation during follow-up. On the other hand, with the recent remarkable development of imaging technology, non-invasive real-time imaging tools, such as computerized tomography (CT), magnetic resonance imaging, and endoscopic ultrasound (EUS), have been increasingly applied for assessing the potential malignancy and prognosis of a variety of tumors including GISTs. For example, Chen *et al*[13] indicated that CT features are more useful than EUS features for predicting mitotic counts. Therefore, exploring the association between CT

features and GIST risk stratification may influence the surgical treatment decision for 2-5 cm gastric GISTs. Nevertheless, subjective assessments may overlook abundant information hidden in the images and may be limited by overreliance on observers' experience.

As a combination of texture analysis and machine learning methods, radiomics has been widely used in the field of assisted tumor diagnosis, staging, and prognosis prediction[16,17]. Many studies have indicated that radiomics features can be used to comprehensively assess the biological behavior of malignant cells, improving the accuracy of diagnosis, prognosis, and prediction[18-20]. Radiomics has also been used to preoperatively predict the malignant potential of GISTs[21]. However, the study on 2-5 cm gastric GISTs has not yet been reported.

The aim of the current study was to propose a radiomics model for predicting the malignant potential of 2-5 cm gastric GISTs by preoperative enhanced CT images. The method may be helpful for preoperative design of individualized treatment strategy for patients with 2-5 cm gastric GISTs.

MATERIALS AND METHODS

Subjects

This retrospective study was approved by our institutional review board, and patient's informed consent was waived. A total of 695 gastric GIST patients with histologically confirmed 2-5 cm gastric GISTs who were treated at our hospital were consecutively enrolled between January 2010 and December 2019. The inclusion criteria were the following: Patients who underwent surgery for primary gastric GISTs with curative intent, patients who underwent standard contrast-enhanced CT less than 15 d before surgical resection; patients with complete clinicopathologic data; and patients with a tumor size of 2-5 cm.

The exclusion criteria were: Patients who received imatinib therapy or other tyrosine kinase inhibitor as a neoadjuvant therapy before surgery; and patients who had tumor rupture before or during surgery.

Finally, 592 patients were excluded due to the above reasons, and 103 patients were included in this study (48 males and 55 females; mean age, 58.31 ± 9.20 years). The included patients were randomly divided into a training group (n = 69) and a test group (n = 34) in a portion of 2:1 ratio with equal proportions of positive and negative samples. The inclusion and exclusion criteria are shown in Figure 1.

CT imaging

Contrast-enhanced CT examinations were performed using one of the following CT scanners: GE LightSpeed VCT (n = 62) or GE Discovery CT750 HD (n = 41). All patients were fasted for at least 8 h before the examination. They were given 6 g of gas production powder orally before the examination to ensure adequate expansion of the gastric cavity. CT images were obtained during breath holding. Both scanners used 5 mm slice thickness, 5 mm slice increment, 0.9 pitch, 120 kV tube voltage, and 300 mA tube current.

Contrast-enhanced scanning was performed for all subjects. They were intravenously administered 70-100 mL of a nonionic contrast agent (iohexol, 300 mg I/L; General Electric) at a rate of 2.5-3.5 mL/s. For the arterial phase, a delay time of 30 s was used. Venous phase and delayed phase scanning were performed 60 s and 120 s after contrast agent injection.

Axial, sagittal, and coronal multiplanar reconstructions images were obtained with a reconstruction thickness of 2-5 mm. CT images were sent to the picture archiving and communication system (PACS) for interpretation at the workstations.

CT findings and radiological model

Two radiologists with 14 years and 5 years of experience in abdominal imaging independently reviewed all images. In case of disagreement, the two readers jointly reviewed the findings to reach a consensus for further analysis. The radiologists were blinded to the pathological data.

The following CT findings were recorded: tumor size (cm), location (cardiac region, fundus, body, or antrum), necrosis (present or absent), ulceration (present or absent), calcification (present or absent), growth pattern, tumor contour (irregular or regular), and tumor margin (poorly or well defined). Tumor size was defined as the maximal diameter on the transverse, coronal, or sagittal plane. Ulceration was defined as a focal mucosal defect/indentation filled with air or fluid or when contrast material was found on the endoluminal surface of the lesion. Growth patterns were classified as endoluminal, exophytic, or mixed. The tumor contour was considered as either regular/round/ovoid or irregular/lobulated. The mean CT value (Hounsfield unit) was measured in the plain phase, arterial phase, venous phase, and delayed phase. Univariate analysis was used to select useful CT findings. A radiological model was constructed by the selected CT findings using backward logistic regression.

Tumor delineation

The regions of GISTs were manually delineated by a junior radiologist (with 5 years of experience in abdominal imaging diagnosis) with the 3D Slicer (version 4.8.1) in the axial direction. A senior

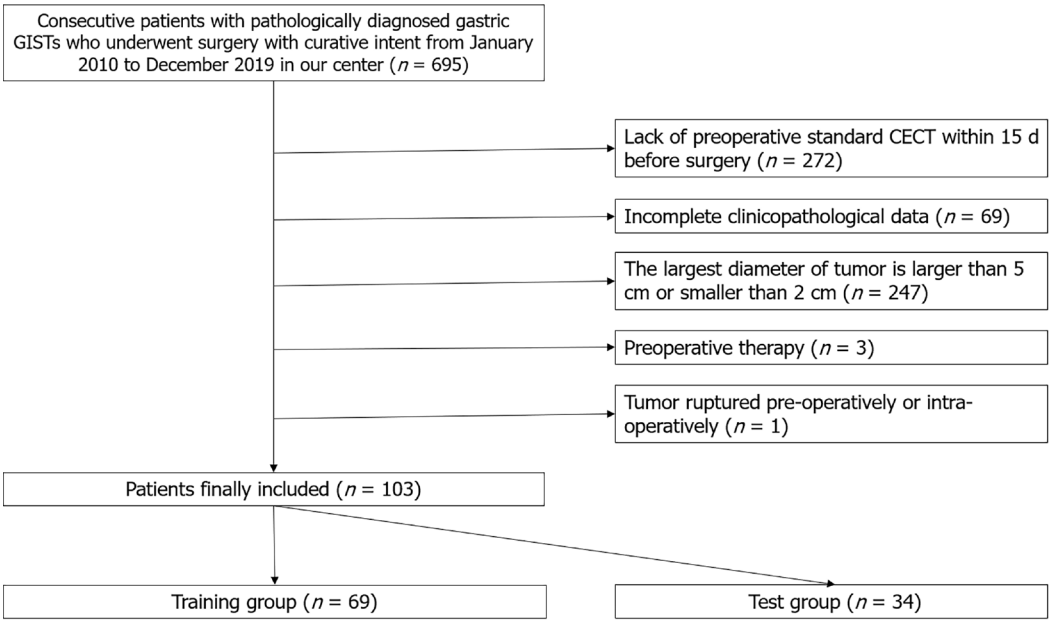

DOI: 10.4251/wjgo.v14.i5.1014

Figure 1 Flowchart of patient inclusion and exclusion. CECT: Contrast-enhanced computerized tomography; GISTs: Gastrointestinal stromal tumors.

radiologist (with 14 years of experience) evaluated the delineations and made modifications if needed. Delineation was performed on each slice of CT images from the artery phase to cover the whole tumor. Both radiologists were blinded to the risk classification of patients. One example is shown in Figure 2.

Feature extraction

Pyradiomic (version 3.0.1) was used to extract 851 features from the region of interest (ROI), including 14 shape features, 18 first-order features, 75 second-order (texture) features (24 gray level co-occurrence matrix features, 14 gray level dependence matrix features, 16 gray level run length matrix features, 16 gray level size zone matrix features, 5 neighboring gray-tone difference matrix features), and their 8 kinds of wavelet transforms ([18 + 75] × 8 + 18 + 75 + 14 = 851).

Low-grade and high-grade malignant potential

According to the NIH–modified criteria[11], mitotic counts > 5/50 HPFs were categorized into high grade, and mitotic counts < 5/50 HPFs were categorized into low grade. Then patients were divided into the very low/low-risk group (low-grade malignant potential group, n = 82) and the moderate/high-risk group (high-grade malignant potential group, n = 21). Low grade was labeled 0, and high grade was labeled 1 as the ground truth for training and test.

Radiomics model

First, a t-test examination was performed to compare all the features between the high-grade and low-grade groups. The features with $P > 0.05$ were removed. Second, the correlation was calculated between each pair of the features. If the absolute value of correlation was > 0.5, the feature with a smaller T value in the t-test was removed. Third, the XGboost algorithm was used to construct a model with remaining features and ground truth.

Due to the small sample size, the maximum estimator number and the maximum depth were set to 3 to avoid overfitting. A 3-fold cross-validation was used to determine the optimal tree number and depth. After cross-validation, the whole training group was trained again by the fixed hyperparameter to obtain the predictive model. A radiomics score was generated by the model for each patient. Finally, the model was assessed in the test group.

Nomogram model

Logistic regression was performed in the training group to classify high-grade and low-grade by combining radiomics scores with CT findings. Nomogram was used to visualize the combination of radiomics score and the selected CT findings. A risk score was generated by the nomogram and evaluated in the test group.

Decision curve of analysis

Decision curve of analysis (DCA) was performed to study the benefit of radiomics model. Net benefit was calculated by subtracting the proportion of all patients who were false positive from the proportion

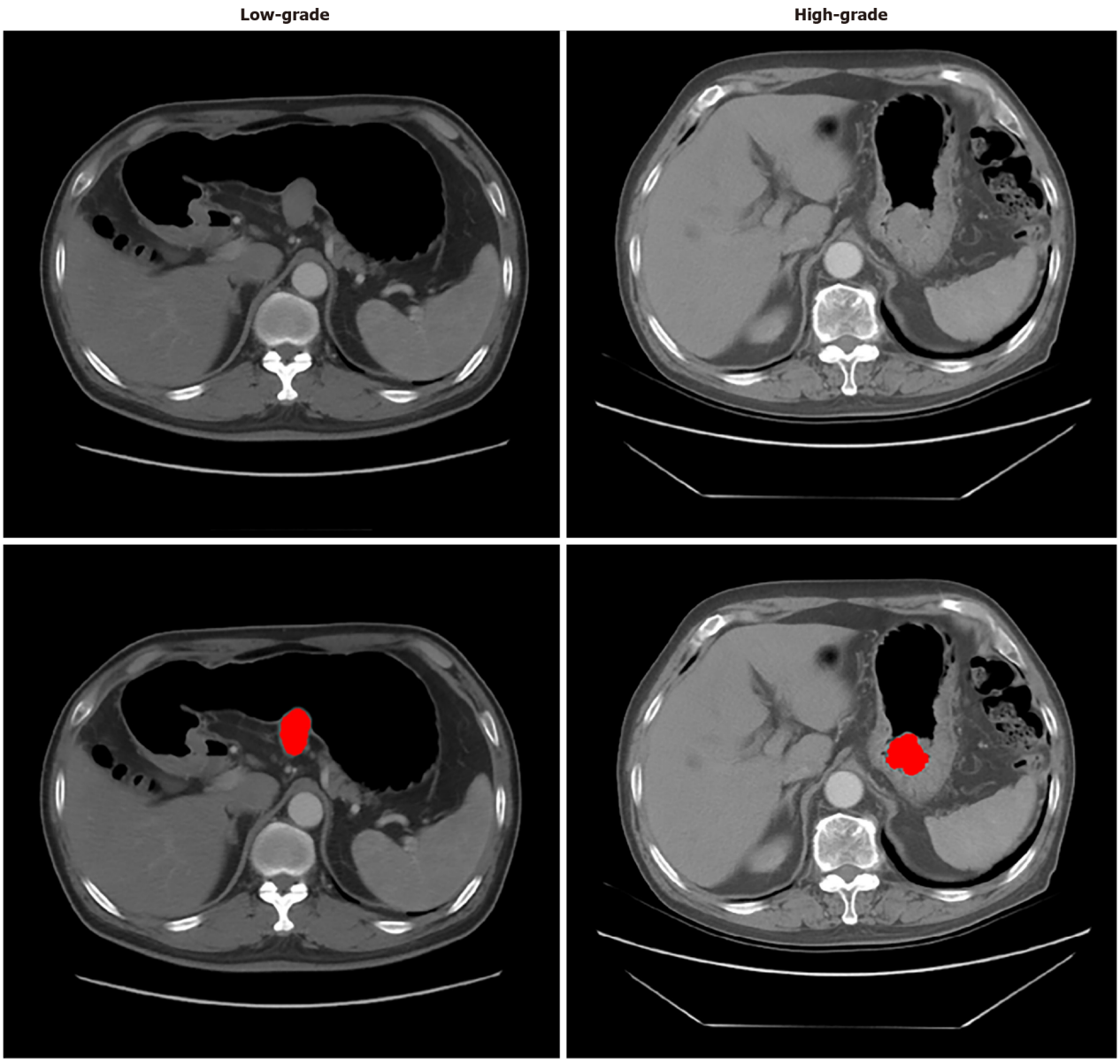

DOI: 10.4251/wjgo.v14.i5.1014

Figure 2 Two examples of computerized tomography images and tumor delineation (red color). The left one was proven low-grade malignant potential, and the right one was proven high-grade malignant potential by pathological analyses with mitotic counts.

of those who were true positive, weighted by the relative harm of forgoing treatment compared with the negative consequences of unnecessary treatments. Standardized net benefit scaled the net benefit into the range between 0 and 1. The relative harm was the ratio of the harm of false positive harm to false negative harm.

Statistical analyses

Independent samples *t*-test was used to compare the continuous variables in the low and high malignant potential groups. Chi-squared test or Fisher's exact test was applied for categorical variables. Receiver operating characteristic (ROC) curves were used to evaluate the predictive model. The cutoff value between low grade and high grade was selected by maximizing the Youden index (sensitivity + specificity-1). The area under the curve (AUC) was compared by the DeLong method.

RESULTS

Patient characteristics

The clinical characteristics and CT findings between the low-grade and high-grade malignant potential groups are analyzed in Table 1. In univariate analyses, tumor diameter, necrosis, ulceration, tumor

Table 1 Patients' characteristics between low-grade and high-grade malignant potential groups

Characteristics	Low-grade, *n* = 82	High-grade, *n* = 21	*t* or χ^2 value	*P* value
Age in year	58.57 ± 8.90	57.28 ± 10.47	0.570	0.570
Sex, *n* (%)			0.354	0.552
Male	37 (45.1)	11 (52.4)		
Female	45 (59.9)	10 (47.6)		
Largest diameter	32.66 ± 8.77	38.76 ± 9.09	2.824	0.006[a]
Location, *n* (%)			2.109	0.550
Cardia	2 (2.4)	0 (0)		
Fundus	40 (48.8)	12 (57.1)		
Body	28 (34.1)	8 (38.1)		
Antrum	12 (14.6)	1 (4.8)		
Growth patterns, *n* (%)			2.196	0.334
Endoluminal	39 (47.6)	11 (52.4)		
Exophytic	24 (29.3)	3 (14.3)		
Mixed	19 (23.2)	7 (33.3)		
Contour, *n* (%)			4.646	0.031[a]
Regular	56 (68.3)	9 (42.9)		
Irregular	26 (31.7)	12 (57.1)		
Margin, *n* (%)			5.645	0.018[a]
Well-defined	67 (81.7)	12 (57.1)		
Poorly	15 (18.3)	9 (42.9)		
Necrosis, *n* (%)			4.268	0.039[a]
Absent	48 (58.5)	7 (33.3)		
Present	34 (41.5)	14 (66.7)		
Calcification, *n* (%)			0.630	0.427
Absent	75 (91.5)	18 (85.7)		
Present	7 (8.5)	3 (14.3)		
Ulceration, *n* (%)			7.823	0.005[a]
Absent	67 (81.7)	11 (52.4)		
Present	15 (18.3)	10 (47.6)		
Plain CT value	34.65 ± 37.92	31.10 ± 13.23	0.421	0.674
Arterial phase CT value	63.70 ± 36.50	59.81 ± 18.58	0.471	0.639
Venous phase CT value	71.78 ± 35.76	63.43 ± 17.32	1.035	0.303
Delayed phase CT value	73.65 ± 34.96	66.14 ± 14.39	0.960	0.339

[a]$P < 0.05$.

Independent samples *t*-test was applied in continuous variables. χ^2 test was applied for categorical variables. CT: Computerized tomography.

margin, and tumor contour significantly differed between the different risk stratification groups (all $P < 0.05$). No significant differences were found in other subjective features between the two groups, including tumor location, growth pattern, calcification, density, and the degree of enhancement in each phase of CT between the different risk stratification groups (all $P \geq 0.05$). Table 2 compares the basic characteristics between the training and the test group. Moreover, there was no significant difference in age, sex, and ground truth between the two groups.

Table 2 Patients' characteristics between the training group and the test group

Characteristics	Training, *n* = 69	Test, *n* = 34	*t* or χ^2 value	*P* value
Age in year	58.30 ± 9.02	58.32 ± 9.71	0.01	0.992
Sex, *n* (%)			0.004	0.948
Male	32 (53.6)	16 (52.9)		
Female	37 (46.4)	18 (47.1)		
Ground truth, *n* (%)			0.001	0.972
Low-grade	55 (79.7)	27 (79.4)		
High-grade	14 (20.3)	7 (20.6)		

Prediction by radiological model

A radiological model was constructed by backward logistic regression using five selected CT findings including tumor diameter, necrosis, ulceration, tumor margin, and tumor contour. Two features were retained in the final model, including the largest diameter (P = 0.032; odds ratio [OR] = 1.082, 95% confidence interval [CI]: 1.007-1.163) and ulceration (P = 0.061; OR = 3.618, 95%CI: 0.943-13.876). The performance of this radiological model is summarized in Table 3. The AUC value was 0.753 (95%CI: 0.597-0.909) for the training group and 0.642 (95%CI: 0.379-0.870) for the test group.

Prediction by radiomics model

After the removal of features *via* *t*-test and correlation, 13 features remained. XGboost method selected four features by three-fold cross-validation with an optimal learning rate of 0.03. The four selected features and their importance were: gray-level nonuniformity (wavelet-HHH glszm feature type) with an importance of 0.703, mean absolute deviation (wavelet-HHH first-order feature type) with an importance of 0.154, small dependence low gray level emphasis (wavelet-LHH gldm feature type) with an importance of 0.098, and maximum (wavelet-LHL_firstorder) with an importance of 0.045. Figure 3 shows the two trees (estimators) for classification. The radiomics score is the summation of the scores from the two trees. The prediction results by radiomics score are summarized in Table 3. The AUC of the prediction by radiomics model was 0.919 (95%CI: 0.828-1.000) for the training group and 0.881 (95%CI: 0.772-0.990) for the test group.

Prediction by nomogram model

Three CT findings were selected by linear regression to combine with the radiomics score above, including necrosis, calcification, and ulcer. Nomogram was plotted as shown in Figure 4. The prediction result by the risk calculated from the nomogram is also summarized in Table 3. The AUC predicted by the nomogram model was 0.916 (95%CI: 0.801-1.000) for the training group and 0.894 (95%CI: 0.773-1.000) for the test group. The ROC curves of the radiological model, radiomics model, and nomogram model were plotted as shown in Figure 5. The AUC of the nomogram model was significantly larger than that of the radiological model in both the training group (Z = 2.795, P = 0.0052) and the test group (Z = 2.785, P = 0.0054).

DCA

Figure 6 shows the result of DCA. The y-axis measured the net benefit. The red line represents the prediction by the nomogram model. The blue line represents the assumption that all patients have high-grade malignant potential GISTs. The horizontal green line represents the assumption that all patients have low-grade malignant potential GTSTs. A 95%CI (dashed line) was determined by 1000 bootstraps. The results showed that the nomogram model produced increased benefit across the whole risk threshold range.

DISCUSSION

GISTs initiate from very early forms of Cajal cells in the gastrointestinal tract wall[22]. GISTs have complex and unpredictable biological behavior, with KIT or platelet-derived growth factor receptor A (PDGFRA) being the main pathogenetic pathways[23]. Up-to-date clinical practice guidelines suggest that the standard treatment for localized GISTs is complete surgical excision. R0 excision (microscopically negative margins) is the goal, especially for patients with a high risk of recurrence. According to recent studies, when surgery is technically challenging (rectum, duodenum, and gastroesophageal junction surgeries) and preoperative cytoreduction may facilitate tumor R0 excision, preoperative imatinib should be considered. Imatinib is currently the first-line molecular targeted drug for the

Table 3 The sensitivity, specificity, positive predictive value, and negative predictive value of the prediction by radiological model, radiomics model, and nomogram model with their 95% confidential intervals

Model	AUC	Sensitivity	Specificity	PPV	NPV
Radiological training	0.753 (0.597-0.909)	42.9 (17.7-71.1)	96.4 (87.5-99.6)	75.0 (34.9-96.8)	86.9 (75.8-94.2)
Radiological test	0.642 (0.379-0.870)	71.4 (29.0-96.3)	66.7 (46.0-83.5)	35.7 (12.8-64.9)	90.0 (68.3-98.8)
Radiomic training	0.919 (0.828-1.000)	92.9 (66.1-99.8)	80.0 (67.0-89.6)	54.2 (32.8-74.4)	97.8 (88.2-99.9)
Radiomic test	0.881 (0.772-0.990)	100.0 (59.0-100.0)	66.7 (46.0-83.5)	43.7 (19.8-70.1)	100.0 (81.5-100.0)
Nomogram training	0.916 (0.801-1.000)	85.7 (57.2-98.2)	90.9 (80.0-97.0)	70.6 (44.0-89.7)	96.2 (86.8-99.5)
Nomogram test	0.894 (0.773-1.000)	100.0 (59.0-100.0)	66.7 (46.0-83.5)	43.7 (19.8-70.1)	100.0 (81.5-100.0)

AUC: Area under the curve; NPV: Negative predictive value; PPV: Positive predictive value.

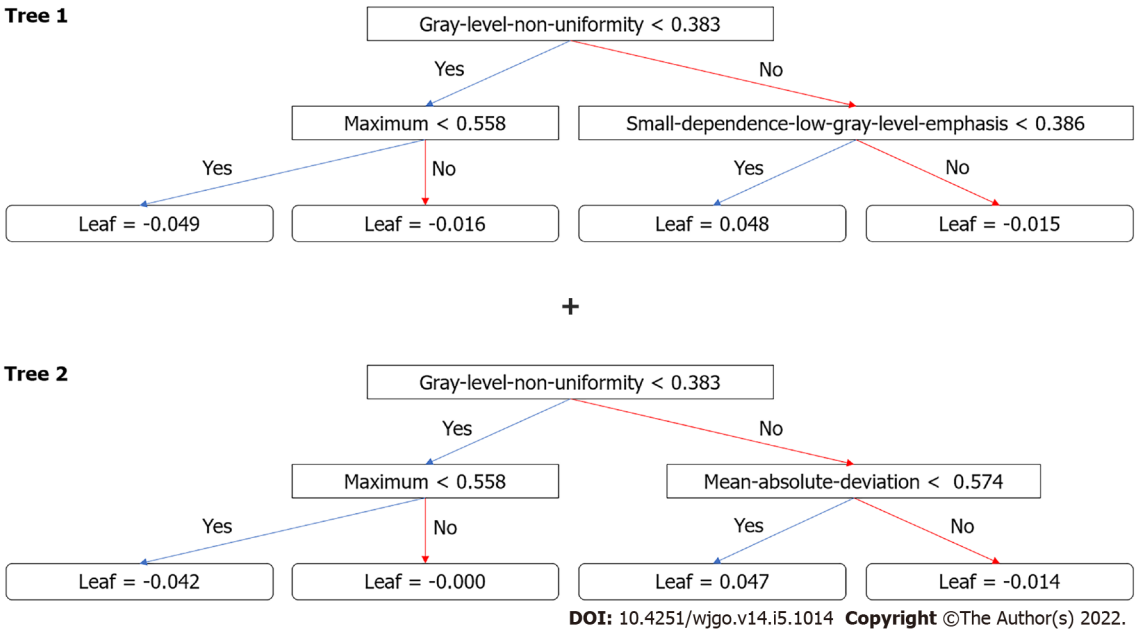

DOI: 10.4251/wjgo.v14.i5.1014

Figure 3 Decision trees generated by XGboost method for classification. Radiomics score is the sum of the scores from the two trees.

treatment of GISTs, and can be used in combination with KIT and PDGFRA[24]. The current guidelines recommend more than 3 years of adjuvant treatment for high-risk GISTs patients[25]. Patients with low malignant potential (low and very low risk) generally have a good prognosis and do not require further adjuvant imatinib therapy[26-28]. The majority of GISTs < 2 cm usually have risk of metastasis and their mitotic counts are < 5 per 50 HPFs in general. Conversely, for GISTs between 2-5 cm, there is a 10-fold difference in metastasis frequency between low- and high-mitosis groups[10]. According to the current diagnosis and treatment paradigm, individualized preoperative prediction of recurrence is particularly important for 2-5 cm GISTs. While the modified NIH consensus criteria are frequently used to estimate the risk of recurrence, the key criteria are only postoperatively accessible. A biopsy may provide preoperative estimation. However, a core needle biopsy may not provide an accurate mitotic count and a full-scale malignant potential assessment of the tumor. Therefore, a new robust risk assessment standard is needed.

Contrast-enhanced CT is the standard imaging method for the pretreatment and follow-up evaluation of GISTs. Several studies have investigated the predictive value of multiple CT findings for the malignant potential of GISTs[13,29-31]. The results varied, possibly due to the different inclusion criteria and subjective assessment standards. A previous study noted that CT findings were predictors of risk stratification for GISTs[29]. In this study, univariate analyses revealed that high-grade malignant potential tumors tended to have an irregular shape, indistinct tumor margins, necrosis, and ulceration, consistent with previous studies[30,32]. Our results also showed that high-grade malignant potential tumors frequently displayed tumors with a larger size. Tateishi *et al*[33] reported that an extrinsic epicenter and an unclear border were the most significant predictors for high-grade tumors, according to multiple stepwise logistic regression analysis. In our series, tumor size, shape, margins, the presence

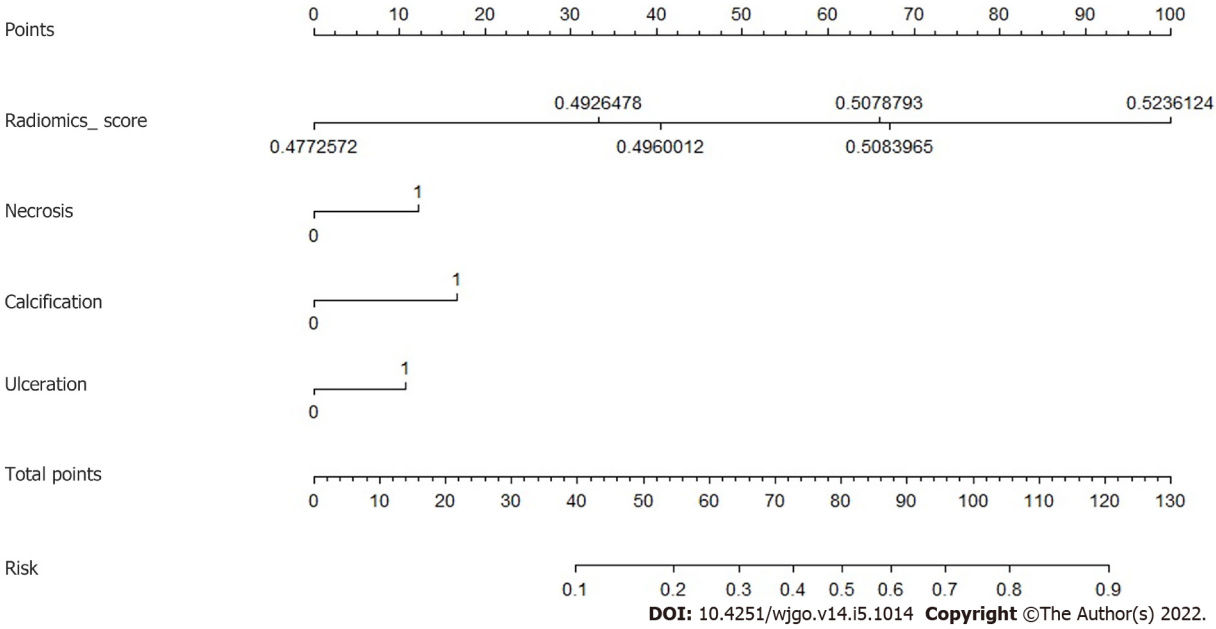

DOI: 10.4251/wjgo.v14.i5.1014 **Copyright** ©The Author(s) 2022.

Figure 4 Nomogram for the prediction. The radiomics score was combined with three computerized tomography findings: Necrosis, calcification, and ulceration.

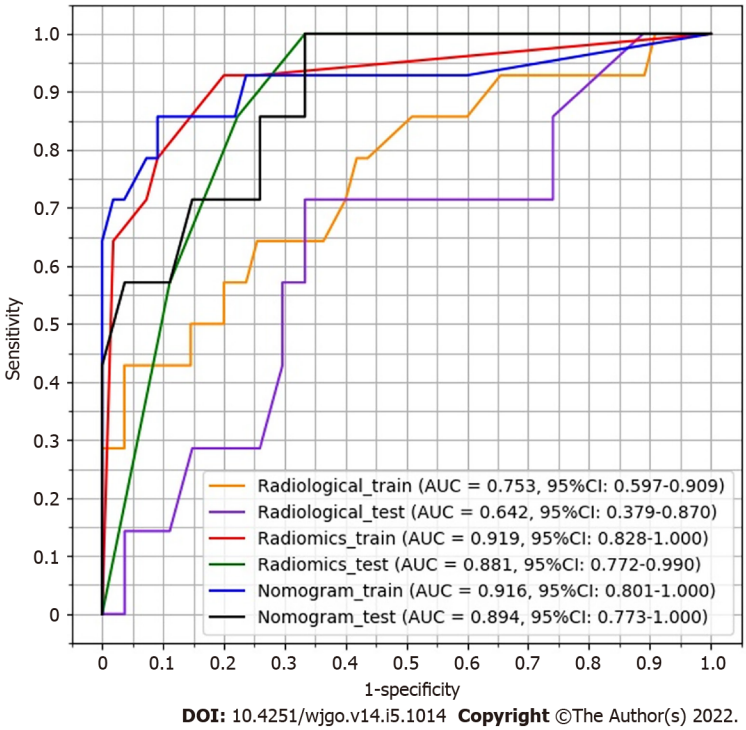

DOI: 10.4251/wjgo.v14.i5.1014 **Copyright** ©The Author(s) 2022.

Figure 5 Receiver operating characteristic curves for radiological model, radiomics model, and nomogram model. AUC: Area under the curve.

of necrosis, and ulceration were statistically significant factors for risk stratification of 2-5 cm gastric GISTs in the univariate analysis. Nevertheless, our radiological model showed that only the largest diameter and the presence of ulceration were independent predictors in backward logistic regression for high malignant potential. Limited by the inadequate predictive power of subjective CT findings, the AUC of the radiological model (0.642 for the test group) was unsatisfactory for clinical application.

Compared with subjective CT findings, both our radiomics and nomogram models had greater predictive power, as indicated by higher AUC values. Significant AUC difference was found between the radiological model and nomogram model despite a small test sample. This demonstrated that our radiomics approach with quantitative analysis had an advantage over the subjective CT findings. Unlike the radiomics models proposed by Chen *et al*[21], this study focused on the GISTs with the largest

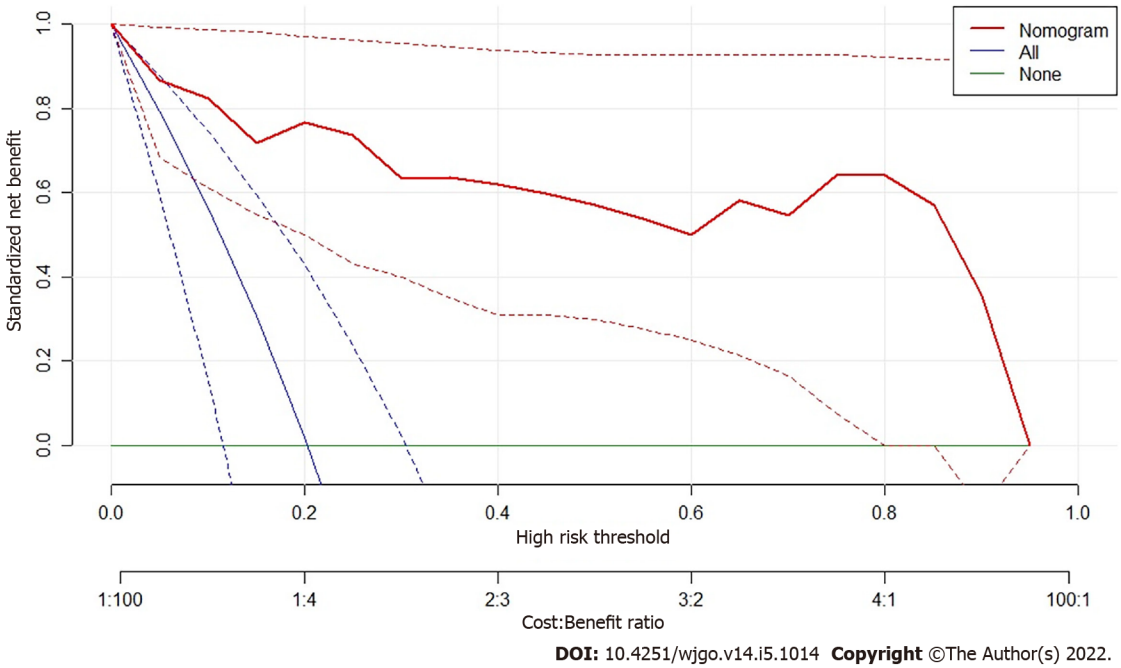

DOI: 10.4251/wjgo.v14.i5.1014

Figure 6 Decision curve of analysis. The nomogram model produces increased benefit in the whole range of risk thresholds.

diameter of 2-5 cm. According to the modified NIH criteria, the risk stratification of gastric GISTs is mainly based on the size of the tumor and mitotic count. GISTs larger than 5 cm tend to be classified into the high-risk group. It is more challenging to predict the potential risk of smaller GISTs. Therefore, it is clinically important to construct a prediction model, especially for the 2-5 cm GISTs. In this study, the ground truth of risk was determined only by mitotic counts. Mitotic counts > 5/50 HPFs were categorized into high-grade malignant potential, and mitotic counts < 5/50 HPFs were categorized into low-grade malignant potential. Therefore, the impact of tumor size was excluded, which was reasonable because 2-5 cm GISTs tended to have a uniform tumor size. In this study, although the largest diameter showed a significant difference in *t*-test examination and was included in the radiological mode, the CT findings were not selected in the final nomogram model. This indicated that tumor size was not crucial for predicting the potential risk for 2-5 cm GISTs . It is possible that manual measurement of 2-5 cm GISTs on CT images was relatively unstable compared with the quantitative features from radiomics models.

In the radiomics model, four features were selected to construct the decision trees by XGboost. The feature with the largest importance showed the gray level nonuniformity from the gray-level size zone matrix. It was used as the root node for both two decision trees. A gray-level zone was defined as the number of connected voxels that share the same gray level intensity. Gray level nonuniformity measures the variability of gray-level intensity values in the image, with a lower value indicating more homogeneity in intensity values. Therefore, signal inhomogeneity inside the tumor region in the arterial phase of CT images is important for predicting the potential risk 2-5 cm GISTs. Due to the small training samples, only four features and two trees with a depth of 2 were included in the radiomics model to avoid overfitting. The similar accuracy between the training and test group indicated a good fitting for both radiomics and nomogram models. In the nomogram, three CT findings were combined with the radiomics score to calculate the risk. This provides a simple way to incorporate the subjective findings with the result of machine learning. Although the presence of calcification was not selected in the *t*-test or logistic regression, it appeared useful in the nomogram. Probably, the mutual effect of calcification and radiomics score contributed to the improvement of the prediction accuracy.

This study had some limitations. First, our data were collected retrospectively, so further prospective research was needed. Second, this study was a single-center study. Although two scanners were used, the scanning parameters were the same. Third, a relatively small sample size limited the complexity of machine learning models. In addition, we did not have information on whether the patients experienced recurrence or death due to the lack of long-term follow-up. Nevertheless, to the best of our knowledge, this was the first study that predicted the malignant potential of 2-5 cm gastric GISTs patients by radiomics. More cohort validation and more integrable factors such as KIT and PDGFRA mutations should be considered in future research[3,34].

CONCLUSION

In this study, we developed a radiomics model and a nomogram to predict the malignant potential of 2-5 cm gastric GISTs. The models revealed more accurate predictive power compared to subjective CT findings.

ARTICLE HIGHLIGHTS

Research background

Gastrointestinal stromal tumors (GISTs) are clinically heterogeneous with varying degrees of malignant potential. Therefore, preoperative evaluation of the biological behavior of GISTs is important for surgical decision-making. Endoscopic resection is an effective and safe treatment for gastric GISTs smaller than 2 cm. Nevertheless, whether endoscopic surgery can be used in resecting gastric GISTs between 2 and 5 cm remains controversial considering the potential risk of metastasis and recurrence. The difficulty in assessing the malignant potential of 2-5 cm gastric GISTs present challenges to surgeons.

Research motivation

Preoperative prediction of the malignant potential and prognosis of GISTs is crucial for clinical decision-making. Radiomics has also been used to preoperatively predict the malignant potential of GISTs. However, the study on 2-5 cm gastric GISTs has not yet been reported.

Research objectives

As stated above, we proposed a radiomics method for predicting the malignant potential of 2-5 cm gastric GISTs based on preoperative enhanced computerized tomography (CT) images. The method may be helpful for preoperative design of individualized treatment strategy for patients with 2-5 cm gastric GISTs.

Research methods

This was a retrospective study in which three models were constructed, including radiological model, radiomics model, and nomogram model. A radiological model was constructed based on CT findings and clinical characteristics. XGboost method was used to construct a radiomics model. Nomogram was constructed by combining the radiomics score with CT findings.

Research results

The area under the curve (AUC) of the nomogram model was significantly larger than the AUC of the radiological model in both the training group and the test group. The decision curve of analysis showed that the nomogram model produces increased benefit across the entire risk threshold range.

Research conclusions

In this study, we developed a radiomics model and a nomogram for malignancy differentiation of 2-5 cm gastric GISTs, which achieved satisfactory discrimination and had the potential to act as a reproducible imaging marker to support the decision-making support in a noninvasive and effective way.

Research perspectives

Future research should be considered on model validation and more integral factors such as KIT and PDGFRA mutations.

FOOTNOTES

Author contributions: Sun XF designed the study and was responsible for the work; Sun XF, Tang L, and Ji WY conducted data collection; Sun XF and Zhang XY conducted image measurement; Zhu HT and Li XT conducted statistical analyses; Sun XF wrote the paper; all authors edited the paper.

Supported by Beijing Hospitals Authority Ascent Plan, No. 20191103; Beijing Municipal Administration of Hospitals Clinical Medicine Development of Special Funding Support, No. ZYLX201803; Beijing Natural Science Foundation, No. Z180001 and No. Z200015; and PKU-Baidu Fund, No. 2020BD027.

Institutional review board statement: This retrospective study was approved by the Institutional Review Board of Peking University Cancer Hospital & Institute.

Informed consent statement: Patients were not required to give informed consent to the study because the analysis used anonymous clinical data that were obtained after each patient agreed to treatment by written consent.

Conflict-of-interest statement: The authors have no conflicts to declare.

Data sharing statement: The authors do not want to share the data.

Country/Territory of origin: China

ORCID number: Xue-Feng Sun 0000-0001-9910-5125; Hai-Tao Zhu 0000-0002-2058-5806; Wan-Ying Ji 0000-0002-9360-8642; Xiao-Yan Zhang 0000-0003-2700-7627; Xiao-Ting Li 0000-0003-2758-3843; Ying-Shi Sun 0000-0001-9424-1910.

S-Editor: Yan JP
L-Editor: Filipodia
P-Editor: Li X

REFERENCES

1 **Polkowski M**. Endoscopic ultrasound and endoscopic ultrasound-guided fine-needle biopsy for the diagnosis of malignant submucosal tumors. *Endoscopy* 2005; **37**: 635-645 [PMID: 16010608 DOI: 10.1055/s-2005-861422]
2 **Nishida T**, Blay JY, Hirota S, Kitagawa Y, Kang YK. The standard diagnosis, treatment, and follow-up of gastrointestinal stromal tumors based on guidelines. *Gastric Cancer* 2016; **19**: 3-14 [PMID: 26276366 DOI: 10.1007/s10120-015-0526-8]
3 **Joensuu H**, Hohenberger P, Corless CL. Gastrointestinal stromal tumour. *Lancet* 2013; **382**: 973-983 [PMID: 23623056 DOI: 10.1016/S0140-6736(13)60106-3]
4 **Corless CL**, Barnett CM, Heinrich MC. Gastrointestinal stromal tumours: origin and molecular oncology. *Nat Rev Cancer* 2011; **11**: 865-878 [PMID: 22089421 DOI: 10.1038/nrc3143]
5 **Nishida T**, Kawai N, Yamaguchi S, Nishida Y. Submucosal tumors: comprehensive guide for the diagnosis and therapy of gastrointestinal submucosal tumors. *Dig Endosc* 2013; **25**: 479-489 [PMID: 23902569 DOI: 10.1111/den.12149]
6 **An W**, Sun PB, Gao J, Jiang F, Liu F, Chen J, Wang D, Li ZS, Shi XG. Endoscopic submucosal dissection for gastric gastrointestinal stromal tumors: a retrospective cohort study. *Surg Endosc* 2017; **31**: 4522-4531 [PMID: 28374257 DOI: 10.1007/s00464-017-5511-3]
7 **Shen C**, Chen H, Yin Y, Chen J, Han L, Zhang B, Chen Z. Endoscopic versus open resection for small gastric gastrointestinal stromal tumors: safety and outcomes. *Medicine (Baltimore)* 2015; **94**: e376 [PMID: 25569663 DOI: 10.1097/MD.0000000000000376]
8 **Andalib I**, Yeoun D, Reddy R, Xie S, Iqbal S. Endoscopic resection of gastric gastrointestinal stromal tumors originating from the muscularis propria layer in North America: methods and feasibility data. *Surg Endosc* 2018; **32**: 1787-1792 [PMID: 28916847 DOI: 10.1007/s00464-017-5862-9]
9 **Kim MY**, Park YS, Choi KD, Lee JH, Choi KS, Kim DH, Song HJ, Lee GH, Jung HY, Kim JH, Yun SC, Kim KC, Yook JH, Oh ST, Kim BS, Ryu MH, Kang YK. Predictors of recurrence after resection of small gastric gastrointestinal stromal tumors of 5 cm or less. *J Clin Gastroenterol* 2012; **46**: 130-137 [PMID: 21617541 DOI: 10.1097/MCG.0b013e31821f8bf6]
10 **Miettinen M**, Lasota J. Gastrointestinal stromal tumors: pathology and prognosis at different sites. *Semin Diagn Pathol* 2006; **23**: 70-83 [PMID: 17193820 DOI: 10.1053/j.semdp.2006.09.001]
11 **Joensuu H**. Risk stratification of patients diagnosed with gastrointestinal stromal tumor. *Hum Pathol* 2008; **39**: 1411-1419 [PMID: 18774375 DOI: 10.1016/j.humpath.2008.06.025]
12 **von Mehren M**, Randall RL, Benjamin RS, Boles S, Bui MM, Ganjoo KN, George S, Gonzalez RJ, Heslin MJ, Kane JM, Keedy V, Kim E, Koon H, Mayerson J, McCarter M, McGarry SV, Meyer C, Morris ZS, O'Donnell RJ, Pappo AS, Paz IB, Petersen IA, Pfeifer JD, Riedel RF, Ruo B, Schuetze S, Tap WD, Wayne JD, Bergman MA, Scavone JL. Soft Tissue Sarcoma, Version 2.2018, NCCN Clinical Practice Guidelines in Oncology. *J Natl Compr Canc Netw* 2018; **16**: 536-563 [PMID: 29752328 DOI: 10.6004/jnccn.2018.0025]
13 **Chen T**, Xu L, Dong X, Li Y, Yu J, Xiong W, Li G. The roles of CT and EUS in the preoperative evaluation of gastric gastrointestinal stromal tumors larger than 2 cm. *Eur Radiol* 2019; **29**: 2481-2489 [PMID: 30617491 DOI: 10.1007/s00330-018-5945-6]
14 **Nishida T**, Sakai Y, Takagi M, Ozaka M, Kitagawa Y, Kurokawa Y, Masuzawa T, Naito Y, Kagimura T, Hirota S; members of the STAR ReGISTry Study Group. Adherence to the guidelines and the pathological diagnosis of high-risk gastrointestinal stromal tumors in the real world. *Gastric Cancer* 2020; **23**: 118-125 [PMID: 31041650 DOI: 10.1007/s10120-019-00966-4]
15 **Ren C**, Wang S, Zhang S. Development and validation of a nomogram based on CT images and 3D texture analysis for preoperative prediction of the malignant potential in gastrointestinal stromal tumors. *Cancer Imaging* 2020; **20**: 5 [PMID: 31931874 DOI: 10.1186/s40644-019-0284-7]
16 **Hodgdon T**, McInnes MD, Schieda N, Flood TA, Lamb L, Thornhill RE. Can Quantitative CT Texture Analysis be Used

to Differentiate Fat-poor Renal Angiomyolipoma from Renal Cell Carcinoma on Unenhanced CT Images? *Radiology* 2015; **276**: 787-796 [PMID: 25906183 DOI: 10.1148/radiol.2015142215]

17 **Lambin P**, Rios-Velazquez E, Leijenaar R, Carvalho S, van Stiphout RG, Granton P, Zegers CM, Gillies R, Boellard R, Dekker A, Aerts HJ. Radiomics: extracting more information from medical images using advanced feature analysis. *Eur J Cancer* 2012; **48**: 441-446 [PMID: 22257792 DOI: 10.1016/j.ejca.2011.11.036]

18 **Gillies RJ**, Kinahan PE, Hricak H. Radiomics: Images Are More than Pictures, They Are Data. *Radiology* 2016; **278**: 563-577 [PMID: 26579733 DOI: 10.1148/radiol.2015151169]

19 **Wu S**, Zheng J, Li Y, Yu H, Shi S, Xie W, Liu H, Su Y, Huang J, Lin T. A Radiomics Nomogram for the Preoperative Prediction of Lymph Node Metastasis in Bladder Cancer. *Clin Cancer Res* 2017; **23**: 6904-6911 [PMID: 28874414 DOI: 10.1158/1078-0432.CCR-17-1510]

20 **Huang YQ**, Liang CH, He L, Tian J, Liang CS, Chen X, Ma ZL, Liu ZY. Development and Validation of a Radiomics Nomogram for Preoperative Prediction of Lymph Node Metastasis in Colorectal Cancer. *J Clin Oncol* 2016; **34**: 2157-2164 [PMID: 27138577 DOI: 10.1200/JCO.2015.65.9128]

21 **Chen T**, Ning Z, Xu L, Feng X, Han S, Roth HR, Xiong W, Zhao X, Hu Y, Liu H, Yu J, Zhang Y, Li Y, Xu Y, Mori K, Li G. Radiomics nomogram for predicting the malignant potential of gastrointestinal stromal tumours preoperatively. *Eur Radiol* 2019; **29**: 1074-1082 [PMID: 30116959 DOI: 10.1007/s00330-018-5629-2]

22 **von Mehren M**, Joensuu H. Gastrointestinal Stromal Tumors. *J Clin Oncol* 2018; **36**: 136-143 [PMID: 29220298 DOI: 10.1200/JCO.2017.74.9705]

23 **Singer S**, Rubin BP, Lux ML, Chen CJ, Demetri GD, Fletcher CD, Fletcher JA. Prognostic value of KIT mutation type, mitotic activity, and histologic subtype in gastrointestinal stromal tumors. *J Clin Oncol* 2002; **20**: 3898-3905 [PMID: 12228211 DOI: 10.1200/JCO.2002.03.095]

24 **Lennartsson J**, Jelacic T, Linnekin D, Shivakrupa R. Normal and oncogenic forms of the receptor tyrosine kinase kit. *Stem Cells* 2005; **23**: 16-43 [PMID: 15625120 DOI: 10.1634/stemcells.2004-0117]

25 **Blay JY**, Levard A. Adjuvant imatinib treatment in gastrointestinal stromal tumor: which risk stratification criteria and for how long? *Anticancer Drugs* 2016; **27**: 71-75 [PMID: 26457546 DOI: 10.1097/CAD.0000000000000286]

26 **Rutkowski P**, Przybył J, Zdzienicki M. Extended adjuvant therapy with imatinib in patients with gastrointestinal stromal tumors : recommendations for patient selection, risk assessment, and molecular response monitoring. *Mol Diagn Ther* 2013; **17**: 9-19 [PMID: 23355099 DOI: 10.1007/s40291-013-0018-7]

27 **Blay JY**, Rutkowski P. Adherence to imatinib therapy in patients with gastrointestinal stromal tumors. *Cancer Treat Rev* 2014; **40**: 242-247 [PMID: 23931926 DOI: 10.1016/j.ctrv.2013.07.005]

28 **López RL**, del Muro XG. Management of localized gastrointestinal stromal tumors and adjuvant therapy with imatinib. *Anticancer Drugs* 2012; **23** Suppl: S3-S6 [PMID: 22739667 DOI: 10.1097/CAD.0b013e3283559fab]

29 **Zhou C**, Duan X, Zhang X, Hu H, Wang D, Shen J. Predictive features of CT for risk stratifications in patients with primary gastrointestinal stromal tumour. *Eur Radiol* 2016; **26**: 3086-3093 [PMID: 26699371 DOI: 10.1007/s00330-015-4172-7]

30 **Kim HC**, Lee JM, Kim KW, Park SH, Kim SH, Lee JY, Han JK, Choi BI. Gastrointestinal stromal tumors of the stomach: CT findings and prediction of malignancy. *AJR Am J Roentgenol* 2004; **183**: 893-898 [PMID: 15385278 DOI: 10.2214/ajr.183.4.1830893]

31 **Mazzei MA**, Cioffi Squitieri N, Vindigni C, Guerrini S, Gentili F, Sadotti G, Mercuri P, Righi L, Lucii G, Mazzei FG, Marrelli D, Volterrani L. Gastrointestinal stromal tumors (GIST): a proposal of a "CT-based predictive model of Miettinen index" in predicting the risk of malignancy. *Abdom Radiol (NY)* 2020; **45**: 2989-2996 [PMID: 31506758 DOI: 10.1007/s00261-019-02209-7]

32 **Burkill GJ**, Badran M, Al-Muderis O, Meirion Thomas J, Judson IR, Fisher C, Moskovic EC. Malignant gastrointestinal stromal tumor: distribution, imaging features, and pattern of metastatic spread. *Radiology* 2003; **226**: 527-532 [PMID: 12563150 DOI: 10.1148/radiol.2262011880]

33 **Tateishi U**, Hasegawa T, Satake M, Moriyama N. Gastrointestinal stromal tumor. Correlation of computed tomography findings with tumor grade and mortality. *J Comput Assist Tomogr* 2003; **27**: 792-798 [PMID: 14501372 DOI: 10.1097/00004728-200309000-00018]

34 **Joensuu H**, Wardelmann E, Sihto H, Eriksson M, Sundby Hall K, Reichardt A, Hartmann JT, Pink D, Cameron S, Hohenberger P, Al-Batran SE, Schlemmer M, Bauer S, Nilsson B, Kallio R, Junnila J, Vehtari A, Reichardt P. Effect of KIT and PDGFRA Mutations on Survival in Patients With Gastrointestinal Stromal Tumors Treated With Adjuvant Imatinib: An Exploratory Analysis of a Randomized Clinical Trial. *JAMA Oncol* 2017; **3**: 602-609 [PMID: 28334365 DOI: 10.1001/jamaoncol.2016.5751]

World Journal of Gastrointestinal Oncology

Submit a Manuscript: https://www.f6publishing.com

World J Gastrointest Oncol 2022 May 15; 14(5): 1027-1036

DOI: 10.4251/wjgo.v14.i5.1027

ISSN 1948-5204 (online)

ORIGINAL ARTICLE

Retrospective Study

Improving the accuracy and consistency of clinical target volume delineation for rectal cancer by an education program

Yang-Zi Zhang, Xiang-Gao Zhu, Ma-Xiaowei Song, Kai-Ning Yao, Shuai Li, Jian-Hao Geng, Hong-Zhi Wang, Yong-Heng Li, Yong Cai, Wei-Hu Wang

Specialty type: Oncology

Provenance and peer review: Unsolicited article; Externally peer reviewed.

Peer-review model: Single blind

Peer-review report's scientific quality classification

Grade A (Excellent): 0
Grade B (Very good): B
Grade C (Good): C, C, C, C
Grade D (Fair): 0
Grade E (Poor): 0

P-Reviewer: Bustamante-Lopez LA, Brazil; Kang MK, South Korea; Paun VP, Romania; Sano W, Japan

Received: December 10, 2021
Peer-review started: December 10, 2021
First decision: January 12, 2022
Revised: January 24, 2022
Accepted: April 24, 2022
Article in press: April 24, 2022
Published online: May 15, 2022

Yang-Zi Zhang, Xiang-Gao Zhu, Ma-Xiaowei Song, Kai-Ning Yao, Shuai Li, Jian-Hao Geng, Hong-Zhi Wang, Yong-Heng Li, Yong Cai, Wei-Hu Wang, Department of Radiation Oncology, Key Laboratory of Carcinogenesis and Translational Research (Ministry of Education/Beijing), Peking University Cancer Hospital & Institute, Beijing 100142, China

Corresponding author: Wei-Hu Wang, MD, Chief Physician, Department of Radiation Oncology, Key Laboratory of Carcinogenesis and Translational Research (Ministry of Education/Beijing), Peking University Cancer Hospital & Institute, No. 52 Fucheng Road, Haidian District, Beijing 100142, China. wangweihu88@163.com

Abstract

BACKGROUND

Accurate target volume delineation is the premise for the implementation of precise radiotherapy. Inadequate target volume delineation may diminish tumor control or increase toxicity. Although several clinical target volume (CTV) delineation guidelines for rectal cancer have been published in recent years, significant interobserver variation (IOV) in CTV delineation still exists among radiation oncologists. However, proper education may serve as a bridge that connects complex guidelines with clinical practice.

AIM

To examine whether an education program could improve the accuracy and consistency of preoperative radiotherapy CTV delineation for rectal cancer.

METHODS

The study consisted of a baseline target volume delineation, a 150-min education intervention, and a follow-up evaluation. A 42-year-old man diagnosed with stage IIIC (T3N2bM0) rectal adenocarcinoma was selected for target volume delineation. CTVs obtained before and after the program were compared. Dice similarity coefficient (DSC), inclusiveness index (IncI), conformal index (CI), and relative volume difference [Δ V (%)] were analyzed to quantitatively evaluate the disparities between the participants' delineation and the standard CTV. Maximum volume ratio (MVR) and coefficient of variation (CV) were calculated to assess the IOV. Qualitative analysis included four common controversies in CTV delineation concerning the upper boundary of the target volume, external iliac area, groin area, and ischiorectal fossa.

RESULTS

Of the 18 radiation oncologists from 10 provinces in China, 13 completed two sets of CTVs. In quantitative analysis, the average CTV volume decreased from 809.82 cm^3 to 705.21 cm^3 (P = 0.001) after the education program. Regarding the indices for geometric comparison, the mean DSC, IncI, and CI increased significantly, while ΔV (%) decreased remarkably, indicating improved agreement between participants' delineation and the standard CTV. Moreover, an 11.80% reduction in MVR and 18.19% reduction in CV were noted, demonstrating a smaller IOV in delineation after the education program. Regarding qualitative analysis, the greatest variations in baseline were observed at the external iliac area and ischiorectal fossa; 61.54% (8/13) and 53.85% (7/13) of the participants unnecessarily delineated the external iliac area and the ischiorectal fossa, respectively. However, the education program reduced these variations.

CONCLUSION

Wide variations in CTV delineation for rectal cancer are present among radiation oncologists in mainland China. A well-structured education program could improve delineation accuracy and reduce IOVs.

Key Words: Rectal cancer; Radiotherapy; Clinical target volume; Delineation; Interobserver variation; Education

Core Tip: Accurate clinical target volume (CTV) delineation is essential to ensure appropriate tumor control while minimizing the exposure of surrounding normal tissues. However, a large degree of variation in CTV delineation for rectal cancer still exists, despite the availability of several CTV delineation guidelines. Our study aimed to evaluate the impact of an education program on CTV delineation for rectal cancer. The results first confirmed the wide variations in CTV delineation for rectal cancer among radiation oncologists from mainland China and proved that a well-structured education program could improve the accuracy and consistency of delineation.

Citation: Zhang YZ, Zhu XG, Song MX, Yao KN, Li S, Geng JH, Wang HZ, Li YH, Cai Y, Wang WH. Improving the accuracy and consistency of clinical target volume delineation for rectal cancer by an education program. *World J Gastrointest Oncol* 2022; 14(5): 1027-1036
URL: https://www.wjgnet.com/1948-5204/full/v14/i5/1027.htm
DOI: https://dx.doi.org/10.4251/wjgo.v14.i5.1027

INTRODUCTION

Colorectal cancer is one of the most common cancers in China, with morbidity and mortality occupying the fifth place among all malignant tumors[1]. Due to occult symptoms, most rectal cancer patients would have progressed to locally advanced stages (cT3-4/N+) at diagnosis, which are associated with high risks of both locoregional recurrence and distant metastasis. Neoadjuvant chemoradiotherapy has become one of the standard treatment strategies for locally advanced rectal cancer, with the ability to increase resectability and the chance of sphincter preservation, as well as improve local control[2,3]. Compared with conventional three-dimensional conformal radiation therapy, intensity-modulated radiation therapy (IMRT) can yield superior plans with respect to target coverage, homogeneity, and conformality, while lowering the dose to adjacent critical organs-at-risk[4]. However, accurate target volume delineation is the premise for the implementation of IMRT. An omission of the target volume may decrease tumor control rate, whereas inappropriate expansion of the irradiation area would result in added normal tissue damage.

Nevertheless, defining a radiation field requires a combination of knowledge from multiple disciplines, including oncology, anatomy, imaging, radiophysics, and radiobiology. Differences in the personal theoretical understanding and clinical experience of radiation oncologists may lead to inaccurate and inconsistent target volume delineation. Although several clinical target volume (CTV) delineation guidelines for rectal cancer[5-7] have been published in recent years, significant interobserver variations (IOV) still exist in target volume delineation among radiation oncologists[8-10]. However, proper education may serve as a bridge that connects complex guidelines with clinical practice. Given the importance of accurate target volume delineation and the fact that no study concerning educational interventions within the target volume delineation field for rectal cancer is

available, we conducted this study to examine the variations in preoperative radiotherapy CTV for rectal cancer among Chinese radiation oncologists and assess the short-term effects of an education program on target volume delineation.

MATERIALS AND METHODS

Participants of the education program

The study consisted of a baseline CTV delineation, a 150-min education intervention, and a follow-up evaluation. The study protocol was approved by the Beijing Cancer Hospital Research Ethics Committee. A total of 18 radiation oncologists from 18 tertiary hospitals in 10 provinces located in north, south, central, and northeast China participated in the education program. Their median age was 37 (range, 31-49) years, and the ratio of men to women was 1.25:1. Regarding their educational background, 72.22% of the participants (13/18) had a master's degree or above. As for their professional title, 33.33% (6/18) were attending physicians; the remaining 66.67% (12/18) were associate chief physicians. The median number of rectal cancer target volumes that they had delineated before the program was 38 (range, 6-300).

Baseline target area delineation

A 42-year-old male patient diagnosed with stage IIIC (T3N2bM0) rectal adenocarcinoma according to the seventh American Joint Committee on Cancer/Union for International Cancer Control TNM staging system[11] was selected for target volume delineation. The tumor was located 4 cm from the anal verge and extended cranially for 4 cm with mesorectal nodes and left internal iliac node metastases. The anal canal was not infiltrated. This patient was selected for clarifying several important issues in delineation and avoiding divergence at the same time. He underwent contrast-enhanced computed tomography (CT) and magnetic resonance imaging (MRI) simulations with 5 mm slice thickness from the L2-L3 junction to the proximal femur, in the supine position with a full bladder and an empty rectum. The simulation images were transferred to a Pinnacle 9.10 Treatment Planning System (Elekta, Sweden). The patient's medical history, physical examination, colonoscopy results, and a full set of pelvic MRI images were introduced through PowerPoint software. All the radiation oncologists participating in the education program were required to independently delineate a CTV on the CT-MRI fusion images based on their previous clinical experience. The window width and the window level used for contouring were 400 Hounsfield units (HU) and 40 HU, respectively.

Education intervention

Subsequently, a 150-min education program on CTV delineation for rectal cancer was conducted. The program consisted of four parts. First, a lecture on the lymphatic drainage mode and the postoperative recurrence pattern of rectal cancer was given. Second, the 2006 version of the definition and delineation of the CTV for rectal cancer[5], the 2009 version of the Radiation Therapy Oncology Group contouring atlas[6], and the 2016 version of the international consensus guidelines on CTV delineation[7] were introduced. Third, a standard CTV (CTV-ref) based on the 2016 version of the CTV delineation guidelines was displayed, and the anatomical boundaries of each lymphatic drainage area were explained in detail. The standard CTV was contoured by an expert who has been engaged in rectal cancer radiotherapy for more than 20 years in our center and was determined through discussion by the entire department; the CTV included the mesorectal and presacral regions, obturator and internal iliac lymph node drainage areas, and 2 cm margins from the cephalic and caudal extents of the primary lesion in the rectum. Fourth, real-time feedback on each participant's delineation deficiencies was conducted, and a question-and-answer period was provided for further clarification. Then, after the training session, the participants were asked to contour a CTV again on the same CT-MRI fusion images.

Parameter analysis

Quantitative evaluation of the target volume parameters: The volumes delineated by each participant before and after the education program were imported to a single Pinnacle 9.10 Treatment Planning System (Elekta, Sweden) for analysis. First, the average volumes and lengths of the CTVs were compared. Then, taking the standard CTV contoured by the expert as a reference (V_{ref}), the two sets of CTVs delineated by the participants (V_{stu}) were compared with V_{ref} for geometric comparison analysis. The indices used for comparison included the Dice similarity coefficient (DSC) index[12], inclusiveness index (IncI)[13], concordance index (CI)[14], and relative volume difference [ΔV (%)][13]. These indices were calculated for measuring the participants' delineation accuracy relative to the standard contour. The definitions and formulas of the above indices are listed in Table 1. The DSC, IncI, and CI can vary between 0 and 1, where 0 means there is a complete disagreement between the V_{stu} and V_{ref}, and 1 indicates perfect agreement. A ΔV (%) of 0 means that the V_{stu} is exactly the same as the V_{ref}, and the higher the value, the greater the difference between the two volumes.

Table 1 Definitions and formulas of the indices used for comparison

	Indices	Definition	Formula
Indices for geometric comparison analysis	Dice similarity coefficient index	Intersection of V_{stu} and V_{ref} divided by their average	$2 (V_{stu} \cap V_{ref})/(V_{stu} + V_{ref})$
	Inclusiveness index	Intersection of V_{stu} and V_{ref} divided by V_{stu}	$(V_{ref} \cap V_{stu})/V_{stu}$
	Concordance index	Intersection of V_{stu} and V_{ref} divided by their union	$(V_{ref} \cap V_{stu})/(V_{ref} \cup V_{stu})$
	Relative volume difference	Difference between V_{stu} and V_{ref} divided by V_{ref} and multiplied by 100	$(V_{stu}-V_{ref})/V_{ref} \times 100$
Indices for interobserver variation	Maximum volume ratio	Ratio of the maximum volume to minimum volume contoured by the participants	V_{max}/V_{min}
	Coefficient of variation	Standard deviation of the volumes contoured by the participants multiplied by 100 and divided by the mean value	SD × 100/mean

V_{stu}: Target volume delineated by the participants; V_{ref}: Standard target volume delineated by the expert; V_{max}: Maximum volume contoured by the participants; V_{min}: Minimum volume contoured by the participants; SD: Standard deviation.

Evaluation of IOV: The indices used for evaluating the IOV were the maximum volume ratio (MVR) and coefficient of variation (CV). The MVR expresses the greatest extent of the difference between the volumes, and the CV expresses the dispersion of volumes around the mean (see definitions and formulas in Table 1), with larger values representing greater variability and lower values suggesting higher consistency among the participants[15]. The MVR and CV were calculated to assess the impact of the education program on IOV.

Qualitative analysis of areas of variability: Qualitative analysis included the following four common controversies in the delineation of preoperative radiotherapy CTV for rectal cancer: (1) Should the upper boundary of the target volume start from the bifurcation of the abdominal aorta, the bifurcation of the common iliac artery or the superior border of the first sacral vertebrae? (2) Whether the external iliac area should be included; (3) Whether the groin area should be included; and (4) Whether the ischiorectal fossa should be included.

Statistical analysis

Continuous data were expressed as mean ± SD, and their normality of distribution was tested using the Shapiro-Wilk test. Comparisons were made using paired *t*-test when both groups of data had normal distribution, whereas the Wilcoxon singed-rank test was used when any group of data deviated from the normal distribution. Categorical variables were expressed as numbers (*n*) and percentages (%) and compared using the χ^2 test or Fisher's exact test. All the analyses were performed using SPSS for Windows (version 22.0, IBM Corp., Armonk, NY, United States). *P* values < 0.05 were considered statistically significant.

RESULTS

Target volume submission status

Although all the 18 radiation oncologists participating in the education program were asked to delineate two sets of CTVs, only 14 completed the baseline target volume delineation, and 13 submitted two sets of CTVs that could be used for analysis. Figure 1 displays the transverse and sagittal planes of the CTVs delineated by the 13 participants before and after the training sessions.

Quantitative evaluation of target volume parameters

Table 2 shows the results of the quantitative analysis of the target volume parameters. After the education program, the average volume of the delineated CTVs decreased significantly from 809.82 ± 141.17 cm^3 to 705.21 ± 100.53 cm^3 (*P* = 0.001). However, no remarkable difference was observed in the average length of the delineated CTVs (18.19 ± 1.01 cm *vs* 17.77 ± 0.60 cm, *P* = 0.175). Regarding the indices for geometric comparison, the mean DSC, IncI, and CI increased significantly, while the Δ V (%) decreased remarkably, *P* values were 0.009, 0.002, 0.011, and 0.002, respectively.

Evaluation of IOV

The results of the comparison analysis for IOV are displayed in Table 3. The mean MVR decreased by

Table 2 Quantitative analysis of target volume parameters

Indices	Before the education program	After the education program	*t*/*Z* value	*P* value
Volume (cm^3)	809.82 ± 141.17 (624.69-1112.79)	705.21 ± 100.53 (603.97-949.53)	-3.180	0.001
Length (cm)	18.19 ± 1.01 (16.50-20.00)	17.77 ± 0.60 (17.00-19.00)	1.442	0.175
DSC	0.78 ± 0.06 (0.68-0.87)	0.84 ± 0.04 (0.71-0.88)	-2.621	0.009
IncI	0.69 ± 0.10 (0.57-0.83)	0.79 ± 0.08 (0.58-0.87)	-3.926	0.002
CI	0.65 ± 0.08 (0.52-0.77)	0.73 ± 0.06 (0.56-0.78)	-2.551	0.011
Δ V (%)	30.79 ± 10.65 (17.33-47.65)	21.43 ± 7.80 (12.93-41.70)	3.926	0.002

Data are presented as mean ± SD (range). DSC: Dice similarity coefficient index; IncI: Inclusiveness index; CI: Concordance index; Δ V (%): Relative volume difference.

Table 3 Quantitative analysis of interobserver variation

	V_{max} (cm^3)	V_{min} (cm^3)	Mean (cm^3)	SD (cm^3)	MVR	CV
Before the education program	1112.79	624.69	809.82	141.17	1.78	17.43
After the education program	949.53	603.97	705.21	100.53	1.57	14.26
Decrease ratio	14.67%	3.32%	12.92%	28.79%	11.80%	18.19%

V_{max}: Maximum volume contoured by the participants; V_{min}: Minimum volume contoured by the participants; SD: Standard deviation; MVR: Maximum volume ratio; CV: Coefficient of variation.

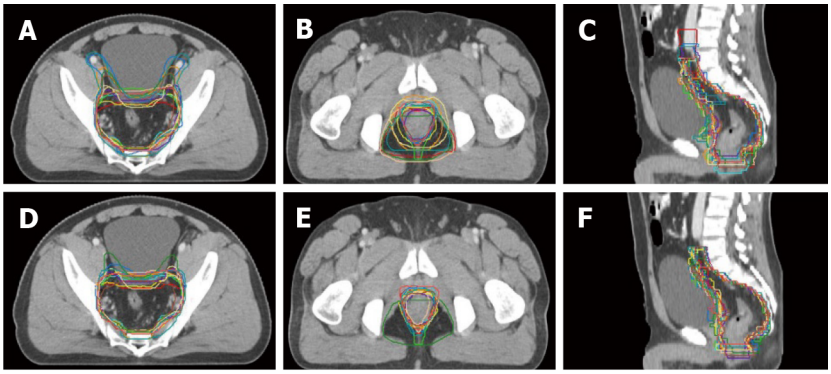

DOI: 10.4251/wjgo.v14.i5.1027

Figure 1 Example images showing the differences in clinical target volume delineation variation before and after the education program. A: Junction slice of rectum and sigmoid colon (before the education program); B: Slice of the ischiorectal fossa (before the education program); C: Sagittal view (before the education program); D: Junction slice of rectum and sigmoid colon (after the education program); E: Slice of the ischiorectal fossa (after the education program); F: Sagittal view (after the education program). Target volumes delineated by different participants are displayed in different colors.

11.80% from 1.78 to 1.57, and the mean CV decreased by 18.19% from 17.43 to 14.26, demonstrating a smaller IOV in delineation after the education program.

Qualitative assessment of target volume variations

Table 4 shows the qualitative assessment of target volume variations before and after the education program. The greatest variations in the CTVs were observed at the external iliac area and the ischiorectal fossa; 61.54% of the participants (8/13) delineated the external iliac area and 53.85% of the participants (7/13) delineated the ischiorectal fossa unnecessarily at the baseline. However, after the education program, the proportion significantly decreased. Regarding the upper boundary, eight CTVs started from the bifurcation of the common iliac artery, three started from the bifurcation of the abdominal aorta or above, and two started from the superior border of the first sacral vertebrae at the baseline. After the education program, 12 CTVs started from the bifurcation of the common iliac artery, and one started from the superior border of the first sacral vertebrae. However, the difference was not statistically significant. The inguinal area was consistently excluded from the CTVs regardless of the

Table 4 Qualitative analysis of target volume variations

Parameters	Before the education program		After the education program		*P* value
	Yes	No	Yes	No	
CTV start from the bifurcation of the common iliac artery	8 (61.54%)	5 (38.46%)	12 (92.31%)	1 (7.69%)	0.16
Delineate external iliac area	8 (61.54%)	5 (38.46%)	1 (7.69%)	12 (92.31%)	0.01
Delineate inguinal area	0 (0%)	13 (100%)	0 (0.00%)	13 (100%)	NA
Delineate ischiorectal fossa	7 (53.85%)	6 (46.15%)	1 (7.69%)	12 (92.31%)	0.03

CTV: Clinical target volume; NA: Not applicable.

education program.

DISCUSSION

This study confirmed the presence of wide variations in preoperative CTV contouring for rectal cancer among radiation oncologists from mainland China and indicated that a well-structured education program could improve delineation accuracy and reduce IOVs. To our knowledge, this is the first study to evaluate the impact of an education program on CTV delineation for rectal cancer.

The participants in this study represented the levels of major tertiary hospitals in China; all of them were attending physicians or above, and 72.22% had a master's or doctor's degree. They all had experience in rectal cancer radiotherapy, and half of them had delineated more than 30 cases of rectal cancer previously. However, our data showed a 1.8-fold variation in CTVs (range, 624.69-1112.79 cm^3) at baseline. After the education program, the delineation accuracy of the participants relative to the standard contour improved remarkably and the IOV decreased. Besides, we found a statistically significant reduction in the average volume of the delineated CTVs. Qualitative analysis indicated that the larger CTV at baseline was associated with an inaccurate higher superior border as well as an inappropriate inclusion of the external iliac region and the ischiorectal fossa.

The 2009 version of the guidelines clearly stated that the most cephalad aspect of the CTV should be where the common iliac vessels bifurcate into the external/internal iliac vessels[6]. The 2016 version of the guidelines generally agreed on this point except for cases with T3N0 and circumferential resection margin (-) disease[7]. An approximate bony landmark is the sacral promontory, which is commonly used as the upper border of radiation fields in traditional two-dimensional radiotherapy. However, occasionally, these two anatomical locations are not equal; under that situation, the correct choice should be where the common iliac vessels bifurcate. Our study revealed that two participants still used the bony landmark as the upper border, and three participants mistakenly increased the CTV's upper border to the bifurcation of the abdominal aorta at baseline. The external iliac region does not belong to the regional lymph nodes of rectal cancer. Elective irradiation of the external iliac region is only recommended for patients with positive obturator lymph nodes or T4b disease with anterior organ invasion[7]. The case in our study had clinical stage T3 without obturator lymph node metastasis; thus, the external iliac region was unnecessary to be included. Nevertheless, 61.54% of the participants (8/13) delineated this area at baseline. The variation in the delineation of the ischiorectal fossa may be related to the alteration in the guidelines recommendation. The 2006 version of the guidelines suggested the inclusion of the inferior pelvic subsite in the irradiated volume when the tumor is located within 6 cm from the anal margin[5]. However, currently, it is believed that inferior pelvic recurrences are more related to tumor spillage during inadequate surgical procedures[7]. Besides, irradiation of the ischiorectal fossa could increase the rate of perineal wound complications after abdominoperineal resection[16]. Therefore, the 2016 version of the guidelines suggested that ischiorectal fossa irradiation can be omitted unless the primary tumor directly invades this area or the external anal sphincter[7]. The case in our study was a low rectal cancer without ischiorectal fossa or external anal sphincter infiltration. Yet 53.85% of the participants (7/13) delineated this area at baseline. However, following the education program, delineation accuracy was improved for the above areas. These qualitative findings, which have not been demonstrated in previous studies, are notable and instructive for the clinical practice of radiation oncologists.

Why was the variability so large among the radiation oncologists? The reasons could be multifactorial. First, radiation oncologists might be unsure about which areas to delineate. Second, they might be unfamiliar with the anatomical borders of each lymphatic drainage area. Third, their knowledge might not have been updated following the publication of new guidelines. Fourth, there is incoherence between knowledge and practice. Considering the vast area of mainland China, the real variations among different levels of medical institutions may be much larger. The geometric inaccuracy

in target volume delineation has proved to have a significant impact on dosimetric coverage of CTV, which probably affects the clinical outcomes[15]. Further, major multi-institutional clinical trials also require consistent delineation of the target area to ensure the accuracy of results in the correlation analysis among various dosimetric data and clinical outcomes. A key question is whether any effective measures could be adopted to reduce these variations.

Literature regarding interventions to reduce IOV in target volume delineation included the importation of additional imaging into the radiotherapy planning system, the implementation of auto-contouring systems, the introduction of standardized guidelines or protocols, and specific teaching interventions. The advances in imaging modalities can help us better distinguish the boundaries between tumors and normal tissues. The use of registered positron emission tomography scans improved gross target volume (GTV) contouring in lung cancer[17] and rectal cancer[18]. Registered MRI scans decreased IOV in target volume delineation for prostate cancer[19] and avoided inadvertent geographical misses during postoperative radiotherapy treatment planning for brain tumors[20]. However, these improvements were more associated with GTV rather than CTV. The implementation of auto-contour systems increased contouring accuracy and saved work time[13,21]. Nevertheless, even with the aid of a computer-assistant system, an accurate target volume delineation still requires the radiation oncologist's own knowledge and judgement.

Nijkamp *et al*[9] found that a reduction of delineation variation in early-stage rectal cancer was achieved by establishing national consensus guidelines. The study of Fuller *et al*[8] revealed that including a visual atlas in addition to written instructions can improve conformance to a reference expert's contours and reduce IOV. However, substantial residual variability still exists in rectal target volume delineation after atlas use[8]. One possible explanation is that the guidelines themselves are complex, which require considerable study and repeated practice before profound understanding and proficient application, especially for non-native English speakers[10]. After the residency program, most clinicians gain knowledge through reading literature or attending academic conferences. However, simply reading literature by themselves is not very effective, and general academic conferences do not include the skills of target volume delineation. Therefore, it is necessary to develop continuing education programs, such as the one in this study, to train clinicians on how to transform the guidelines into clinical practice.

When performing an education program, a simply didactic lecture is not sufficient; hands-on practical sessions and interactive communication are essential. Dewas *et al*'s[22] study revealed that didactic teaching did not significantly improve lung cancer delineation. The experience of Davis *et al*[23] suggested that a combination of didactic and interactive learning was more effective in changing clinicians' practice than didactic sessions alone. Our specially designed education program organically integrated theoretical knowledge, clinical practice, and real-time feedback, provided two chances for target area delineation, and achieved favorable teaching effects in a relatively short period. This education program generated a positive response and has been incorporated into the national continuing education programs.

This study had several limitations, including the small sample size and only a single case for contouring. Furthermore, the long-term outcomes were not assessed; thus, it is unclear whether the education program is associated with lasting effects. Further studies need to include more participants and rule out possible selection biases resulting from a single patient and anatomic differences by tumor locations. Moreover, a prolonged follow-up period is needed to investigate the long-term effects of the education program.

CONCLUSION

Wide variations in the delineation of CTV for rectal cancer were present among radiation oncologists from mainland China. Inappropriate inclusion of the external iliac area and ischiorectal fossa were the two main issues in the CTV contouring. A well-structured education program could improve delineation accuracy and reduce IOVs. It is feasible to incorporate such a program into the continuing education programs for radiation oncologists.

ARTICLE HIGHLIGHTS

Research background

Accurate target volume delineation is essential for precise radiotherapy. Inappropriate target volume may reduce local control or bring more normal tissue damage. However, defining a radiation field is not easy since it requires an integration of knowledge from multiple disciplines and rich clinical experience.

Research motivation

Previous studies have proved that wide variations in clinical target volume (CTV) delineation for rectal

cancer were present among radiation oncologists despite the availability of several guidelines. Thus, how to improve the delineation accuracy and consistency has emerged as a key question in the era of precise radiotherapy. However, no study regarding the current situation of CTV delineation for rectal cancer is available in China, and there is also a lack of study on the impact of educational interventions on rectal cancer target delineation.

Research objectives

To examine the interobserver variation (IOV) in CTV delineation for rectal cancer among radiation oncologists in mainland China and evaluate whether an education program could improve the accuracy and consistency of delineation.

Research methods

The study consisted of a baseline CTV delineation, a 150-min education intervention, and a follow-up CTV delineation. CTVs contoured by the participants before and after the program were obtained and compared. Quantitative evaluation included the indices for measuring the delineation accuracy of the participants relative to the standard contour and the indices for assessing IOV. Qualitative analysis included four common problems in CTV delineation.

Research results

Eighteen radiation oncologists from 10 provinces in China attended the education program and 13 of them completed two sets of CTVs. After the education program, a statistically significant reduction in the average volume of the delineated CTVs was detected (P = 0.001). The agreement between the participants' delineation and the standard CTV improved remarkably and the IOV decreased. Qualitative analysis indicated that 61.54% of the participants (8/13) delineated the external iliac area, and 53.85% of the participants (7/13) delineated the ischiorectal fossa unnecessarily at the baseline, and the proportions reduced significantly after the program.

Research conclusions

Our study first confirmed the wide variations in CTV delineation for rectal cancer among radiation oncologists from mainland China and proved that education interventions could improve the accuracy and consistency of delineation.

Research perspectives

Further studies need to recruit more participants and include more cases for target volume delineation. Besides, the long-term effects of the education program also need to be investigated.

ACKNOWLEDGEMENTS

The authors would like to thank the radiation oncologists who participated in the study.

FOOTNOTES

Author contributions: Zhang YZ drafted the manuscript, and was involved with data analysis; Zhu XG, Yao KN, Li S, and Geng JH participated in the collection and analysis of the data; Song MX, Wang HZ, and Li YH revised the article critically for important intellectual content; Wang WH and Cai Y participated in the design of the study and revision of the article; and all authors read and approved the final manuscript.

Supported by the Beijing Municipal Science & Technology Commission, No. Z181100001718192; the Capital's Funds for Health Improvement and Research, No. 2020-2-1027 and No. 2020-1-4021; the National Natural Science Foundation, No. 82073333; and the Beijing Natural Science Foundation, No. 1212011.

Institutional review board statement: This study was reviewed and approved by the Beijing Cancer Hospital Research Ethics Committee (Approval No. 2021YJZ111).

Informed consent statement: The participants of the study were not required to give informed consent to the study because the analysis used anonymous image data that were obtained from the education program.

Conflict-of-interest statement: The authors declare that there is no conflict of interest.

Data sharing statement: The datasets used and/or analyzed during the current study are available from the corresponding authors on reasonable request.

Country/Territory of origin: China

ORCID number: Yang-Zi Zhang 0000-0001-7371-1709; Xiang-Gao Zhu 0000-0002-6739-8047; Ma-Xiaowei Song 0000-0002-0537-9502; Kai-Ning Yao 0000-0002-9269-5836; Shuai Li 0000-0002-7577-9704; Jian-Hao Geng 0000-0003-1625-5406; Hong-Zhi Wang 0000-0001-6040-796X; Yong-Heng Li 0000-0002-2101-2014; Yong Cai 0000-0002-8862-2909; Wei-Hu Wang 0000-0003-4969-398X.

S-Editor: Wang JJ
L-Editor: A
P-Editor: Wang JJ

REFERENCES

1 **Chen W**, Zheng R, Baade PD, Zhang S, Zeng H, Bray F, Jemal A, Yu XQ, He J. Cancer statistics in China, 2015. *CA Cancer J Clin* 2016; **66**: 115-132 [PMID: 26808342 DOI: 10.3322/caac.21338]
2 **Glynne-Jones R**, Wyrwicz L, Tiret E, Brown G, Rödel C, Cervantes A, Arnold D; ESMO Guidelines Committee. Rectal cancer: ESMO Clinical Practice Guidelines for diagnosis, treatment and follow-up. *Ann Oncol* 2017; **28**: iv22-iv40 [PMID: 28881920 DOI: 10.1093/annonc/mdx224]
3 **National Comprehensive Cancer Network**. NCCN Clinical Practice Guidelines in Oncology: Rectal Cancer. Version 1. 2021. [cited 22 December 2020]. Available from: https://www.poijaya.org/wp-content/uploads/2021/08/rectal.pdf
4 **Mok H**, Crane CH, Palmer MB, Briere TM, Beddar S, Delclos ME, Krishnan S, Das P. Intensity modulated radiation therapy (IMRT): differences in target volumes and improvement in clinically relevant doses to small bowel in rectal carcinoma. *Radiat Oncol* 2011; **6**: 63 [PMID: 21651775 DOI: 10.1186/1748-717X-6-63]
5 **Roels S**, Duthoy W, Haustermans K, Penninckx F, Vandecaveye V, Boterberg T, De Neve W. Definition and delineation of the clinical target volume for rectal cancer. *Int J Radiat Oncol Biol Phys* 2006; **65**: 1129-1142 [PMID: 16750329 DOI: 10.1016/j.ijrobp.2006.02.050]
6 **Myerson RJ**, Garofalo MC, El Naqa I, Abrams RA, Apte A, Bosch WR, Das P, Gunderson LL, Hong TS, Kim JJ, Willett CG, Kachnic LA. Elective clinical target volumes for conformal therapy in anorectal cancer: a radiation therapy oncology group consensus panel contouring atlas. *Int J Radiat Oncol Biol Phys* 2009; **74**: 824-830 [PMID: 19117696 DOI: 10.1016/j.ijrobp.2008.08.070]
7 **Valentini V**, Gambacorta MA, Barbaro B, Chiloiro G, Coco C, Das P, Fanfani F, Joye I, Kachnic L, Maingon P, Marijnen C, Ngan S, Haustermans K. International consensus guidelines on Clinical Target Volume delineation in rectal cancer. *Radiother Oncol* 2016; **120**: 195-201 [PMID: 27528121 DOI: 10.1016/j.radonc.2016.07.017]
8 **Fuller CD**, Nijkamp J, Duppen JC, Rasch CR, Thomas CR Jr, Wang SJ, Okunieff P, Jones WE 3rd, Baseman D, Patel S, Demandante CG, Harris AM, Smith BD, Katz AW, McGann C, Harper JL, Chang DT, Smalley S, Marshall DT, Goodman KA, Papanikolaou N, Kachnic LA; Radiation Oncology Committee of the Southwest Oncology Group. Prospective randomized double-blind pilot study of site-specific consensus atlas implementation for rectal cancer target volume delineation in the cooperative group setting. *Int J Radiat Oncol Biol Phys* 2011; **79**: 481-489 [PMID: 20400244 DOI: 10.1016/j.ijrobp.2009.11.012]
9 **Nijkamp J**, de Haas-Kock DF, Beukema JC, Neelis KJ, Woutersen D, Ceha H, Rozema T, Slot A, Vos-Westerman H, Intven M, Spruit PH, van der Linden Y, Geijsen D, Verschueren K, van Herk MB, Marijnen CA. Target volume delineation variation in radiotherapy for early stage rectal cancer in the Netherlands. *Radiother Oncol* 2012; **102**: 14-21 [PMID: 21903287 DOI: 10.1016/j.radonc.2011.08.011]
10 **Franco P**, Arcadipane F, Trino E, Gallio E, Martini S, Iorio GC, Piva C, Moretto F, Ruo Redda MG, Verna R, Tseroni V, Bona C, Pozzi G, Fiandra C, Ragona R, Bertetto O, Ricardi U. Variability of clinical target volume delineation for rectal cancer patients planned for neoadjuvant radiotherapy with the aid of the platform Anatom-e. *Clin Transl Radiat Oncol* 2018; **11**: 33-39 [PMID: 29928706 DOI: 10.1016/j.ctro.2018.06.002]
11 **Edge SB**, Compton CC. The American Joint Committee on Cancer: the 7th edition of the AJCC cancer staging manual and the future of TNM. *Ann Surg Oncol* 2010; **17**: 1471-1474 [PMID: 20180029 DOI: 10.1245/s10434-010-0985-4]
12 **Zou KH**, Warfield SK, Bharatha A, Tempany CM, Kaus MR, Haker SJ, Wells WM 3rd, Jolesz FA, Kikinis R. Statistical validation of image segmentation quality based on a spatial overlap index. *Acad Radiol* 2004; **11**: 178-189 [PMID: 14974593 DOI: 10.1016/S1076-6332(03)00671-8]
13 **La Macchia M**, Fellin F, Amichetti M, Cianchetti M, Gianolini S, Paola V, Lomax AJ, Widesott L. Systematic evaluation of three different commercial software solutions for automatic segmentation for adaptive therapy in head-and-neck, prostate and pleural cancer. *Radiat Oncol* 2012; **7**: 160 [PMID: 22989046 DOI: 10.1186/1748-717X-7-160]
14 **Konert T**, Vogel WV, Everitt S, MacManus MP, Thorwarth D, Fidarova E, Paez D, Sonke JJ, Hanna GG. Multiple training interventions significantly improve reproducibility of PET/CT-based lung cancer radiotherapy target volume delineation using an IAEA study protocol. *Radiother Oncol* 2016; **121**: 39-45 [PMID: 27663950 DOI: 10.1016/j.radonc.2016.09.002]
15 **Peng YL**, Chen L, Shen GZ, Li YN, Yao JJ, Xiao WW, Yang L, Zhou S, Li JX, Cheng WQ, Guan Y, Xia HQ, Liu S, Zhao C, Deng XW. Interobserver variations in the delineation of target volumes and organs at risk and their impact on dose distribution in intensity-modulated radiation therapy for nasopharyngeal carcinoma. *Oral Oncol* 2018; **82**: 1-7 [PMID:

29909882 DOI: 10.1016/j.oraloncology.2018.04.025]
16 **Bullard KM**, Trudel JL, Baxter NN, Rothenberger DA. Primary perineal wound closure after preoperative radiotherapy and abdominoperineal resection has a high incidence of wound failure. *Dis Colon Rectum* 2005; **48**: 438-443 [PMID: 15719190 DOI: 10.1007/s10350-004-0827-1]
17 **Morarji K**, Fowler A, Vinod SK, Ho Shon I, Laurence JM. Impact of FDG-PET on lung cancer delineation for radiotherapy. *J Med Imaging Radiat Oncol* 2012; **56**: 195-203 [PMID: 22498194 DOI: 10.1111/j.1754-9485.2012.02356.x]
18 **Whaley JT**, Fernandes AT, Sackmann R, Plastaras JP, Teo BK, Grover S, Perini RF, Metz JM, Pryma DA, Apisarnthanarax S. Clinical utility of integrated positron emission tomography/computed tomography imaging in the clinical management and radiation treatment planning of locally advanced rectal cancer. *Pract Radiat Oncol* 2014; **4**: 226-232 [PMID: 25012830 DOI: 10.1016/j.prro.2013.09.002]
19 **Villeirs GM**, Van Vaerenbergh K, Vakaet L, Bral S, Claus F, De Neve WJ, Verstraete KL, De Meerleer GO. Interobserver delineation variation using CT *vs* combined CT + MRI in intensity-modulated radiotherapy for prostate cancer. *Strahlenther Onkol* 2005; **181**: 424-430 [PMID: 15995835 DOI: 10.1007/s00066-005-1383-x]
20 **Datta NR**, David R, Gupta RK, Lal P. Implications of contrast-enhanced CT-based and MRI-based target volume delineations in radiotherapy treatment planning for brain tumors. *J Cancer Res Ther* 2008; **4**: 9-13 [PMID: 18417895 DOI: 10.4103/0973-1482.39598]
21 **Ma CY**, Zhou JY, Xu XT, Guo J, Han MF, Gao YZ, Du H, Stahl JN, Maltz JS. Deep learning-based auto-segmentation of clinical target volumes for radiotherapy treatment of cervical cancer. *J Appl Clin Med Phys* 2022; **23**: e13470 [PMID: 34807501 DOI: 10.1002/acm2.13470]
22 **Dewas S**, Bibault JE, Blanchard P, Vautravers-Dewas C, Pointreau Y, Denis F, Brauner M, Giraud P. Delineation in thoracic oncology: a prospective study of the effect of training on contour variability and dosimetric consequences. *Radiat Oncol* 2011; **6**: 118 [PMID: 21929770 DOI: 10.1186/1748-717X-6-118]
23 **Davis D**, O'Brien MA, Freemantle N, Wolf FM, Mazmanian P, Taylor-Vaisey A. Impact of formal continuing medical education: do conferences, workshops, rounds, and other traditional continuing education activities change physician behavior or health care outcomes? *JAMA* 1999; **282**: 867-874 [PMID: 10478694 DOI: 10.1001/jama.282.9.867]

World Journal of Gastrointestinal Oncology

Submit a Manuscript: https://www.f6publishing.com

World J Gastrointest Oncol 2022 May 15; 14(5): 1037-1049

DOI: 10.4251/wjgo.v14.i5.1037

ISSN 1948-5204 (online)

ORIGINAL ARTICLE

Observational Study

Digital single-operator cholangioscopy for biliary stricture after cadaveric liver transplantation

Jian-Feng Yu, Dong-Lei Zhang, Yan-Bin Wang, Jian-Yu Hao

Specialty type: Microscopy

Provenance and peer review: Unsolicited article; Externally peer reviewed.

Peer-review model: Single blind

Peer-review report's scientific quality classification

Grade A (Excellent): 0
Grade B (Very good): B, B
Grade C (Good): C
Grade D (Fair): 0
Grade E (Poor): 0

P-Reviewer: Incorvaia L, Italy; Kitagawa K, Japan; Tsou YK, Taiwan

Received: December 20, 2021
Peer-review started: December 20, 2021
First decision: February 21, 2022
Revised: April 8, 2022
Accepted: April 24, 2022
Article in press: April 24, 2022
Published online: May 15, 2022

Jian-Feng Yu, Dong-Lei Zhang, Yan-Bin Wang, Jian-Yu Hao, Department of Gastroenterology, Beijing Chao-Yang Hospital, Capital Medical University, Beijing 100020, China

Corresponding author: Jian-Yu Hao, MD, PhD, Chief Physician, Department of Gastroenterology, Beijing Chao-Yang Hospital, Capital Medical University, No. 8 Gongti South Road, Chaoyang District, Beijing 100020, China. haojianyuxhnk@sina.cn

Abstract

BACKGROUND

Biliary strictures after liver transplantation (LT) remain clinically arduous and challenging situations, and endoscopic retrograde cholangiopancreatography (ERCP) has been considered as the gold standard for the management of biliary strictures after LT. Nevertheless, in the treatment of biliary strictures after LT with ERCP, many studies show that there is a large variation in diagnostic accuracy and therapeutic success rate. Digital single-operator peroral cholangioscopy (DSOC) is considered a valuable diagnostic modality for indeterminate biliary strictures.

AIM

To evaluate DSOC in addition to ERCP for management of biliary strictures after LT.

METHODS

Nineteen patients with duct-to-duct biliary reconstruction who underwent ERCP for suspected biliary complications between March 2019 and March 2020 at Beijing Chaoyang Hospital, Capital Medical University, were consecutively enrolled in this observational study. After evaluating bile ducts using fluoroscopy, cholangioscopy using a modern digital single-operator cholangioscopy system (SpyGlass DS™) was performed during the same procedure with patients under conscious sedation. All patients received peri-interventional antibiotic prophylaxis. Biliary strictures after LT were classified according to the manifestations of choledochoscopic strictures and the manifestations of transplanted hepatobiliary ducts.

RESULTS

Twenty-one biliary strictures were found in a total of 19 patients, among which anastomotic strictures were evident in 18 (94.7%) patients, while non-anastomotic strictures in 2 (10.5%), and space-occupying lesions in 1 (5.3%). Stones were found

in 11 (57.9%) and loose sutures in 8 (42.1%). A benefit of cholangioscopy was seen in 15 (78.9%) patients. Cholangioscopy was crucial for selective guidewire placement prior to planned intervention in 4 patients. It was instrumental in identifying biliary stone and/or loose sutures in 9 patients in whom ERCP failed. It also provided a direct vision for laser lithotripsy. A space-occupying lesion in the bile duct was diagnosed by cholangioscopy in one patient. Patients with biliary stricture after LT displayed four types: (A) mild inflammatory change (n = 9); (B) acute inflammatory change edema, ulceration, and sloughing (n = 3); (C) chronic inflammatory change; and (D) acute suppurative change. Complications were seen in three patients with post-interventional cholangitis and another three with hyperamylasemia.

CONCLUSION

DSOC can provide important diagnostic information, helping plan and perform interventional procedures in LT-related biliary strictures.

Key Words: Cholangioscopy; Endoscopic retrograde cholangiopancreatography; Liver transplantation; Biliary strictures; Biliary complications; Biliary anastomotic stricture

Core Tip: Biliary strictures represent a leading cause of morbidity and mortality in liver transplant recipients. To date, endoscopic retrograde cholangiopancreatography remains the gold standard for diagnosing and treating such complications. The present study examined the benefit of complementary digital single-operator cholangioscopy. Our results are encouraging and demonstrate strong evidence for a diagnostic and therapeutic advantage of additional cholangioscopy for the management of biliary disorders following liver transplantation.

Citation: Yu JF, Zhang DL, Wang YB, Hao JY. Digital single-operator cholangioscopy for biliary stricture after cadaveric liver transplantation. *World J Gastrointest Oncol* 2022; 14(5): 1037-1049
URL: https://www.wjgnet.com/1948-5204/full/v14/i5/1037.htm
DOI: https://dx.doi.org/10.4251/wjgo.v14.i5.1037

INTRODUCTION

Liver transplantation (LT) has become a standard of care in patients with end-stage liver disease[1]. Despite improvements in surgical techniques, graft preservation technology, immunosuppressive therapy, and close follow-up[2], a biliary stricture is still the most common adverse event (AE) after LT, occurring in 5 % to 19 % of patients[3-6]. Biliary strictures include a wide array of biliary abnormalities that have different anatomical locations, clinical presentation, and pathogenesis. Biliary strictures after LT can be either anastomotic (AS) or non-anastomotic (NAS) based on the morphology and location of stenosis observed during imaging procedures[7,8]. AS account for approximately 80% of the post LT biliary strictures, are usually isolated, localized within 5 mm to the anastomosis site, and formed over short ductal lengths[9]. NAS account for the remaining 10% to 25%, are found more than 5 mm proximal to the anastomosis[10]; which can occur in both the extrahepatic or intrahepatic ducts and often develop at multiple sites and over greater lengths[10-12]. The first-line approach to resolving biliary strictures involves endoscopic retrograde cholangiopancreatography (ERCP), with stenosis dilatation and placement of multiple plastic stents, and fully covered self-expandable metallic stents[13-16]. Currently, ERCP represents the gold standard for the diagnosis and treatment of biliary strictures after LT[17]. The success rate of endoscopic therapy of the bile duct is 80%-100% in cases of LT[13,14], but successful long-term outcomes of endoscopic management of biliary anastomotic strictures after liver transplantation are 36.9%-100%[11,18,19]. Because not all strictures can be correctly diagnosed and treated with ERCP alternative methods are needed.

In 2015, digital single-operator cholangioscopy (DSOC), a high-resolution cholangioscopy (SpyGlass DS™), was introduced by Boston Scientific (Boston Scientific Corp.), enabling high-definition imaging of bile ducts. DSOC provides detailed imaging of the biliary tree, assisting both with diagnosis and treatment through biopsy under direct vision, lithotripsy of difficult stones, retrieval of migrated stents, foreign body removal, and guidewire placement[20]. Therefore, since its development, DSOC has gained increasing attention in the field of management of biliary strictures after LT[21].

A few case reports and small case series analyzing the role of single-operator cholangioscopy (SOC) for management of biliary strictures after LT suggest that this approach is safe and feasible and can

identify distinct features of anastomotic strictures[18-24]. This additional information may help guide effective treatment and predict patient outcomes. However, further studies are needed to fully evaluate the benefits of SOC in this respect, while for DSOC, to the best of our knowledge, there is little data available on its effect on the management of biliary strictures in LT recipients.

As it is likely that DSOC will benefit endoscopic management of biliary strictures after LT, by providing important high-resolution information of the bile duct, we decided to undertake an observational study of its use. Therefore, this study aimed to examine the role of complementary DSOC using the SpyGlass DS system during ERCP for the management of biliary strictures following LT.

MATERIALS AND METHODS

Subjects

This retrospective, observational study was performed at the Beijing ChaoYang Hospital, Capital Medical University, China. The study was performed in accordance with the guidelines of the Declaration of Helsinki and was approved by the Ethics Committee of ChaoYang Hospital (Beijing, China). All patients signed written informed consent for surgery. The statistical methods of this study were reviewed by Dr. Li-Rong Liang from the Department of Clinical Epidemiology, Beijing Chao-Yang Hospital, Capital Medical University. Patients with LT and duct-to-duct biliary anastomosis who presented with clinical or biochemical signs of biliary strictures and/or suspected biliary complications based upon imaging and/or histology between February 2019 and March 2020 were included in the study.

Inclusion criteria: (1) Patients after LT with clinical manifestations or biochemical changes of biliary stricture from February 2019 to March 2020; and (2) Imaging examinations by B-ultrasound, computed tomography, or magnetic resonance cholangiopancreatography (MRCP) suggested biliary stricture. Exclusion criteria: (1) Severe changes in the anatomical structure of the upper digestive tract; (2) Patients with severe coagulopathy; (3) Patients with severe cardiopulmonary insufficiency; and (4) Patients who cannot tolerate anesthesia.

Procedures

All patients underwent transabdominal ultrasound. In the case of inconclusive findings on transabdominal ultrasound (common bile duct cannot be shown due to excessive gastrointestinal gas) and the absence of clinically evident cholangitis, MRCP was performed before ERCP. All patients received ERCP performed using a large diameter channel duodenoscope (TJF-260V, Olympus Corp., Tokyo, Japan). If a plastic biliary stent was previously placed in the patient, it was removed before cannulation. Cannulation of the bile duct was guidewire-assisted (0.035 inches, Hydra Jagwire™, Boston Scientific Corp) using a cannulating sphincterotome (Autotome RX, Boston Scientific Corp). If necessary, biliary sphincterotomy was performed. During the procedures, patients received conscious sedation with propofol and sufentanil.

Cholangioscopy

ERCP was followed by cholangioscopy during the same procedure. Cholangioscopy was carried out using a single operator cholangioscopy device (SpyGlass DS; Boston Scientific Corp.) that was pushed along the guidewire through the working channel of the duodenoscope into the bile duct. The guidewire was then removed, and cholangioscopy was conducted under visual guidance. A biopsy was performed in case of unrecognized bile duct mucosal lesions. After the intervention, patients remained hospitalized for at least 3 d.

The interventions were performed by two highly experienced investigators with a yearly case volume of more than 200 endoscopic biliary interventions. Procedure-related complications were evaluated according to the American Society for Gastrointestinal Endoscopy guidelines[10].

Peri-interventional antibiotics

Standard antibiotic prophylaxis included intravenous cefoxitin (New Asia Pharmaceutical Co. Ltd) at least 6 h before the procedure and up to 3 d thereafter. During ERCP/cholangioscopy, bile was collected for microbial analysis and for antibiotic susceptibility testing.

Immunosuppression

All patients were maintained on a calcineurin inhibitor (Ciclosporin A, Novartis Pharma Stein AG) alone or in combination with either an mTOR inhibitor (rapamycin, Kerry Centre) or mycophenolate mofetil (Roche).

Interpretation of ERCP findings

Strictures were determined as an abrupt narrowing of the bile duct with a delayed outflow of contrast media through the stricture. Bile strictures were fluoroscopically subdivided into AS at the site of biliary

Table 1 Patients' characteristics

Patient No.	Age (yr)	Sex	Indication for LT	Post-LT time (mo)	Stent placement status	Number of previous ERCPs
1	42	M	Hepatitis B liver cirrhosis	25	Y	3
2	55	M	Alcoholic liver cirrhosis	6	Y	1
3	55	M	Alcoholic liver cirrhosis	9	Y	1
4	52	M	Hepatitis B liver cirrhosis	7	Y	1
5	47	M	Cryptogenic liver cirrhosis	11	N	0
6	63	F	Hepatitis C liver cirrhosis	6	N	0
7	52	F	Primary biliary cholangitis	17	Y	2
8	52	F	Hepatitis B liver cirrhosis	36	Y	3
9	44	M	Alcoholic liver cirrhosis	26	N	0
10	37	F	Drug-induced liver injury, acute liver failure	2	N	0
11	37	F	Drug-induced liver injury, acute liver failure	4	Y	1
12	54	M	Alcoholic liver cirrhosis	4	N	1
13	42	M	Hepatitis B liver cirrhosis, acute liver failure	30	N	0
14	54	M	Hepatocellular carcinoma/hepatitis B	17	Y	2
15	72	F	Cryptogenic liver cirrhosis	20	N	0
16	41	F	Primary biliary cholangitis	21	N	0
17	59	M	Cryptogenic liver cirrhosis	13	N	0
18	49	M	Alcoholic liver cirrhosis	15	N	0
19	49	M	Hepatitis B liver cirrhosis	17	Y	0

LT: Liver transplantation; ERCP: Endoscopic retrograde cholangiopancreatography.

anastomosis and NAS affecting donor bile ducts that were proximal to the biliary anastomosis. Dilatation was determined as an abrupt increase of the diameter of the bile duct, leading to a bag or column appearance of the bile duct. Bile duct stones were determined as intraluminal filling defects of contrast media, which were rounded or cloud-like, free-moving, and could be pushed by endoscopic instruments.

Interpretation of cholangioscopy findings

Strictures were determined as above and were visible as an abrupt substantial narrowing of bile ducts compared with distal and proximal segments of the bile duct. Stones were determined as free-moving, hard, foreign bodies in the bile duct or soft floccule stuck to the wall of the bile duct. A loose suture was determined as wire floating in the bile duct near the anastomosis. A neoplasm was determined as a quasi-circular lesion protruding into the lumen of the bile duct, which was connected with the wall of the bile duct.

The biliary stricture could be characterized into 4 types (Type A, B, C, and D) based on the cholangioscopic appearance of the mucosa at the anastomotic site and donor bile duct.

Observation indicators

The main observation indicators were the success rate of ERCP intubation, the success rate of DSOC auxiliary guide wire passing through the stenosis, the correct rate of ERCP and DSOC to diagnose the nature of stenosis, routine blood analysis 2h and 24h postoperatively, serum total bilirubin, serum direct bilirubin, serum amylase.

ERCP was intubated through the duodenal papilla, and if the guidewire failed to enter the intrahepatic bile duct through the stenosis, it was judged as a failure of ERCP.

Table 2 Patients' endoscopic diagnosis and treatment

Patient No.	Finding of ERCP	Findings of DSOC	Biliary stricture classification by DSOC	Endoscopic intervention
1	NAS	NAS; AS; stone; suture	Type B	Extraction of stones; MSP
2	NAS	AS; stone; suture	Type C	Extraction of stones; MSP
3	NAS	AS; stone; suture	Type D	MSP; ENBD
4	NAS	AS; stone	Type B	CAGP; balloon dilation; extraction of stones; MSP
5	AS	AS; stone; suture	Type A	CAGP; laser lithotripsy; balloon dilation; extraction of stones; MSP
6	NAS	Space-occupying lesions		Biopsy
7	AS	AS; stone; suture	Type B	Extraction of stones; MSP
8	AS	AS; stone; suture	Type B	Extraction of stones; MSP
9	AS, stone	AS; stone	Type A	Balloon dilation; laser lithotripsy; extraction of stones; ENBD
10	AS	AS; stone; suture	Type B	Balloon dilation; SSP
11	AS	AS; suture	Type B	Balloon dilation; MSP
12	AS	AS	Type B	Balloon dilation; MSP
13	AS, stone	AS; stone	Type A	Extraction of stones; ENBD
14	NAS; stone	AS; stone	Type B	Extraction of stones; MSP
15	AS	AS	Type A	CAGP; bougienage; SSP
16	AS	AS	Type A	CAGP; bougienage; SSP
17	AS	AS	Type A	Balloon dilation; SSP
18	AS	AS	Type C	ENBD
19	NAS	NAS; AS	Type B	MSP

AS: Anastomotic stricture; non-AS: Non-anastomotic stricture; DSOC: Digital single-operator peroral cholangioscopy; ERCP: Endoscopic retrograde cholangiopancreatography; CAGP: Cholangioscopy-assisted guidewire placement; SSP: Single plastic stent placement; MSP: Multiple plastic stent placement; ENBD: Endoscopic nasobiliary drainage.

Statistical analysis

Statistical analysis was conducted using SPSS 24 (IBM Corp., Armonk, NY, United States). All data are presented as absolute and relative frequencies or reported as mean ± SD. Categorical variables were compared using Fisher's exact test. P values < 0.05 were considered statistically significant.

RESULTS

Patients' characteristics

Over the course of our study, 19 patients (12 males and 7 females), with a median age of 50.3 ± 8.9, underwent ERCP followed by cholangioscopy. Procedures were carried out at a median of 13.7 ± 8.2 mo after LT. 9 of the 19 patients underwent ERCP and had plastic stent placement in the common bile duct within three months prior to this study, while the remaining 10 received the procedure for the first time after LT. The patients' clinical and demographic data are shown in Table 1.

Findings of ERCP and DSOC

During ERCP, AS were observed in 12 patients, NAS in 7, and stones in 3 (Table 2). Observation with cholangioscopy revealed AS in 18 patients, NAS in 2, stones in 11, loose suture in 7, and a space-occupying lesion in one (Table 2).

The biliary stricture could be characterized into 4 types. Type A (Figure 1) was found in 6 patients, which showed mild inflammatory changes, including fibrotic stenosis with mild erythema at the anastomotic site, pale smooth mucosa of the donor hepatobiliary duct, dimly visible branching of the submucosal vessels, and circular or elliptic opening of the intrahepatic bile duct. Type B (Figure 1) was

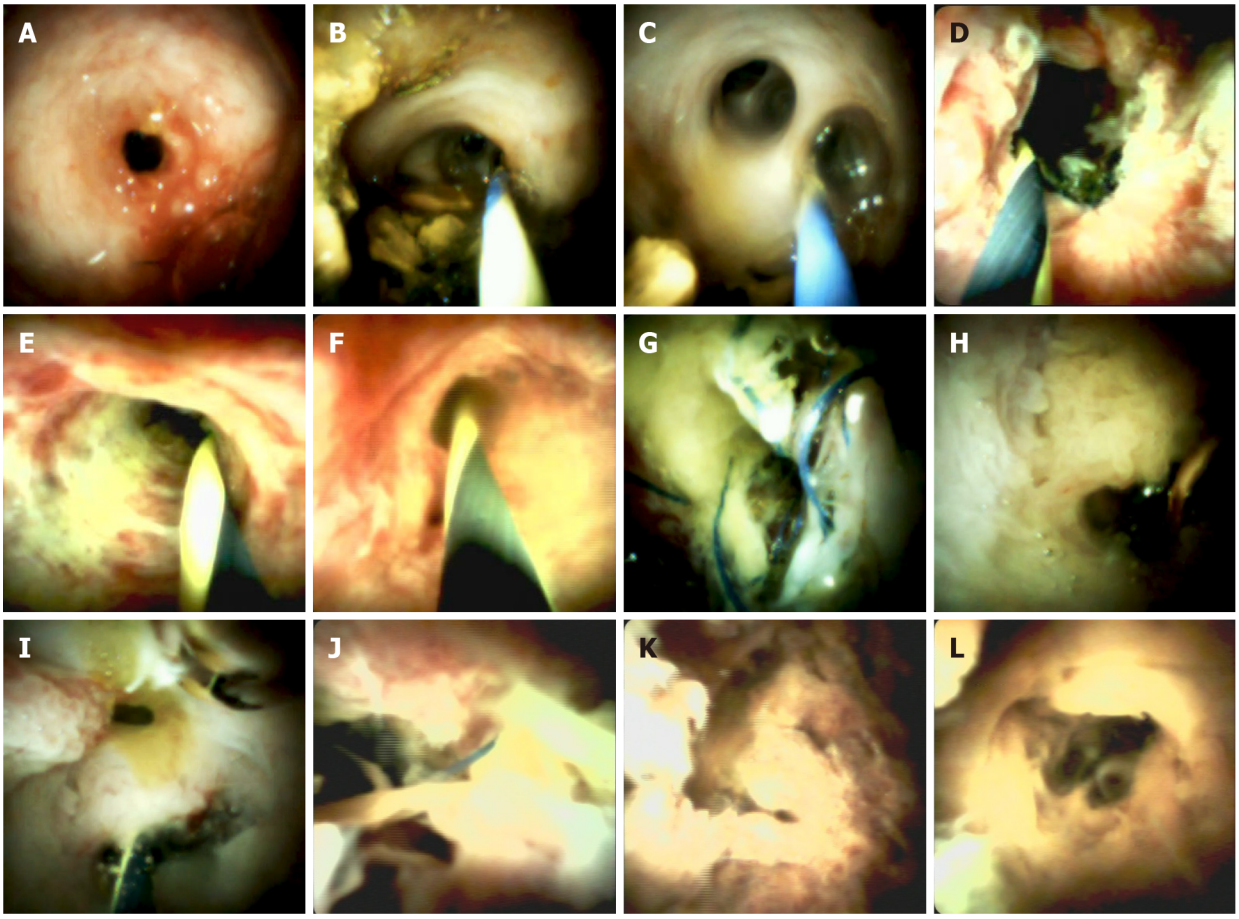

DOI: 10.4251/wjgo.v14.i5.1037

Figure 1 Representative cholangioscopic appearance of the donor bile duct mucosa. A: Cholangioscopic image of the anastomotic stricture with erythema (Type A); B: Pale smooth mucosa of the donor hepatobiliary duct and dimly visible branching of the submucosal vessels (Type A); C: circular or elliptic opening of the intrahepatic bile duct in the hepatic portal system (Type A); D: Cholangioscopic image of the anastomotic stricture with hyperemia, edema, and polypoid growth tissues (Type B); E: hyperemia mucosa of the donor hepatobiliary duct with longitudinal ulcer (Type B); F: hyperemia mucosa of the intrahepatic bile duct in the hepatic portal system (Type B); G: Cholangioscopic image of the anastomotic stricture with sludge and suture (Type C); H: Deformed intrahepatic bile duct opening and granular mucosal surface without vessels (Type C); I: the villous mucosal surface of intrahepatic ducts (Type C); J: Cholangioscopic image of the anastomotic stricture with necrotic material and suture (Type D); K: The wall of intrahepatic bile duct with a mass of necrotic material (Type D); L: Deformed intrahepatic bile duct opening with necrotic material (Type D).

found in 9 patients, which showed acute inflammatory changes, including anastomotic stenosis with hyperemia, edema, or polypoid growth tissues. In addition, the donor bile duct might show hyperemia, edema, clear submucosal vessels, and other manifestations of acute inflammation and even ulceration. This type was often associated with the presence of stones and sludge. Type C (Figure 1) was found in 2 patients, showing chronic inflammatory changes in anastomotic and donor hepatobiliary ducts. The mucosa of the anastomotic site and the donor hepatobiliary duct were thickened and pale, the surface was granular or villous, submucosa vessels had become thinner or disappeared, and the form of the intrahepatic bile duct opening had changed. When combined with acute inflammation, the mucosa could have also shown signs of hyperemia, edema, or other acute inflammatory manifestations. Type D (Figure 1) was found in one patient, which showed suppurative changes of the anastomotic site and donor hepatobiliary ducts. The mucosa of the anastomotic site and donor bile duct was greyish-yellow, the lumen of the bile duct was filled with pus and looked dirty, and submucosal vessels appeared.

Comparison between ERCP and cholangioscopy

Cannulation was successful in 14 of the 18 patients attempted during ERCP. Selective guidewire placement was achieved during DSOC under direct vision in the remaining 4 patients that had failed during ERCP (Figure 2). Furthermore, cholangioscopy successfully identified stones and sludge in 8 more patients (P = 0.005) that ERCP missed. It also successfully detected loose sutures in 8 patients (P = 0.008) that ERCP failed to detect (Figure 3). Four patients diagnosed with NAS by ERCP were later determined to be AS by choledochoscopy, with 2 type A, 1 type B, and 1 type C. The findings of ERCP and cholangioscopy, as well as endoscopic intervention, are summarized in Table 2.

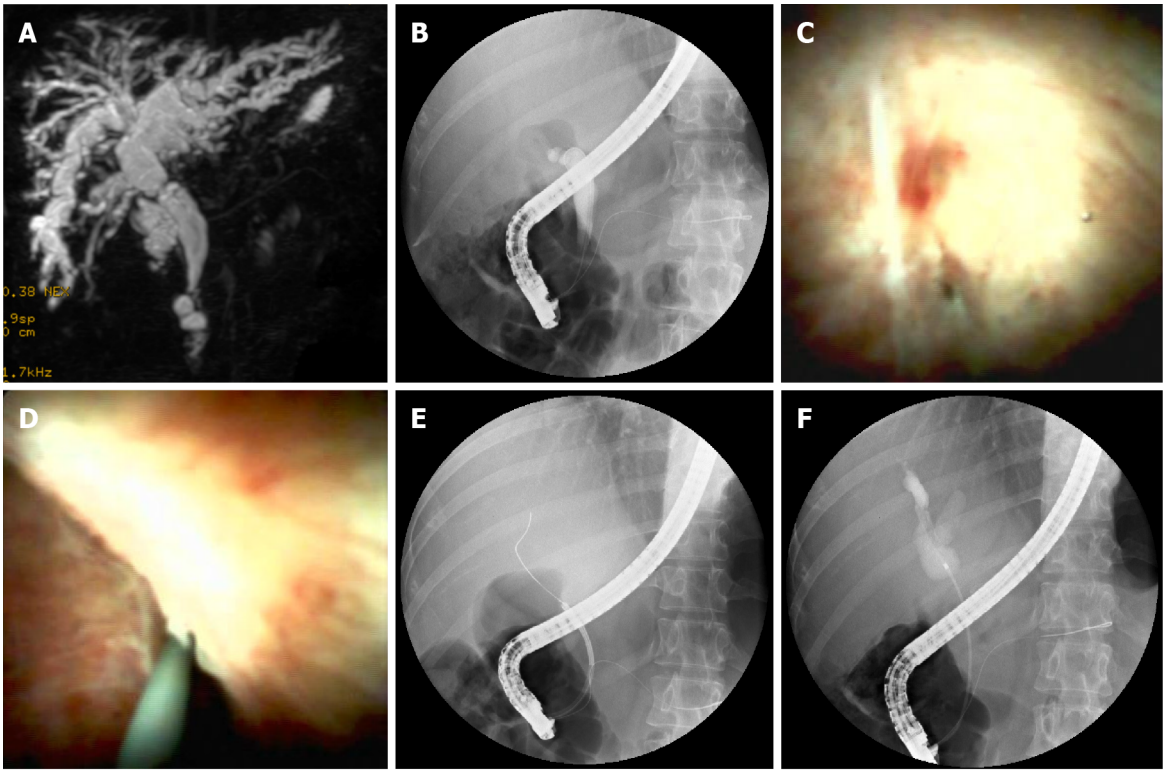

DOI: 10.4251/wjgo.v14.i5.1037

Figure 2 Cholangioscopy-assisted guidewire placement. A: MRCP image shows anastomotic stricture and dilated bile duct above and below the stricture; B: ERCP image shows the guidewire failed to pass through the stricture; C: A narrow needle-like anastomosis (black arrow); D: Cholangioscopic image shown guidewire inserted through the anastomosis; E: ERCP image shown guidewire inserted into the intrahepatic bile duct; F: ERCP image shown dilated bile duct above anastomosis.

Histological findings

A total of 8 biopsies were obtained. Studies of the histology of 7 anastomotic stricture samples, including 3 type A, 3 type B, and 1 type C, demonstrated fibrous hyperplasia with mixed infiltration of lymphocytes, plasmacytes, and granulocytes, as well as granulation tissue and scars. A neoplasm with a red surface (Figure 4) in the donor bile tract was observed in one patient. Histology of the biopsy revealed a large number of infiltrating lymphocytes with uniform, diffuse distribution, and obvious atypia. Liver-localized post-transplantation lymphoproliferative disease (LL-PTLD) was confirmed by immunohistochemistry in this patient.

Endoscopic treatment

In patients with biliary strictures, a total of 7 balloon dilatations, 2 bougienage of a tight stricture, 9 extractions of stones, 10 multiple plastic stent placement, 4 endoscopic nasobiliary drainage, 4 single plastic stent placement, and 2 Laser lithotripsies under direct vision were performed (Figure 5).

Complications

No serious adverse events occurred in any of the cases. However, mild complications were observed in 6/19 (31.6%), in which 3 were documented as post-ERCP cholangitis, and 3 were hyperamylasemia (15.7%). All cases of DSOC-related complications had a mild clinical course and were treated successfully with conservative therapeutic approaches.

DISCUSSION

The aim of this study was to evaluate whether the use of DSOC added any benefits for patients undergoing ERCP for the management of biliary strictures after LT. The results from 19 patients showed that during ERCP, AS was observed in 12 patients, NAS in 7, and stones in 3. However, DSOC revealed AS in 18 patients, NAS in 2, stones in 11, loose suture in 7, and a space-occupying lesion in one patient. The DSOC also meant that AS could be characterized into 4 types (A to D) based on the cholangioscopic appearance of the donor bile duct mucosa. Therefore, these results suggest that DSOC can provide important diagnostic information for patients with suspected biliary strictures after LT.

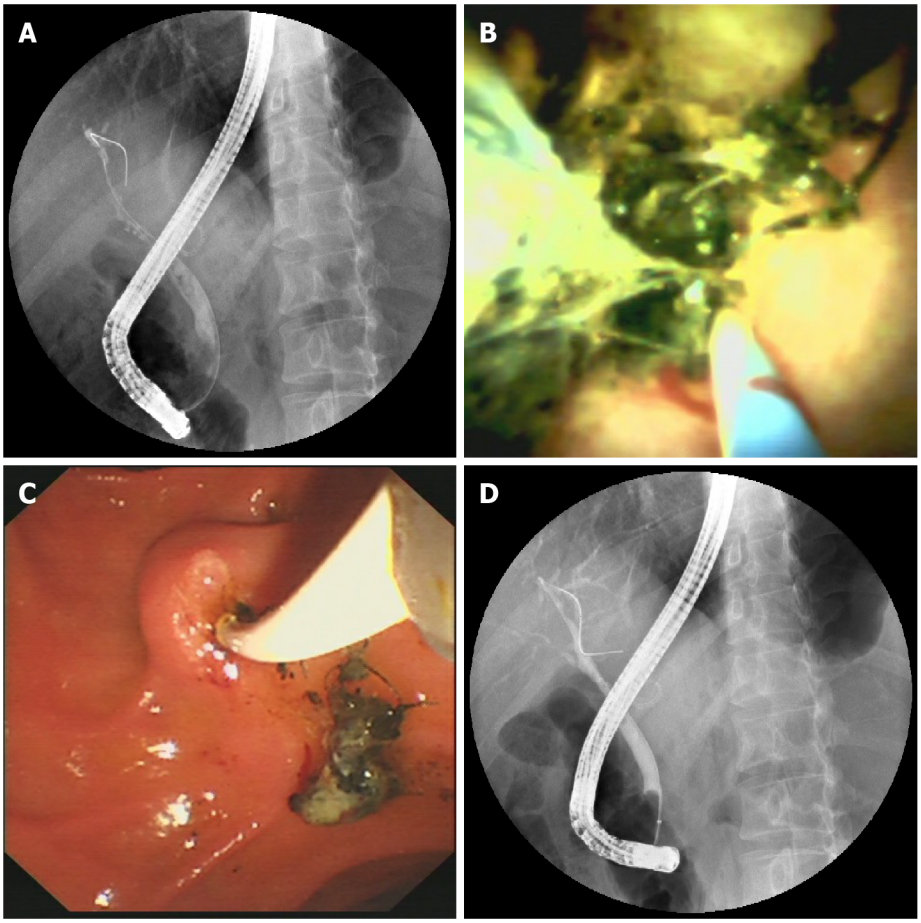

DOI: 10.4251/wjgo.v14.i5.1037

Figure 3 Biliary stenosis caused by stones and sutures. A: ERCP image shows stricture between anastomosis and hilus region; B: Cholangioscopic image shows stones and suture in donor bile duct; C: Duodenoscopic image shows a mixture of sludge and sutures taken out by balloon; D: ERCP image shows the biliary stricture disappeared after extraction of the mixture.

The results of this study agree with those of previous studies that have shown SOC can identify biliary strictures in patients after LT[21-24]. Our results also suggest DSOC provided a more accurate diagnosis of biliary stenosis than ERCP. Similar to Hüsing-Kabar *et al*[23] who found a benefit of cholangioscopy in 46.2% of patients, our study potentially showed an even greater benefit, in 15 (78.9%) patients. Initially, seven patients were diagnosed with NAS by ERCP, but of these, only two were confirmed with choledochoscopy. Among the five remaining patients, four were confirmed with AS, including 2 type B cases, 1 type C case, and 1 type D case; and one patient was diagnosed with LL-PTLD according to histology. These five patients all presented with NAS-like imaging in ERCP, possibly due to a large number of stones and sludge adhered to the donor's bile duct wall, which made the angiography images resemble multi-segment bile duct stenosis. The biliary strictures resolved after the extraction of stones and sludge. However, it is not known whether the NAS-like imaging resulting from mural calculi above the stenosis is a misleading phenomenon or actually an early manifestation of NAS, and further study is needed to investigate this. In our study, one case of NAS diagnosed by ERCP was found to be a neoplasm in the bile tract under direct vision of cholangioscopy, which was later confirmed as LL-PTLD based on histology. Our finding indicated that AS and NAS are not the only etiologies of biliary stenosis after LT. Thus, the use of DSOC in our study may have provided an additional advantage.

A previous study by Balderramo *et al*[22] divided AS into two patterns according to cholangioscopy finding of anastomosis: (A) the presence of mild erythema and scarring of the AS; and (B) the presence of severe edema and erythema plus ulceration with sloughing at the AS. Based on cholangioscopy imaging of the anastomosis and donor bile duct, we divided them into four types. It should be noted that one patient in type C and one patient in type D underwent second liver transplantation for chronic rejection within 6 mo, which indicated that patients with type C or D might have a poor prognosis after treatment. Further research is needed to confirm whether this classification method has guiding significance for treatment and prognosis.

In our study, cholangioscopy was superior to ERCP in the detection of stones and sludge, discovered in 11(61.1%) patients by DSOC, while only 3 (16.7%) by ERCP. This may be because these tiny stones and sludge were kept close to the wall of the bile duct and were difficult to discern by ERCP. The

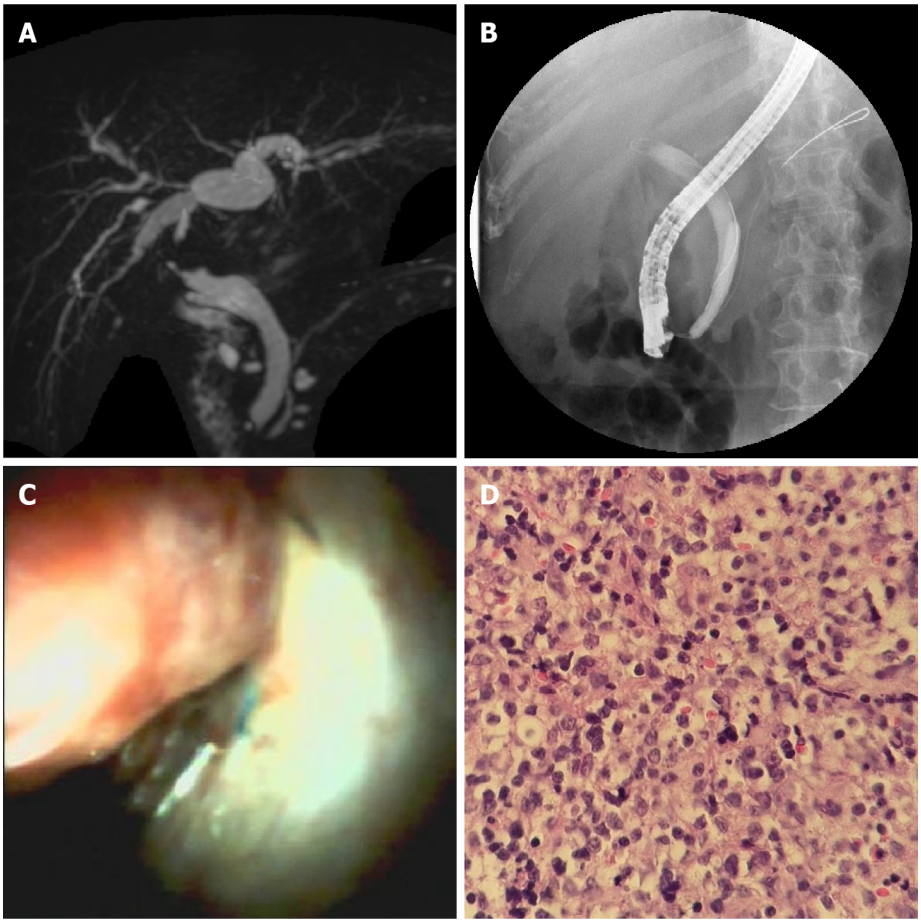

DOI: 10.4251/wjgo.v14.i5.1037

Figure 4 A neoplasm in donor bile duct. A: Magnetic resonance cholangiopancreatography image shows stricture between anastomosis and hilus region; B: Endoscopic retrograde cholangiopancreatography image shows guidewire failed to pass through the stricture; C: Cholangioscopic image shows the neoplasm with a red surface in the donor bile tract; D: Pathological sections of the neoplasm show many identical lymphocytes with distinct atypia.

presence of bile stones, including sludge and casts formation, is a common biliary complication after LT, with a reported incidence of 5% to 10%[25]. Early diagnosis and treatment of stones are crucial for patient and graft survival. Therefore, DSOC could be more helpful than ERCP in post LT care.

In addition, loose sutures at the anastomotic site, one of the causes of calculus formation, were found with DSOC but not ERCP in 7 (41.2%) patients in our study. In 1897, Homans reported the first case of migration of silk sutures into the common bile duct and the formation of gallstones[26]. Since then, many cases of bile duct stone formation around sutures have been reported[27,28]. The stone can form over the nidus of the introduced unabsorbable suture material when cholesterol and/or pigment aggregate around it. Thus, bile duct anastomosis with absorbable sutures may help to reduce stone formation. However, there is no consensus on the use of suitable suture material for anastomosis of bile ducts in LT. Although DSOC provides a great tool to locate the loose sutures at the anastomotic site, currently, there is no suitable device to remove these sutures. We have attempted to remove the loose sutures with balloons but only achieved the removal of sutures with a small amount of tissue in two patients.

Passing the stricture with a guidewire is a fundamental prerequisite for the technical success of endoscopic stricture management. In LT patients, the strictures are often very tight and twisted due to the presence of dense fibrotic tissue and the hypertrophic transplanted liver, rendering this procedure challenging. The incidence of failed guidewire passage through the stricture is between 16%-38%[11,29]. While ERCP can only determine the location, length, and morphology of the coronary plane, by contrast, choledochoscopy can distinguish the mucosal manifestations of the bile duct, the presence or absence of attachments, as well as the morphology of the horizontal plane. It is plausible that DSOC may facilitate the passage of a guidewire through the more challenging strictures under direct visualization in LT patients[21,30]. A study by Woo *et al*[21] revealed poor performance of cholangioscopy-assisted guidewire placement in 60% of cases. However, Hüsing-Kabar *et al*[23] reported that they steered the guidewire over the stricture successfully under direct vision in all patients for whom conventional cannulation failed. In our study, cholangioscopy-assisted guidewire placement was performed successfully in four patients for whom the procedure failed previously in ERCP. The low success rate of guidewire placement in Woo *et al*[21] study may be due to the fact that their study was

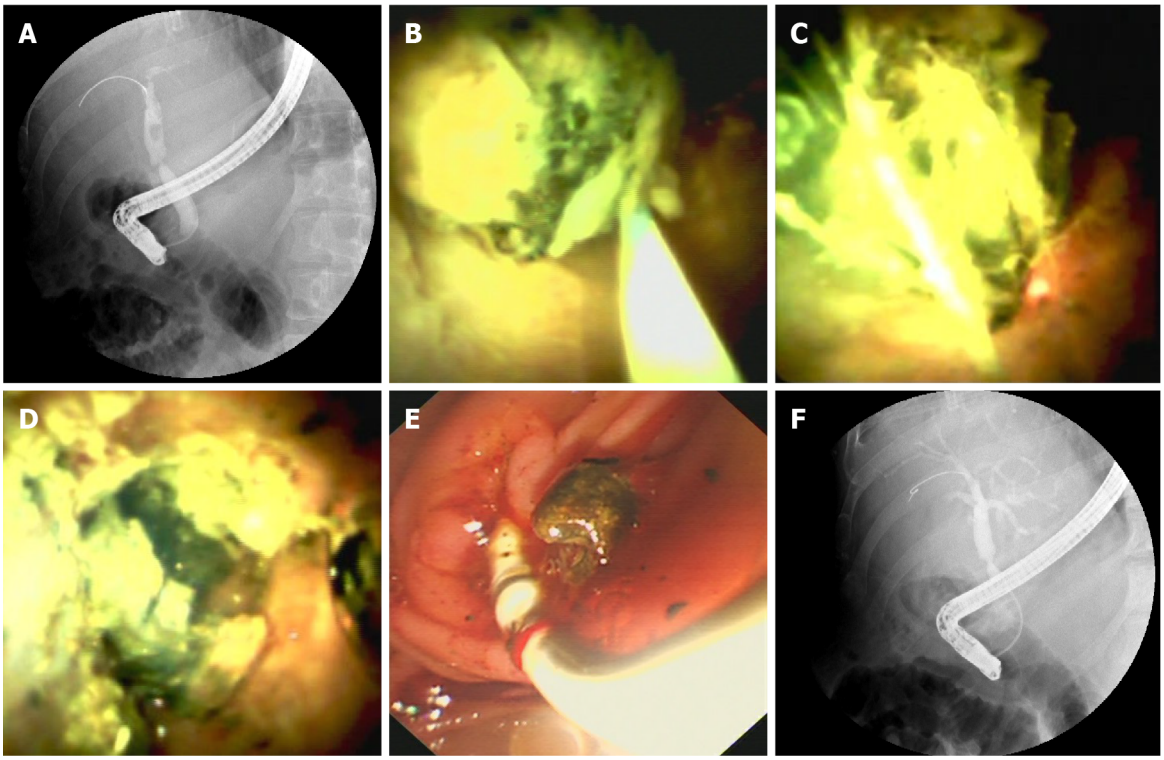

DOI: 10.4251/wjgo.v14.i5.1037

Figure 5 Laser lithotripsy under direct vision. A: Endoscopic retrograde cholangiopancreatography (ERCP) image shows a stone in the bile duct above an anastomotic stricture; B: Cholangioscopic image shows a green stone in the donor bile duct; C: Optical fiber inserted through the cholangioscopy channel touching the stone; D: Cholangioscopic image shows the stone was shattered by laser; E: Duodenoscopic image shows crushed stone taken out by balloon; F: ERCP image shows the stone was completely extracted.

performed in patients receiving living donor LT, which involved special and sometimes complex anatomy of bile ducts and required complicated bile duct anastomosis[20]. In contrast, all patients included in our study underwent whole cadaveric LT.

We successfully performed laser lithotripsy with DSOC in one patient. The calculi with bile duct stricture after LT are most commonly located above the anastomosis, and AS makes it difficult to extract the stones. We broke the stone with the laser under direct visualization and then extracted the rubble successfully with a balloon into the duodenum. This approach avoids the risk of cholangitis resulting from long-term stent implantation and stone stimulation. We believed it was a good choice for the complex stone treatment.

In our study, post-DSOC cholangitis occurred in 15.8% (3/19) of the patients, which was higher than that was reported with ERCP alone (0.5%-3.0%)[31]. Sethi *et al*[32] reported that cholangioscopy increased the risk of post-ERCP cholangitis in a retrospective study. LT recipients are more likely to develop post-ERCP cholangitis during choledochoscopy due to immunosuppressive medications, water injection during choledochoscopy, and incomplete biliary drainage. Therefore, proper evaluation of selected indications to identify patients who may benefit most for such procedures and attention to detail at peri-procedure, such as antibiotic prophylaxis and appropriate water injection pressure and speed, are crucial for the prevention of post-ERCP cholangitis. Furthermore, microbial analysis of bile collected during bile duct interventions should be regularly performed to guide the treatments in case of post-ERCP septic complications.

Some limitations of this study should be noted. First, this study is retrospective, and the number of analyzed patients was small, making it necessary to treat statistical comparisons with caution. Second, this was a single-center study, and the procedures were performed by physicians with ample experience in the management of biliary complications after LT. Thus, these results may not be applicable to all centers. Finally, we did not include patients who underwent living donor LT or recipients of transplants from donors after cardiac death, who have a higher incidence of AS *vs* recipients of cadaveric donors.

CONCLUSION

In conclusion, DSOC is feasible and safe in LT recipients with biliary strictures and offers useful diagnostic information in addition to ERCP. These results suggest that cholangioscopy is superior to

ERCP in diagnosing and classifying biliary strictures after LT, diagnosing biliary stones and sludge, and optimizing treatment in the patients concerned. Therefore, we recommend performing DSOC concurrently with the first ERCP procedure in LT recipients with strictures who require choledochoscopy-assisted guidewire placement or need laser lithotripsy under direct visualization.

ARTICLE HIGHLIGHTS

Research background

Liver transplantation (LT) has become a standard of care in patients with end-stage liver disease. Biliary strictures after LT can be either anastomotic or non-anastomotic based on the morphology and location of stenosis observed during imaging procedures. The first-line approach to resolving biliary strictures involves endoscopic retrograde cholangiopancreatography (ERCP), with stenosis dilatation and placement of multiple plastic stents, and fully covered self-expandable metallic stents.

Research motivation

Biliary strictures after LT remain clinically arduous and challenging situations, and ERCP has been considered as the gold standard for the management of biliary strictures after LT. Nevertheless, in the treatment of biliary strictures after LT with ERCP, many studies show that there is a large variation in diagnostic accuracy and therapeutic success rate. Digital single-operator peroral cholangioscopy (DSOC) is considered a valuable diagnostic modality for indeterminate biliary strictures.

Research objectives

This study aimed to evaluate DSOC in addition to ERCP for management of biliary strictures after LT.

Research methods

Total 19 patients with duct-to-duct biliary reconstruction who underwent ERCP for suspected biliary complications were consecutively enrolled in this observational study. After evaluating bile ducts using fluoroscopy, cholangioscopy using a modern digital single-operator cholangioscopy system was performed during the same procedure with patients under conscious sedation. Biliary strictures after LT were classified according to the manifestations of choledochoscopic strictures and the manifestations of transplanted hepatobiliary ducts.

Research results

Twenty-one biliary strictures were found in a total of 19 patients, among which anastomotic strictures were evident in 18 (94.7%) patients, while non-anastomotic strictures in 2 (10.5%), and space-occupying lesions in 1 (5.3%). Stones were found in 11 (57.9%) and loose sutures in 8 (42.1%). A benefit of cholangioscopy was seen in 15 (78.9%) patients. It was instrumental in identifying biliary stone and/or loose sutures in 9 patients in whom ERCP failed. It also provided a direct vision for laser lithotripsy.

Research conclusions

The present study examined the benefit of complementary DSOC. DSOC can provide important diagnostic information, helping plan and perform interventional procedures in LT-related biliary strictures. Our results are encouraging and demonstrate strong evidence for a diagnostic and therapeutic advantage of additional cholangioscopy for the management of biliary disorders following liver transplantation.

Research perspectives

This study was retrospective, and prospective multicenter trials should be performed. Patients with living donor LT should also be investigated.

FOOTNOTES

Author contributions: Hao JY provided supervision, guidance, and constant encouragement during the study and during the writing; Wang YB contributed to the study concept and design; Zhang DL contributed to the drafting of the manuscript; four colleagues (Lang R, Fan H, Liu Y, and Li LX) from Department of Hepatobiliary Surgery, Beijing Chaoyang Hospital, Capital Medical University contributed to data collection; Yu JF contributed to the revision of the manuscript; and all authors approved the final version of the report.

Institutional review board statement: The present study was approved by the Ethics Committee of Chao-Yang Hospital (Approval number: 2020-25).

Informed consent statement: Written informed consent was obtained from the patients.

Conflict-of-interest statement: The authors declare that they have no competing interests.

Data sharing statement: Data sharing is not applicable to this article as no datasets were generated or analyzed during the current study.

STROBE statement: The authors have read the STROBE Statement - checklist of items, and the manuscript was prepared and revised according to the STROBE Statement - checklist of items.

Country/Territory of origin: China

ORCID number: Jian-Feng Yu 0000-0001-6862-8257; Dong-Lei Zhang 0000-0002-0933-2015; Yan-Bin Wang 0000-0003-1646-0397; Jian-Yu Hao 0000-0001-9504-8987.

S-Editor: Wang JL
L-Editor: A
P-Editor: Wang JL

REFERENCES

1 **Halliday N**, Westbrook RH. Liver transplantation: need, indications, patient selection and pre-transplant care. *Br J Hosp Med (Lond)* 2017; **78**: 252-259 [PMID: 28489446 DOI: 10.12968/hmed.2017.78.5.252]
2 **Charlton MR**. Roadmap for improving patient and graft survival in the next 10 years. *Liver Transpl* 2016; **22**: 71-78 [PMID: 27514705 DOI: 10.1002/lt.24602]
3 **Akamatsu N**, Sugawara Y, Hashimoto D. Biliary reconstruction, its complications and management of biliary complications after adult liver transplantation: a systematic review of the incidence, risk factors and outcome. *Transpl Int* 2011; **24**: 379-392 [PMID: 21143651 DOI: 10.1111/j.1432-2277.2010.01202.x]
4 **Kochhar G**, Parungao JM, Hanouneh IA, Parsi MA. Biliary complications following liver transplantation. *World J Gastroenterol* 2013; **19**: 2841-2846 [PMID: 23704818 DOI: 10.3748/wjg.v19.i19.2841]
5 **Nemes B**, Gámán G, Doros A. Biliary complications after liver transplantation. *Expert Rev Gastroenterol Hepatol* 2015; **9**: 447-466 [PMID: 25331256 DOI: 10.1586/17474124.2015.967761]
6 **Suárez F**, Otero A, Solla M, Arnal F, Lorenzo MJ, Marini M, Vázquez-Iglesias JL, Gómez M. Biliary complications after liver transplantation from maastricht category-2 non-heart-beating donors. *Transplantation* 2008; **85**: 9-14 [PMID: 18192905 DOI: 10.1097/01.tp.0000297945.83430.ce]
7 **Rao HB**, Prakash A, Sudhindran S, Venu RP. Biliary strictures complicating living donor liver transplantation: Problems, novel insights and solutions. *World J Gastroenterol* 2018; **24**: 2061-2072 [PMID: 29785075 DOI: 10.3748/wjg.v24.i19.2061]
8 **Thethy S**, Thomson BNj, Pleass H, Wigmore SJ, Madhavan K, Akyol M, Forsythe JL, James Garden O. Management of biliary tract complications after orthotopic liver transplantation. *Clin Transplant* 2004; **18**: 647-653 [PMID: 15516238 DOI: 10.1111/j.1399-0012.2004.00254.x]
9 **Balderramo D**, Navasa M, Cardenas A. Current management of biliary complications after liver transplantation: emphasis on endoscopic therapy. *Gastroenterol Hepatol* 2011; **34**: 107-115 [PMID: 20692731 DOI: 10.1016/j.gastrohep.2010.05.008]
10 **ASGE Standards of Practice Committee**, Chandrasekhara V, Khashab MA, Muthusamy VR, Acosta RD, Agrawal D, Bruining DH, Eloubeidi MA, Fanelli RD, Faulx AL, Gurudu SR, Kothari S, Lightdale JR, Qumseya BJ, Shaukat A, Wang A, Wani SB, Yang J, DeWitt JM. Adverse events associated with ERCP. *Gastrointest Endosc* 2017; **85**: 32-47 [PMID: 27546389 DOI: 10.1016/j.gie.2016.06.051]
11 **Hsieh TH**, Mekeel KL, Crowell MD, Nguyen CC, Das A, Aqel BA, Carey EJ, Byrne TJ, Vargas HE, Douglas DD, Mulligan DC, Harrison ME. Endoscopic treatment of anastomotic biliary strictures after living donor liver transplantation: outcomes after maximal stent therapy. *Gastrointest Endosc* 2013; **77**: 47-54 [PMID: 23062758 DOI: 10.1016/j.gie.2012.08.034]
12 **Chang JH**, Lee IS, Choi JY, Yoon SK, Kim DG, You YK, Chun HJ, Lee DK, Choi MG, Chung IS. Biliary Stricture after Adult Right-Lobe Living-Donor Liver Transplantation with Duct-to-Duct Anastomosis: Long-Term Outcome and Its Related Factors after Endoscopic Treatment. *Gut Liver* 2010; **4**: 226-233 [PMID: 20559526 DOI: 10.5009/gnl.2010.4.2.226]
13 **Seehofer D**, Eurich D, Veltzke-Schlieker W, Neuhaus P. Biliary complications after liver transplantation: old problems and new challenges. *Am J Transplant* 2013; **13**: 253-265 [PMID: 23331505 DOI: 10.1111/ajt.12034]
14 **Tringali A**, Barbaro F, Pizzicannella M, Boškoski I, Familiari P, Perri V, Gigante G, Onder G, Hassan C, Lionetti R, Ettorre GM, Costamagna G. Endoscopic management with multiple plastic stents of anastomotic biliary stricture following liver transplantation: long-term results. *Endoscopy* 2016; **48**: 546-551 [PMID: 26859556 DOI: 10.1055/s-0042-100277]
15 **Nacif LS**, Bernardo WM, Bernardo L, Andraus W, Torres L, Chaib E, D'Albuquerque LC, Maluf-Filho F. Endoscopic

treatment of post-liver transplantation anastomotic biliary stricture: systematic review and meta-analysis. *Arq Gastroenterol* 2014; **51**: 240-249 [PMID: 25296086 DOI: 10.1590/s0004-28032014000300014]

16 **Landi F**, de'Angelis N, Sepulveda A, Martínez-Pérez A, Sobhani I, Laurent A, Soubrane O. Endoscopic treatment of anastomotic biliary stricture after adult deceased donor liver transplantation with multiple plastic stents *vs* self-expandable metal stents: a systematic review and meta-analysis. *Transpl Int* 2018; **31**: 131-151 [PMID: 29090502 DOI: 10.1111/tri.13089]

17 **Hüsing A**, Cicinnati VR, Beckebaum S, Wilms C, Schmidt HH, Kabar I. Endoscopic ultrasound: valuable tool for diagnosis of biliary complications in liver transplant recipients? *Surg Endosc* 2015; **29**: 1433-1438 [PMID: 25159653 DOI: 10.1007/s00464-014-3820-3]

18 **Ranjan P**, Bansal RK, Mehta N, Lalwani S, Kumaran V, Sachdeva MK, Kumar M, Nundy S. Endoscopic management of post-liver transplant billiary complications: A prospective study from tertiary centre in India. *Indian J Gastroenterol* 2016; **35**: 48-54 [PMID: 26873087 DOI: 10.1007/s12664-016-0625-4]

19 **Kim TH**, Lee SK, Han JH, Park DH, Lee SS, Seo DW, Kim MH, Song GW, Ha TY, Kim KH, Hwang S, Lee SG. The role of endoscopic retrograde cholangiography for biliary stricture after adult living donor liver transplantation: technical aspect and outcome. *Scand J Gastroenterol* 2011; **46**: 188-196 [PMID: 20955089 DOI: 10.3109/00365521.2010.522722]

20 **Karagyozov P**, Boeva I, Tishkov I. Role of digital single-operator cholangioscopy in the diagnosis and treatment of biliary disorders. *World J Gastrointest Endosc* 2019; **11**: 31-40 [PMID: 30705730 DOI: 10.4253/wjge.v11.i1.31]

21 **Woo YS**, Lee JK, Noh DH, Park JK, Lee KH, Lee KT. SpyGlass cholangioscopy-assisted guidewire placement for post-LDLT biliary strictures: a case series. *Surg Endosc* 2016; **30**: 3897-3903 [PMID: 26684207 DOI: 10.1007/s00464-015-4695-7]

22 **Balderramo D**, Sendino O, Miquel R, de Miguel CR, Bordas JM, Martinez-Palli G, Leoz ML, Rimola A, Navasa M, Llach J, Cardenas A. Prospective evaluation of single-operator peroral cholangioscopy in liver transplant recipients requiring an evaluation of the biliary tract. *Liver Transpl* 2013; **19**: 199-206 [PMID: 23404861 DOI: 10.1002/lt.23585]

23 **Hüsing-Kabar A**, Heinzow HS, Schmidt HH, Stenger C, Gerth HU, Pohlen M, Thölking G, Wilms C, Kabar I. Single-operator cholangioscopy for biliary complications in liver transplant recipients. *World J Gastroenterol* 2017; **23**: 4064-4071 [PMID: 28652659 DOI: 10.3748/wjg.v23.i22.4064]

24 **Franzini T**, Moura R, Rodela G, Andraus W, Herman P, D'Albuquerque L, de Moura E. A novel approach in benign biliary stricture - balloon dilation combined with cholangioscopy-guided steroid injection. *Endoscopy* 2015; **47** Suppl 1: E571-E572 [PMID: 26610089 DOI: 10.1055/s-0034-1393370]

25 **Ayoub WS**, Esquivel CO, Martin P. Biliary complications following liver transplantation. *Dig Dis Sci* 2010; **55**: 1540-1546 [PMID: 20411422 DOI: 10.1007/s10620-010-1217-2]

26 **Homans J**. VIII. Gall-Stones formed around Silk Sutures Twenty Months after Recovery from Cholecystotomy. *Ann Surg* 1897; **26**: 114-116 [PMID: 17860458]

27 **Beardsley C**, Lim J, Gananadha S. Nonabsorbable suture material in the biliary tract. *J Gastrointest Surg* 2012; **16**: 2182-2183 [PMID: 22573113 DOI: 10.1007/s11605-012-1903-9]

28 **Li Q**, Tao L, Wu X, Mou L, Sun X, Zhou J. Bile duct stone formation around a Prolene suture after cholangioenterostomy. *Pak J Med Sci* 2016; **32**: 263-266 [PMID: 27022388 DOI: 10.12669/pjms.321.8985]

29 **Tsujino T**, Isayama H, Sugawara Y, Sasaki T, Kogure H, Nakai Y, Yamamoto N, Sasahira N, Yamashiki N, Tada M, Yoshida H, Kokudo N, Kawabe T, Makuuchi M, Omata M. Endoscopic management of biliary complications after adult living donor liver transplantation. *Am J Gastroenterol* 2006; **101**: 2230-2236 [PMID: 16952286 DOI: 10.1111/j.1572-0241.2006.00797.x]

30 **Parsi MA**, Guardino J, Vargo JJ. Peroral cholangioscopy-guided stricture therapy in living donor liver transplantation. *Liver Transpl* 2009; **15**: 263-265 [PMID: 19177445 DOI: 10.1002/lt.21584]

31 **Dumonceau JM**, Kapral C, Aabakken L, Papanikolaou IS, Tringali A, Vanbiervliet G, Beyna T, Dinis-Ribeiro M, Hritz I, Mariani A, Paspatis G, Radaelli F, Lakhtakia S, Veitch AM, van Hooft JE. ERCP-related adverse events: European Society of Gastrointestinal Endoscopy (ESGE) Guideline. *Endoscopy* 2020; **52**: 127-149 [PMID: 31863440 DOI: 10.1055/a-1075-4080]

32 **Sethi A**, Chen YK, Austin GL, Brown WR, Brauer BC, Fukami NN, Khan AH, Shah RJ. ERCP with cholangiopancreatoscopy may be associated with higher rates of complications than ERCP alone: a single-center experience. *Gastrointest Endosc* 2011; **73**: 251-256 [PMID: 21106195 DOI: 10.1016/j.gie.2010.08.058]

World Journal of Gastrointestinal Oncology

Submit a Manuscript: https://www.f6publishing.com

World J Gastrointest Oncol 2022 May 15; 14(5): 1050-1056

DOI: 10.4251/wjgo.v14.i5.1050

ISSN 1948-5204 (online)

CASE REPORT

Primary hepatic angiosarcoma manifesting as hepatic sinusoidal obstruction syndrome: A case report

Fu-Shuang Ha, Hua Liu, Tao Han, De-Zhao Song

Specialty type: Oncology

Provenance and peer review: Unsolicited article; Externally peer reviewed.

Peer-review model: Single blind

Peer-review report's scientific quality classification

Grade A (Excellent): 0
Grade B (Very good): 0
Grade C (Good): C, C
Grade D (Fair): 0
Grade E (Poor): E

P-Reviewer: Ferraioli G, Italy; Ghannam WM, Egypt; Kumar A, India

Received: November 27, 2021
Peer-review started: November 27, 2021
First decision: January 8, 2022
Revised: January 20, 2022
Accepted: April 20, 2022
Article in press: April 20, 2022
Published online: May 15, 2022

Fu-Shuang Ha, Hua Liu, Tao Han, De-Zhao Song, The Third Central Clinical College of Tianjin Medical University, Tianjin 300170, China

Fu-Shuang Ha, Hua Liu, Tao Han, De-Zhao Song, Tianjin Key Laboratory of Extracorporeal Life Support for Critical Diseases, Tianjin 300170, China

Fu-Shuang Ha, Hua Liu, Tao Han, De-Zhao Song, Artificial Cell Engineering Technology Research Center, Tianjin 300170, China

Fu-Shuang Ha, Hua Liu, Tao Han, De-Zhao Song, Tianjin Institute of Hepatobiliary Disease, Tianjin 300170, China

Tao Han, Tianjin Union Medical Center, Naikai University Affiliated Hospital, Tianjin 300121, China

Corresponding author: Tao Han, MD, PhD, Professor, The Third Central Clinical College of Tianjin Medical University, No. 83 Jintang Road, Tianjin 300170, China. hantaomd@126.com

Abstract

BACKGROUND

Primary hepatic angiosarcoma (PHA) is a rare malignancy with a poor prognosis. It is difficult to diagnose PHA because of the lack of specific symptoms or tumour markers, and it rapidly progresses and has a high mortality. To our knowledge, PHA has not been reported to mimic hepatic sinusoidal obstruction syndrome. Herein, we present a case of PHA manifesting as hepatic sinusoidal obstruction syndrome, diagnosed using transjugular liver biopsy, that resulted in the death of the patient.

CASE SUMMARY

A 71-year-old man was admitted with the primary complaint of abdominal distension, decreased appetite, fatigue in the previous month, and loss of 10 kg of weight in the past 2 years. Both the liver and spleen were enlarged, and the liver had a medium-hard texture on percussion. Laboratory examinations were performed, and abdominal plain computed tomography (CT) and contrast-enhanced CT showed hepatomegaly and splenomegaly, as well as diffuse low-density shadows distributed in the liver and spleen. Contrast-enhanced CT revealed diffuse, hypodense, nodular or flake shadows in the liver and heterogeneous enhancement in the spleen. A transjugular liver biopsy was performed. Based on the pathology results, the patient was diagnosed with hepatic sinusoidal

obstruction syndrome secondary to PHA. The patient's status further deteriorated and he developed serious hepatic failure. The patient was discharged, and died 3 d later.

CONCLUSION
PHA is rare and has a poor prognosis; however, transjugular liver biopsy can be safely performed to aid in diagnosis.

Key Words: Hepatic angiosarcoma; Hepatic sinusoidal obstruction syndrome; Outcome; Primary cancer; High mortality; Case report

Core Tip: To our knowledge, primary hepatic angiosarcoma (PHA) has not been reported to mimic hepatic sinusoidal obstruction syndrome. Here, we present a patient who died from PHA, which manifested as hepatic sinusoidal obstruction syndrome and was diagnosed by transjugular liver biopsy.

Citation: Ha FS, Liu H, Han T, Song DZ. Primary hepatic angiosarcoma manifesting as hepatic sinusoidal obstruction syndrome: A case report. *World J Gastrointest Oncol* 2022; 14(5): 1050-1056
URL: https://www.wjgnet.com/1948-5204/full/v14/i5/1050.htm
DOI: https://dx.doi.org/10.4251/wjgo.v14.i5.1050

INTRODUCTION

Primary hepatic angiosarcoma (PHA) is a rare form of malignancy, accounting for 2% of all primary liver tumours. Despite the low incidence, PHA is still the most common malignant mesenchymal tumour of the liver and the third most common primary liver malignancy[1,2]. Accurate diagnosis of this tumour is usually difficult because the symptoms and signs are not specific, and tumours are difficult to distinguish radiologically from other hepatic tumours[3]. In addition, a tissue sample is required for a diagnosis, and very few patients opt to undergo a needle biopsy[4]. Herein, we report a case of PHA, which manifested as hepatic sinusoidal obstruction syndrome.

CASE PRESENTATION

Chief complaints

A 71-year-old man was admitted to our hospital with the primary complaint of abdominal distension that commenced a fortnight before presentation.

History of present illness

The patient had ingested herbal medicine for 20 d prior, to maintain his health, but complained of decreased appetite and fatigue in the previous month, and had lost 10 kg of weight in the past 2 years.

History of past illness

The patient denied any history of hepatitis, diabetes mellitus, or cancer.

Personal and family history

The patient was not a habitual drinker and did not have any significant history of exposure to carcinogenic chemicals such as thorium dioxide, vinyl chloride monomer, or arsenic.

Physical examination

Both the liver and spleen were enlarged, and the liver had a medium-hard texture on percussion.

Laboratory examinations

Laboratory examinations on admission were as follows: White blood cell count, 6.57 × 10^9/L; haemoglobin, 88 g/L; platelet count, 45 × 10^9/L; albumin, 32.5 g/L; alanine aminotransferase, 90 U/L; aspartate transaminase, 124 U/L; alkaline phosphatase, 231 U/L; γ-glutamyl transpeptidase, 257 U/L; total bilirubin, 82.6 μmol/L; direct bilirubin, 48.2 μmol/L; prothrombin time, 18.9 s; international normalised ratio, 1.6; and plasma D-dimer, > 10 mg/L. Tumour markers, including α-fetoprotein,

carcinoembryonic antigen, and carbohydrate antigen 19-9, were within normal ranges. Screening tests for autoantibodies and viral hepatitis returned negative results.

Imaging examinations

Abdominal plain computed tomography (CT) and contrast-enhanced CT showed hepatomegaly and splenomegaly, as well as diffuse low-density shadows distributed in the liver and spleen (Figure 1A). Contrast-enhanced CT revealed diffuse, hypodense, nodular or flake shadows in the liver and heterogeneous enhancement in the spleen (Figure 1B).

FINAL DIAGNOSIS

The patient presented with abdominal distension, jaundice, ascites, and hepatomegaly, in conjunction with the evidence on enhanced computed tomography; in addition, Budd-Chiari syndrome was ruled out because there were no communicating branches between the narrowed hepatic veins. The patient had a history of herbal medicine intake. After excluding other known causes of liver injury, a preliminary diagnosis of hepatic sinusoidal obstruction syndrome was made; however, there remained some doubts as the herbal medicine that the patient had ingested in its common form does not contain pyrrolidine alkaloid and splenomegaly was significant in the acute phase. The occurrence of splenomegaly during the acute phase of hepatic sinusoidal obstruction syndrome is rare. A transjugular liver biopsy was subsequently performed to improve the diagnosis.

Anticoagulation therapy was administered the following day. Three days later, pathological examination of a liver biopsy sample showed that the hepatic sinusoids were obviously dilated and filled with red blood cells. Hepatocytes around the sinusoid atrophy were found. Significant cytological atypia was observed with anastomosing channels, which was suggestive of angiosarcoma (Figure 2). Immunohistochemically, the specimen was positive for CD31, CD34, and electroretinography (ERG), supporting the diagnosis of PHA (Figure 3). The Ki-67 proliferative index was almost 20%–30%. Based on the pathology results, the patient was diagnosed with hepatic sinusoidal obstruction syndrome secondary to PHA.

TREATMENT

Whole-body positron emission tomography/CT fusion scanning was performed after administration of 18F-fluorodeoxyglucose (^{18}F-FDG) for staging purposes to identify metastatic sites. Diffuse areas of increased uptake were seen in the liver, which corresponded to images on CT (Figure 4A). The maximum standardised uptake value in the liver was 4.3. In addition, multiple areas of increased uptake were detected in the spleen and right ilium, suggestive of spleen dissemination (Figure 4A) and bone metastasis (Figure 4B), respectively.

OUTCOME AND FOLLOW-UP

The patient's status further deteriorated, with the development of serious hepatic failure, and progressive reduction in haemoglobin levels and platelet counts. The patient complained of further aggravated abdominal distension. At the family's request, the patient was discharged; he died 3 d later.

DISCUSSION

This case highlights the rarity and complex nature of the diagnosis of PHA. Owing to its rare occurrence, nonspecific symptomatology, nonspecific tumour makers, challenging radiographic findings, and low biopsy rate, confirming a diagnosis of PHA is difficult. The aetiology of PHA remains unclear. According to an epidemiological study, vinyl chloride monomer, thorium dioxide, arsenic, and androgenic anabolic steroids are associated with the development of PHA in 25% of all cases[5].

The symptoms of PHA are variable. Most patients have nonspecific symptoms including abdominal pain, fatigue, weakness, anorexia, weight loss, fever, and low back pain, and these symptoms mimic chronic liver diseases[6]. PHA is more predominantly found in men, with a male to female diagnosis ratio of 3:1, and presents in the fifth or sixth decade of life[7].

It has been suggested that PHA can be elucidated by counting the number and size of hepatic tumours on CT images. PHA can appear as multiple nodules, a dominant mass, or a mixed pattern of a dominant mass and multiple nodules, but rarely manifests as an infiltrative, micronodular subtype[1]. In our case, the tumour manifested as an infiltrative, micronodular subtype and the findings on

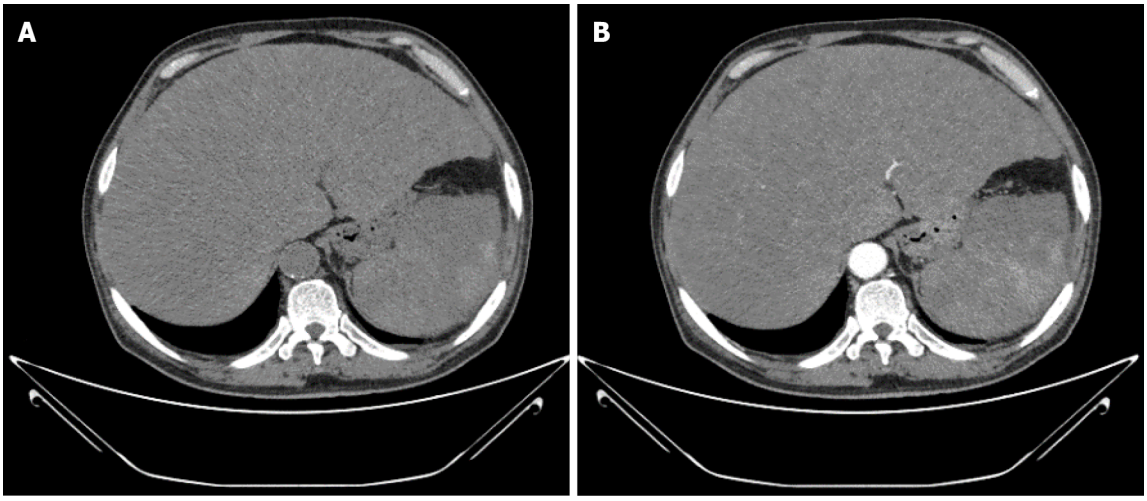

DOI: 10.4251/wjgo.v14.i5.1050

Figure 1 Abdominal plain computed tomography and contrast-enhanced computed tomography images. A: Abdominal plain computed tomography (CT) image; B: Contrast-enhanced CT image. Abdominal plain CT and contrast-enhanced CT showed hepatomegaly and splenomegaly and diffuse low-density shadows distributed in the liver and spleen. Contrast-enhanced CT revealed diffuse, hypodense, nodular or flake shadows in the liver and heterogeneous enhancement in the spleen.

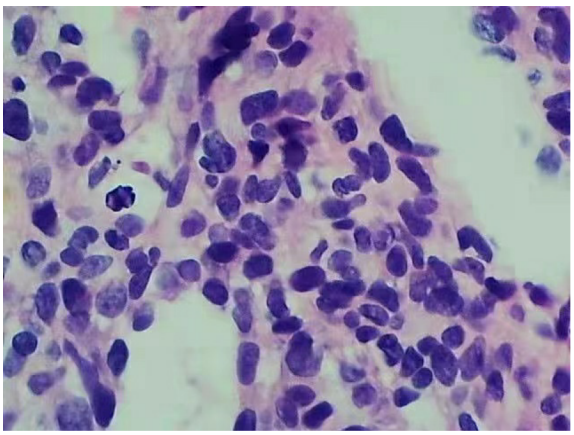

DOI: 10.4251/wjgo.v14.i5.1050

Figure 2 Haematoxylin and eosin-stained liver biopsy (× 400) demonstrating significant cytological atypia with anastomosing channels.

contrast-enhanced CT were consistent with hepatic sinusoidal obstruction syndrome. To our knowledge, this is the first reported case of hepatic sinusoidal obstruction syndrome that was diagnosed as PHA.

The history of herbal medicine intake made this diagnosis more difficult. In China, hepatic sinusoidal obstruction syndrome is often associated with the oral intake of plants that contain pyrrolidine alkaloids. Our case met the 'Nanjing criteria' for the diagnosis of hepatic sinusoidal obstruction syndrome except that the herbal medicine that the patient had ingested does not contain pyrrolidine alkaloid in its common form[8]. Budd-Chiari syndrome, especially the type with simple hepatic vein obstruction, can be easily misdiagnosed. Communicating branches between the narrowed hepatic veins are seen in Budd-Chiari syndrome and are a critical feature that distinguishes Budd-Chiari syndrome from other similar conditions[8].

The patient's condition progressed rapidly. Thus, the diagnosis was questionable. A liver biopsy was necessary to establish a definitive diagnosis. However, because the patient's platelet count continued to decline and coagulation disorders and jaundice could not be controlled, a percutaneous liver biopsy was not performed, due to the associated increased risk of bleeding. There is evidence that transjugular liver biopsy is a highly efficacious, well-tolerated, and safe procedure. It can be safely performed multiple times in the same patient or in critically ill patients with severe coagulopathy and does not significantly increase the rate of complications while maintaining an extremely favourable diagnostic yield[9]. It is difficult to make a diagnosis of PHA using only a CT scan, and a biopsy might be a reasonable option; however, percutaneous liver biopsy in patients with PHA is not safe because of the vascular nature of the tumour and its tendency to haemorrhage[2]. Thus, sometimes, transjugular liver biopsy is a good

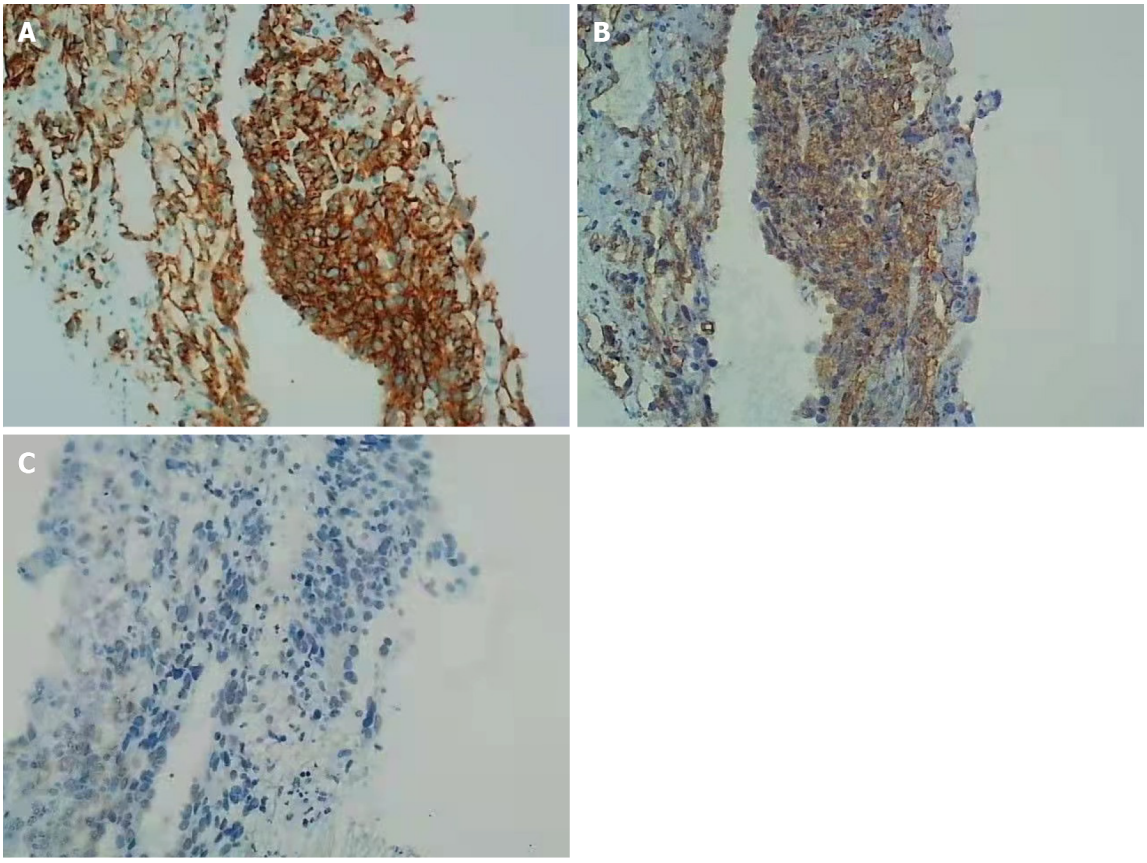

DOI: 10.4251/wjgo.v14.i5.1050

Figure 3 Immunohistochemical staining. The hepatic angiosarcoma components are positive for CD31 and CD34 and weakly positive for electroretinography (ERG) (original magnification, × 200). A: CD31; B: CD34; C: ERG.

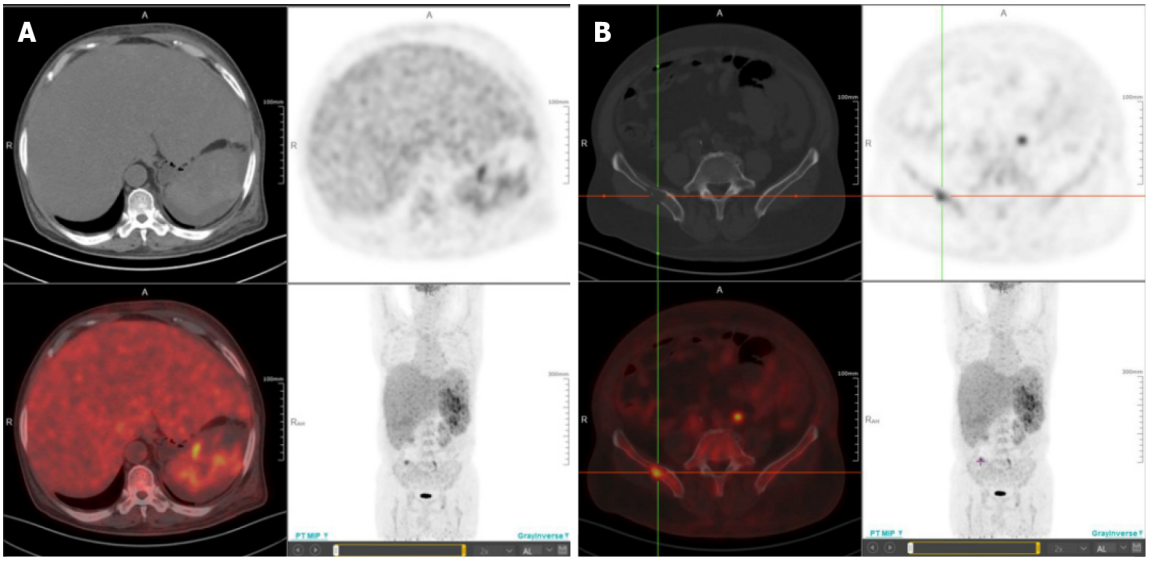

DOI: 10.4251/wjgo.v14.i5.1050

Figure 4 18F-fluorodeoxyglucose positron emission tomography/computed tomography images. A: 18F-fluorodeoxyglucose (^{18}F-FDG) positron emission tomography/computed tomography (PET/CT) images show marked FDG accumulation within the liver and spleen; B: ^{18}F-FDG PET/CT images show marked FDG accumulation within the right ilium.

choice.

Microscopic examination could show cytological atypia such as spindle-shaped cells, and immunohistochemical staining positive for CD31, CD34, ERG, and factor VIII in patients with PHA[10,11].

There is report that ^{18}F-FDG positron emission tomography is helpful for distinguishing between PHA and giant cavernous hepatic haemangioma[8], and it can help to identify metastatic sites for staging purposes. At the time of presentation, most patients with PHA have metastatic lesions, such as lung or spleen lesions[12].

The treatment of PHA has not been defined owing to its rarity and association with high mortality. The median survival duration is 6 mo if the patient does not undergo treatment, and only 3% of patients live longer than 2 years[2]. There are several choices of treatment for patients with PHA. Ideal treatment is complete resection, especially when the tumour is limited to one segment of the liver[13]. The prognoses of these patients depend on the ability to achieve complete tumour resection[14]. However, more than 80% of patients are diagnosed at advanced stage, with only a few patients meeting the criteria for tumour resection, thus curative surgery is difficult to perform[15]. PHA is considered to be a contraindication for liver transplantation as survival is poor and recurrence rates are high[16].

PHA is also reported to be radioresistant[3]. Alternative palliative therapies, including transarterial chemoembolization and systemic chemotherapy, are considered to be effective for unresectable PHA[17, 18]. Transarterial chemoembolization is useful to treat acute arterial bleeding from the liver of patients with PHA[18].

CONCLUSION

PHA is a rare malignancy with a poor prognosis. This case highlights the rarity of the disease, and the difficulty of diagnosis. Transjugular liver biopsy may be a safe choice in patients with PHA to aid in diagnosis.

FOOTNOTES

Author contributions: Ha FS and Liu H contributed equally to this work; Ha FS and Liu H wrote the original draft; Song DZ performed the transjugular liver biopsy; Han T reviewed and edited the manuscript; all authors have read and approved the final manuscript.

Supported by Tianjin Science and Technology Plan Project, No. 19ZXDBSY00030; and Beijing iGandan Foundation, No. RGGJJ-2021-014.

Informed consent statement: The patient and his legal guardian provided informed written consent prior to the case report.

Conflict-of-interest statement: Nothing to disclosed.

CARE Checklist (2016) statement: The authors have read the CARE checklist (2016), and the manuscript was prepared and revised according to the CARE checklist (2016).

Country/Territory of origin: China

ORCID number: Fu-Shuang Ha 0000-0001-9287-3965; Hua Liu 0000-0002-0729-2021; Tao Han 0000-0003-4216-6968; De-Zhao Song 0000-0003-3405-531X.

S-Editor: Fan JR
L-Editor: Wang TQ
P-Editor: Fan JR

REFERENCES

1 **Koyama T**, Fletcher JG, Johnson CD, Kuo MS, Notohara K, Burgart LJ. Primary hepatic angiosarcoma: findings at CT and MR imaging. *Radiology* 2002; **222**: 667-673 [PMID: 11867783 DOI: 10.1148/radiol.2223010877]

2 **Locker GY**, Doroshow JH, Zwelling LA, Chabner BA. The clinical features of hepatic angiosarcoma: a report of four cases and a review of the English literature. *Medicine (Baltimore)* 1979; **58**: 48-64 [PMID: 368508 DOI: 10.1097/00005792-197901000-00003]

3 **Molina E**, Hernandez A. Clinical manifestations of primary hepatic angiosarcoma. *Dig Dis Sci* 2003; **48**: 677-682 [PMID: 12741455 DOI: 10.1023/a:1022868221670]

4 **Kew MC**, Dos Santos HA, Sherlock S. Diagnosis of primary cancer of the liver. *Br Med J* 1971; **4**: 408-411 [PMID: 5124443 DOI: 10.1136/bmj.4.5784.408]

5 **Falk H**, Herbert J, Crowley S, Ishak KG, Thomas LB, Popper H, Caldwell GG. Epidemiology of hepatic angiosarcoma in the United States: 1964-1974. *Environ Health Perspect* 1981; **41**: 107-113 [PMID: 7199426 DOI: 10.1289/ehp.8141107]

6 **Zhu YP**, Chen YM, Matro E, Chen RB, Jiang ZN, Mou YP, Hu HJ, Huang CJ, Wang GY. Primary hepatic angiosarcoma: A report of two cases and literature review. *World J Gastroenterol* 2015; **21**: 6088-6096 [PMID: 26019478 DOI: 10.3748/wjg.v21.i19.6088]

7 **Abegunde AT**, Aisien E, Mba B, Chennuri R, Sekosan M. Fulminant hepatic failure secondary to primary hepatic angiosarcoma. *Case Rep Gastrointest Med* 2015; **2015**: 869746 [PMID: 25815217 DOI: 10.1155/2015/869746]

8 **Zhuge Y**, Liu Y, Xie W, Zou X, Xu J, Wang J; Chinese Society of Gastroenterology Committee of Hepatobiliary Disease. Expert consensus on the clinical management of pyrrolizidine alkaloid-induced hepatic sinusoidal obstruction syndrome. *J Gastroenterol Hepatol* 2019; **34**: 634-642 [PMID: 30669184 DOI: 10.1111/jgh.14612]

9 **Sue MJ**, Lee EW, Saab S, McWilliams JP, Durazo F, El-Kabany M, Kaldas F, Busuttil RW, Kee ST. Transjugular Liver Biopsy: Safe Even in Patients With Severe Coagulopathies and Multiple Biopsies. *Clin Transl Gastroenterol* 2019; **10**: e00063 [PMID: 31259750 DOI: 10.14309/ctg.0000000000000063]

10 **Wang ZB**, Wei LX. [Primary hepatic angiosarcoma: a clinical and pathological analysis]. *Zhonghua Bing Li Xue Za Zhi* 2013; **42**: 376-380 [PMID: 24060070 DOI: 10.3760/cma.j.issn.0529-5807.2013.06.005]

11 **Wang ZB**, Yuan J, Chen W, Wei LX. Transcription factor ERG is a specific and sensitive diagnostic marker for hepatic angiosarcoma. *World J Gastroenterol* 2014; **20**: 3672-3679 [PMID: 24707153 DOI: 10.3748/wjg.v20.i13.3672]

12 **Park YS**, Kim JH, Kim KW, Lee IS, Yoon HK, Ko GY, Sung KB. Primary hepatic angiosarcoma: imaging findings and palliative treatment with transcatheter arterial chemoembolization or embolization. *Clin Radiol* 2009; **64**: 779-785 [PMID: 19589416 DOI: 10.1016/j.crad.2009.02.019]

13 **Adson MA**, Beart RW Jr. Elective hepatic resections. *Surg Clin North Am* 1977; **57**: 339-360 [PMID: 322336 DOI: 10.1016/s0039-6109(16)41186-2]

14 **Weitz J**, Klimstra DS, Cymes K, Jarnagin WR, D'Angelica M, La Quaglia MP, Fong Y, Brennan MF, Blumgart LH, Dematteo RP. Management of primary liver sarcomas. *Cancer* 2007; **109**: 1391-1396 [PMID: 17315167 DOI: 10.1002/cncr.22530]

15 **Bioulac-Sage P**, Laumonier H, Laurent C, Blanc JF, Balabaud C. Benign and malignant vascular tumors of the liver in adults. *Semin Liver Dis* 2008; **28**: 302-314 [PMID: 18814083 DOI: 10.1055/s-0028-1085098]

16 **Gatta G**, Ciccolallo L, Kunkler I, Capocaccia R, Berrino F, Coleman MP, De Angelis R, Faivre J, Lutz JM, Martinez C, Möller T, Sankila R; EUROCARE Working Group. Survival from rare cancer in adults: a population-based study. *Lancet Oncol* 2006; **7**: 132-140 [PMID: 16455477 DOI: 10.1016/S1470-2045(05)70471-X]

17 **Ratan R**, Patel SR. Chemotherapy for soft tissue sarcoma. *Cancer* 2016; **122**: 2952-2960 [PMID: 27434055 DOI: 10.1002/cncr.30191]

18 **Leowardi C**, Hormann Y, Hinz U, Wente MN, Hallscheidt P, Flechtenmacher C, Buchler MW, Friess H, Schwarzbach MH. Ruptured angiosarcoma of the liver treated by emergency catheter-directed embolization. *World J Gastroenterol* 2006; **12**: 804-808 [PMID: 16521200 DOI: 10.3748/wjg.v12.i5.804]

World Journal of Gastrointestinal Oncology

Submit a Manuscript: https://www.f6publishing.com

World J Gastrointest Oncol 2022 May 15; 14(5): 1057-1064

DOI: 10.4251/wjgo.v14.i5.1057

ISSN 1948-5204 (online)

CASE REPORT

Successful treatment of pancreatic accessory splenic hamartoma by laparoscopic spleen-preserving distal pancreatectomy: A case report

Shao-Yan Xu, Bo Zhou, Shu-Mei Wei, Ya-Nan Zhao, Sheng Yan

Specialty type: Gastroenterology and hepatology

Provenance and peer review: Unsolicited article; Externally peer reviewed.

Peer-review model: Single blind

Peer-review report's scientific quality classification

Grade A (Excellent): 0
Grade B (Very good): B, B
Grade C (Good): 0
Grade D (Fair): 0
Grade E (Poor): 0

P-Reviewer: Dias E, Portugal; Sugiyama Y, Japan

Received: December 24, 2021
Peer-review started: December 24, 2021
First decision: March 13, 2022
Revised: March 26, 2022
Accepted: April 21, 2022
Article in press: April 21, 2022
Published online: May 15, 2022

Shao-Yan Xu, Bo Zhou, Sheng Yan, Division of Hepatobiliary and Pancreatic Surgery, Department of Surgery, The Second Affiliated Hospital, School of Medicine, Zhejiang University, Hangzhou 310000, Zhejiang Province, China

Shu-Mei Wei, Department of Pathology, The Second Affiliated Hospital, School of Medicine, Zhejiang University, Hangzhou 310000, Zhejiang Province, China

Ya-Nan Zhao, Department of Ultrasound, The Second Affiliated Hospital, School of Medicine, Zhejiang University, Hangzhou 310000, Zhejiang Province, China

Corresponding author: Sheng Yan, PhD, Chief Doctor, Division of Hepatobiliary and Pancreatic Surgery, Department of Surgery, The Second Affiliated Hospital, School of Medicine, Zhejiang University, No. 88 Jiefang Road, Hangzhou 310000, Zhejiang Province, China. shengyan@zju.edu.cn

Abstract

BACKGROUND

Pancreatic accessory spleen (PAS) is an uncommon congenital abnormality of the spleen. Spleen hamartoma (SH) is also rare. Moreover, hamartoma in the PAS has not been reported thus far. We report the first case here.

CASE SUMMARY

A 26-year-old male presented with a one-month history of left upper quadrant abdominal pain, and computerized tomography (CT) examination suggested a mass in the pancreas tail. The patient then attended our hospital for diagnosis and treatment. Ultrasonography, CT, and magnetic resonance imaging revealed a solid mass with cystic degeneration growing from the tail of the pancreas. The tumor marker carbohydrate antigen 19-9 (CA19-9) increased to 96.7 U/mL (normal range 0-37 U/mL). An epidermoid cyst in a PAS was considered preoperatively. However, a malignant tumor cannot be ruled out. We performed laparoscopic surgery, and two pancreatic masses were found growing from the pancreatic tail. The two masses were so closely connected that preoperative imaging examinations suggested only one mass. We carefully isolated the masses from the splenic artery and vein. A laparoscopic spleen-preserving distal pancreatectomy was successfully performed. On pathological examination, the masses were well-defined, homogeneous red-tan, 4 × 3, and 4.5 × 1.5 in size, respectively.

One of them was cystically degenerated. On microscopical examination, the mass contained unorganized small slit-like vascular channels enclosing red blood cells and lined with plump endothelial cells. No area of cytologic atypia was identified. Focal lymphoid aggregates were found in the intravascular areas. White pulp or fibrosis was not observed. The final diagnosis was pancreatic accessory SH with cystic degeneration. After the operation, CA19-9 was reduced to normal. The patient recovered well, and the 34-mo follow-up period was uneventful.

CONCLUSION

Here, we report the first case of pancreatic accessory SH. A laparoscopic spleen-preserving distal pancreatectomy was successfully performed. The patient recovered well and had a good prognosis.

Key Words: Pancreatic accessory spleen; Splenic hamartoma; Cystic degeneration; Laparoscopic spleen-preserving distal pancreatectomy; Case report

Core Tip: Pancreatic accessory spleen (PAS) is an uncommon congenital abnormality of the spleen. Spleen hamartoma (SH) is also rale. Moreover, hamartoma in the PAS has not been reported thus far. Here, we report the first case of pancreatic accessory SH. The tumor marker carbohydrate antigen 19-9 was abnormal. A precise diagnosis was challenging to obtain preoperatively, and a malignant tumor could not be ruled out. We successfully performed laparoscopic spleen-preserving distal pancreatectomy. The patient recovered well and had a good prognosis.

Citation: Xu SY, Zhou B, Wei SM, Zhao YN, Yan S. Successful treatment of pancreatic accessory splenic hamartoma by laparoscopic spleen-preserving distal pancreatectomy: A case report. *World J Gastrointest Oncol* 2022; 14(5): 1057-1064

URL: https://www.wjgnet.com/1948-5204/full/v14/i5/1057.htm

DOI: https://dx.doi.org/10.4251/wjgo.v14.i5.1057

INTRODUCTION

An accessory spleen is a congenital defect caused by fusion failure of the splenic anlage during embryology. Approximately 10%-15% of the general population experiences this event. The splenic hilum is the most common location of an accessory spleen. Tissue is not commonly found in the pancreas (only 16% of cases)[1]. A pancreatic accessory spleen (PAS) is not always recognized preoperatively. Radiologically, the pancreatic accessory spleen appears to be a well-defined, solitary, and hypervascular lesion. The differential diagnosis includes well-differentiated adenocarcinoma, mucinous cystic neoplasm, neuroendocrine neoplasm, solid pseudopapillary tumor, or metastatic tumor to the pancreas[2]. PAS is a benign lesion and rarely causes any symptoms. It is rarely diagnosed preoperatively, and most cases are identified only after surgical resection.

Splenic hamartoma (SH), which was first described in 1861 by Rokitansky, is a rare benign lesion of the spleen[3]. SH is a very rare benign vascular lesion, with fewer than 200 cases reported in the English literature thus far[4]. SH occurs equally in men and women, and adults are the most affected population [5]. SH consists of disorganized sinusoid-like channels, such as red pulp tissue, the lining cells of which can be highlighted by CD8 immunopositivity. In contrast, no white pulp elements are observed in the lesion[6]. SH is generally a single lesion, and multiple lesions are rare. Patients are usually asymptomatic and diagnosed incidentally, while patients with large hamartomas can have symptoms such as nonspecific abdominal pain, thrombocytopenia, splenomegaly, fever, and night sweats[7]. To date, hamartoma in the PAS has not been reported. Here, we report the first case of pancreatic accessory SH. After laparoscopic spleen-preserving distal pancreatectomy, the patient recovered well and had a good prognosis.

CASE PRESENTATION

Chief complaints

A 26-year-old male attended a local hospital because of left upper quadrant abdominal pain.

History of present illness

Laboratory examination revealed carbohydrate antigen 19-9 (CA19-9) 41.7 U/mL (normal range 0-37 U/mL), and computerized tomography (CT) examination suggested a mass in the pancreatic tail. The patient was then referred to our hospital for diagnosis and treatment.

History of past illness

There was no other significant medical history. There was no relevant history, including past interventions and outcomes.

Personal and family history

The patient did not have a history of smoking or drinking alcohol. There was no relevant family history.

Physical examination

The patient's vital signs were stable. The abdomen was soft and nondistended without evidence of a palpable mass.

Laboratory examinations

Levels of the tumor markers CA19-9 were abnormal, 41.7 U/mL, 96.7 U/mL in the local hospital and our hospital, respectively. Tumor markers alpha-fetoprotein, CA125, and carcinoembryonic antigen were in the normal range. Other blood tests, fecal examinations, and coagulation function were normal.

Imaging examinations

On ultrasonography (US), a well-defined, inhomogeneous echoic mass with a size of 5.9 cm × 3.8 cm was seen growing from the tail of the pancreas with both hyperechoic solid and hypoechoic cystic parts, dominated by a solid part (Figure 1A). Color Doppler flow imaging showed dotted blood flow signals in the mass (Figure 1B). On CT imaging, a well-defined, 6.8 cm × 3.7 cm mass with cystic change was found growing from the tail of the pancreas. The mass was isointense relative to the normal splenic parenchyma on plain scanning (Figure 2A). After enhancement, the enhancement of the parenchyma was similar to that of the spleen (Figure 2B), and the mass was close to both the splenic artery (Figure 2C) and splenic vein (Figure 2D). The mass was isointense on T1-weighted magnetic resonance imaging (MRI) (Figure 3A). On T2-weighted MRI, heterogeneous hyperintensity was found, and the signal in the middle of the tumor was higher (Figure 3B). According to these results, an epidermoid cyst in a PAS was considered preoperatively. However, a malignant tumor cannot be ruled out.

Pathological findings and immunohistochemical staining

On pathological examination of surgical specimen, two well-defined, homogeneous red-tan masses were found to be 4 × 3 and 4.5 × 1.5 in size. The former was cystically degenerated. Hemorrhage or necrosis was not found. On microscopical examination, the mass grew from the pancreas (Figure 4A). It contained unorganized small slit-like vascular channels enclosing red blood cells and lined with plump endothelial cells. No area of cytologic atypia was identified. Focal lymphoid aggregates were found in the intravascular areas (Figure 4B). White pulp or fibrosis was not observed. On immunohistochemical staining, CD8 was positive in the lining cells and scattered lymphocytes (Figure 5A); CD34 was positive in vascular lining cells (Figure 5B).

FINAL DIAGNOSIS

The final diagnosis was pancreatic accessory SH with cystic degeneration.

TREATMENT

After sufficient preparation and consent from the patient and his family members, the surgery was performed. The patient was placed in a 45° head high position. Following anesthesia and sterilization of the surgery field, sterile drapes were whisked onto the patient's body. Subsequently, a 10 mm long incision was made in the superior border of the umbilicus. A CO_2 pneumoperitoneum was set up with 15 mmHg intra-abdominal pressure using a Veress needle, and a 10 mm trocar puncture was made to insert a laparoscopic lens. Under direct vision, 10 mm and 5 mm incisions were made in the left and right abdomen, respectively, and corresponding trocars were implanted in each incision. Then, we inserted surgical instruments to operate the surgery. We exposed the pancreas with an ultrasonic scalpel. Two red pancreatic masses were found, close to each other and growing from the pancreatic tail. The upper and lower margins of the middle pancreas were isolated. We dissociated the superior mesenteric artery and portal vein from the lower margin of the pancreas and opened the posterior

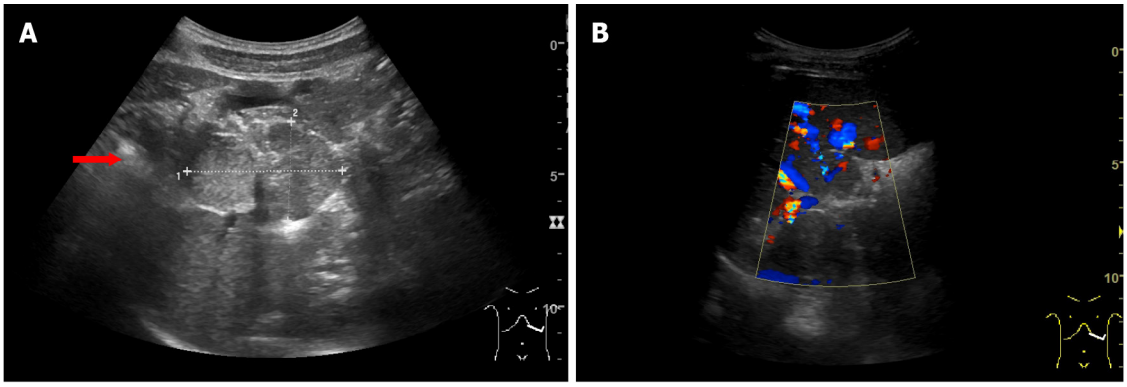

DOI: 10.4251/wjgo.v14.i5.1057

Figure 1 Ultrasound findings. A: A well-defined, inhomogeneous echoic mass (red arrow) with a size of 5.9 cm × 3.8 cm was seen growing from the tail of the pancreas with both hyperechoic solid and hypoechoic cystic parts, dominated by a solid part; B: Color Doppler flow imaging showed dotted blood flow signals in the mass.

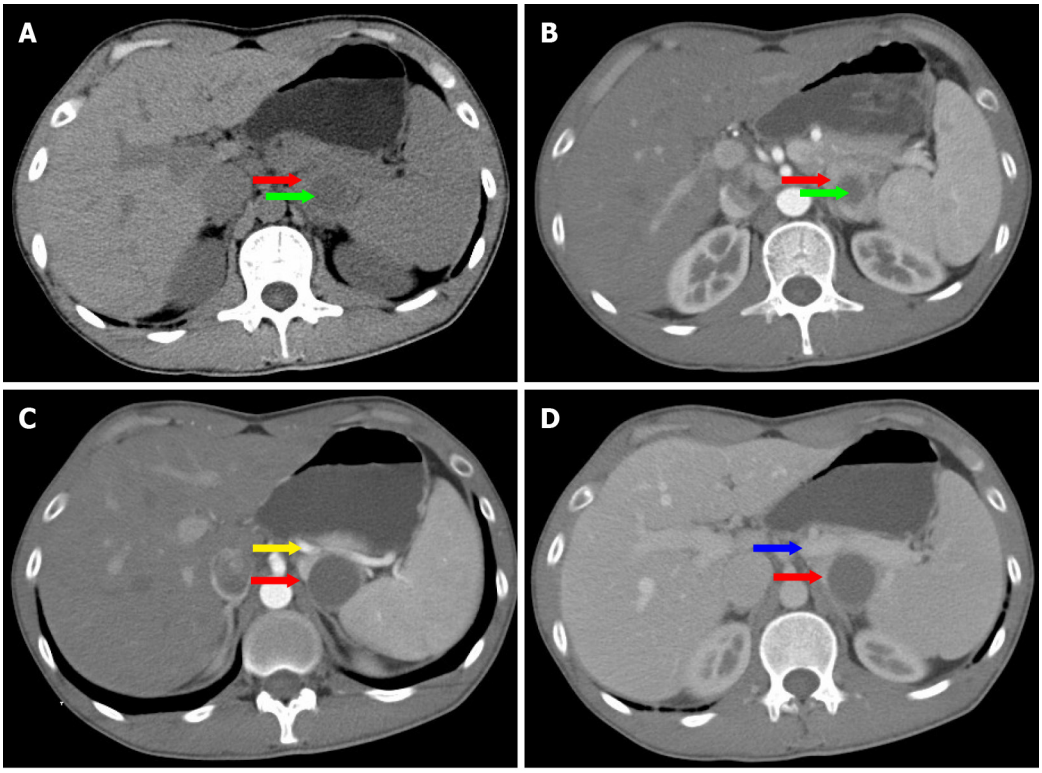

DOI: 10.4251/wjgo.v14.i5.1057

Figure 2 Computerized tomography findings. A: A well-defined, 6.8 cm × 3.7 cm mass (red arrow) with cystic change (green arrow), was found growing from the tail of the pancreas. The mass was isointense relative to the normal splenic parenchyma on plain scanning; B: After enhancement, the enhancement of parenchyma was similar to that of the spleen; C: The mass (red arrow) was close to splenic artery (yellow arrow); D: The mass (red arrow) was close to splenic vein (blue arrow).

pancreatic passage along the portal vein sulcus. The body and tail of the pancreas were isolated toward the splenic hilum. We dissected the distal pancreas, including the masses, with a cutting closure device. The masses were close to both the splenic artery and vein. We carefully isolated the masses from the blood vessels. Finally, the distal pancreas and tumor were removed entirely, and the spleen was preserved by laparoscopic surgery.

OUTCOME AND FOLLOW-UP

The patient recovered well with no pancreatic leakage postoperatively, and CA19-9 was reduced to normal. The patient left our hospital three days later. During the 34-mo follow-up period, the patient

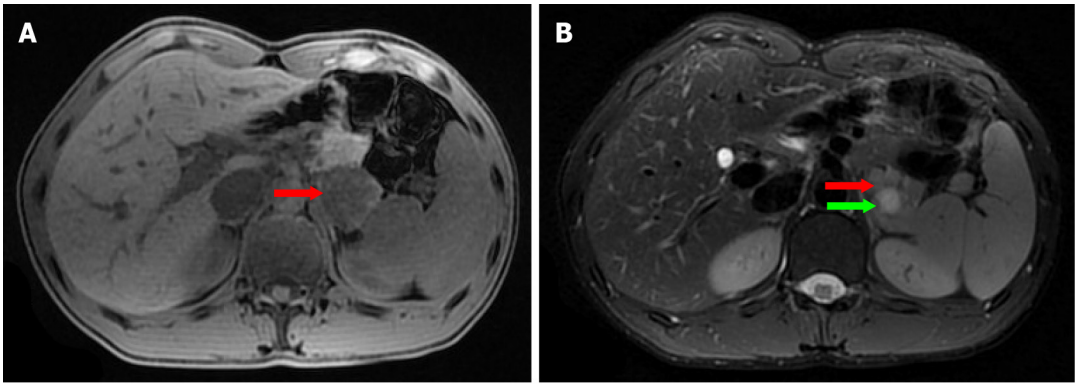

DOI: 10.4251/wjgo.v14.i5.1057

Figure 3 Magnetic resonance imaging findings. A: The mass (red arrow) was isointense on T1-weighted magnetic resonance imaging (MRI); B: On T2-weighted MRI, heterogeneously hyperintense was found, and the signal in the middle of the tumor was higher (green arrow).

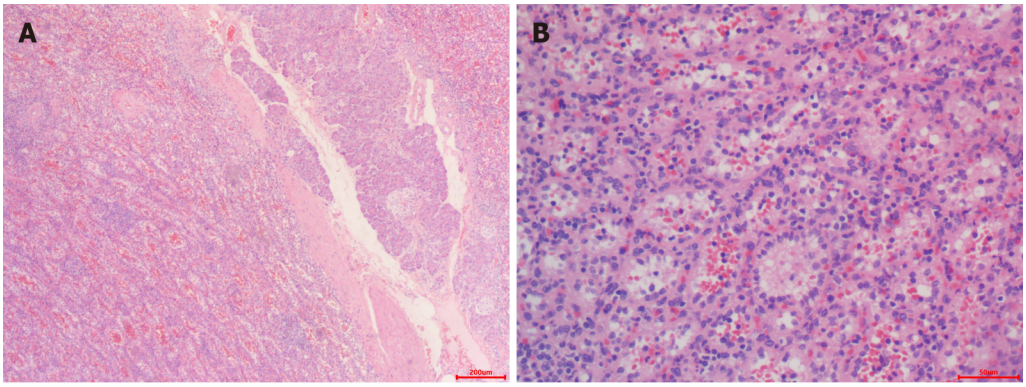

DOI: 10.4251/wjgo.v14.i5.1057

Figure 4 Microscopic examination. A: The mass grew from the pancreas [hematoxylin and eosin (HE), × 40]; B: The mass contained unorganized small slit-like vascular channels enclosing red blood cells and lined with plump endothelial cells. No area of cytologic atypia was identified. Focal lymphoid aggregates were found in the intravascular areas (HE, × 200). White pulp or fibrosis was not observed.

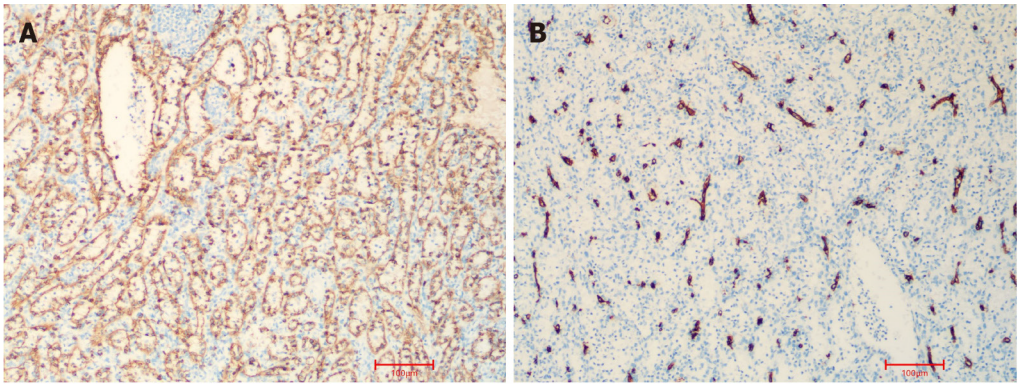

DOI: 10.4251/wjgo.v14.i5.1057

Figure 5 Immunohistochemical staining. A: CD8 immunostaining was positive in the lining cells and scattered lymphocytes (× 10); B: Immunohistochemistry for CD34 was positive in vascular lining cells (× 10).

remained well without any complications.

DISCUSSION

PAS is an uncommon congenital abnormality of the spleen with an incidence of approximately 2%[8]. It

is a benign lesion, and patients are usually asymptomatic. It is difficult to accurately diagnose preoperatively, and they are usually misdiagnosed as hypervascular pancreatic neoplasms. SH is a rare benign "tumor", and fewer than 200 cases have been reported thus far. Moreover, hamartoma in PAS has not been reported. In the present study, we report the first case. SH can occur in any age group, usually asymptomatically with no sex predilection[9]. They are usually found incidentally during physical examination or at autopsy. The tumors vary in size, ranging from a few millimeters to a maximum of 20 cm, with a median size of 5 cm. Women often encounter larger masses, suggesting a hormonal influence [4].

Obtaining an accurate diagnosis of SH through the use of US, CT, and MRI is challenging[10]. On US, the lesion is usually solid and hyperechoic, relative to normal splenic tissue. Color Doppler flow imaging shows dotted blood flow signals in the lesion. It appears on CT as an isodense or hypoattenuating solid lesion compared to the normal splenic tissue. On MRI imaging, SH can show different findings depending on whether it is fibrous or not. Most SHs appear on MRI as isointense lesions on T1-weighted image and heterogeneously hyperintense on T2-weighted image.

Although the use of multiple radiologic imaging techniques makes it possible to detect SH, definitive diagnosis still depends on pathological examination. SHs usually are well demarcated from normal spleen and present as dark red, solitary or multiple masses. Histologically, SH can be classified into white and red pulp subtypes, consisting of lymphoid tissue and a complex of sinuses, respectively[4]. The majority of SHs are mixtures of the different characteristics. Immunohistochemically, the lining cells of sinusoid-like channels are CD8-positive[11]. The cells are also positive for CD31, CD34, factor VIII–related antigen, and vimentin[12-14].

The pathogenesis of SH is still controversial. One hypothesis is that the tumor is a congenital malformation of the red pulp, excessive and disorganized growth of abnormally formed red pulp, a neoplasm, or a reactive lesion to prior trauma[15,16]. SH has also been associated with other hamartomatous masses, such as tuberous sclerosis[17]. In some cases, SHs are combined with hematological disorders. But, the clear relationship between them has not been studied[18].

The radiological differential diagnosis of SH includes lymphoma, inflammatory myofibroblastic and metastatic tumors[19]. Pathologically, SH should be differentially diagnosed from other splenic vascular tumors, such as hemangioma, lymphangioma and so on[6]. Most patient of SH are asymptomatic. When a malignant tumor can not be eliminated, splenectomy may be a good choice for patient with an accidentally found splenic lesion[20]. In the present case, one lesion was found in the tail of the pancreas, and a pancreatic accessory spleen with epidermoid cystic change was considered preoperatively by multiple imaging examinations.

Abnormally elevated CA19-9 often occurs in patients with malignancies or inflammation of the pancreatic, biliary and gynecological systems[21]. SH is a rare benign "tumor", and fewer than 200 cases have been reported thus far. To date, only one study has reported the elevation of serum CA19-9 in a case of spleen hamartoma[22]. However, normalization was not reported after resection. In our case, the patient was symptomatic with left upper quadrant abdominal pain. In addition, laboratory examination revealed that CA19-9 was abnormally elevated (96.7 U/mL). A malignant tumor cannot be ruled out. Therefore, we successfully performed laparoscopic spleen-preserving distal pancreatectomy for the patient. The final diagnosis was pancreatic accessory splenic hamartoma with cystic degeneration. After resection, the serum CA19-9 level was reduced to normal, and CA19-9 immunostaining of the tissue was negative. As the case is extremely rare, the mechanism behind the occasional elevation of serum CA19-9 in the case of spleen hamartoma has not been studied thus far. In our case, the elevation of serum CA19-9 might be caused by the inflammation of the cystic degeneration of pancreatic accessory SH.

CONCLUSION

A PAS is an uncommon congenital abnormality. SH is also rale. Moreover, hamartoma in the PAS has not been reported thus far. Here, we report the first case. The tumor marker CA19-9 was abnormal, and a malignant tumor could not be ruled out preoperatively. We successfully performed laparoscopic spleen-preserving distal pancreatectomy, and the patient recovered well and had a good prognosis.

FOOTNOTES

Author contributions: Xu SY collected case data and prepared the photos; Wei SM proofread the pathologic materials; Xu SY wrote the manuscript; Zhou B, Zhao YN and Yan S proofread and revised the manuscript; all authors approved the final version to be published.

Supported by the Chen Xiao-Ping Foundation for the Development of Science and Technology of Hubei Province, No. CXPJJH11900009-07.

Informed consent statement: Informed written consent was obtained from the patient for publication of this report

and any accompanying images.

Conflict-of-interest statement: The authors declare that they have no conflict of interest.

CARE Checklist (2016) statement: The authors have read the CARE Checklist (2016), and the manuscript was prepared and revised according to the CARE Checklist (2016).

Country/Territory of origin: China

ORCID number: Shao-Yan Xu 0000-0001-8016-0917; Bo Zhou 0000-0002-4139-5462; Shu-Mei Wei 0000-0002-5362-8083; Ya-Nan Zhao 0000-0002-4938-9235; Sheng Yan 0000-0002-4153-3546.

S-Editor: Zhang H
L-Editor: A
P-Editor: Zhang H

REFERENCES

1 **Wadham BM**, Adams PB, Johnson MA. Incidence and location of accessory spleens. *N Engl J Med* 1981; **304**: 1111 [PMID: 7207579 DOI: 10.1056/nejm198104303041822]
2 **Spencer LA**, Spizarny DL, Williams TR. Imaging features of intrapancreatic accessory spleen. *Br J Radiol* 2010; **83**: 668-673 [PMID: 19690077 DOI: 10.1259/bjr/20308976]
3 **Eker T**, Kocaay AF, Sevim Y, Çakmak A. Splenic hamartoma is a rare cause of abdominal pain: Case report and literature review. *Turk J Surg* 2017; **33**: 294-295 [PMID: 29260137 DOI: 10.5152/UCD.2015.3048]
4 **Cheng N**, Chen J, Pan Y, Jiang Y, Zhou J, Shao C. Splenic hamartoma with bizarre stromal cells: a case report and literature review. *Diagn Pathol* 2018; **13**: 8 [PMID: 29378604 DOI: 10.1186/s13000-018-0687-y]
5 **Falk S**, Stutte HJ. Hamartomas of the spleen: a study of 20 biopsy cases. *Histopathology* 1989; **14**: 603-612 [PMID: 2759557 DOI: 10.1111/j.1365-2559.1989.tb02201.x]
6 **Lee H**, Maeda K. Hamartoma of the spleen. *Arch Pathol Lab Med* 2009; **133**: 147-151 [PMID: 19123729 DOI: 10.5858/133.1.147]
7 **Gonzalez Urquijo M**, Rodarte-Shade M, Rangel-Rangel R, Castillo-Meraz JA, Rodriguez-Tejeda JR, Gil-Galindo G. A giant splenic hamartoma associated with hematologic disorders: A case report. *Ann Med Surg (Lond)* 2018; **36**: 199-202 [PMID: 30505440 DOI: 10.1016/j.amsu.2018.11.003]
8 **Zhu HX**, Lou WH, Kuang TT, Wang DS. Post-splenectomy intrapancreatic accessory spleen mimicking endocrine tumor of the pancreas. *Int J Surg Case Rep* 2014; **5**: 1151-1153 [PMID: 25437661 DOI: 10.1016/j.ijscr.2014.11.032]
9 **Lam KY**, Yip KH, Peh WC. Splenic vascular lesions: unusual features and a review of the literature. *Aust N Z J Surg* 1999; **69**: 422-425 [PMID: 10392884 DOI: 10.1046/j.1440-1622.1999.01550.x]
10 **Sim J**, Ahn HI, Han H, Jun YJ, Rehman A, Jang SM, Jang K, Paik SS. Splenic hamartoma: A case report and review of the literature. *World J Clin Cases* 2013; **1**: 217-219 [PMID: 24340270 DOI: 10.12998/wjcc.v1.i7.217]
11 **Zukerberg LR**, Kaynor BL, Silverman ML, Harris NL. Splenic hamartoma and capillary hemangioma are distinct entities: immunohistochemical analysis of CD8 expression by endothelial cells. *Hum Pathol* 1991; **22**: 1258-1261 [PMID: 1748432 DOI: 10.1016/0046-8177(91)90108-2]
12 **Yigit N**, Covey S, Tam W. Massive splenic hamartoma with bizarre stromal cells. *Int J Hematol* 2015; **101**: 315-316 [PMID: 25637257 DOI: 10.1007/s12185-015-1748-6]
13 **Ramdall RB**, Alasio TM, Cai G, Yang GC. Primary vascular neoplasms unique to the spleen: littoral cell angioma and splenic hamartoma diagnosis by fine-needle aspiration biopsy. *Diagn Cytopathol* 2007; **35**: 137-142 [PMID: 17304535 DOI: 10.1002/dc.20568]
14 **Conlon S**, Royston D, Murphy P. Splenic hamartoma. *Cytopathology* 2007; **18**: 200-202 [PMID: 17573768 DOI: 10.1111/j.1365-2303.2006.00371.x]
15 **Silverman ML**, LiVolsi VA. Splenic hamartoma. *Am J Clin Pathol* 1978; **70**: 224-229 [PMID: 696681 DOI: 10.1093/ajcp/70.2.224]
16 **Levy AD**, Abbott RM, Abbondanzo SL. Littoral cell angioma of the spleen: CT features with clinicopathologic comparison. *Radiology* 2004; **230**: 485-490 [PMID: 14752189 DOI: 10.1148/radiol.2302030196]
17 **Darden JW**, Teeslink R, Parrish A. Hamartoma of the spleen: a manfestation of tuberous sclerosis. *Am Surg* 1975; **41**: 564-566 [PMID: 1166974]
18 **Abbott RM**, Levy AD, Aguilera NS, Gorospe L, Thompson WM. From the archives of the AFIP: primary vascular neoplasms of the spleen: radiologic-pathologic correlation. *Radiographics* 2004; **24**: 1137-1163 [PMID: 15256634 DOI: 10.1148/rg.244045006]
19 **Wang JH**, Ma XL, Ren FY, Zuo CJ, Tian JM, Wang ZF, Zheng JM. Multi-modality imaging findings of splenic

hamartoma: a report of nine cases and review of the literature. *Abdom Imaging* 2013; **38**: 154-162 [PMID: 22539044 DOI: 10.1007/s00261-012-9880-8]

20 **Havlik RJ**, Touloukian RJ, Markowitz RI, Buckley P. Partial splenectomy for symptomatic splenic hamartoma. *J Pediatr Surg* 1990; **25**: 1273-1275 [PMID: 2286905 DOI: 10.1016/0022-3468(90)90529-i]

21 **Carleton C**, Hoang L, Sah S, Kiyokawa T, Karamurzin YS, Talia KL, Park KJ, McCluggage WG. A Detailed Immunohistochemical Analysis of a Large Series of Cervical and Vaginal Gastric-type Adenocarcinomas. *Am J Surg Pathol* 2016; **40**: 636-644 [PMID: 26685087 DOI: 10.1097/PAS.0000000000000578]

22 **Fujii T**, Obara T, Shudo R, Tanno S, Maguchi H, Saitoh Y, Ura H, Kohgo Y. Splenic hamartoma associated with thrombocytopenia. *J Gastroenterol* 1997; **32**: 114-118 [PMID: 9058306 DOI: 10.1007/BF01213307]

World Journal of Gastrointestinal Oncology

Submit a Manuscript: https://www.f6publishing.com

World J Gastrointest Oncol 2022 May 15; 14(5): 1065-1066

DOI: 10.4251/wjgo.v14.i5.1065

ISSN 1948-5204 (online)

CORRECTION

Correction to "Efficacy and safety of endoscopic resection in treatment of small gastric stromal tumors: A state-of-the-art review"

Ze-Ming Chen, Min-Si Peng, Li-Sheng Wang, Zheng-Lei Xu

Specialty type: Gastroenterology and hepatology

Provenance and peer review: Unsolicited article; Externally peer reviewed.

Peer-review model: Single blind

Peer-review report's scientific quality classification

Grade A (Excellent): 0
Grade B (Very good): B
Grade C (Good): C
Grade D (Fair): 0
Grade E (Poor): 0

P-Reviewer: Anastasiou I, United States; Ishida T, Japan

Received: October 21, 2021
Peer-review started: October 21, 2021
First decision: March 13, 2022
Revised: March 14, 2022
Accepted: April 25, 2022
Article in press: April 25, 2022
Published online: May 15, 2022

Ze-Ming Chen, Min-Si Peng, Li-Sheng Wang, Zheng-Lei Xu, Department of Gastroenterology, The Second Clinical Medical College, Jinan University (Shenzhen People's Hospital), Shenzhen 518000, Guangdong Province, China

Corresponding author: Zheng-Lei Xu, MD, Chief Doctor, Department of Gastroenterology, The Second Clinical Medical College, Jinan University (Shenzhen People's Hospital), No. 1017 Dongmen North Road, Shenzhen 518000, Guangdong Province, China. 78249073@qq.com

Abstract

We corrected the name of our institution in this study. The correct name should be ""Department of Gastroenterology, The Second Clinical Medical College, Jinan University (Shenzhen People's Hospital), Shenzhen 518000, Guangdong Province, China".

Key Words: Correction; Efficacy; Safety; Endoscopic resection; Small gastric stromal tumors

Core Tip: Correction to "Efficacy and safety of endoscopic resection in treatment of small gastric stromal tumors: A state-of-the-art review".

Citation: Chen ZM, Peng MS, Wang LS, Xu ZL. Correction to "Efficacy and safety of endoscopic resection in treatment of small gastric stromal tumors: A state-of-the-art review". *World J Gastrointest Oncol* 2022; 14(5): 1065-1066
URL: https://www.wjgnet.com/1948-5204/full/v14/i5/1065.htm
DOI: https://dx.doi.org/10.4251/wjgo.v14.i5.1065

TO THE EDITOR

Correction: The name of our institution "Department of Gastroenterology, Shenzhen People's Hospital, The Second Clinical Medical College, Jinan University, Shenzhen 518000, Guangdong Province, China"[1] should be changed to "Department of Gastroenterology, The Second Clinical Medical College, Jinan University (Shenzhen

People's Hospital), Shenzhen 518000, Guangdong Province, China".

FOOTNOTES

Author contributions: Xu ZL wrote this correction; and All authors finally approved it.

Conflict-of-interest statement: There are not any relevant conflicts of interest.

Country/Territory of origin: China

ORCID number: Ze-Ming Chen 0000-0002-8046-7932; Min-Si Peng 0000-0002-7653-846x; Li-Sheng Wang 0000-0002-7418-6114; Zheng-Lei Xu 0000-0002-5413-7390.

S-Editor: Ma YJ
L-Editor: A
P-Editor: Ma YJ

REFERENCES

1 **Chen ZM**, Peng MS, Wang LS, Xu ZL. Efficacy and safety of endoscopic resection in treatment of small gastric stromal tumors: A state-of-the-art review. *World J Gastrointest Oncol* 2021; **13**: 462-471 [PMID: 34163567 DOI: 10.4251/wjgo.v13.i6.462]

Published by **Baishideng Publishing Group Inc**
7041 Koll Center Parkway, Suite 160, Pleasanton, CA 94566, USA
Telephone: +1-925-3991568
E-mail: bpgoffice@wjgnet.com
Help Desk: https://www.f6publishing.com/helpdesk
https://www.wjgnet.com